ISOLATING, CHARACTERIZING, AND ENGINEERING NOVEL CU-PROTEINS AND PEROXIDASES

BY

PARISA HOSSEINZADEH

DISSERTATION

Submitted in partial fulfillment of the requirements
for the degree of Doctor of Philosophy in Biochemistry
in the Graduate College of the
University of Illinois at Urbana-Champaign, 2015

Urbana, Illinois

Doctoral Committee:

Professor Yi Lu, Chair and Director of Research
Professor Robert R. Gennis
Professor Emad Tajkhorshid
Professor Huimin Zhao

ABSTRACT

Metalloproteins are a fascinating class of proteins that function at the heart of several important biological processes including photosynthesis, respiration, and nitrogen fixation. It is even more amazing, considering that nature uses a small set of tertiary structures and metal centers to perform all these different functions with efficiency and selectivity. How nature tunes the activity within these scaffolds has been the area of research for many years. The goal of this work is to understand the underlying mechanisms of such tuning with a special focus on the role of subtle changes of residues in the secondary coordination sphere of the metal ion, an underexplored area of study. I use protein engineering techniques not only to shed light on the mechanisms underlying such changes, but also to design new functionalities within our scaffold proteins and to enhance their properties for specific purposes, such as fuel generation.

This work is divided into three main sections. In the first, I focus on characterizing a novel metalloprotein, N. mar_1307, from the organism *Nitrosopumilus maritimus*. While the protein shares a protein fold and Type 1 copper coordination site with other common electron transfer cupredoxins, the lack of an axial residue creates an open binding position in the Cu center, leading to a novel enzymatic function, NO oxidation. The purification, characterization, and activity assays of the protein are described in detail in chapter 2.

The second and major focus of this work is on tuning the reduction potential of azurin, a common electron transfer protein. In chapter 3 I demonstrate that how by making mutations around the Cu site, and replacing Cu with Ni I can obtain an azurin variant with a reduction potential of nearly 1V, the highest potential that can be observed under physiological conditions, along with other variants with negative potentials. Chapter 4 describes the characterization of a series of Phe114 mutants that were used to understand the role of this critical secondary sphere residue in tuning the reduction potential of the Cu site. Chapter 5 demonstrates the Marcus inverted region of electron transfer in a series of azurin variants with different reduction potentials. Finally, I show my initial attempts toward the design of a high-throughput screening platform for the directed evolution of azurin in chapter 6.

In chapters 7 and 8, I focus on the design of novel functionalities in one of our model scaffolds, cytochrome *c* peroxidase (C*c*P). Chapter 7 describes the work done to enhance the Mn(II) oxidation activity in a designed model of manganese peroxidase within the C*c*P scaffold

based on modifications of the second coordination sphere around the Mn(II) binding site. In chapter 8 I report the design and characterization of a novel C*c*P variant that shows catalase-like activity in "as-purified" form and forms a heme-protein crosslink in the heme-bound form.

To my husband, Amir, for being there for me and for always believing in me.
And to my parents, Mehri and Ahmad, and my sister Nadia, for their never-ending love.

ACKNOWLEDGMENTS

I wish to thank first and foremost my adviser, Professor Yi Lu, for all his support and help. He supported me throughout my PhD both on scientific and personal matters. I feel more mature as a scientist and a person owing to his fatherly care and advice. I would specifically like to thank him for providing an environment in which I can freely talk and discuss ideas. I would like to thank him for never giving up on the idea that I will be a patient person one day, an idea my parents gave up on a long time ago! I also wish to give special thanks to my incredible committee members, Prof. Bob Gennis, Prof. Emad Tajkhorshid, and Prof. Huimin Zhao, from whom I have learned so much. I would especially like to thank Emad for being there for me and patiently listening to my problems. I wish to also thank Chris Weitzel for being the coolest course instructor ever!

I want to acknowledge all the Lu lab members for their kindness and the friendly environment they created that made life pleasant during all these years. My gratitude will go to Dr. Nicholas Marshall, Dr. Kyle Miner, and Dr. Yang Yu for taking part in mentoring me in development of both technical skills and ideas. I would like to specially thank Nick without whom I wouldn't be standing where I am right now. I would like to thank Dr. Seyed-Fakhreddin Torabi and his wife Saleheh Ghasempour for being there for me, as friends and as my family in the states. I would like to thank Li Huey Tan and Shiliang Tian for being the role models of a wonderful person and an amazing scientist. Thanks Ambika Bhagi, Chang Cui, Kevin Harnden, and Evan Mirts for making my last couple of years in the lab a joyful memory and for giving me company. Special thanks will go to Igor Petrik, Julian Reed, and Kevin Hwang for helping me beyond what a colleague will do. Thanks for being there for me, for all your friendship and support, for all the discussions, and for all the amazing moments of climbing!

I wish to thank my friends in Urbana-Champaign that made my graduate experience amazing; friends who turned into part of my family. Without the mental support from them, it would be much harder for me to keep on. Special thanks goes to Omid Alamdari whose presence made my life here a happier experience. I'd like to also thank Dr. Behrouz Touri, Shayan Bordbar, Rezvan Shahoei, Maryam Khademian, Farzaneh Khajouei, Ehsan Totoni, Tanya Perlova, Amir Saberi and Mahdieh Jadaliha for all the happy and sad moments we shared. Thanks to my friends who are not here but never forgot me, specially Faranak Fattahi,

Sadaf Amin, and Mariam Okhovat. Knowing that I have them was enough for me to not feel alone. Thanks to Hanieh Falahati for always checking on me. Thanks to all my volleyball fellows who gave a new dimension to my life, especially Mohammad Naghnaeian and Amin Haghighat. I also wish to thank my MCB fellows, class of 2010, especially Padmaja Venkatarishnian, Paige Sheraden, and Peiwen Wu. And I cannot forget to give my thanks to Mr. Jeff Goldberg (mostly because he will send an email reminding me to do so ☺) who did his best for keeping all Biochemsitry students organized and prepared and for never let us forget any seminars.

I want to thank my parents, Ahmad Hosseinzadeh and Mehri Aminisani who raised me as an independent individual, who respected my decisions and me. I want to specifically thank them for their selfless decision to allow me to take on this journey to continue my studies and for their never-ending support and love. Without them, I would be nothing. My sister, Nadia, made me a better person by giving me her honest and true opinion about me and by reminding me of my mistakes. Her presence even from far away was a reason for me to not give up. I wish to thank my parents-in-law, Souraya Chavoshian and Hossein Nayyeri, and my sister-in-law Ghazal, for all their kindness and for their support during the past couple of years.

And last but definitely not least, I wish to thank my husband, Amir Nayyeri, without whom this journey was impossible. He is my rock. My appreciations for him cannot be described in words. He was my motivation and support throughout the way. He gave meaning to my life and enlightened my moments.

TABLE OF CONTENTS

CHAPTER 1

INTRODUCTION

* Portions of this chapter are from a submitted review to *Biophys. Biochim. Acta-Bioenerg.* As "Designed and fine-tuning redox potentials of metalloproteins involved in electron transfer in biology" (Hosseinzadeh P., Lu Y.)

1.1. Metalloproteins, primary ligands and secondary ligands

Any protein that contains at least one bound metal ion is called a metalloprotein and this classification is regardless of the role the metal ion is playing or whether the metal ion is present alone or is coordinated via an organic framework. Several metal ions can be found within protein scaffolds. The most common metal ions in biology are Fe, Cu, Zn, Mg, Ca and Mn. Other metal ions such as Co, W, V, Ni,and Mo can also be found but in less abundance.

The metal ion can simply serve a structural role within the protein. For example, in Zn-finger proteins the Zn ion stabilizes a kink in the structure, making it optimal for DNA binding.[1] However, the role of metal ions is not limited to structural stabilization as metalloproteins can also participate in storage of metal ions, electron transfer, ligan binding (e.g, O2, NO, H2), and a variety of catalytic activities.[2]

Each metal ion within a protein is directly coordinated by the so-called "primary ligands". Residues that are in some contact with primary ligands but are not coordinating the metal ion are called "secondary coordination residues". The primary ligands determine the geometry of the metal site and some of its most important features. The arrangement of ligands dictates metal geometry and spin based on the ligand field theory. The most common geometries of metal ions are shown in figure 1.1a. Figure 1.1b demonstrates an example of how the ligand field can affect the d-orbital splitting of a transition metal ion. Such effect is due to selective stabilization of one or more sets of d-orbitals over the others in the given field.

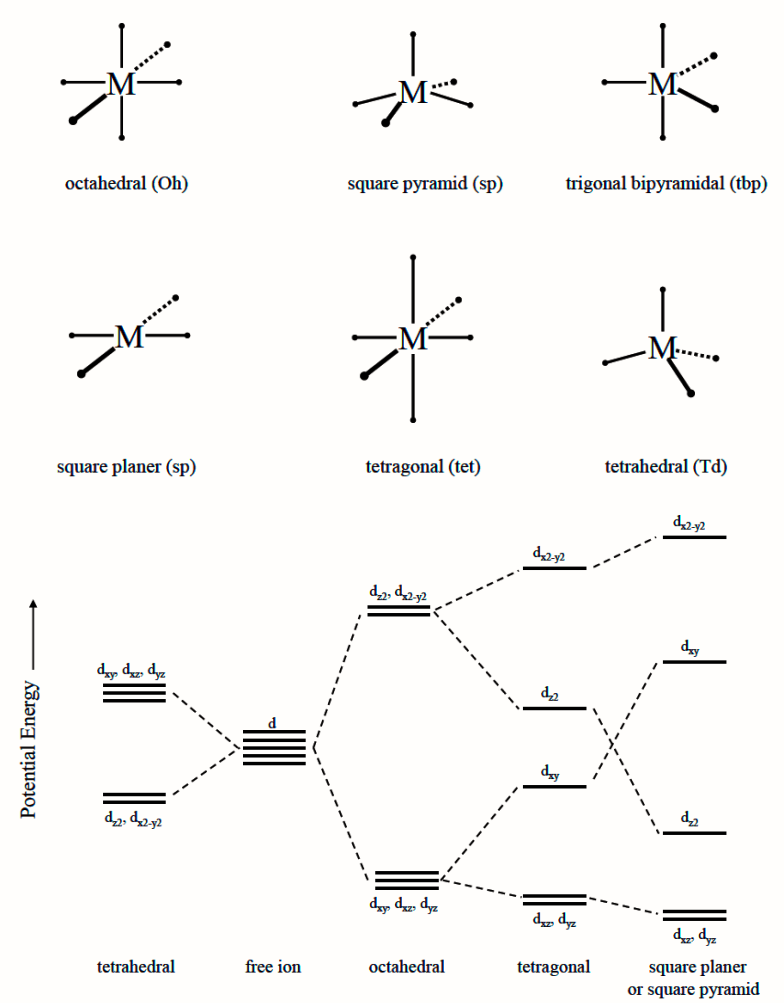

Figure 1.1.(a) Most common coordination geometries of metal ions. (b) Ligand field splitting of d orbitals in selected ligand field geometries.

Another feature of the ligand is its softness, a factor that can be determined based on the hard-soft acid base theory (HSAB). Soft ligands prefer soft metal ions whereas hard ligands would better coordinate hard metal ions. Whether or not a hard ligand is used in place of a soft ligand can affect the equilibrium between one oxidation state of the metal ion vs. the other. Table 1.1 shows the hardness and softness of different metal ions and their preferred ligands. As a general rule, the smaller the ionic radii or the higher the charge, the harder a metal ion is.

Table 1.1. Classification of acids and bases based on HSAB theory.

	Acids	**Bases**
Hard	H^+, Li^+, K^+,Mg^{2+}, Ca^{2+}, Mn^{2+}, Al^{3+}, Ln^{3+}, Cr^{3+}, Co^{3+}, Fe^{3+}, VO^{2+}, MoO^{3+}, SO_3, CO_2	H_2O, ROH, NH_3, RNH_2, RCO_2^-, Cl^-, F^-, PO_4^{3-}, HPO_4^{2-}, $H_2PO_4^-$, SO_4^{2-}

Table 1.1 cont.

Intermediate	Fe^{2+}, Co^{2+}, Ni^{2+}, Cu^{2+}, Zn^{2+}, Pb^{2+}, Sn^{2+}, SO_2, NO^+, Ru^{2+}	Imidazole, pyridine
Soft	Cu^+, Ag^+, Au^+, Tl^+, Hg^+, Cd^{2+}, Pd^{2+}, Pt^{2+}, Hg^{2+}	RSH, R_2S, CN^-, I^-, $S_2O_3^{2-}$

Within a protein scaffold, several amino acids can potentially to coordinate metal ions. A list of these amino acids and their features are shown in table 1.2.

Table 1.2. Endogenuous biological ligands. Adapted from ref. [2]

coordinating group	nomenclature[a] (examples)	pK_a[b]
N-Donors		
amino: side chain	H_2N^{ϵ}·Lys	9–11[c]
N-terminus	H_2N·X (any residue)	
amido: backbone (–NHC(O)–)	HN·X (any residue)	≳13
side chain ($-C(O)NH_2$)	HN^{γ}·Asn, HN^{δ}·Gln	
amidato: backbone $(-N-C(O)-)^-$	$^-$N·X (any residue)	
side chain $(-C(O)NH)^-$	$^-N^{\gamma}$·Asn, $^-N^{\delta}$·Gln	
imidazolyl 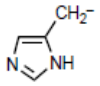	N·His	≳14[d]
imidazolato 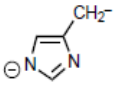	$^-$N·His	
guanidine 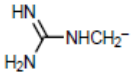	H_2N^{δ}·Arg	>12[e]
O-Donors		
carbamate	O_2CNH·Lys	
carboxylate: side chain	O_2C^{γ}·Asp, O_2C^{δ}–Glu	4–5
C-terminus	O_2C·X (any residue)	
carbonyl: side chain	OC^{γ}·Asn, OC^{δ}·Gln	
backbone	OC·X (any residue)	
phenol	HO·Tyr	10
phenolate	O·Tyr	
hydroxyl	HO·X (X = Ser, Thr)	≳14
olate	O·X (X = Ser, Thr)	
S-Donors		
thioether	S·Met	
thiol	HS·Cys	8–9
thiolate	S·Cys	
disulfide	SS·Cys (cystine)	

imidazolyl, respectively. [a] X = amino acid residue; side chain C-atom designation:

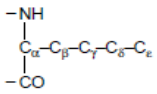

[b] Approximate values in proteins; actual values may vary with protein environment. [c] $-NH_3^+$ form. [d] Imidazolium pK_a 6–7. [e] $-HNC(NH_2)_2^+$ form.

While metal ions can be directly coordinated to protein residues, some of them are found in proteins within organic frames. The most well-known frame is protoporphyrin ring which can accommodate Fe ion. Several types of porphyrins are found in nature with different features, shown in figure 1.2. Corins are Co containing counterparts of porphyrins. Pterins are another common frame clustering W and Mo.

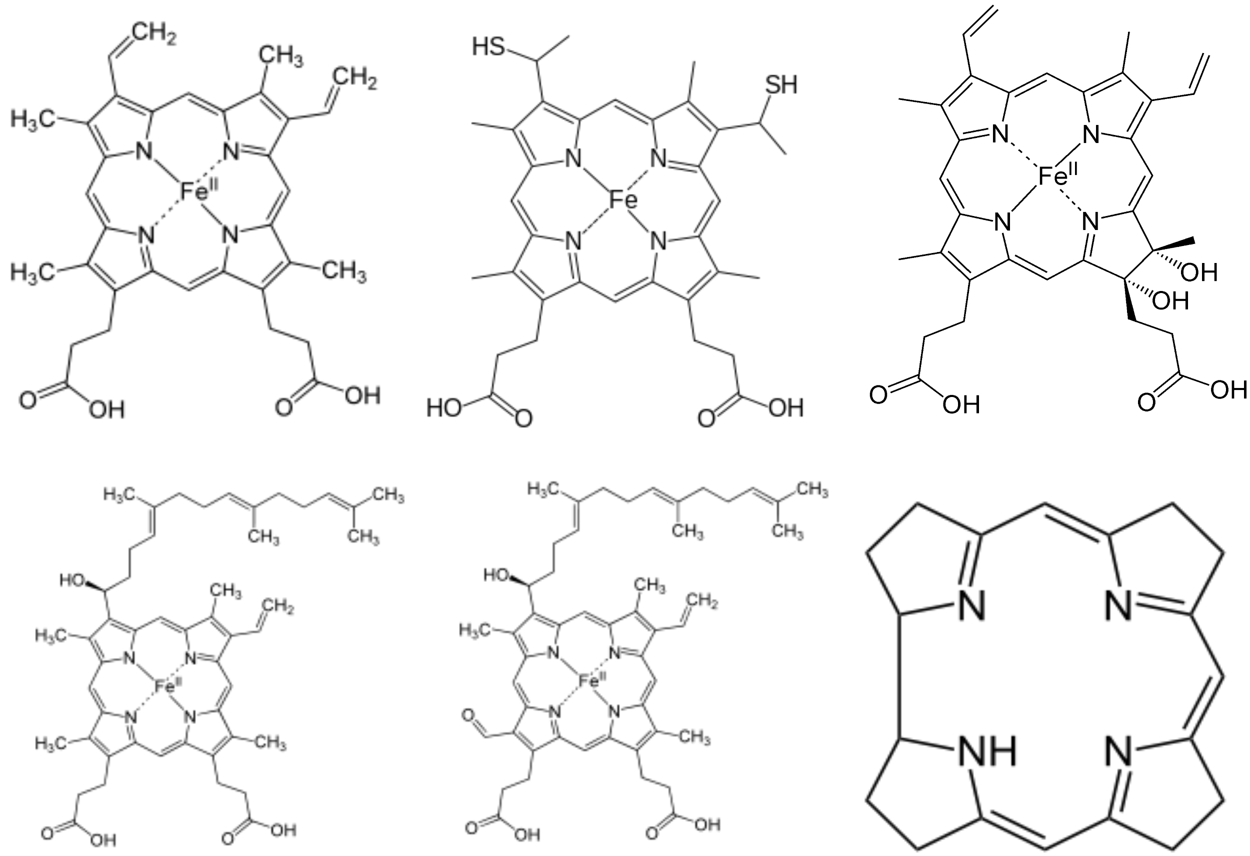

Figure 1.2.Different types of hemes and a corin.

1.2. Functions of metalloproteins

Metalloproteins are involved in a variety of physiological functions vital for cell survival. These functions can be categorized in many ways. One such way is to divide them into two broad categories, redox-based functions and non-redox functions. Table 1.3 summarizes the

most common transition metal centers in biology, their geometry, preferred ligands, and their most common functions.

Table 1.3. Biologically relevant transition metal ions. Adapted from ref [2]

Metal	Function	Common oxidation states	d^n	Common coordination number	Effective geometry	Spin state
Co	Oxidase, alkyl group transfer	+2	d^7	4	T_d	3/2
				5	C_{4v}	3/2
					D_{3h}	3/2
				6	O_h	½
					O_h	3/2
		+3	d^6	6	O_h	0
					O_h	2
Cu	Oxidase, dioxygen transport, electron transfer	+1	d^{10}	2	Linear	0
				3	Trigonal	0
				4	T_d	0
				6	O_h	0
		+2	d^9	4	T_d	½
					D_{4h}	½
				5	C_{4v}	½
					D_{3h}	½
				6	O_h	½
		+3	d^8	6	O_h	1
Fe	Oxidase, dioxygen transport/ storage, electron transfer, nitrogen fixation	+2	d^6	4	T_d	2
					D_{4h}	2
				5	C_{4v}	2
					D_{3h}	2
				6	O_h	0
					O_h	2
		+3	d^5	4	T_d	5/2
					C_{4v}	5/2
				5		3/2
				6	O_h	½
					O_h	5/2

Table 1.3 cont.

Mn	Photosynthesis,	+2	d^5	4	T_d	5/2
	oxidase, structure			5	D_{3h}	5/2
				6	O_h	½
					O_h	5/2
		+3	d^4	5	C_{4v}	2
					D_{3h}	2
				6	O_h	1
					O_h	2
		+4	d^3	4	T_d	3/2
				6	O_h	3/2
Mo	Nitrogen fixation,	+3	d^3	6	O_h	3/2
	oxidase, oxo transfer	+4	d^2	6	O_h	1
		+5	d^1	4	T_d	½
$[MoO]^{3+}$				5	C_{4v}	½
				6	O_h	½
		+6	d^0	4	T_d	0
$[MoO_2]^{2+}$				6	O_h	0
Ni	Hydrogenase,	+2	d^8	4	T_d	1
	hydrolase				D_{4h}	0
				5	C_{4v}	1
					C_{4v}	0
					D_{3h}	1
					D_{3h}	0
				6	O_h	1
		+3	d^7	4	D_{4h}	½
				5	C_{4v}	½
				6	O_h	½
					O_h	3/2
		+4	d^6	6	O_h	0
W	dehydrogenase	+4	d^2	6	O_h	1
$[WO]^{+3}$		+5	d^1	5	C_{4v}	½
				6	O_h	½
		+6	d^0	4	T_d	0
				5	C_{4v}	0
$[WO_2]^{2+}$				6	O_h	0
V	Nitrogen fixation,	+2	d^3	6	O_h	3/2
	oxidase	+3	d^2	6	O_h	1
$[VO]^{2+}$		+4	d^1	5	C_{4v}	½
				6	O_h	½
$[VO_2]^{+}$		+5	d^0	6	T_d	0

Table 1.3 cont.

Zn	Structure, hydrolase	+2	d^1	4	T_d	0
				5	C_{4v}	0
					D_{3h}	0
				6	O_h	0

1.2.1. Non-redox functions

While metalloproteins are mostly known for their redox functions, they perform a wide range of other functions as well. As mentioned earlier, some metalloproteins have a metal ion as a structural element. Two Ca^{2+} binding sites are present in manganese peroxidase and are suggested to give stability to the protein. Disruption of the Ca^{2+} binding sites causes thermal susceptibility in the protein. This thermal inactivation is due to some overall protein structural changes and distinct changes in heme environment [3]. The presences of distal Ca^{2+} gives enzyme extra compactness and rigidity [4]. Presence of metal ion is necessary for proper binding of substrate in a number of enzymes including polymerases. Mg^{2+} is necessary for coordinating to the phosphate backbone of the DNA and placing them in the right position for reaction to happen.[5] Metal binding to a metalloproteins can be a means to regulate gene transcription and protein expression. Metal-responsive transcription factor-1 (MTF-1) is one such protein. In normal condition the protein shuttles between the cytosol and the nucleus. Direct binding of excess Zn or indirect release of Zn due to Cd binding to metallothioneins will direct MTF-1 to the nucleus where it can recruit transcription machinery and regulate gene expression.[6]

Binding to metal ions can cause drastic structural changes in a metalloprotein and hence changes its function. A very well-studied example of such a case is the protein calmodulin. Binding of Ca^{2+} ion to calmodulin will result in drastic structural changes in the protein (see figure 1.3). These structural changes in turn influence protein localization, different modes of binding to other proteins, and target-specific activation.[7]

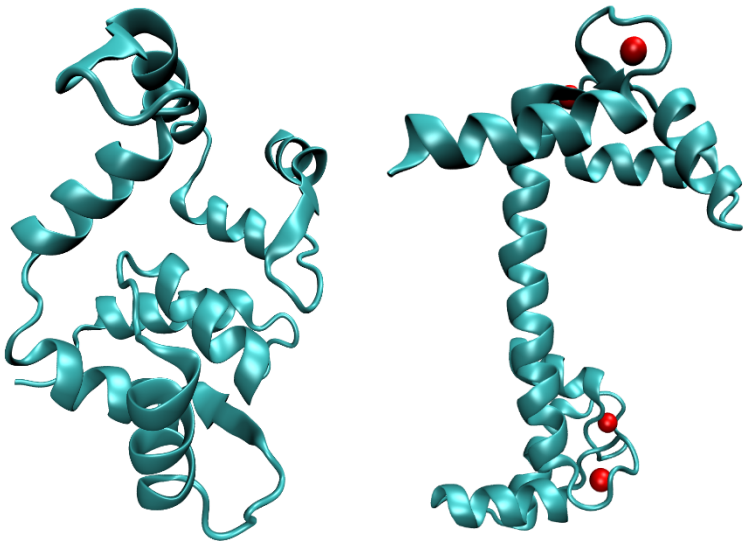

Figure 1.3. Structures of apo-calmodulin (left figure, PDB: 1QX5) and Ca^{2+}-bound calmodulin (figure in right, PDB ID: 1CLL)

Metalloproteins can sometimes serve as storage for the metal ion, releasing their content when required. Ferritins are probably the most well-known example of metal storage proteins acting as huge cages for iron.[8] Metal ions can be found in the active site of proteins, facilitating the reactions through acting as a Lewis acid. Zn^{2+} plays such a role in a variety of enzymes including carbonic anhydrase the mechanism of which is shown in figure 1.4.[9,10]

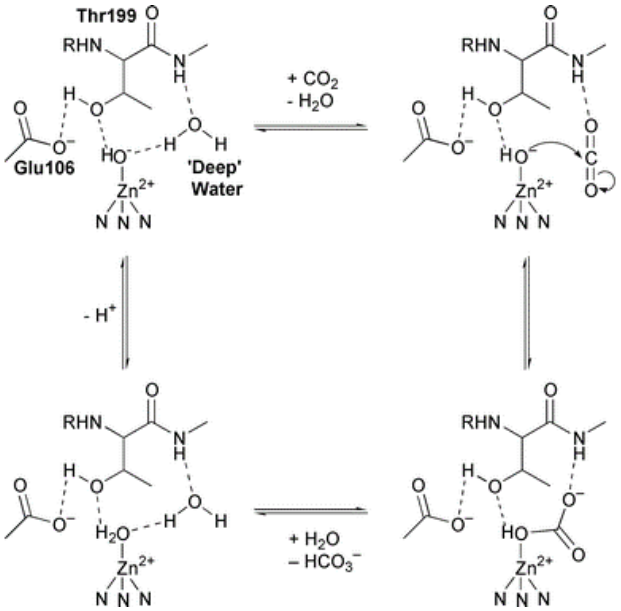

Figure 1.4. Proposed mechanism of CO_2 hydration by carbonic anhydrase. Adapted from ref. 11

1.2.2. Redox-based functions

In redox-based functions, the metal ion goes through a transition between different oxidation states. Such a change in redox state can be used to simply transfer electrons, to perform an enzymatic function, or to facilitate delivery of a small molecule. Electron transfer (ET) is one of the best-studied functions of metalloproteins and some metalloproteins are evolved to just perform this function. The most common classes of metalloproteins involved in ET are cupredoxins (including type 1 copper (T1Cu) proteins and Cu_A centers),[11-17,18,19,20] cytochromes,[20-27] and FeS proteins.[20,28-34] Each class performs ET between different types of redox partners with different range of reduction potential (E°). Cupredoxins usually function at the high end while FeS centers are mostly involved in low reduction potential ET chains.[20]

Redox transition of the metal ion can be accompanied by a catalytic reaction. Numerous metalloenzymes have been reported catalyzing a variety of functions, some of which are essential for life on earth. Cytochrome *c* oxidases (C*c*Os) are the terminal enzymatic complexes in oxidative ET chain, turning O_2 into water and enabling aerobic respiration.[35,36] P450s are one of the most diverse classes of heme enzymes performing several functions such as oxidation, hydroxylation, and alkylation with specificity and high efficiency using very similar reaction mechanisms.[37-43] Hydrogenases can perform one of the most kinetically difficult reactions on earth, catalyzing the reversible oxidation of molecular H_2.[44-49] Reduction potential of the metal center is one of the most important features of these sites for their function as it controls and directs ET events, a requirement for the catalytic activity of above proteins.

1.3. Approaches to study metalloproteins

Researches have been interested in studying metalloproteins from the early days of protein biochemistry. Myoglobin was the first proteins being crystallized in 1958 by the work of Kendrew et al.[50] How these proteins function and what factors contribute to their activity was among the questions that has sparked the interest of several scientists throughout the years. To address such questions, two main approaches have been taken, the top-down approach and the bottom-up approach. A combination of these approaches, so-called the "biosynthetic approach" is also being developed recently. In this section, I will briefly explain the two approaches first and spend some time describing the biosynthetic approach.

1.3.1. The top-down approach

The most common way of gaining mechanistic insights into the activity of metalloproteins was the common biochemical approach. In this approach, specific residues in the protein that are hypothesized to be important for the activity are mutated to other residues. A decrease in or abolishment of the activity is an indicator of a critical role for that residue. The biochemical approach has yielded numerous insightful results with regards to finding critical residues and elements contributing to specific features of metalloproteins. However, there are certain drawbacks to this approach, mostly arising from the complexity of metalloproteins.

One such example is the case of heme copper oxidises (HCOs) and nitric oxide reductases (NORs). Heme-copper oxidases (HCOs)[51-66] and nitric oxide reductases (NORs)[67-70] are two structurally homologous membrane proteins that catalyze $4e^-$ reduction of O_2 to H_2O, and $2e^-$ reduction of NO to N_2O, respectively. The free energy generated from the O_2 reduction by HCOs is used to drive proton (H^+) translocation across the membrane, which is then used to synthesize ATP. NORs, on the other hand, do not drive H^+ translocation.[71] Despite the different functions, both enzymes' active sites consist of a proximal His-coordinated heme, with the major difference being the identity of the nonheme metal (Cu_B in HCO and Fe_B in NOR), and its primary and secondary coordination spheres (SCS) (Fig. 1.5). The Cu_B is ligated by three His, one of which is covalently cross-linked to a Tyr,[72] while Fe_B is coordinated by three His and a Glu.[68] And two more conserved Glu's form a hydrogen-bonding (H-bonding) network to the active site in *c*NOR.[73-75] One of the most intriguing questions about these enzymes is why HCOs are efficient in O-O bond cleavage using a $4e^-$ reduction process, whereas NORs are effective in N-N bond formation using a $2e^-$ reduction process.

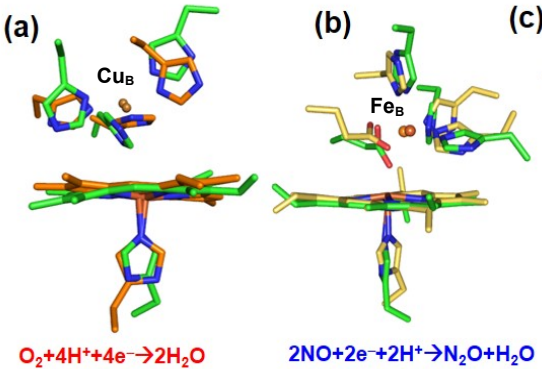

Figure 1.5. Overlays of (a) HCO (1V54, orange) & Cu_BMb model (green);[25] (b) cNOR (3O0R, yellow) & Fe_BMb (3K9Z, green);[30,229] (c) SiR (1AOP, orange) & Fe_4S_4-CcP model (green).[50]

Studies of native heteronuclear metalloenzymes have provided a plethora of information about the enzymes' structure and function.[52,53,64,65,76,77] Despite much progress, it remains difficult to address the above questions, including those mentioned above, for several reasons. First, many of these enzymes are large, membrane-bound systems (e.g. ~200 kDa for bovine HCO) that are difficult to express in large quantities and with the homogeneity required for biochemical and biophysical studies. Moreover, the enzymes often contain multiple metal cofactors, which complicates the study of the active centers due to overlapping spectroscopic features. For example, signals of a low-spin heme far from the heme-Cu center dominate the UV-vis and magnetic circular dichroism (MCD) spectra of HCOs.[78] To address this issue, isotopic or spin labeling are often required. In contrast to smaller and simpler mononuclear or homonuclear enzymes, such labelings are often very difficult to do at selective site(s) for heteronuclear enzymes with additional cofactors (e.g. ^{57}Fe labeling only at the Fe_B site in NOR). The active sites of these enzymes are similar (e.g., using heme-nonheme metal centers), yet can catalyze diverse reactions (e.g., $2e^-$ and $4e^-$ reductions of NO and O_2). One way to overcome such an obstacle is to compare different enzymes in this family to provide a holistic view. However, it is difficult to provide fair comparisons of functional properties of different sites (e.g., Cu_B and Fe_B) that reside in very different protein environments. To address this, one nonheme metal such as Cu_B in HCO could be replaced with another such as Fe, to find out if the replacements will confer any different reactivity. Unfortunately, it is extremely difficult to selectively remove and replace the nonheme metal in the native enzymes, most of which are membranous, and such efforts have resulted in inactive or misfolded proteins (even when the native metal ion was added back), which are not biologically relevant.[79] Finally, a common practice is to use site-directed mutagenesis (SDM) to replace conserved residues in one enzyme with others in another. While this approach is effective in examining individual enzymes, it is difficult to draw general conclusions across two or more enzymes since outcome is difficult to reconcile between different enzymes, especially when similar mutations cause different effects.[75]

1.3.2. The bottom-up approach

To address the limitations of the top-down appraoch, several chemists took the lead and designed synthetic models of the active sites of metalloproteins. These models provide an excellent tool for focusing on specific features of the ligands and metal ions themselves and will

provide an easier platform for studying such active sites and can complement the biochemical top-down approach by providing insights into whether *necessary* structural elements are *enough* for the function of the enzymes. Multiple successful examples of designing a metal active site has been reported during the past couple of decades and those studies provided much insight into the activity of the active sites of interest.[80] One such example is the diiron models of hydrogenases. Detailed studies of these models resulted in a better understanding of the native system.[81] Models of heme porphyrins provide scientist with a simple system to gain experimental insights about the features of Fe-O_2 bonding.[82] Models of Mo ligated to pterin cofactor were used to understand the role of the strength of NH…S hydrogen bond in the reactivity of the model.[83] The synthesis of small molecule models for HCOs and NORs active site also has been an effective approach used by several well-known bioinorganic chemists, including Drs. Richard H. Holm,[84-87] James P. Collman[88-101] and Kenneth D. Karlin,[102-122] and several leading researchers in Europe[123-126] and Japan.[127-130]

This minimalist approach can serve as a touchstone whereby the knowledge obtained from the biochemical, spectroscopic, and X-ray structural studies can be tested. Since the model systems lack other metal-binding sites, they can simplify many structural and functional characterizations and aid to deconvolute spectroscopy. The success of these models is a milestone in bioinorganic chemistry and these models will continue to play an important role in understanding the structure and function of metalloproteins. However, as pointed out by Dr. Collman in a review, the synthetic model approach has limitations and challenges.[94] For example, in case of models of HCOs and NORs, in the approach of studying stoichiometric reactions of reduced synthetic models with O_2 under *nonprotic* conditions,[131] "*the availability of protons in aqueous media may fundamentally change the dioxygen reactivity of the FeCu core*".[99] Synthetic models often result in relatively stable and unreactive bridging oxo or peroxo derivatives with much shorter Fe-Cu distances than that in HCO. Collman attributed this problem to the nonprotic conditions, because the presence of protons in HCO may destabilize the ferric peroxo intermediates (to form the putative ferric-hydroperoxo intermediate, which is known to be very reactive in many heme enzymes). Collman's group has tried to overcome this limitation by studying their models in biologically relevant conditions using electrocatalytic methods. However, as noted in his review, "*this method makes the use of spectroscopic techniques to characterize the system during the catalysis extremely challenging; so far,*

electrocatalytic studies have been a kinetic method".[99] Without spectroscopic results, insights into native HCOs are limited. Collman went on to point out that one of the most interesting and challenging areas in biomimetic modeling is to incorporate synthetic models into a better-defined chemical environment, such as self-assembled monolayers. In addition, it has become increasingly clear from biochemical and biophysical studies that non-covalent interactions, such as active site waters and the associated hydrogen bonding network, play a critical role in HCO and NOR function. This issue is at the frontier of the chemistry and biology and extremely difficult to address because it requires careful design and synthesis of rigid ligands with precise positioning of functional groups, as demonstrated recently by several groups.[132,133] Moreover, the active site models usually are synthesized and perform under non-physiological conditions, which in some cases questions the transferability of the results obtained to physiological conditions. Reduction potential of metal cofactors in general is usually higher inside proteins than in their model counterparts.[134]

1.3.3. Biosynthetic approach

An effective alternative approach towards making synthetic models is to use the same type of "ligands" and structures as native enzymes, which we model with small, stable, easy-to-produce and well-characterized proteins as the scaffold. We call this approach "biosynthetic modeling."[135,136] Compared to small organic ligands, proteins possess several unique features that make them an ideal choice for assembling protein models. First, they can fold into a rigid scaffold where different metal-binding centers can be readily placed in predefined orientations. Second, site-directed mutagenesis (SDM) eliminates the need for protecting groups and complicated synthesis commonly employed in organic synthesis. Third, the protein scaffolds provides additional protection for the metal-binding site, yielding more stable metal-binding centers. Fourth, the complex protein framework of metalloenzymes is amenable to site-specific (as opposed to solvent-induced) modulation of the secondary coordination sphere of the metal-binding site.[137] For example, although the pKa for free glutamic acid is around 4, pKa's for multiple glutamic acids in a single protein may range from 4.0 to 8.2 depending on the local electrostatic environment and hydrophilicity.[138] Finally, biosynthetic models are synthesized and function under physiological conditions using aqueous solvents, and are biodegradable ligands and therefore, environmentally benign.

The historical lack of biosynthetic models using proteins as ligands is mainly due to difficulties in the construction, expression, and purification of proteins. While this situation may have been true a decade or two ago, the rapid development of molecular biology and protein biochemistry has made it possible to synthesize proteins as easily as, or in some cases even more easily than, small molecules. A major advantage of biosynthesis is that, unlike small molecule syntheses where a modification of the ligand might result in quite a different yield, cost, and time investment, a similar protein ligand modification results in less variation of these parameters. These advances in biosynthesis make it much easier to prepare recombinant proteins in a short time (e.g., in a few days) with high yields (e.g., up to a few grams of proteins per liter). At the same time, protein ligands can retain all the structural features of native enzymes, such as rigidity and long-range or secondary sphere interactions, while significantly reducing the complexity of purification and characterization.

Furthermore, current advances in computational protein design provide us with an invaluable tool to use as a guide in our engineering. There have been multiple reports of successful engineering of novel functionalities and drugs inside protein scaffolds using a variety of computational programs such as Dezymer,[139,140] metal search, [141,142] and more recently, the Rosetta Suite,[143-145] with very exciting achievements. [139 146 147-154] The ability to incorporate unnatural amino acids using either expressed protein ligation[155] or orthogonal tRNA/tRNA synthetase systems[156] allows us to introduce novel functionalities inside our protein scaffolds, providing a unique opportunity to study the subtle effect of specific features such as charge distribution without structural perturbation, a task that is not practical in complex protein systems. Because the proteins we have chosen are easy to characterize and crystalize, it is also easier for us to offer deep insights into the reaction mechanisms that they mimic. The ultimate goal of protein engineering is to use *de novo* protein scaffolds, and much progress has been made in building existing or novel functionalities inside such scaffolds.[157-161] However, *de novo* design of protein scaffolds has its own challenges. In our approach, we overcome the scaffold difficulties by focusing mostly on designing the active site inside already available natural scaffolds. Being subjected to evolution and selection, this natural repertoire is more stable against mutations than *de novo* scaffolds. Moreover, the higher diversity in natural scaffolds than *de novo* motifs enables us to mimic a greater number of activities. Based on this approach, we have succeeded in demonstrating the importance of these long-range interactions in fine-tuning redox potentials of

azurin beyond the natural range of cupredoxins,[137] and in conferring and fine-tuning enzymatic activities.[162-164]

An overall comparison of the approaches mentioned above is summarized in table 1. 4.

Native enzymes	Synthetic models	Biosynthetic models
Difficult to obtain homogeneous sample in large quantities	Long synthesis of models of heteronuclear centers with low yields	Easy to obtain large quantities in short times
Function under physiological conditions	Usually functional under non-physiological conditions	Function under physiological conditions
SCS interactions differ in same enzymes from different sources	Very difficult to incorporate SCS interactions into the model	Role of SCS interactions can be easily studied through SDM in one scaffold
Residing in different protein environments hampers the comparison between similar enzymes	Different active centers can be designed within the same overall scaffold	Different active centers can be designed within the same overall scaffold
Difficult to crystallize	Easy to crystallize; can be soaked	Easy to crystallize; can be soaked
Overlapping features of other metal cofactors	Focus only on the active center	Focus only on the active center
Difficult to remove cofactors such as heme or nonheme metal ions without loss of function and/or structure	Can use different cofactors	Easy to replace heme, nonheme metal ion, or other cofactors
Difficult to trap intermediates using site specific labeling	Intermediates can be trapped	Site specific labeling is easily achievable via techniques such as UAA incorporation
Difficult to perform systematic studies of specific features such as heme E°, pKa of residues, and ET rates	Amenable to systematic studies using different ligands or reaction conditions	Amenable to systematic studies using cofactor replacement or UAA incorporation

1.4. Thesis goals and outlook

Metalloproteins form 50% of all the proteins on earth[165] and play essential roles for maintaining life on earth. Photosynthesis, respiration, DNA replication, and nitrogen assimilation are just a few examples of reactions that rely on presence of metalloproteins. Despite their importance, there are still many proteins that are reported as putative metal binders without their physiological function being understood. Moreover, there are several questions regarding the known proteins that remain elusive. This thesis aims to address such issues.

In chapter two, I describe my efforts in purifying and characterizing a putative Cu-binding protein from the marine archaea, *Nitrosopumilus maritimus*. While the protein is hypothesized to be a simple cupredoxins, my coworkers and I showed that it has an open binding site and have NO oxidation activity.

Chapters three to five focus mainly on addressing the question of what are the factors important in tuning the reduction potential in azurin, as a case study for cupredoxin class of ET

proteins, what are the applications of such tuning and whether we can engineer this protein to span the entire range of physiological potential. I would first start with description of the successful design of azurin to span the entire range of physiological potential, from 970 to -950 mV vs. standard hydrogen electrode (SHE) using only five mutations and two metal cofactors, Ni and Cu. I will then talk about more detailed studies of the role of residue 114 in such tuning in chapter four. Chapter five focuses on one application of the designed proteins, which is to provide a platform to study and understand Marcus inverted region in protein systems. Along these lines and as a means to provide more robust proteins as redox reagents, in chapter six I describe my efforts in designing a high-throughput screening platform to obtain stable variants with desired reduction potentials.

Chapter seven is focused on my attempts in understanding the role of interactions beyond the primary metal ligands to tune the activity and metal binding in our MnP model in CcP, MnC*c*P. I showed here how adding or removing hydrogen bonds to the metal ligand will affect metal binding. I also showed the effect of removal of steric hindrance and increasing flexibility in the activity.

In chapter eight, I will describe the characterization of a new C*c*P variant in which the loop containing residues 178 to 180 is replaced with that in MnP. I describe the unexpected results of presence of a Cys residue in position 184 in the protein. The catalase-like activity of the as-purified protein is investigated together with my studies in characterizing this state. Also, comprehensive studies of the heme-protein crosslink that is formed during heme addition to the protein are provided.

1.5. References

(1) Yu, F.; Cangelosi, V. M.; Zastrow, M. L.; Tegoni, M.; Plegaria, J. S.; Tebo, A. G.; Mocny, C. S.; Ruckthong, L.; Qayyum, H.; Pecoraro, V. L. Protein design: Toward functional metalloenzymes;*Chem. Rev.* **2014**, *114*, 3495.

(2) Holm, R. H.; Kennepohl, P.; Solomon, E. I. Structural and Functional Aspects of Metal Sites in Biology;*Chem. Rev.* **1996**, *96*, 2239.

(3) Sutherland, G. R.; Zapanta, L. S.; Tien, M.; Aust, S. D. Role of calcium in maintaining the heme environment of manganese peroxidase;*Biochemistry* **1997**, *36*, 3654.

(4) Sutherland, G. R. J.; Aust, S. D. Thermodynamics of Binding of the Distal Calcium to Manganese Peroxidase;*Biochemistry* **1997**, *36*, 8567.

(5) Beard, W. A.; Wilson, S. H. Structural insights into the origins of DNA polymerase fidelity;*Structure* **2003**, *11*, 489.

(6) Gunther, V.; Lindert, U.; Schaffner, W. The taste of heavy metals: gene regulation by MTF-1;*Biochim. Biophys. Acta* **2012**, *1823*, 1416.

(7) Chin, D.; Means, A. R. Calmodulin: a prototypical calcium sensor;*Trends Cell Biol.* **2000**, *10*, 322.

(8) Massover, W. H. Ultrastructure of ferritin and apoferritin: a review;*Micron* **1993**, *24*, 389.

(9) Bertini, I.; Lanini, G.; Luchinat, C.; Messori, L.; Monnanni, R.; Scozzafava, A. Investigation of Cu_2Co_2SOD and its anion derivatives. Proton NMR and electronic spectra;*J. Am. Chem. Soc.* **1985**, *107*, 4391.

(10) Sprigings, T. G.; Hall, C. D. A simple carbonic anhydrase model which achieves catalytic hydrolysis by the formation of an 'enzyme-substrate'-like complex;*J. Chem. Soc., Perkin Trans. 2* **2001**, 2063.

(11) Farver, O.; Pecht, I. Electron transfer processes of blue copper proteins;*Met. Ions Biol.* **1981**, *3*, 151.
(12) Stevens, T. H.; Martin, C. T.; Wang, H.; Brudvig, G. W.; Scholes, C. P.; Chan, S. I. The nature of copperA in cytochrome c oxidase;*J. Biol. Chem.* **1982**, *257*, 12106.
(13) Dennison, C.; Canters, G. W. The CuA site of cytochrome c oxidase;*Receuil des Travaux Chimiques des Pays-Bas* **1996**, *115*, 345.
(14) Battistuzzi, G.; Borsari, M.; Loschi, L.; Righi, F.; Sola, M. Redox Thermodynamics of Blue Copper Proteins;*J. Am. Chem. Soc.* **1999**, *121*, 501.
(15) De Rienzo, F.; Gabdoulline, R. R.; Menziani, M. C.; Wade, R. C. Blue copper proteins: A comparative analysis of their molecular interaction properties;*Protein Sci.* **2000**, *9*, 1439.
(16) Gray, H. B.; Malmstrom, B. G.; Williams, R. J. Copper coordination in blue proteins;*J. Biol. Inorg. Chem.* **2000**, *5*, 551.
(17) Lu, Y. In *Biocoordination Chemistry*; Que, J. L., Tolman, W. B., Meyer, T. J., Eds.; Elsevier: Oxford, UK, 2004; Vol. 8; 8, p 91.
(18) Rorabacher, D. B. Electron Transfer by Copper Centers;*Chem. Rev.* **2004**, *104*, 651.
(19) Wilson, T. D.; Yu, Y.; Lu, Y. Understanding Copper-thiolate Containing Electron Transfer Centers by Incorporation of Unnatural Amino Acids and the CuA Center into the Type 1 Copper Protein Azurin;*Coord. Chem. Rev.* **2012**, *257*, 260.
(20) Liu, J.; Chakraborty, S.; Hosseinzadeh, P.; Yu, Y.; Tian, S.; Petrik, I.; Bhagi, A.; Lu, Y. Metalloproteins containing cytochrome, iron-sulfur, or copper redox centers;*Chem. Rev.* **2014**, *114*, 4366.
(21) Keilin, D.; Hartree, E. F. Cytochrome and cytochrome oxidase;*Proc. R. Soc. London, Ser. B* **1939**, *127*, 167.
(22) Lember, R.; Barrett, J. *Cytochromes*; Academic Press: London, 1973.
(23) Vonjagow, G.; Sebald, W. B-Type Cytochromes;*Annu. Rev. Biochem* **1980**, *49*, 281.
(24) Meyer, T. E.; Kamen, M. D. New Perspectives on C-Type Cytochromes;*Adv. Protein Chem.* **1982**, *35*, 105.
(25) Pettigrew, G. W.; Moore, G. R. *Cytochromes C: Biological Aspects*; Springer: Berlin, 1987.
(26) Coutinho, I. B.; Xavier, A. V. Tetraheme cytochromes;*Methods Enzymol.* **1994**, *243*, 119.
(27) Rodgers, K. R.; Lukat-Rodgers, G. S. In *Comprehensive Coordination Chemistry II*; McCleverty, J. A., Meyer, T. J., Eds.; Elsevier Ltd.: Amsterdam, 2004; Vol. 8, p 17.
(28) Tsibris, J. C. M.; Woody, R. W. Structural studies of iron-sulfur proteins.;*Coord. Chem. Rev.* **1970**, *5*, 417.
(29) Beinert, H.; Holm, R. H.; Munck, E. Iron-sulfur clusters: nature's modular, multipurpose structures;*Science* **1997**, *277*, 653.
(30) Sticht, H.; Rosch, P. The structure of iron-sulfur proteins.;*Prog. Biophys. Mol. Biol.* **1998**, *70*, 95.
(31) Anand, B. N. Iron-sulfur proteins and their synthetic analogs: structure, reactivity and redox properties.;*Resonance* **1998**, *3*, 52.
(32) Kummerle, R.; Kyritsis, P.; Gaillard, J.; Moulis, J.-M. Electron transfer properties of iron-sulfur proteins.;*J. Inorg. Biochem.* **2000**, *79*, 83.
(33) Meyer, J. Iron-sulfur protein folds, iron-sulfur chemistry, and evolution.;*J. Biol. Inorg. Chem.* **2008**, *13*, 157.
(34) Lill, R. Function and biogenesis of iron-sulfur proteins.;*Nature* **2009**, *460*, 831.
(35) Michel, H. The mechanism of proton pumping by cytochrome c oxidase;*Proc. Natl. Acad. Sci. U S A* **1998**, *95*, 12819.
(36) Yoshikawa, S.; Muramoto, K.; Shinzawa-Itoh, K. Proton-pumping mechanism of cytochrome *c* oxidase;*Annu. Rev. Biophys.* **2011**, *40*, 205.
(37) Murray, R. I.; Fisher, M. T.; Debrunner, P. G.; Sligar, S. G. Structure and chemistry of cytochrome P-450;*Top. Mol. Struct. Biol.* **1985**, *6*, 157.
(38) Sligar, S. G. Nature's universal oxygenases: the cytochromes P450;*Essays Biochem.* **1999**, *34*, 71.
(39) Coon, M. J. Cytochrome P450: nature's most versatile biological catalyst;*Annu. Rev. Pharmacol. Toxicol.* **2005**, *45*, 1.
(40) Denisov, I. G.; Makris, T. M.; Sligar, S. G.; Schlichting, I. Structure and chemistry of cytochrome P 450;*Chem. Rev.* **2005**, *105*, 2253.
(41) Schuler, M. A.; Sligar, S. G. Diversities and similarities in P450 systems: an introduction;*Met. Ions Life Sci.* **2007**, *3*, 1.
(42) Denisov, I. G. In *Physical inorganic chemistry: Principles, methods, and models*; Bakac, A., Ed.; John Wiley & Sons, Inc.: Hoboken, NJ, USA, 2010, p 109.
(43) Jung, S. T.; Lauchli, R.; Arnold, F. H. Cytochrome P 450: taming a wild type enzyme;*Curr. Opin. Biotechnol.* **2011**, *22*, 809.
(44) Constant, P.; Hallenbeck, P. C. In *Biohydrogen*; Pandey, A., Chang, J.-S., Hallenbeck, P., Larroche, C., Eds.; Elsevier: 2013, p 75.
(45) Winkler, M.; Esselborn, J.; Happe, T. Molecular basis of [FeFe]-hydrogenase function;*Biochim. Biophys. Acta, Bioenerg.* **2013**, *1827*, 974.
(46) Fritsch, J.; Lenz, O.; Friedrich, B. Structure, function and biosynthesis of O_2-tolerant hydrogenases;*Nat. Rev. Microbiol.* **2013**, *11*, 106.
(47) Lubitz, W.; Ogata, H.; Ruediger, O.; Reijerse, E. Hydrogenases;*Chem. Rev.* **2014**, *114*, 4081.
(48) Armstrong, F. A. Electrochemistry of hydrogenases;*Electroanal. Chem.* **2014**, *25*, 33.
(49) Bagyinka, C. How does the ([NiFe]) hydrogenase enzyme work?;*Int. J. Hydrogen Energy* **2014**, *39*, 18521.
(50) Kendrew, J. C.; Bodo, G.; Dintzis, H. M.; Parrish, R. G.; Wyckoff, H.; Phillips, D. C. A three-dimensional model of the myoglobin molecule obtained by x-ray analysis;*Nature* **1958**, *181*, 662.
(51) Babcock, G. T.; Varotsis, C.; Zhang, Y. Oxygen activation in cytochrome oxidase and in other heme proteins;*Biochim. Biophys. Acta* **1992**, *1101*, 192.

(52) Woodruff, W. H. Coordination dynamics of heme-copper oxidases. The ligand shuttle and the control and coupling of electron transfer and proton translocation;*J. Bioenerg. Biomembr.* **1993**, *25*, 177.
(53) Iwata, S.; Ostermeier, C.; Ludwig, B.; Michel, H. Structure at 2.8 Å resolution of cytochrome *c* oxidase from *Paracoccus denitrificans*;*Nature* **1995**, *376*, 660.
(54) Tsukihara, T.; Aoyama, H.; Yamashita, E.; Tomizaki, T.; Yamaguchi, H.; Shinzawa-Itoh, K.; Nakashima, R.; Yaono, R.; Yoshikawa, S. Structures of metal sites of oxidized bovine heart cytochrome *c* oxidase at 2.8 Å.;*Science* **1995**, *269*, 1069.
(55) Tsukihara, T.; Aoyama, H.; Yamashita, E.; Tomizaki, T.; Yamaguchi, H.; Shinzawa-Itoh, K.; Nakashima, R.; Yaono, R.; Yoshikawa, S. The whole structure of the 13-subunit oxidized cytochrome c oxidase at 2.8 Angstrom;*Science* **1996**, *272*, 1136.
(56) Ostermeier, C.; Harrenga, A.; Ermler, U.; Michel, H. Structure at 2.7 Å resolution of the *Paracoccus denitrificans* two-subunit cytochrome *c* oxidase complexed with an antibody Fv fragment;*Proc. Natl. Acad. Sci. U S A* **1997**, *94*, 10547.
(57) Yoshikawa, S.; Shinzawa-itoh, K.; Nakashima, R.; Yaono, R.; Yamashita, E.; Inoue, N.; Yao, M.; Fei, M. J.; Libeu, C. P.; Mizushima, T.; Yamaguchi, H.; Tomizaki, T.; Tsukihara, T. Redox-coupled crystal structural changes in bovine heart cytochrome *c* oxidase;*Science* **1998**, *280*, 1723.
(58) Abramson, J.; Riistama, S.; Larsson, G.; Jasaitis, A.; Svensson-Ek, M.; Laakkonen, L.; Puustinen, A.; Iwata, S.; Wikstrom, M. The structure of the ubiquinol oxidase from *Escherichia coli* and its ubiquinone binding site;*Nature structural biology* **2000**, *7*, 910.
(59) Fei, M. J.; Yamashita, E.; Inoue, N.; Yao, M.; Yamaguchi, H.; Tsukihara, T.; Shinzawa-Itoh, K.; Nakashima, R.; Yoshikawa, S. X-ray structure of azide-bound fully oxidized cytochrome *c* oxidase from bovine heart at 2.9 Å resolution;*Acta Crystallogr. Sect. D. Biol. Crystallogr.* **2000**, *D56*, 529.
(60) Soulimane, T.; Buse, G.; Bourenkov, G. P.; Bartunik, H. D.; Huber, R.; Than, M. E. Structure and mechanism of the aberrant ba_3-cytochrome *c* oxidase from *Thermus thermophilus.*;*EMBO J.* **2000**, *19*, 1766.
(61) Yoshikawa, S. Reaction mechanism of bovine heart cytochrome oxidase;*Keio Journal of Medicine* **2000**, *49*, 99.
(62) Svensson-Ek, M.; Abramson, J.; Larsson, G.; Tornroth, S.; Brzezinski, P.; Iwata, S. The X-ray crystal structures of wild-type and EQ(I-286) mutant cytochrome *c* oxidases from Rhodobacter sphaeroides;*J. Mol. Biol.* **2002**, *321*, 329.
(63) Tsukihara, T.; Shimokata, K.; Katayama, Y.; Shimada, H.; Muramoto, K.; Aoyama, H.; Mochizuki, M.; Shinzawa-itoh, K.; Yamashita, E.; Yao, M.; Ishimura, Y.; Yoshikawa, S. The low-spin heme of cytochrome *c* oxidase as the driving element of the proton-pumping process.;*Proc. Natl. Acad. Sci. U S A* **2003**, *100*, 15304.
(64) Namslauer, A.; Brzezinski, P. Structural elements involved in electron-coupled proton transfer in cytochrome *c* oxidase;*FEBS Lett.* **2004**, *567*, 103.
(65) McMahon, B. H.; Fabian, M.; Tomson, F.; Causgrove, T. P.; Bailey, J. A.; Rein, F. N.; Dyer, R. B.; Palmer, G.; Gennis, R. B.; Woodruff, W. H. FTIR studies of internal proton transfer reactions linked to inter-heme electron transfer in bovine cytochrome *c* oxidase;*Biochim. Biophys. Acta* **2004**, *1655*, 321.
(66) Wikström, M. Cytochrome *c* oxidase: 25 years of the elusive proton pump;*Biochim. Biophys. Acta* **2004**, *1655*, 241.
(67) Moënne-Loccoz, P. Spectroscopic characterization of heme iron-nitrosyl species and their role in NO reductase mechanisms in diiron proteins;*Nat. Prod. Reports* **2007**, *24*, 610.
(68) Hino, T.; Matsumoto, Y.; Nagano, S.; Sugimoto, H.; Fukumori, Y.; Murata, T.; Iwata, S.; Shiro, Y. Structural basis of biological N_2O generation by bacterial nitric oxide reductase;*Science* **2010**, *330*, 1666.
(69) Matsumoto, Y.; Tosha, T.; Pisliakov, A. V.; Hino, T.; Sugimoto, H.; Nagano, S.; Sugita, Y.; Shiro, Y. Crystal structure of quinol-dependent nitric oxide reductase from Geobacillus stearothermophilus;*Nat. Struct. Mol. Biol.* **2012**, *19*, 238.
(70) Shiro, Y.; Sugimoto, H.; Tosha, T.; Nagano, S.; Hino, T. Structural basis for nitrous oxide generation by bacterial nitric oxide reductases.;*Philos. Trans. R. Soc. London, Ser. B* **2012**, *367*, 1195.
(71) Blomberg, M. R. A.; Siegbahn, P. E. M. Why is the reduction of NO in cytochrome *c* dependent nitric oxide reductase (cNOR) not electrogenic?;*Biochim. Biophys. Acta* **2013**, *1827*, 826.
(72) Hemp, J.; Christian, C.; Barquera, B.; Gennis, R. B.; Martinez, T. J. Helix switching of a key active-site residue in the cytochrome cbb_3 oxidases;*Biochemistry* **2005**, *44*, 10766.
(73) Thorndycroft, F. H.; Butland, G.; Richardson, D. J.; Watmough, N. J. A new assay for nitric oxide reductase reveals two conserved glutamate residues form the entrance to a proton-conducting channel in the bacterial enzyme;*Biochem. J.* **2007**, *401*, 111.
(74) Flock, U.; Lachmann, P.; Reimann, J.; Watmough, N. J.; Ädelroth, P. Exploring the terminal region of the proton pathway in the bacterial nitric oxide reductase;*J. Inorg. Biochem.* **2009**, *103*, 845.
(75) Schurig-Briccio, L. A.; Venkatakrishnan, P.; Hemp, J.; Bricio, C.; Berenguer, J.; Gennis, R. B. Characterization of the nitric oxide reductase from *Thermus thermophilus*;*Proc. Natl. Acad. Sci. U S A* **2013**, *110*, 12613.
(76) García-Horsman, J. A.; Barquera, B.; Rumbley, J.; Ma, J.; Gennis, R. B. The Superfamily of Heme-Copper Respiratory Oxidases;*J. Bacteriol.* **1994**, *176*, 5587.
(77) Ferguson-Miller, S.; Babcock, G. T. Heme/Copper terminal oxidases.;*Chem. Rev.* **1996**, *96*, 2889.
(78) Watmough, N. J.; Cheesman, M. R.; Butler, C. S.; Little, R. H.; Greenwood, C.; Thomson, A. J. The dinuclear center of cytochrome bo_3 from *Escherichia coli*;*J. Bioenerg. Biomembr.* **1998**, *30*, 55.
(79) Gennis, R.; Ferguson-Miller, S. Structure of Cytochrome c Oxidase, Energy Generator of Aerobic Life;*Science* **1995**, *269*, 1063.
(80) Tolman, W. B. Editorial for the Virtual Issue on Models of Metalloenzymes;*Inorg. Chem.* **2013**, *52*, 7307.

(81) Silakov, A.; Olsen, M. T.; Sproules, S.; Reijerse, E. J.; Rauchfuss, T. B.; Lubitz, W. EPR/ENDOR, Mössbauer, and Quantum-Chemical Investigations of Diiron Complexes Mimicking the Active Oxidized State of [FeFe]Hydrogenase;*Inorg. Chem.* **2012**, *51*, 8617.
(82) Wilson, S. A.; Kroll, T.; Decreau, R. A.; Hocking, R. K.; Lundberg, M.; Hedman, B.; Hodgson, K. O.; Solomon, E. I. Iron L-Edge X-ray Absorption Spectroscopy of Oxy-Picket Fence Porphyrin: Experimental Insight into Fe–O2 Bonding;*J. Am. Chem. Soc.* **2013**, *135*, 1124.
(83) Okamura, T.-a.; Ushijima, Y.; Omi, Y.; Onitsuka, K. Systematic Investigation of Relationship between Strength of NH···S Hydrogen Bond and Reactivity of Molybdoenzyme Models;*Inorg. Chem.* **2013**, *52*, 381.
(84) Lee, S. C.; Holm, R. H. Synthesis and characterization of an asymmetric bridged assembly containing the unsupported [Fe^{III}-O-Cu^{II}] bridge: an analog of the binuclear site in oxidized cytochrome *c* oxidase;*J. Am. Chem. Soc.* **1993**, *115*, 11789.
(85) Lee, M.; Saijoh, K.; Kobayshi, T.; Fujii, M.; Fukunaga, T.; Sumino, K. Gene regulation of metalloproteins under exposure of heavy metals;*Proc.ICMR Semin.* **1994**, 115.
(86) Baeg, J.-O. Covalently supported porphyrins as ligands for the preparation of heme a_3/Cu_B binuclear active site analogues of heme–copper terminal oxidases and metallation under mild conditions;*Chem. Commun.* **1998**, 571.
(87) Holm, R. H. Chemical approaches to bridged biological metal assemblies;*Pure Appl.Chem.* **1995**, *67*, 217.
(88) Collman, J. P.; Fu, L. Synthetic Models for Hemoglobin and Myoglobin;*Acc.Chem.Res.* **1999**, *32*, 455.
(89) Ozaki, S.; Hara, I.; Matsui, T.; Watanabe, Y. Molecular engineering of myoglobin: The improvement of oxidation activity by replacing Phe-43 with tryptophan;*Biochemistry* **2001**, *40*, 1044.
(90) Collman, J. P.; Eberspacher, T.; Fu, L.; Herrmann, P. C. Functional models for the oxygen binding/activating hemeproteins, myoglobin and cytochrome c oxidase;*J.Mol.Catal.A: Chem.* **1997**, *117*, 9.
(91) Collman, J. P.; Fu, L.; Herrmann, P. C.; Zhang, X. A functional model related to cytochrome *c* oxidase and its electrocatalytic four-electron reduction of O_2;*Science* **1997**, *275*, 949.
(92) Collman, J. P.; Wang, Z. Synthetic heme chemistry: the cradle of functional molecules and catalysts;*Chemtracts* **1999**, *12*, 229.
(93) Collman, J. P.; Rapta, M.; Broering, M.; Raptova, L.; Schwenninger, R.; Boitrel, B.; Fu, L.; L'Her, M. Close Structural Analogs of the Cytochrome c Oxidase Fea3/CuB Center Show Clean 4e- Electroreduction of O2 to H2O at Physiological pH;*J.Am.Chem.Soc.* **1999**, *121*, 1387.
(94) Collman, J. P.; Boulatov, R.; Sunderland, C. J.; Fu, L. Functional analogues of cytochrome *c* oxidase, myoglobin, and hemoglobin;*Chem. Rev.* **2004**, *104*, 561.
(95) Collman, J. P.; Boulatov, R.; Sunderland, C. J. In *The porphyrin handbook*; Kadish, K. M., Smith, K. M., Guilard, R., Eds.; Academic press: San Diego, 2003; Vol. 11, p 1.
(96) Collman, J. P.; Shiryaeva, I. M.; Boulatov, R. Effect of Electron Availability on Selectivity of O2 Reduction by Synthetic Monometallic Fe Porphyrins;*Inorg. Chem.* **2003**, *42*, 4807.
(97) Collman, J. P.; Boulatov, R. Electrocatalytic O_2 reduction by synthetic analogues of the heme/Cu site of cytochrome oxidase incorporated in a lipid film;*Angew. Chem. Int. Ed.* **2002**, *41*, 3487.
(98) Collman, J. P.; Rapta, M.; Broering, M.; Raptova, L.; Schwenninger, R.; Boitrel, B.; Fu, L.; L'Her, M. Close structural analogs of the cytochrome *c* oxidase Fe-a_3/Cu_B center show clean 4e^- electroreduction of O_2 to H_2O at physiological pH;*J. Am. Chem. Soc.* **1999**, *121*, 1387.
(99) Collman, J. P.; Decreau, R. A.; Zhang, C. Synthesis of cytochrome *c* oxidase models bearing a Tyr244 mimic;*J. Org. Chem.* **2004**, *69*, 3546.
(100) Collman, J. P.; Yang, Y.; Dey, A.; Decreau, R. A.; Ghosh, S.; Ohta, T.; Solomon, E. I. A functional nitric oxide reductase model.;*Proc. Natl. Acad. Sci. U S A* **2008**, *105*, 15660.
(101) Collman, J. P.; Dey, A.; Barile, C. J.; Ghosh, S.; Decreau, R. A. Inhibition of Electrocatalytic O2 Reduction of Functional CcO Models by Competitive, Non-Competitive, and Mixed Inhibitors;*Section Title: Enzymes*, ACS ASAP.
(102) Nanthakumar, A.; Nasir, M. S.; Karlin, K. D.; Ravi, N.; Huynh Boi, H. A cytochrome *c* oxidase reactivity model: generation of a peroxo-bridged iron/copper dinuclear complex;*J. Am. Chem. Soc.* **1992**, *114*, 6564.
(103) Nanthakumar, A.; Fox, S.; Murthy, N. N.; Karlin, K. D.; Ravi, N.; Huynh, B. H.; Orosz, R. D.; Day, E. P.; Hagen, K. S.; Blackburn, N. J. Oxo- and hydroxo-bridged (porphyrin)iron(III)-copper(II) species as cytochrome c oxidase models: acid-base interconversions and x-ray structure of the Fe(III)-(O2-)-Cu(II) complex;*J.Am.Chem.Soc.* **1993**, *115*, 8513.
(104) Karlin, K. D.; Nanthakumar, A.; Fox, S.; Murthy, N. N.; Ravi, N.; Huynh, B. H.; Orosz, R. D.; Day, E. P. X-ray structure and physical properties of the oxo-bridged complex [(F_8-TPP)Fe-O-Cu(TMPA)]$^+$, F_8-TPP = Tetrakis(2,6-difluorophenyl)porphyrinate(2-), TMPA = Tris(2-pyridylmethyl)amine: Modeling the cytochrome *c* oxidase Fe-Cu heterodinuclear active site;*J. Am. Chem. Soc.* **1994**, *116*, 4753.
(105) Karlin, K. D.; Fox, S.; Nanthakumar, A.; Murthy, N. N.; Wei, N.; Obias, H. V.; Martens, C. F. Copper-dioxygen chemistry and modeling the Fe-Cu center in cytochrome c oxidase;*Pure Appl.Chem.* **1995**, *67*, 289.
(106) Nanthakumar, A.; Fox, S.; Murthy, N. N.; Karlin, K. D. Inferences from the ^{1}H-NMR spectroscopic study of an antiferromagnetically coupled heterobinuclear Fe(III)−(X)−Cu(II) S=2 spin system (X = O^{2-}, OH^-);*J. Am. Chem. Soc.* **1997**, *119*, 3898.
(107) Kopf, M.-A.; Karlin, K. D. Dioxygen Reactivity of Reduced Heme and Heme-Copper Complexes Utilizing Tetraarylporphyrinates Tethered with Both a Pyridyl Axial Ligand and N,N-Bis[2-(2-pyridyl)ethyl]amine Chelate;*Inorg.Chem.* **1999**, *38*, 4922.

(108) Kopf, M.-A.; Neuhold, Y.-M.; Zuberbuehler, A. D.; Karlin, K. D. Oxo- and Hydroxo-Bridged Heme-Copper Assemblies Formed from Acid-Base or Metal-Dioxygen Chemistry;*Inorg.Chem.* **1999**, *38*, 3093.
(109) Ghiladi, R. A.; Ju, T. D.; Lee, D.-H.; Moeenne-Loccoz, P.; Kaderli, S.; Neuhold, Y.-M.; Zuberbuehler, A. D.; Woods, A. S.; Cotter, R. J.; Karlin, K. D. Formation and Characterization of a High-Spin Heme-Copper Dioxygen (Peroxo) Complex;*J.Am.Chem.Soc.* **1999**, *121*, 9885.
(110) Kim, E.; Helton, M. E.; Wasser, I. M.; Karlin, K. D.; Lu, S.; Huang, H.-w.; Moënne-Loccoz, P.; Incarvito, C. D.; Rheingold, A. L.; Honecker, M.; Kaderli, S.; Zuberbühler, A. D. Superoxo, μ-peroxo, and μ-oxo complexes from heme/O_2 and heme-Cu/O_2 reactivity: Copper ligand influences in cytochrome *c* oxidase models;*Proc. Natl. Acad. Sci. U S A* **2003**, *100*, 3623.
(111) Kamaraj, K.; Kim, E.; Galliker, B.; Zakharov, L. N.; Rheingold, A. L.; Zuberbuehler, A. D.; Karlin, K. D. Copper(I) and copper(II) complexes possessing cross-linked imidazole-phenol ligands: Structures and dioxygen reactivity;*J. Am. Chem. Soc.* **2003**, *125*, 6028.
(112) Ghiladi, R. A.; Karlin, K. D. Low-Temperature UV-Visible and NMR Spectroscopic Investigations of O2 Binding to (6L)FeII, a Ferrous Heme Bearing Covalently Tethered Axial Pyridine Ligands;*Inorg. Chem.* **2002**, *41*, 2400.
(113) Ghiladi, R. A.; Hatwell, K. R.; Karlin, K. D.; Huang, H.-w.; Moeenne-Loccoz, P.; Krebs, C.; Huynh, B. H.; Marzilli, L. A.; Cotter, R. J.; Kaderli, S.; Zuberbuehler, A. D. Dioxygen Reactivity of Mononuclear Heme and Copper Components Yielding A High-Spin Heme-Peroxo-Cu Complex;*J. Am. Chem. Soc.* **2001**, *123*, 6183.
(114) Ghiladi, R. A.; Kretzer, R. M.; Guzei, I.; Rheingold, A. L.; Neuhold, Y.-M.; Hatwell, K. R.; Zuberbuehler, A. D.; Karlin, K. D. (F8TPP)FeII/O2 Reactivity Studies {F8TPP = Tetrakis(2,6-difluorophenyl)porphyrinate(2-)}: Spectroscopic (UV-Visible and NMR) and Kinetic Study of Solvent-Dependent (Fe/O2 = 1:1 or 2:1) Reversible O2-Reduction and Ferryl Formation;*Inorg. Chem.* **2001**, *40*, 5754.
(115) Kopf, M.-A.; Karlin, K. D. Models of copper enzymes and heme-copper oxidases;*Biomimetic Oxidations Catalyzed by Transition Metal Complexes* **2000**, 309.
(116) Kim, D.; Guengerich, F. P. Enhancement of 7-methoxyresorufin O-demethylation activity of human cytochrome P450 1A2 by molecular breeding;*Section Title: Enzymes* **2004**, *432*, 102.
(117) Wasser, I. M.; Huang, H.-w.; Moënne-Loccoz, P.; Karlin, K. D. Heme/non-heme diiron(II) complexes and O_2, CO, and NO adducts as reduced and substrate-bound models for the active site of bacterial nitric oxide reductase;*J. Am. Chem. Soc.* **2005**, *127*, 3310.
(118) Kim, E.; Helton, M. E.; Lu, S.; Moeenne-Loccoz, P.; Incarvito, C. D.; Rheingold, A. L.; Kaderli, S.; Zuberbuehler, A. D.; Karlin, K. D. Tridentate Copper Ligand Influences on Heme-Peroxo-Copper Formation and Properties: Reduced, Superoxo, and m-Peroxo Iron/Copper Complexes;*Inorg. Chem.* **2005**, *44*, 7014.
(119) del Río, D.; Sarangi, R.; Chufán, E. E.; Karlin, K. D.; Hedman, B.; Hodgson, K. O.; Solomon, E. I. Geometric and electronic structure of the heme−peroxo−copper complex [(F_8TPP)Fe^{III}−(O_2^{2-})−Cu^{II}>(TMPA)](ClO_4);*J. Am. Chem. Soc.* **2005**, *127*, 11969.
(120) Kim, E.; Kamaraj, K.; Galliker, B.; Rubie, N. D.; Moeenne-Loccoz, P.; Kaderli, S.; Uhler, A. D. Z.; Karlin, K. D. Dioxygen Reactivity of Copper and Heme-Copper Complexes Possessing an Imidazole-Phenol Cross-Link;*Inorg. Chem.* **2005**, *44*, 1238.
(121) Ghiladi, R. A.; Huang, H.-w.; Moenne-Loccoz, P.; Stasser, J.; Blackburn, N. J.; Woods, A. S.; Cotter, R. J.; Incarvito, C. D.; Rheingold, A. L.; Karlin, K. D. Heme-copper/dioxygen adduct formation relevant to cytochrome c oxidase: spectroscopic characterization of [(6L)FeIII-(O22-)-CuII]+;*JBIC, Journal of Biological Inorganic Chemistry* **2005**, *10*, 63.
(122) Kim, E.; Shearer, J.; Lu, S.; Moeenne-Loccoz, P.; Helton, M. E.; Kaderli, S.; Zuberbuehler, A. D.; Karlin, K. D. Heme/Cu/O2 Reactivity: Change in FeIII-(O22-)-CuII Unit Peroxo Binding Geometry Effected by Tridentate Copper Chelation;*J. Am. Chem. Soc.* **2004**, *126*, 12716.
(123) Serr, B. R.; Headford, C. E. L.; Anderson, O. P.; Elliott, C. M.; Spartalian, K.; Fainzilberg, V. E.; Hatfield, W. E.; Rohrs, B. R.; Eaton, S. S.; Eaton, G. R. Cytochrome c oxidase models: a dinuclear iron(III) porphyrin-copper(II) complex with a sulfur bridge;*Inorg.Chem.* **1992**, *31*, 5450.
(124) Casella, L.; Monzani, E.; Gullotti, M.; Gliubich, F.; De Gioia, L. Cytochrome c oxidase models: synthesis and reactivity of iron(III)-copper(II) complexes of deuterohemin-polybenzimidazole dinucleating ligands;*J.Chem.Soc., Dalton Trans.* **1994**, 3203.
(125) Franceschi, F.; Gullotti, M.; Monzani, E.; Casella, L.; Papaefthymiou, V. Cytochrome c oxidase models. A novel dinuclear iron-copper complex derived from a covalently modified deuteroporphyrin-L-histidine-bis(benzimidazole) ligand;*Chem.Commun.* **1996**, 1645.
(126) Monzani, E.; Casella, L.; Gullotti, M.; Panigada, N.; Franceschi, F.; Papaefthymiou, V. Cytochrome c oxidase models. Dinuclear iron/copper complexes derived from covalently modified deuteroporphyrins;*J.Mol.Catal.A: Chem.* **1997**, *117*, 199.
(127) Davydov, R.; Kofman, V.; Fujii, H.; Yoshida, T.; Ikeda-Saito, M.; Hoffman, B. M. Catalytic Mechanism of Heme Oxygenase through EPR and ENDOR of Cryoreduced Oxy-Heme Oxygenase and Its Asp 140 Mutants;*J. Am. Chem. Soc.* **2002**, *124*, 1798.
(128) Crusats, J.; Suzuki, A.; Mizutani, T.; Ogoshi, H. Regioselective Porphyrin Bridge Cleavage Controlled by Electronic Effects. Coupled Oxidation of 3-Demethyl-3-(trifluoromethyl)mesohemin IX and Identification of Its Four Biliverdin Derivatives;*J.Org.Chem.* **1998**, *63*, 602.
(129) Chishiro, T.; Shimazaki, Y.; Tani, F.; Tachi, Y.; Naruta, Y.; Karasawa, S.; Hayami, S.; Maeda, Y. Isolation and crystal structure of a peroxo-bridged heme-copper complex;*Angew.Chem., Int.Ed.Engl.* **2003**, *42*, 2788.
(130) Liu, J.-G.; Naruta, Y.; Tani, F. A functional model of the cytochrome c oxidase active site: Unique conversion of a heme-m-peroxo-CuII intermediate into heme-superoxo/CuI;*Angew. Chem. Int. Ed.* **2005**, *44*, 1836.

(131) Ju, T. D.; Woods, A. S.; Cotter, R. J.; Moenne-Loccoz, P.; Karlin, K. D. Dioxygen and nitric oxide reactivity of a reduced heme/non-heme diiron(II) complex [(5L)FeII...FeII-Cl]+. Using a tethered tetraarylporphyrin for the development of an active site reactivity model for bacterial nitric oxide reductase;*Inorg. Chim. Acta* **2000**, *297*, 362.
(132) MacBeth, C. E.; Gupta, R.; Mitchell-Koch, K. R.; Young, V. G., Jr.; Lushington, G. H.; Thompson, W. H.; Hendrich, M. P.; Borovik, A. S. Utilization of hydrogen bonds to stabilize M-O(H) units: synthesis and properties of monomeric iron and manganese complexes with terminal oxo and hydroxo ligands.;*J. Am. Chem. Soc.* **2004**, *126*, 2556.
(133) Borovik, A. S. Bioinspired hydrogen bond motifs in ligand design: The role of noncovalent interactions in metal ion mediated activation of dioxygen.;*Acc. Chem. Res.* **2005**, *38*, 54.
(134) Kassner, R. J. Effects of nonpolar environments on the redox potentials of heme complexes;*Proc. Natl. Acad. Sci. U S A* **1972**, *69*, 2263.
(135) Lu, Y. Biosynthetic Inorganic Chemistry;*Angew. Chem. Int. Ed.* **2006**, *45*, 5588.
(136) Lu, Y.; Yeung, N.; Sierecki, N.; Marshall, N. M. Design of functional metalloproteins;*Nature* **2009**, 855.
(137) Marshall, N. M.; Garner, D. K.; Wilson, T. D.; Gao, Y.-G.; Robinson, H.; Nilges, M. J.; Lu, Y. Rationally tuning the reduction potential of a single cupredoxin beyond the natural range;*Nature* **2009**, *462*, 113.
(138) Fersht, A. *Enzyme structure and mechanism* New York, 1985.
(139) Hellinga, H. W.; Richards, F. M. Construction of new ligand binding sites in proteins of known structure: I. Computer-aided modeling of sites with pre-defined geometry;*J. Mol. Biol.* **1991**, *222*, 763.
(140) Hellinga, H. W. Metalloprotein design;*Curr. Opin. Biotechnol.* **1996**, *7*, 437.
(141) Clarke, N. D.; Yuan, S.-M. Metal Search: A computer program that helps design tetrahedral metal-binding sites;*Proteins: Struct., Funct., Genet.* **1995**, *23*, 256.
(142) Desjarlais, J. R.; Clarke, N. D. Computer search algorithms in protein modification and design;*Curr. Opin. Struct. Biol.* **1998**, *8*, 471.
(143) Richter, F.; Leaver-Fay, A.; Khare, S. D.; Bjelic, S.; Baker, D. De novo enzyme design using Rosetta3;*PLOS ONE* **2011**, *6*, e19230.
(144) Wang, S.; Yang, S.; An, B.; Yin, Y.; Lu, Y.; Xu, Y.; Hao, D. Molecular dynamics analysis reveals structural insights into mechanism of nicotine N-demethylation catalyzed by tobacco cytochrome p450 mono-oxygenase;*PLOS ONE* **2011**, *6*, e23342.
(145) Koga, N.; Tatsumi-Koga, R.; Liu, G.; Xiao, R.; Acton, T. B.; Montelione, G. T.; Baker, D. Principles for designing ideal protein structures;*Nature* **2012**, *491*, 222.
(146) Robertson, D. E.; Farid, R. S.; Moser, C. C.; Urbauer, J. L.; Mulholland, S. E.; Pidikiti, R.; Lear, J. D.; Wand, A. J.; DeGrado, W. F.; Dutton, P. L. Design and synthesis of multi-haem proteins;*Nature* **1994**, *368*, 425.
(147) Klemba, M.; Gardner, K. H.; Marino, S.; Clarke, N. D.; Regan, L. Novel metal-binding proteins by design;*Nat. Struct. Biol.* **1995**, *2*, 368.
(148) Hecht, M. H.; West, M. W.; Roy, S.; Rojas, N. R.; Kamtekar, S.; McLean, J.; Helmer, K. J.; Simons, C. T.; Beasley, J. R. Design of libraries of de novo proteins by binary patterning of polar and nonpolar amino acids;*Protein Eng.* **1997**, *10*, 20.
(149) Huang, P. S.; Love, J. J.; Mayo, S. L. A de novo designed protein protein interface;*Protein Sci.* **2007**, *16*, 2770.
(150) Murphy, P. M.; Bolduc, J. M.; Gallaher, J. L.; Stoddard, B. L.; Baker, D. Alteration of enzyme specificity by computational loop remodeling and design;*Proceedings of the National Academy of Sciences* **2009**.
(151) Yarov-Yarovoy, V.; DeCaen, P. G.; Westenbroek, R. E.; Pan, C.-Y.; Scheuer, T.; Baker, D.; Catterall, W. A. Structural basis for gating charge movement in the voltage sensor of a sodium channel;*Proceedings of the National Academy of Sciences* **2011**.
(152) Wargacki, A. J.; Leonard, E.; Win, M. N.; Regitsky, D. D.; Santos, C. N. S.; Kim, P. B.; Cooper, S. R.; Raisner, R. M.; Herman, A.; Sivitz, A. B.; Lakshmanaswamy, A.; Kashiyama, Y.; Baker, D.; Yoshikuni, Y. An Engineered Microbial Platform for Direct Biofuel Production from Brown Macroalgae;*Science* **2012**, *335*, 308.
(153) Whitehead, T. A.; Chevalier, A.; Song, Y.; Dreyfus, C.; Fleishman, S. J.; De Mattos, C.; Myers, C. A.; Kamisetty, H.; Blair, P.; Wilson, I. A.; Baker, D. Optimization of affinity, specificity and function of designed influenza inhibitors using deep sequencing;*nature biotechnol* **2012**, 1546.
(154) Privett, H. K.; Kiss, G.; Lee, T. M.; Blomberg, R.; Chica, R. A.; Thomas, L. M.; Hilvert, D.; Houk, K. N.; Mayo, S. L. Iterative approach to computational enzyme design;*Proceedings of the National Academy of Sciences* **2012**, *109*, 3790.
(155) Muir, T. W.; Sondhi, D.; Cole, P. A. Expressed protein ligation: A general method for protein engineering;*Proc. Natl. Acad. Sci. U S A* **1998**, *95*, 6705.
(156) Xie, J.; Schultz, P. G. Adding amino acids to the genetic repertoire;*Biopolymers / Model systems* **2005**, *9*, 548.
(157) Dieckmann, G. R.; McRorie, D. K.; Tierney, D. L.; Utschig, L. M.; Singer, C. P.; O'Halloran, T. V.; Penner-Hahn, J. E.; DeGrado, W. F.; Pecoraro, V. L. De Novo design of mercury-binding two- and three-helical bundles;*J. Am. Chem. Soc.* **1997**, *119*, 6195.
(158) Klemba, M. W.; Munson, M.; Regan, L. De novo design of protein structure and function;*Proteins* **1998**, 313.
(159) DeGrado, W. F.; Summa, C. M. De Novo design and structural characterizationof proteins and metalloproteins;*Annu.Rev.Biochem.* **1999**, *68*, 77.
(160) Choi, S.; Isaacs, A.; Clements, D.; Liu, D.; Kim, H.; Scott, R. W.; Winkler, J. D.; DeGrado, W. F. De novo design and in vivo activity of conformationally restrained antimicrobial arylamide foldamers;*Proceedings of the National Academy of Sciences* **2009**, *106*, 6968.
(161) Zastrow, M. L.; Peacock, A. F. A.; Stuckey, J. A.; Pecoraro, V. L. Hydrolytic catalysis and structural stabilization in a designed metalloprotein;*Nature Chem* **2012**, *4*, 118.

(162) Yeung, N.; Lin, Y.-W.; Gao, Y.-G.; Zhao, X.; Russell, B. S.; Lei, L.; Miner, K. D.; Robinson, H.; Lu, Y. Rational design of a structural and functional nitric oxide reductase;*Nature* **2009**, *462*, 1079.
(163) Lin, Y. W.; Yeung, N.; Gao, Y. G.; Miner, K. D.; Tian, S.; Robinson, H.; Lu, Y. Roles of glutamates and metal ions in a rationally designed nitric oxide reductase based on myoglobin;*Proc. Natl. Acad. Sci. U S A* **2010**, *107*, 8581.
(164) Lin, Y.-W.; Yeung, N.; Gao, Y.-G.; Miner, K. D.; Lei, L.; Robinson, H.; Lu, Y. Introducing a 2-His-1-Glu nonheme iron center into myoglobin confers nitric oxide reductase activity;*J. Am. Chem. Soc.* **2010**, *132*, 9970.
(165) Degtyarenko, K. In *Encyclopedia of Genetics, Genomics, Proteomics and Bioinformatics*; John Wiley & Sons, Ltd: 2004.

CHAPTER 2

PURIFICATION AND CHARACTERIZATION OF A NOVEL CUPREDOXIN-LIKE PROTEIN FROM *NITROSOPUMILUS MURITI*

* Portions of this chapter are taken from a manuscript, not submitted yet, as "A novel purple cupredoxins from *Nitrosopumilus maritimus* displays NO oxidase activity" (Hosseinzadeh P.*, Marshall N.M.*, Tian S.*, Hemp J., Mullen T., Gao Y-G., Nilges M.J., Robinson H., Gennis R.B., Lu Y.). Marshal N.M. started the purification and initial characterizations. Tian S. performed activity assays and related figures. Dr. Hemp J. initially found the sequence and designed the expression vector without the transmembrane helix.

2.1. Introduction

Every year new classes of microorganisms[1] and species are being discovered. A recent study has estimated that 86% of all organisms on earth and 91% of species in the ocean have yet to be fully described.[2] While some of these organisms are new strains of a previously know species, some are entirely new ones with functions essential to life on earth. One such organism is *Nitrosopumilu maritimus*, discovered in a filter in the Seattle aquarium[3] and soon shown to be a major player in N_2 cycle on earth. In this chapter, after a brief introduction to N_2 cycle in general and *N. mar.* in specific, I will focus on my efforts in understanding a small putative cupredoxin from this archeon, N.mar._1307.

2.1.1. N_2 cycle

Nitrogen gas is an essential nutrient and among the most abundant molecules on the earth atmosphere composing about 78% of the total air content. Despite its abundance as a gas, this form of nitrogen cannot be absorbed by most organisms and should be converted to ammonia (NH_3) in order to be absorbed by plants and being used in building blocks of life, amino acids, (deoxy)ribonucleotides, and sugars.[4] The process of adsorbing gaseous N_2 and changing it into NH_3 is called nitrogen fixation. Nitrogen fixation is only a part of the N_2 cycle. Other parts involved in changing the ammonia back to gaseous N_2 to close the cycle. Figure 2.1 shows a schematic view of the cycle.[4]

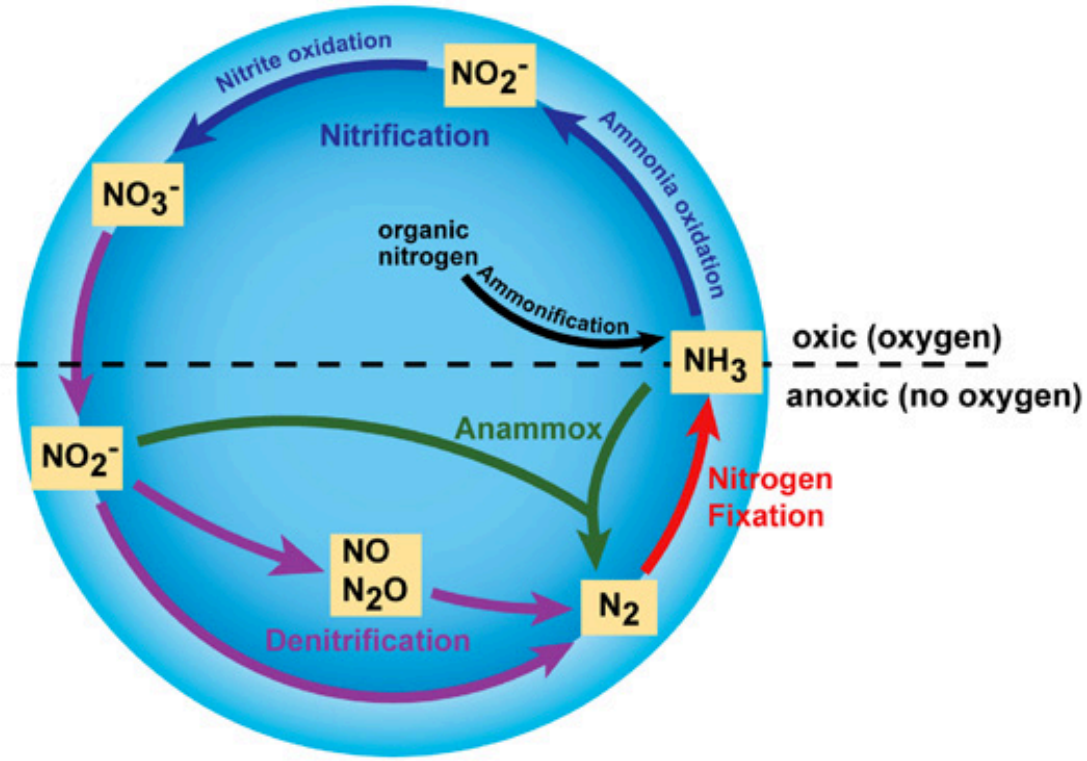

Figure 2.1. Schematic representation of N_2 cycle on earth. Figure adapted from ref. [4]

Nitrification is referred to a series of reactions in the N_2 cycle through which the NH_3 is converted to nitrite and then nitrate. Before discovery of archea, nitrification was believed to be solely carried out by bacteria.[5] Several studies focused on understanding of the nitrification process in bacteria. A summary of the results is shown below. In the first step, NH_3 is converted to the intermediate hydroxylamine (NH_2OH) by a class of enzymes called ammonia monooxygenase. This intermediate is then converted to nitrite upon the action of hydroxylamine oxidoreductase. Nitrite would then be converted to nitrate by nitrite oxidoreductase.[6,7]

1. $2\ NH_4^+ + 3\ O_2 \rightarrow 2\ NO_2^- + 2\ H_2O + 4\ H^+$ (Nitrosomonas)
2. $2\ NO_2^- + O_2 \rightarrow 2\ NO_3^-$ (Nitrobacter, Nitrospina)
3. $NH_3 + O_2 \rightarrow NO_2^- + 3H^+ + 2e^-$
4. $NO_2^- + H_2O \rightarrow NO_3^- + 2H^+ + 2e^-$

Later, several families of archaea were shown to be involved in denitrification as well,[8,9] first of which was *Thaumarchaeota.*[10] In contrast to ammonia-oxidizing bacteria (AOB), the enzymology and reaction steps in ammonia-oxidizing archaea (AOA) is less well-established. [8,9] For example, the quest for finding a putative hydroxylamine oxidoreductase in one of the most abundant of such archaea, *Nitrosopumilus maritimus,* which is suggested to be a major player in N_2 cycle in the oceans, has failed so far.

2.1.2. Nitrospumilus Maritimus

Nitrosopumilus maritimus (N. mar.) was discovered in a filter in the Seattle aquarium by ribosomal RNA sequencing.[3] This and similar strains have since been shown to exist throughout the oceans in the world.[11-27] *N. mar.* is a straight rod-shape archeaon of 0.5-0.9 mm length and 0.17-0.2 mm diameter (Figure 2.2).

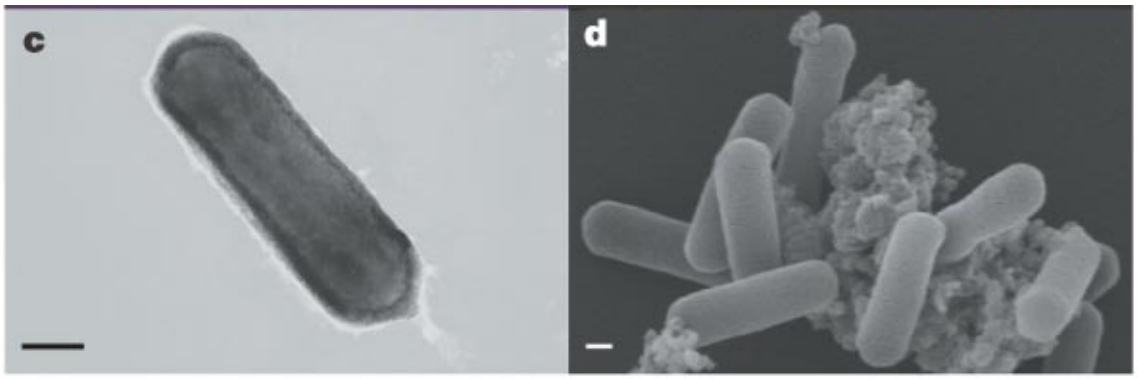

Figure 2.2. TEM (c) and SEM (d) of *N. mar.* Scale bars are 0.1 mm. Figures from ref. [3]

What is interesting about *N. mar.* is the large number of genes encoding putative copper proteins in its genome. *N. mar* is missing the genes coding for cytochromes *c*, the most ubiquitous class of electron transfer (ET) proteins and appears to have replaced these by cupredoxin-like proteins. While *N. mar* still utilizes many heme proteins for other functions, copper proteins appear to have evolved to completely take over the role of electron transfer. In some cases, functions carried out by heme proteins in every other known form of life are believed to be performed by copper proteins in *N. mar*.

N. mar has been shown to grow and oxidize ammonia even at the low ammonia concentrations found in the ocean.[3,14] Therefore, it is a major player in converting dissolved ammonia in the oceans to nitrite, a critical step in the global nitrogen cycle.[13,14,24,26]

Given the important role that *N. mar* plays in the global nitrogen cycle, and its unusual replacement of heme-based ET proteins with copper-based counterparts, isolating, purifying and characterizing some of the cupredoxin-like proteins from the *N. mar* would expand our understanding of the interplay between heme-based and copper-based biochemical processes. Furthermore, many of the smaller cupredoxin-like proteins are proposed to be involved in critical metabolic pathways in *N. mar*, including a putative mononuclear copper protein that could catalyze NO oxidation to NO_2^-.[24] Therefore it would be interesting to find out structural features responsible for such function.

2.1.3. N.mar_1307

Soon after realization of the critical role of *N. mar.* in the N_2 cycle, genomic-based studies were performed to discover enzymes with putative role in denitrification process. Along with several candidates with enzymatic activity, a putative Cu-binding protein was discovered that was highly expressed in the organism with ammonia-dependent expression. The protein, called N. mar_1307 was predicted to be anchored to membrane via a single trans-membrane helix and to have a common cupredoxin fold and $(His)_2$-Cys Cu-binding motif. Due to these structural similarities, a common ET role was predicted for the protein. Dr. James Hemp (who performed the initial studies mentioned above) then asked us to characterize this protein.

Herein, I describe the purification and characterization of N. mar_1307. Our results suggest a more interesting role for this highly expressed protein and interesting new chemistries for a type 1 Cu (T1 Cu) protein.

2.2. Materials and methods

2.2.1. Cell culture and expression of N. mar proteins

The protein coding DNA sequences of *N. mar_* 1307 was cloned into the pET-22b periplasmic expression vector (Novagen) from genomic DNA. *N. mar_* 1307 natively has an N-terminal helix that anchors the protein to the cell membrane. These membrane associated helices were omitted from the cloned sequence here in order to result in solubly expressed protein.

Rosetta strain *E. coli* (Novagen) were then transformed with the cloned sequences. This strain of *E. coli* was used because the codon usage of *N. mar* is very different from that of *E. coli*

and Rosetta cells have extra translational machinery and tRNAs to compensate for this. Transformed cells were then used to streak LB plates with 100 mg/L ampicillin. These plates were incubated at 37°C overnight to obtain single colonies. Single colonies were then used to inoculate 5 mL LB cultures with 100 μg/mL of ampicillin, which were then incubated at 37°C until an OD_{600} of 0.6-0.8 was achieved. A 2 L portion of 2xYT media was then inoculated with 1 mL of the 5 mL culture and 100 mg/L of ampicillin. The 2 L cultures were then incubated at 37°C overnight, typically reaching an OD_{600} of around 1.5 after 18 hours. In the morning, cells were induced with 100 mg/L of Isopropyl β-D-1-thiogalactopyranoside (IPTG) and allowed to express protein at 37°C for an additional 4 hours. After expressing for 4 hours, proteins were extracted *via* the osmotic shock procedure outlined below.

The volumes in the procedure outlined below were scaled based on the volume of the original culture. After harvesting the *E. coli* by centrifugation, the cells were re-suspended in 1/8 the volume of the original culture of a solution containing 20 % w/v sucrose, 50 mM tris HCl buffer at pH 8.0, and 5 mM ethylenediaminetetraacetate (EDTA). The cells were incubated in this solution at room temperature for 1 hour and re-harvested. The supernatant was discarded and the cells were re-suspended in 1/8 the volume of the original culture of a solution with 4 mM NaCl and 1 mM dithiothreitol (DTT) to lyse the periplasmic membrane. Cells were left in this solution for 10 minutes at 4°C to effectively lyse the periplamsic membrane. Solids were then removed by centrifuging and the supernantant was collected. The pH of the supernatant was then lowered to 4.0 by slowly adding a solution of 500 mM sodium acetate at pH 4.0 (1/10 the volume of the supernatant). Lowering the pH in this way caused more solids to precipitate, which were again removed by centrifuging and the supernatant was collected.

2.2.2. Column purification of N. mar_1307 and re-constitution with copper

After extracting the protein from the cells by the osmotic shock procedure above, the pH of the N. mar_1307 supernatant solution was raised to 6.0 by slow addition of aqueous NaOH. The supernatant was then applied to a FF Q-sepharose column (50 mL, GE Healthcare) equilibrated in 50 mM sodium acetate buffer at pH 6.0 by adding the beads directly to the supernatant and letting it shake on an orbital shaker at 4°C overnight. The protein was eluted from the column by a NaCl gradient on an Akta basic FPLC (GE Healthcare). The desired protein typically eluted at around 300 mM NaCl.

N. mar_1307 was then reconstituted with copper by adding a slight excess of $CuSO_4$ to the partially purified protein solution. Full incorporation took several hours to complete. It was believed that the slow incorporation of copper compared to some other cupredoxin proteins may have been due to binding of another exogenous metal in the metal binding site, but first dialyzing the protein versus an excess of EDTA to remove exogenous metal did not increase the copper incorporation rate. The increase in absorbances at 415 and 570 nm were monitored to estimate copper incorporation. Full copper incorporation was assumed to be the point at which no further increase in the visible absorbances was seen upon addition of more copper. Copper incorporated protein was then separated from non-copper bound protein and other contaminants by re-applying the protein to a Q-sepharose column and re-eluting it with a NaCl gradient. The purity of the final protein solution was assessed with SDS-Page and electrospray ionization mass spectrometry (ESI-MS).

2.2.3. Electrochemical characterization of N. mar_1307

The reduction potential of the copper site in N. mar*_1307* was measured by a modified protein film voltammetry (PFV) techniques reported previously.[28,29] Pyrolitic graphite edge electrodes (PGEs) were modified with a layer of multi-wall carbon nanotubes (1 mg/ml in DMF, sonicated for 4 hours to homogeneity) overnight. 10 mM 1-pyrene butyric acid in DMF was added to electrode. After 1 hour, the electrode was rinsed and a mixture of freshly prepared 1-ethyl-3-(3-dimethyl aminopropyl carbodimide (0.4 M) and N0hydroxy sulfosuccinamide (0.1 M) was added for 20 min. the electrode was rinsed and a solution of 1 mM protein reconstituted at pH 4 was added to the electrode and incubated for 45 min. The CV values were recorded at scan rates from 0.01 to 1 V/s in 50 mM Tris buffer pH 8 with 200 mM NaCl.

2.2.4. Spectroscopic characterization of N. mar_1307

ESI-MS was collected on a Waters Quattro II Tandem Quadrupole/Hexapole/Quadrupole instrument by adding formic acid to samples to ionize. UV-visible spectra of N. mar_1307 were collected on a Carey 5E (Varian) in temperature independent (TIP) pH 7.0 buffer. For pH studies of the UV-visible absorbances, the protein was exchanged into mixed buffer consisting of 50 mM sodium phosphate, 50 mM sodium acetate, 40 mM MES, 40 mM MOPS, 40 mM CAPS and 100 mM NaCl at the various pH values. The protein was brought to each pH by exchanging it

into the proper buffer with a PD-10 size exclusion column (GE Healthcare). EPR spectra were taken at 30 K in TIP 7, or UB at different pH (4, 7 or 9) buffer as a glass with 20% glycerol. Spectra were collected on a Varian 122 spectrometer with an Air Products Helitran cryostat.

2.2.5. Crystallization of N. mar_1307

Crystals of N. mar_1307 were grown by the hanging drop vapor diffusion method. Protein solution was prepared in 50 mM sodium acetate buffer at pH 6.0 to a concentration of about 2 mM. A 2 μL portion of this protein solution was then mixed with 2 μL of a well buffer solution consisting of 0.1 M TrisHCl at pH 8.0, 20mM $CuSO_4$, 0.1M $LiNO_3$ and varying amounts of polyethylene glycol (PEG). The highest quality crystals formed from wells with 35 % w/v PEG 4000 after about 2 months at 4°C.

2.2.6. Activity tests

Cu(II) Loaded N.mar_1307 protein solution in 50 mM BisTris pH7.0 buffer was degassed in a Schlenk line and transferred to an anaerobic chamber (Coy Laboratories). Five molar equivalents of NONOate solution (from a 50 mM stock solution) was added to 2000 μl of 150 μM Cu(II)-N. mar_1307 solution in 50 mM BisTris pH7.0 buffer. The UV-vis spectra were monitored by an Agilent 8453 photodiode array spectrometer located inside the chamber. The extinction coefficient at 560 nm (ε_{560nm} = 906 $M^{-1}cm^{-1}$) was used to calculate the concentration of Cu(II)-N.mar_1307 solution. The concentration of Proli NONOate (Cayman Chemical, MI) was determined using ε_{252nm} = 8400 $M^{-1}cm^{-1}$.

EPR spectra were collected at 30 K on an X-band Varian E-122 spectrometer at the Illinois EPR Research Center equipped with an Air Products Helitran Cryostat and EIP frequency counter. The EPR samples were prepared same as described above except 2.0 mM protein concentration was used for better resolution. Glycerol was added to a final 20% v/v and the solution was quickly frozen in liquid nitrogen.

2.2.7. Griess assay

The Griess reagent kit for nitrite quantitation containing *N*-(1-naphthyl)ethylenediamine dihydrochloride, sulfanilic acid and nitrite standard solution was purchased from Life technologies and stored refrigerated at 4 ^{o}C, protected from light. Sodium nitrite solutions with

concentrations between 1-100 μM were prepared by diluting the nitrite standard solution with Millipore water. Equal volumes of *N*-(1-naphthyl)ethlyenediamine and sulfanilic acid was mixed to form the Griess reagent. A mixture of 10 μL of Griess reagent, 30 μL of the nitrite-containing sample and 260 μL of Millipore waterwas incubated for 30 minutes at room temperature. To obtain the standard curve, concentration of nitrite was plotted against absorbance of the mixture at 548 nm, measured relative to the reference sample containing 10 μL Griess reagent and 290 μL Millipore water.

To investigate whether the protein produces nitrite, Cu(II)-N.mar_1307 was mixed with 5 molar equivalents of Proli NONOate solution in 100 mM Tris pH8.0 according to the procedure described above. After the solution turned colorless, 30 μL of the solution was mixed with 10 μL of Griess reagent and 260 μL of Millipore water. In the meanwhile, a solution of only Proli NONOate in 100 mM Tris pH8.0 was used as a control which was also incubated with Griess reagent at room temperature for 30 min. Measure the absorbance at 548 nm and read nitrite concentrations corresponding to the absorbance of experimental samples from the standard plot.

2.2.8. Protein oligomerization analysis

4-20% pre-cast SDS gels from BioRad was used for gel analysis. The protein was loaded on the gel either before or after crosslinking with gluteraldehyde. Gluteraldehyde crosslinking protocol was adapted from previous reports.[30] In brief, 2.3% gluteraldehyde was added to protein in different concentrations and the reaction proceeded for 5 min at room temperature. The protein was then mixed with blue stain and run for one hour at 120 V. Native gels were prepared using the protocol previously used in our lab.[31]

Gel chromatography was performed on a 50 ml sephadex size exclusion column. The standard was from life technologies, catalog number LC0725. Buffer was 50 mM sodium acetate, pH 6.3.

2.3. Results and discussion

2.3.1. Expression of N. mar proteins

An inspection of the amino acid sequence of the N. mar_1307 suggests that it contains an N-terminal transmembrane helix (Figure 2.3). N. Mar_1307 was cloned without this anchor to obtain the soluble copper-containing domain.

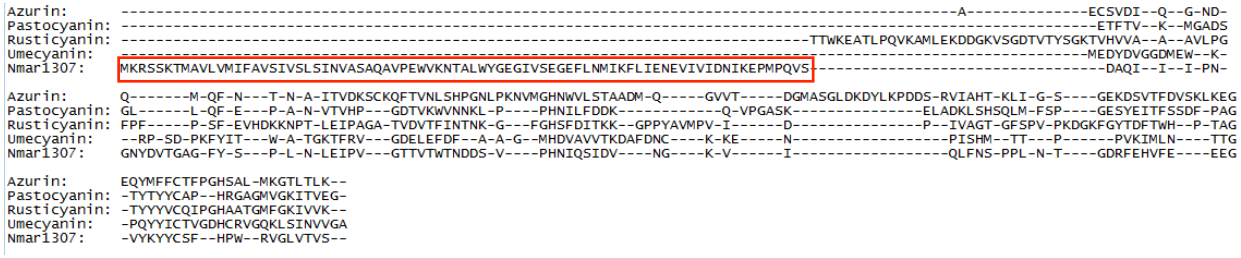

Figure 2.3. Structure-based sequence alignment of Nmar 1307 and a number of other cupredoxins proteins. The initial sequence shown in a red box is the membrane part that we excluded to express the protein in a soluble form.

The protein was expressed in *E. coli* and purified by using two consecutive ion exchange chromatographic steps (Figure 2.4).

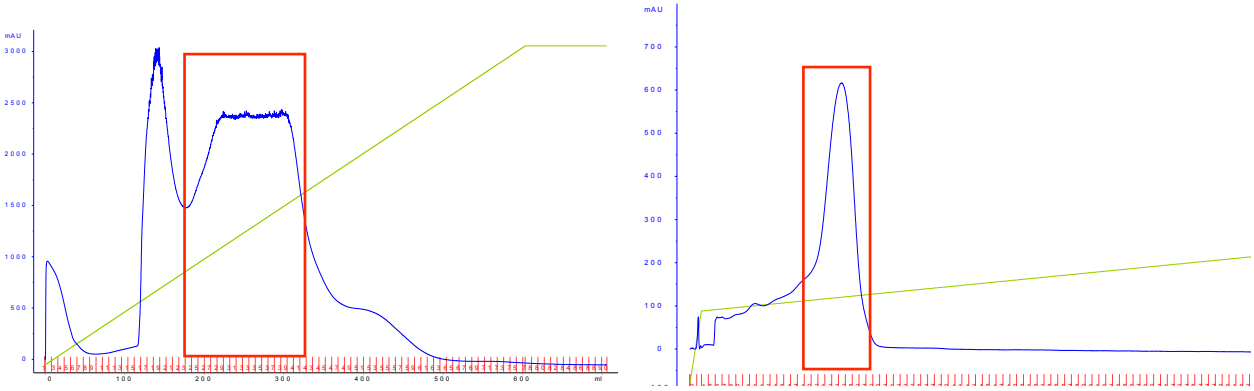

Figure 2.4. (a) FPLC trace of metal free Nmar-1307. The blue line indicates absorption at 280 and the green line represents the concentration of buffers. Collected fractions are shown in red box. After metal reconstitution, the holo-protein is loaded into a second Q FF column. The trace is shown in (b).

An electrospray ionization mass spectrometry (ESI) of the purified protein showed a peak with a mass of 10,746±1 Da (see Figure 2.5), which is within the experimental error of the calculated mass of apo-N.mar_1307 (10,747 Da). No other major peak was observed in the mass range, indicating that the N. Mar_1307 was successfully expressed and purified in its copper-free apo form.

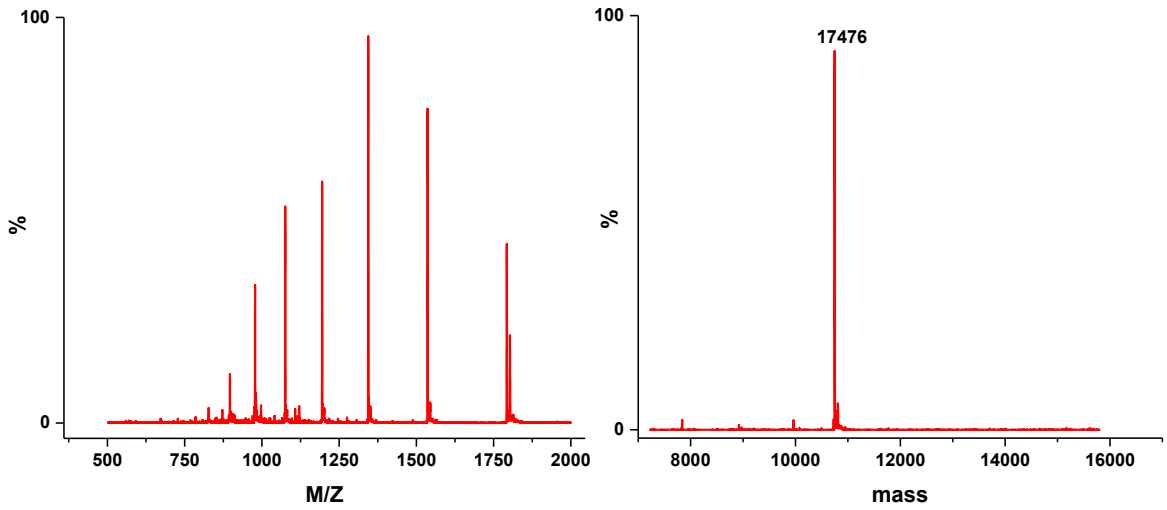

Figure 2.5. Representative ESI-MS of N. mar_1307.

Addition of Cu(II) to the apo-N. Mar_1307 converted the colorless protein to one with a purple color. After column purification protein was shown to be > 95 % pure based on SDS-PAGE (Figure 2.6).

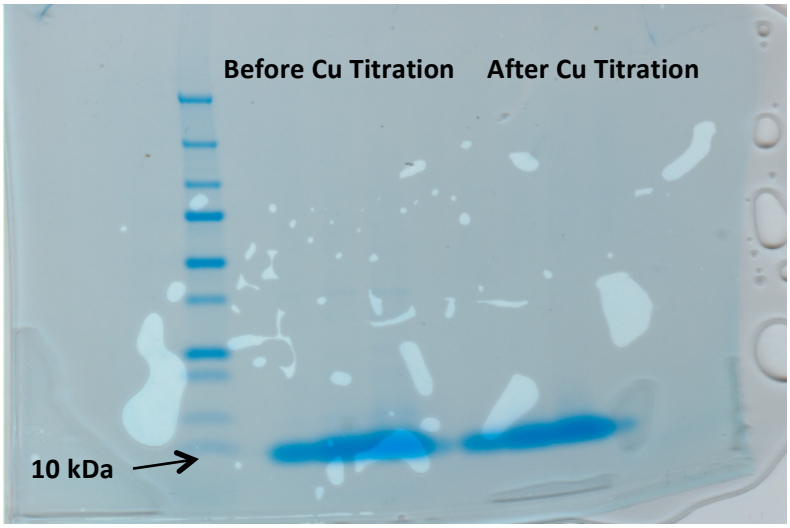

Figure 2.6. SDS-PAGE gel of column purified *N. mar*_1307 both before and after copper incorporation.

The UV-visible spectroscopy of the resulting protein (Figure 2.7) is strongly dependent on the pH at which the Cu titration occurs. with peaks at 412 nm and 560 nm with extinction coefficients at pH 4 of 732 ±6 $M^{-1}cm^{-1}$ and 906 ±8 $M^{-1}cm^{-1}$, respectively.

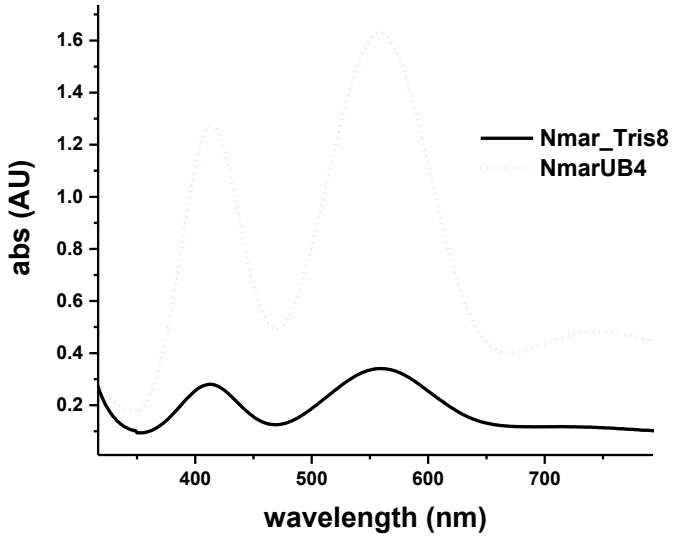

Figure 2.7. Titration of Cu(II) at two different pH results in different intensities of observed peaks. The protein concentration is the same in two samples.

SDS-PAGE analysis of protein crosslinked with gluteraldehyde as well as gel filtration analysis showed that the protein is in a dimer state in solution and this dimer state can be formed by heating the protein in the presence of stain (Figure 2.8). Interestingly, even without crosslinking, the protein forms a covalent dimer upon addition of dye and hearting in the holo state.

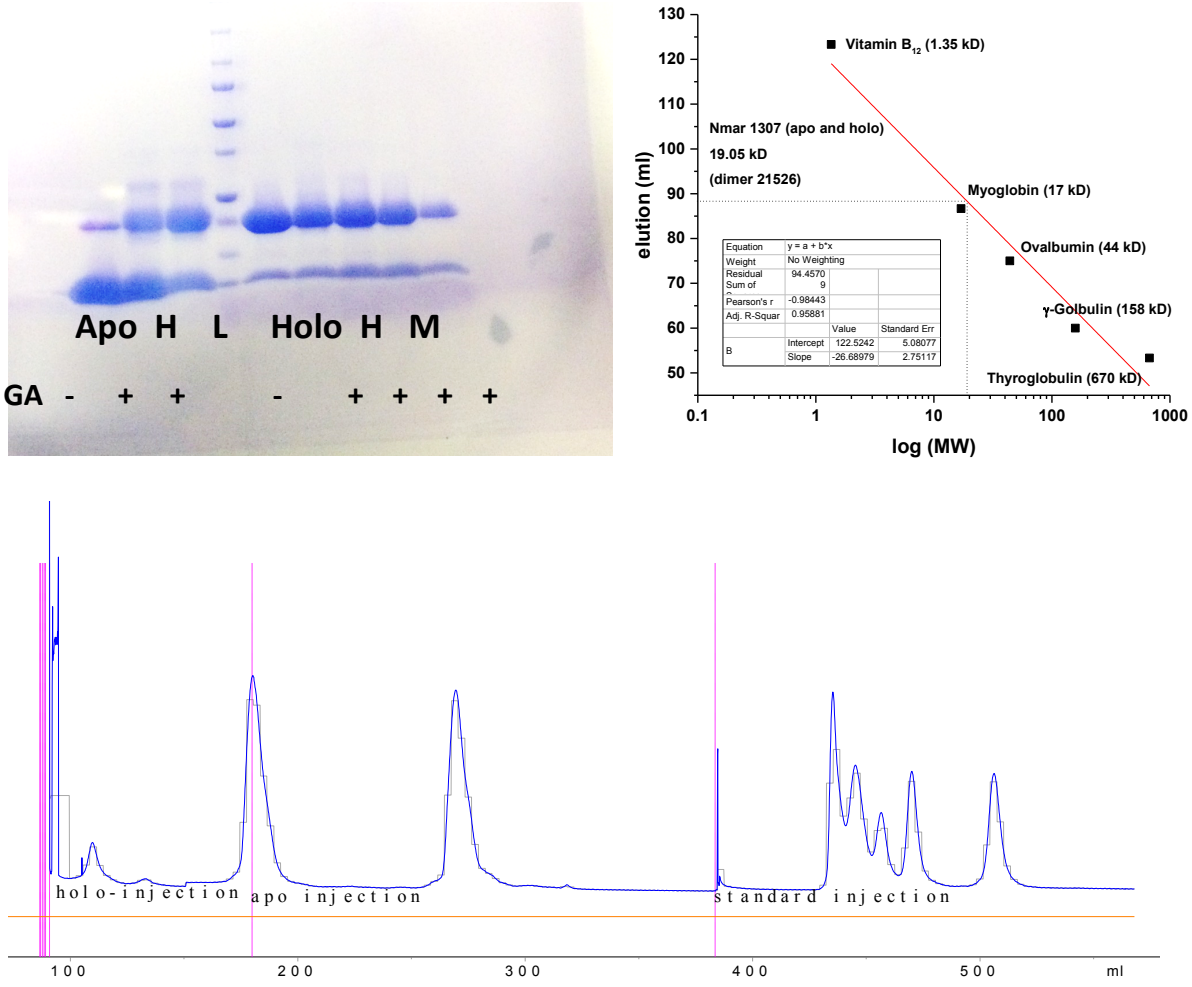

Figure 2.8. Gel filteration and SDS-PAGE analysis of the protein suggests a dimeric state in the solution.

2.3.2. Electron Paramagnetic Resonance spectroscopy

The EPR spectrum, shown in Figure 2.9, is also highly pH-dependent. Below pH 5, the spectrum is similar to that of a typical T1, blue cupredoxins (see table 2.1).[32] At pH > 5 and is most similar to the Cys49Ala variant of the copper chaperone BSco from *B. subtilis*.[33]

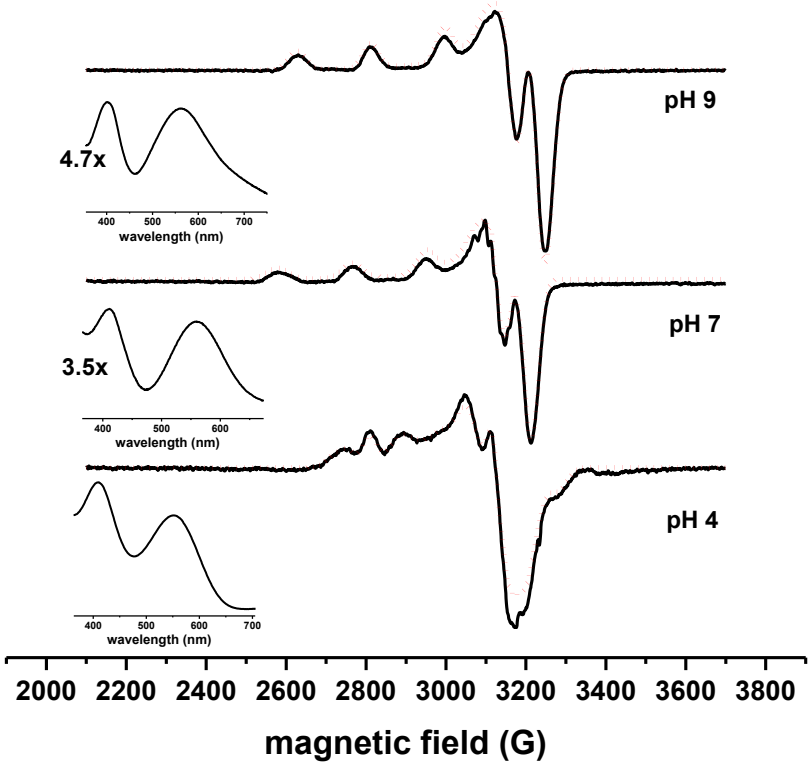

Figure 2.9. Representative UV-vis and EPR spectra of Cu(II) addition into N. mar_1307 at pH 4, 7, and 9. The red dotted lines are simulation results.

Table 2.1. Simulation parameters of EPR of different N. mar_1307 Species.

Sample	species	g_x, g_y, g_z	A_x, A_y, A_z (10^{-4} cm^{-1})
UB-9	100% one species	2.0587, 2.0391, 2.2270	17.6, 7, 191.3
UB-7	Mostly one species,	2.0633, 2.0375, 2.2351	14.3, 3.3, 194.3
	N splitting added	3, 33, 19	16, 44, 13
UB-4	51.5 % species 1	2.0330, 2.0561, 2.2741	67, 9.7, 61.3
	48.5% species 2	2.0567, 2.0493, 2.2659	47.3, 0.3, 92.7

The copper in the high-pH species was readily removed by the addition of EDTA to the solution. In contrast, EDTA did not remove the copper from the low-pH protein species (Figure 2.10) . These data suggest that the affinity of the apo-protein for Cu(II) is substantially greater for the low-pH species.

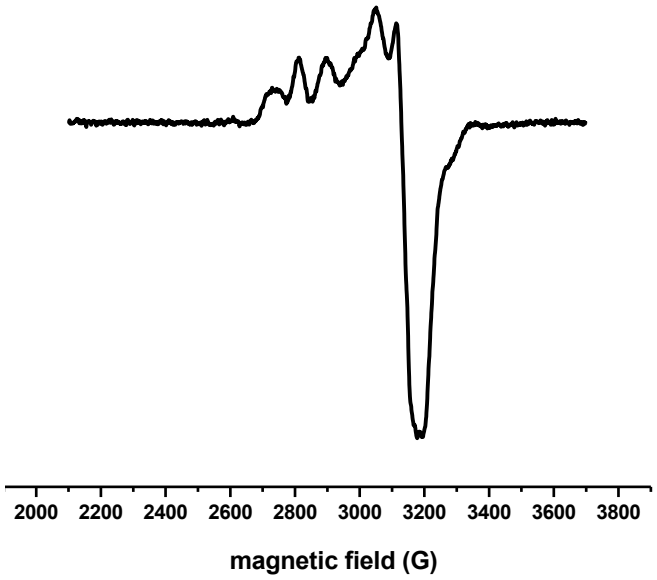

Figure 2.10. The representative EPR spectra of EDTA treated holo-N. mar_1307 at pH 7.

2.3.3. Structure of Nmar-1307

The three dimensional structure of N. mar_1307 (Figure 2.11a) was determined by X-ray crystallography. The protein crystallized with 4 molecules in the asymmetric unit, with each of the four molecules being the same except for different conformations of a few surface residues that display a high degree of freedom.

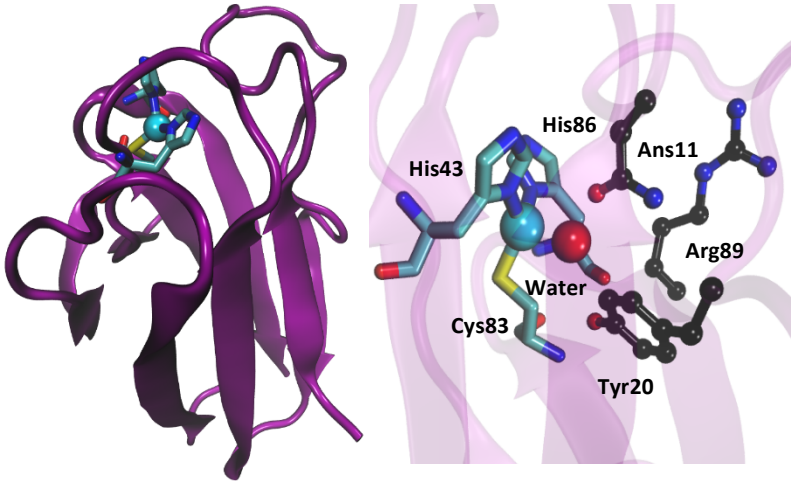

Figure 2.11. Crystal structure of *N. mar*_1307. a) Full structure with the backbone shown in ribbon representation and the primary copper ligands in stick. B) Zoom in of the copper binding site with nearby amino acids shown in ball-and-stick representation. The coordinating water is shown as a red ball.

Relevant crystallographic parameters are provided in Tables 2.2 and 2.3. The copper is coordinated to one Cys and two His in a trigonal plane (S^{γ}_{Cys83}-Cu = 2.30 Å, N^{δ}_{His43}-Cu = 1.97 Å and N^{δ}_{His86}-Cu = 1.99), which closely resemble typical values for a cupredoxin.[34] However, unlike most T1 cupredoxins that contain a Met, Leu or Gln residue in the axial position above the trigonal plane, in N. mar_1307 the site is occupied by a water ligand. Based on sequence homology with other cupredoxin proteins, the residue that is in the same position in the sequence of N. mar_1307 as the axial ligand in other cupredoxins is Arg89. The structure of N. mar_1307, however, clearly shows that Arg89 rotates away from the copper creating an open coordination site (figure 2.11b). The next closest possible copper ligands are the O^{δ} from Asn11 or the O^{η} from Tyr20. Both atoms are > 4 Å from the most likely copper position, which is much too long to consider these residues strong copper ligands. Extra electron density 2.31 Å from the T1 Cu is assigned as a water molecule within the Cu coordination sphere. This water is 2.44 Å and 3.01 Å away from potential hydrogen bonding groups of Asn11 and Tyr20, respectively. On the other side of the trigonal plane, a backbone carbonyl oxygen atom from Pro42 is located near the copper center as in other cupredoxin proteins, such as azurin, where computational work has shown that there is a strong ionic interaction between the copper and the dipole from the oxygen.[35] However, the distance between the oxygen and copper in N. mar_1307 is more than 4 Å, suggesting that any ionic contribution would be weak.

Table 2.2. Crystallogrpahic parameters from data collection of N. mar_1307 crystal.

Resolution range (Å)	45.87 - 1.6 (1.657 - 1.6)
Space group	P 41 21 2
Unit cell	68.887 68.887 184.45 90 90 90
Total reflections	
Unique reflections	59603 (5817)
Multiplicity	
Completeness (%)	99.97 (99.74)
Mean I/sigma(I)	17.74 (5.31)
Wilson B-factor	18.70

Table 2.2. cont.

Reflections used for R-free	
R-work	0.1703 (0.2032)
R-free	0.1918 (0.2411)
CC(work)	
CC(free)	
Number of non-hydrogen atoms	3609
macromolecules	3012
ligands	6
water	591
Protein residues	384
RMS(bonds)	0.006
RMS(angles)	1.07
Ramachandran favored (%)	97
Ramachandran allowed (%)	
Ramachandran outliers (%)	0
Clashscore	2.57
Average B-factor	22.90
macromolecules	20.80
ligands	24.10
solvent	33.40

Table 2.3. Relevant bond length near the Cu binding site of N. mar_1307

Atoms	Chain A (Å)	Chain B (Å)	Chain C (Å)	Chain D (Å)	Average distance (Å)
S^{γ}_{Cys83}-Cu	2.30	2.32	2.29	2.29	2.30
N^{δ}_{His43}-Cu	1.97	1.98	1.95	1.99	1.97
N^{δ}_{His86}-Cu	1.99	1.99	1.99	1.99	1.99
O_{Pro42}-Cu	4.29	4.36	4.23	4.34	4.30
O^{δ}_{Asn11}-Cu	3.98	3.93	3.96	3.89	3.94
O^{δ}_{Asn11}-O_{water}	2.49	2.40	2.46	2.43	2.44
O^{η}_{Tyr20}-Cu	4.94	4.80	4.89	4.87	4.87
O^{η}_{Tyr20}-O_{water}	3.06	2.95	2.87	3.18	3.01
O_{water}-Cu	2.28	2.30	2.44	2.22	2.31

2.3.4. Electrochemical characterization of N. mar_1307

The presence of a water ligand in the oxidized form of the protein was further confirmed by cyclic voltammetry experiments. A representative cyclic voltammogram (CV) of T1-Cu like N. mar_1307, reconstituted with Cu(II) at pH 4, is shown in Figure 2.12. A strong current response that was dependent upon protein was seen at 263±24 mV vs. Ag/AgCl (468 mV vs SHE) upon voltage sweep in 50 mM TrisHCl, pH 8.0 The unusually big separation between the oxidative and reductive peak in the CV spectra also suggests a high reorganization energy associated with redox process which can be contributed to the loss of water in the reduced state. The same water coordination and loss thereof have been observed previously in nitrosocyanin.[36] CV of EDTA titrated sample gave very similar results (figure 2.12)

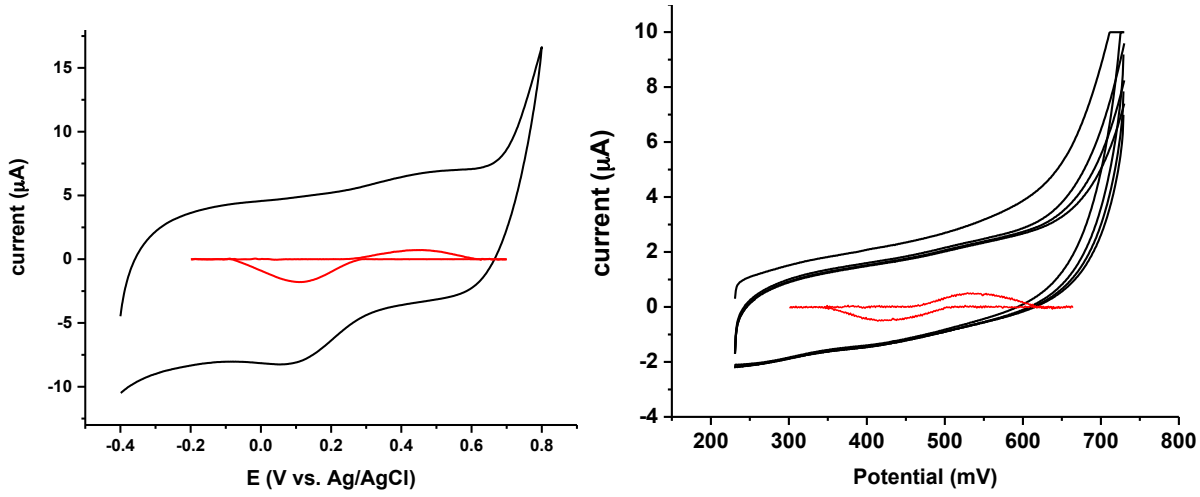

Figure 2.12. CV of N. mar_1307 on modified PGE and of EDTA-treated sample on DDAB-treated PGE. (first at 10 mV/S and the later at 200 mV/s)

2.3.5. NO oxidation assay

The open coordination site and binding of a solvent molecule directly to the copper, which is probably absent in the reduced form based on CV data, suggest that this protein might be an enzyme. The ability of N. mar_1307 to oxidize NO to NO_2 was tested. Exposure of 0.15 mM of N. mar_1307 to 5 molar equivalents of NO at pH 7.0 resulted in slow bleaching of the visible absorbances, suggesting reduction of the copper site to Cu(I) and subsequent oxidation of NO to NO_2^- (Figure 2.13a).

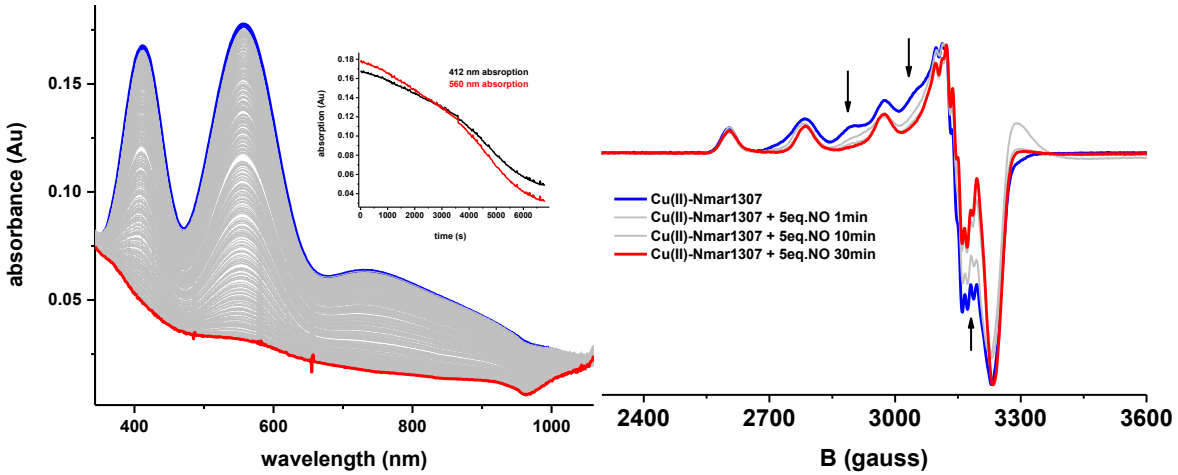

Figure 2.13. a) Time course of UV-vis spectra upon bleaching the LMCT bands of Cu(II)-N.mar1307 with 1ml NO gas in 100 mM Tris buffer pH8.0 under anaerobic condition. b) x-band EPR spectra of Cu(II)-N.mar1307 reacting with NO in 50 mM BisTris pH7.0: Cu(II)-N.mar1307 before reaction (black), 1 min after reacting with NO (red), 10 min after reacting with NO (green) and 30 min after reacting with NO (blue).

NO_2^- production was confirmed using the Griese assay (figure 2.14).[37] Monitoring the reaction through EPR showed a decrease in signal from the T1-like EPR active species, while the signal from the weakly absorbing species remained intact (Figure 2.13b). These data suggest that the purple species is the active form of the protein

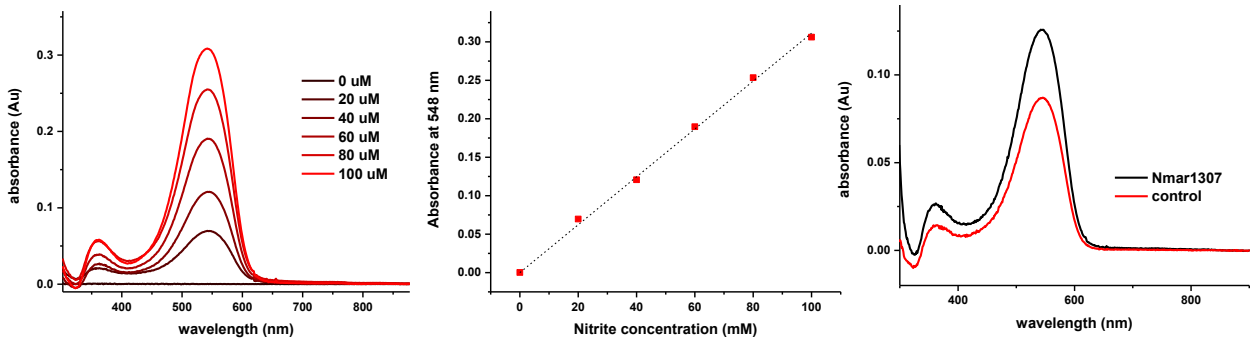

Figure 2.14. (a) , (b) show standard curve of Griese reagent for NO_2^- production. (c) Production of NO_2^- in buffer control (27.9 µM) compared with N. mar_1307 (40.2 µM) after 30 min time with starting ?? concentration of NO. The NO_2^- production is buffer is due to side reaction of NONOate.

Without a way to reoxidize the Cu, the reactivity studies were limited to a single turnover.

$$NO_{aq} + H_2O + [Cu^{2+}] \text{Ä} \quad NO_2^- + 2H^+ + [Cu^+]$$

The reaction with NO is highly pH dependent. Complete reduction of Cu(II) to Cu(I) by NO is observed only at pH > 7.0. At pH 5.0, no bleaching of the ligand-to-metal charge transfer (LMCT) bands is observed. We also observed that at pH 5.0, the reduced N. mar_1307 is oxidized by NO_2^- to result in a Cu(II) species identical to the original Cu(II) form of N. mar_1307 and presumably aqueous NO. At pH 7.0, no Cu(II) species formation was observed upon treatment of reduced N. mar_1307 with NO_2^-.

2.4. Summary and conclusion

The high midpoint potential of the Cu (468 mV) favors the oxidation of NO to nitrite under standard state conditions (E_{m7}=200mV SHE, for NO_{aq}). Acidic conditions will increase the E_{m7} by about 120 mV per pH unit below pH 8. Hence, it is consistent with the observations that at pH 8 and an excess of NO and no nitrite, the reaction will favor the 1-electron reduction of NO to nitrite. At lower pH and an excess of nitrite over NO, the reaction with the result in the reduction of the Cu in N. mar_1307.

Physiologically, *N. mar*. converts ammonia to nitrite. In Nitrosomonas europaea, this is accomplished by the ammonia monooxygenase, which generates hydroxylamine, and hydroxylamine oxidoreductase, which converts hydroxylamine to nitrite. However, no gene that can be annotated as hydroxylamine oxidoreductase is present in the genome of *N. mar.* It is possible that the pathway utilized by N. mar. differs from the canonical pathway. Possibly, NO is the produced and then oxidized to nitrite by N. mar._1307. Such production of NO has recently been observed in ammonia aoxidizing archaea.[38] However, an immediate electron acceptor remains to be identified to reoxidize N.mar_1307 and multiple turnovers demonstrated.

What is clear from the current work is that N. mar_1307 is a unique cupredoxin which has an axial water molecule that can be displaced, allowing 1-electron chemistry to a substrate. The midpoint potential of the Cu is sufficiently high at pH 8 to oxidize NO to nitrite under conditions where the ratio of NO/nitrite is sufficiently high. Other copper-containing nitrite reductases contain a type-2 copper at the active site coordinated to three His and water and the favored direction of the reaction favors the reduction of nitrite to NO due to the relatively low midpoint potential of the electron donor. In the case of N. mar_1307, the type-1 copper has a relatively

high midpoint potential and it is reasonable to assume that the electron acceptor has an even higher potential, hence shifting the direction of the catalyzed reaction to favor the formation of nitrite. Given that *N. mar.* is a significant producer of oceanic nitrite, it is important to clarify the enzymology.

2.5. References

(1) Brown, C. T.; Hug, L. A.; Thomas, B. C.; Sharon, I.; Castelle, C. J.; Singh, A.; Wilkins, M. J.; Wrighton, K. C.; Williams, K. H.; Banfield, J. F. Unusual biology across a group comprising more than 15% of domain Bacteria;*Nature* **2015**, *523*, 208.

(2) Mora, C.; Tittensor, D. P.; Adl, S.; Simpson, A. G. B.; Worm, B. How Many Species Are There on Earth and in the Ocean?;*PLoS Biol.* **2011**, *9*, e1001127.

(3) Könneke, M.; Bernhard, A. E.; de, l. T. J. R.; Walker, C. B.; Waterbury, J. B.; Stahl, D. A. Isolation of an autotrophic ammonia-oxidizing marine archaeon;*Nature* **2005**, *437*, 543.

(4) Bernhard, A. The Nitrogen Cycle: Processes, Players, and Human Impact;*Nature Education Knowledge* **2010**, *3*, 25.

(5) Thamdrup, B. New Pathways and Processes in the Global Nitrogen Cycle;*Annual Review of Ecology, Evolution, and Systematics* **2012**, *43*, 407.

(6) Prosser, J. I. Autotrophic nitrification in bacteria;*Adv. Microb. Physiol.* **1989**, *30*, 125.

(7) Ward, B. B. Nitrification and Denitrification: Probing the Nitrogen Cycle in Aquatic Environments;*Microb. Ecol.* **1996**, *32*, 247.

(8) Wuchter, C.; Abbas, B.; Coolen, M. J.; Herfort, L.; van Bleijswijk, J.; Timmers, P.; Strous, M.; Teira, E.; Herndl, G. J.; Middelburg, J. J.; Schouten, S.; Sinninghe Damste, J. S. Archaeal nitrification in the ocean;*Proc. Natl. Acad. Sci. U. S. A.* **2006**, *103*, 12317.

(9) Hatzenpichler, R. Diversity, physiology, and niche differentiation of ammonia-oxidizing archaea;*Appl. Environ. Microbiol.* **2012**, *78*, 7501.

(10) Pester, M.; Schleper, C.; Wagner, M. The Thaumarchaeota: an emerging view of their phylogeny and ecophysiology;*Curr. Opin. Microbiol.* **2011**, *14*, 300.

(11) Foesel, B. U.; Gieseke, A.; Schwermer, C.; Stief, P.; Koch, L.; Cytryn, E.; de, l. T. J. R.; van, R. J.; Minz, D.; Drake, H. L.; Schramm, A. Nitrosomonas Nm143-like ammonia oxidizers and Nitrospira marina-like nitrite oxidizers dominate the nitrifier community in a marine aquaculture biofilm;*FEMS Microbiol. Ecol.* **2008**, *63*, 192.

(12) Ingalls, A. E.; Shah, S. R.; Hansman, R. L.; Aluwihare, L. I.; Santos, G. M.; Druffel, E. R. M.; Pearson, A. Quantifying archaeal community autotrophy in the mesopelagic ocean using natural radiocarbon;*Proceedings of the National Acadamy of Sciences* **2006**, *103*, 6442.

(13) Labrenz, M.; Sintes, E.; Toetzke, F.; Zumsteg, A.; Herndl, G. J.; Seidler, M.; Jurgens, K. Relevance of a crenarchaeotal subcluster related to Candidatus Nitrosopumilus maritimus to ammonia oxidation in the suboxic zone of the central Baltic Sea;*ISME Journal* **2010**, *4*, 1496.

(14) Martens-Habbena, W.; Berube, P. M.; Urakawa, H.; de, l. T. J. R.; Stahl, D. A. Ammonia oxidation kinetics determine niche separation of nitrifying Archaea and Bacteria;*Nature* **2009**, *461*, 976.

(15) Martinez-Garcia, M.; Stief, P.; Diaz-Valdes, M.; Wanner, G.; Ramos-Espla, A.; Dubilier, N.; Anton, J. Ammonia-oxidizing Crenarchaeota and nitrification inside the tissue of a colonial ascidian;*Environ. Microbiol.* **2008**, *10*, 2991.

(16) Matsutani, N.; Nakagawa, T.; Nakamura, K.; Takahashi, R.; Yoshihara, K.; Tokuyama, T. Enrichment of a novel marine ammonia-oxidizing archaeon obtained from sand of an eelgrass zone;*Microbes Environ.* **2011**, *26*, 23.

(17) Mincer, T. J.; Church, M. J.; Taylor, L. T.; Preston, C.; Karl, D. M.; DeLong, E. F. Quantitative distribution of presumptive archaeal and bacterial nitrifiers in Monterey Bay and the North Pacific Subtropical Gyre;*Environ. Microbiol.* **2007**, *9*, 1162.

(18) Moin, N. S.; Nelson, K. A.; Bush, A.; Bernhard, A. E. Distribution and diversity of archaeal and bacterial ammonia oxidizers in salt marsh sediments;*Applied and Environmental Microbiology* **2009**, *75*, 7461.

(19) Nelson, K. A.; Moin, N. S.; Bernhard, A. E. Archaeal diversity and the prevalence of Crenarchaeota in salt marsh sediments;*Applied and Environmental Microbiology* **2009**, *75*, 4211.

(20) Porat, I.; Vishnivetskaya, T. A.; Mosher, J. J.; Brandt, C. C.; Yang, Z. K.; Brooks, S. C.; Liang, L.; Drake, M. M.; Podar, M.; Brown, S. D.; Palumbo, A. V. Characterization of archaeal community in contaminated and uncontaminated surface stream sediments;*Microbial Ecology* **2010**, *60*, 784.

(21) Quaiser, A.; Zivanovic, Y.; Moreira, D.; Lopez-Garcia, P. Comparative metagenomics of bathypelagic plankton and bottom sediment from the Sea of Marmara;*ISME J.* **2011**, *5*, 285.

(22) Siboni, N.; Ben-Dov, E.; Sivan, A.; Kushmaro, A. Global distribution and diversity of coral-associated Archaea and their possible role in the coral holobiont nitrogen cycle;*Environ. Microbiol.* **2008**, *10*, 2979.

(23) Urakawa, H.; Martens-Habbena, W.; Stahl, D. A. High abundance of ammonia-oxidizing Archaea in coastal waters, determined using a modified DNA extraction method;*Applied and Environmental Microbiology* **2010**, *76*, 2129.

(24) Walker, C. B.; de, l. T. J. R.; Klotz, M. G.; Urakawa, H.; Pinel, N.; Arp, D. J.; Brochier-Armanet, C.; Chain, P. S. G.; Chan, P. P.; Gollabgir, A.; Hemp, J.; Hugler, M.; Karr, E. A.; Konneke, M.; Shin, M.; Lawton, T. J.; Lowe, T.; Martens-Habbena, W.; Sayavedra-Soto, L. A.; Lang, D.; Sievert, S. M.; Rosenzweig, A. C.; Manning, G.; Stahl, D. A. Nitrosopumilus maritimus genome reveals unique mechanisms for nitrification and autotrophy in globally distributed marine crenarchaea;*Proc. Natl. Acad. Sci. U. S. A., Early Ed.* **2010**, 1.
(25) Woebken, D.; Fuchs, B. M.; Kuypers, M. M. M.; Amann, R. Potential interactions of particle-associated anammox bacteria with bacterial and archaeal partners in the Namibian upwelling system;*Applied and Environmental Microbiology* **2007**, *73*, 4648.
(26) You, J.; Das, A.; Dolan, E. M.; Hu, Z. Ammonia-oxidizing archaea involved in nitrogen removal;*Water Res.* **2009**, *43*, 1801.
(27) Zeng, Y.; Li, H.; Jiao, N. Phylogenetic diversity of planktonic archaea in the estuarine region of East China Sea;*Microbiol. Res.* **2007**, *162*, 26.
(28) Armstrong, F. A. Insights from protein film voltammetry into mechanisms of complex biological electron-transfer reactions;*J. Chem. Soc., Dalton Trans.* **2002**, 661.
(29) Krishnan, S.; Armstrong, F. A. Order-of-magnitude enhancement of an enzymatic hydrogen-air fuel cell based on pyrenyl carbon nanostructures;*Chem. Sci.* **2012**, *3*, 1015.
(30) Fadouloglou, V. E.; Kokkinidis, M.; Glykos, N. M. Determination of protein oligomerization state: two approaches based on glutaraldehyde crosslinking;*Anal. Biochem.* **2008**, *373*, 404.
(31) Torabi, S. F.; Wu, P.; McGhee, C. E.; Chen, L.; Hwang, K.; Zheng, N.; Cheng, J.; Lu, Y. In vitro selection of a sodium-specific DNAzyme and its application in intracellular sensing;*Proc. Natl. Acad. Sci. U. S. A.* **2015**, *112*, 5903.
(32) Solomon, E. I. Spectroscopic Methods in Bioinorganic Chemistry: Blue to Green to Red Copper Sites;*Inorg. Chem.* **2006**, *45*, 8012.
(33) Siluvai, G. S.; Mayfield, M.; Nilges, M. J.; Debeer George, S.; Blackburn, N. J. Anatomy of a red copper center: spectroscopic identification and reactivity of the copper centers of Bacillus subtilis Sco and its Cys-to-Ala variants;*J Am Chem Soc* **2010**, *132*, 5215.
(34) Gray, H. B.; Malmstrom, B. G.; Williams, R. J. Copper coordination in blue proteins;*J. Biol. Inorg. Chem.* **2000**, *5*, 551.
(35) Nar, H.; Messerschmidt, A.; Huber, R.; van de Kamp, M.; Canters, G. W. Crystal structure analysis of oxidized Pseudomonas aeruginosa azurin at pH 5·5 and pH 9·0 : A pH-induced conformational transition involves a peptide bond flip;*J. Mol. Biol.* **1991**, *221*, 765.
(36) Arciero, D. M.; Pierce, B. S.; Hendrich, M. P.; Hooper, A. B. Nitrosocyanin, a red cupredoxin-like protein from Nitrosomonas europaea;*Biochemistry* **2002**, *41*, 1703.
(37) Tsikas, D. Analysis of nitrite and nitrate in biological fluids by assays based on the Griess reaction: appraisal of the Griess reaction in the L-arginine/nitric oxide area of research;*J. Chromatogr. B Analyt. Technol. Biomed. Life Sci.* **2007**, *851*, 51.
(38) Martens-Habbena, W.; Qin, W.; Horak, R. E.; Urakawa, H.; Schauer, A. J.; Moffett, J. W.; Armbrust, E. V.; Ingalls, A. E.; Devol, A. H.; Stahl, D. A. The production of nitric oxide by marine ammonia-oxidizing archaea and inhibition of archaeal ammonia oxidation by a nitric oxide scavenger;*Environ. Microbiol.* **2015**, *17*, 2261.

CHAPTER 3

DESIGN OF A SINGLE SCAFFOLD PROTEIN, AZURIN, TO SPAN THE ENTIRE RANGE OF PHYSIOLOGICAL REDUCTION POTENTIAL

* Portions of this chapter are from a manuscript submitted to PNAS, as "Design of a single scaffold protein that spans the entire 2V range of physiological redox potential" (Hosseinzadeh P.*, Marshall N.M.*, Chacón K.N., Yu Y., Nilges M.J., Blackburn N.J., Lu Y.). Marshall N.M initiated the projects and performed several initial assays and experiments that are presented in the SI and CV data of the protein. EXAFS simulations were performed by Chacón K.N. and some of EXAFS data were collected by Chacón K.N. and Yu Y.
* Portions of the introduction are from a review submitted to Biophys. Biochim. Acta as "Designed and fine-tuning redox potentials of metalloproteins involved in electron transfer in biology" (Hosseinzadeh P., Lu Y.)

3.1. Introduction

3.1.1. Importance of tuning Reduction potential

The reduction potential (E°) of a metal center is best described as the tendency of the center to acquire electrons and thus to be reduced (Eq. 3.1). The more positive the value of E°, often called high E° centers, the more favorable the reduction of the metal center becomes, and thus it is called an oxidant.[1] Similarly, centers with less positive values of E° are often referred to as low E° centers and their oxidation is more favorable, hence are better reductants.[1]

$$M^m + ne^- \rightarrow M^{m-n} \qquad \text{Eq. 3.1}$$

As can be deduced from the definition, the value of E° is relative. The most common standard used for defining the E° value is the standard hydrogen electrode (SHE) which is the potential of a platinum electrode in a theoretical electrode/solution interface, where the concentration of H^+ is 1 M. The value of SHE has been arbitrarily assigned to be 0.0 mV. All E° values mentioned in this review are referred vs. SHE. Any factor that stabilizes a higher oxidation state or destabilizes a lower oxidation state of the metal ion will decrease the E°, i.e. the metal ion is easier to be oxidized or more difficult to be reduced. Similarly, factors stabilizing lower oxidation states of the metal ion will increase E°, causing the metal to be reduced more easily.

Another important factor to consider when discussing ET is the rate at which the process occurs. Several factors can influence the rate of ET, based on Marcus equation (Eq. 3.2).

$$k_{ET} = \frac{2\pi}{\hbar} |H_{AB}|^2 \frac{1}{\sqrt{4\pi\lambda k_B T}} \exp\left(-\frac{(\lambda+\Delta G^\circ)^2}{4\lambda k_B T}\right) \qquad \text{Eq. 3.2}$$

where k_{ET} is the rate constant of electron transfer, H_{AB} is the electron coupling between the initial and final states, λ is the reorganization energy, and ΔG° is is the total Gibbs free energy change for the ET reaction, often called the driving force of the reaction.[2]

Among the factors that influence the ET rate, E° can play a major role, as it provides the driving force (ΔG°) for the ET reaction. By tuning E° of different metal centers within a protein, the ET rate can be precisely controlled. A primary example of such tuning is observed in ET reactions in photosynthesis and respiration.

In photosynthesis, the reaction center, also called light harvesting complex, is responsible for harvesting the energy in the form of light through several chlorophylls and pigments to ensure the maximum capture of visible light. [3,4] In the light-dependent stage of photosynthesis, the excited chlorophyll in photosystem II (PS-II) loses one electron, which is first transferred to a quinone (plastoquinone in plants) and then to cytochrome b_6f, an ET protein (plastocyanin in plants), and finally photosystem I (PS-I). Upon additional exposure to light, the electron is excited and transferred to another molecule, usually a membrane bound FeS protein, then to ferredoxins, and through the action of ferredoxin-NADPH reductase (FNR), to its ultimate acceptor, $NADP^+$. The electron that left PS-II is restored through oxidation of water.[3,4] Through these series of reactions electrons flow thermodynamically downhill. The energy provided by these electrons results in the generation of a proton gradient across the membrane, which is later used to produce ATP through the action of ATP synthase. The newly produced NADPH will then take part in the next stage of photosynthesis, called the dark cycle, to help store the energy in the form of C-C bonds via a process called carbon fixation.[5,6] Special requirements for proteins that are involved in photosynthetic reaction centers have been discussed by Dutton and coworkers in detail.[3,7] The production of a proton-motive force, and subsequently ATP, is dependent on the downhill movement of electrons, which in turn is controlled by the E° of the redox partners involved in each reaction (Figure 3.1).

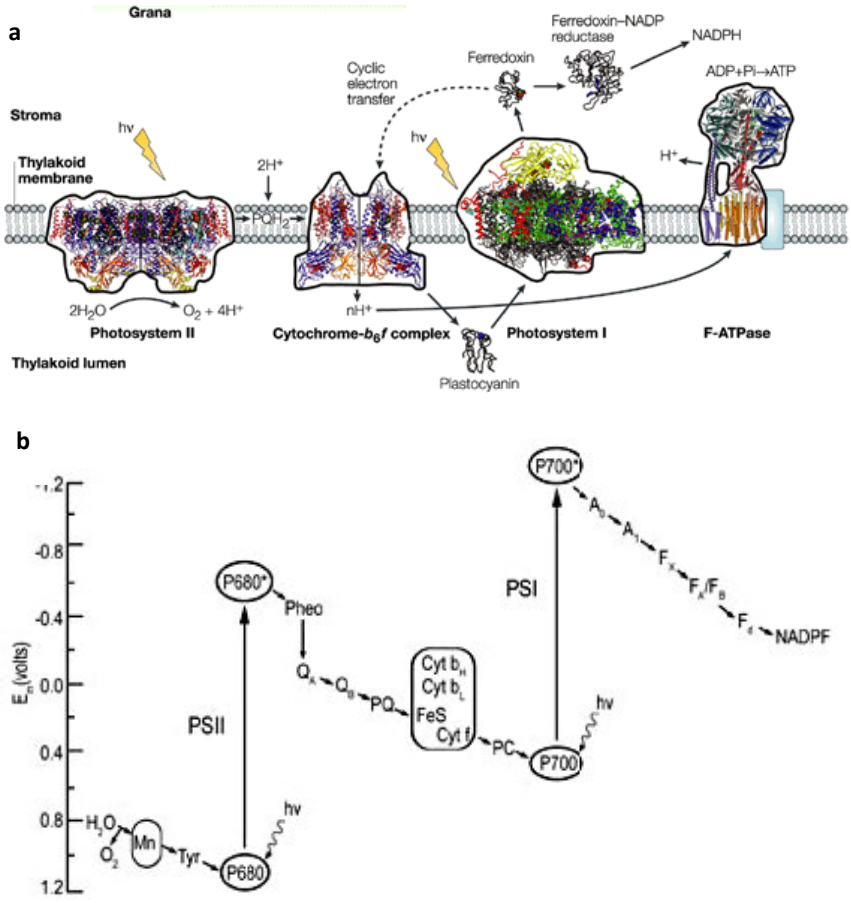

Figure 3.1. (a) Schematic representation of molecules involved in light stage of photosynthesis. (b) Z-scheme of photosynthesis showing the electron flow and the potential of redox pairs involved. Figures adapted with permission from Ref. [5] (Copyright © 2004, Rights Managed by Nature Publishing Group and [8] (Copyright © 1992, Kluwer Academic Publishers., respectively.

Similar tuning of the E° is also observed in the respiratory electron transport chain (Figure 3.2). In aerobic respiration, electrons generated from the oxidation of NADH to NAD^+ are transferred to complex I (NADH-coenzyme Q reductase), and then to ubiquinone (coenzyme Q). Ubiquinone can also accept electrons from complex II (succinate dehydrogenase) that are generated through conversion of succinate to fumarate. Reduced ubiquinone will then pass its electrons to complex III (cytochrome $bc_{1)}$, then to cytochrome *c*, and finally to complex IV (cytochrome *c* oxidase) which transfers electrons to their ultimate acceptor, O_2, generating water in the process.[9-13]

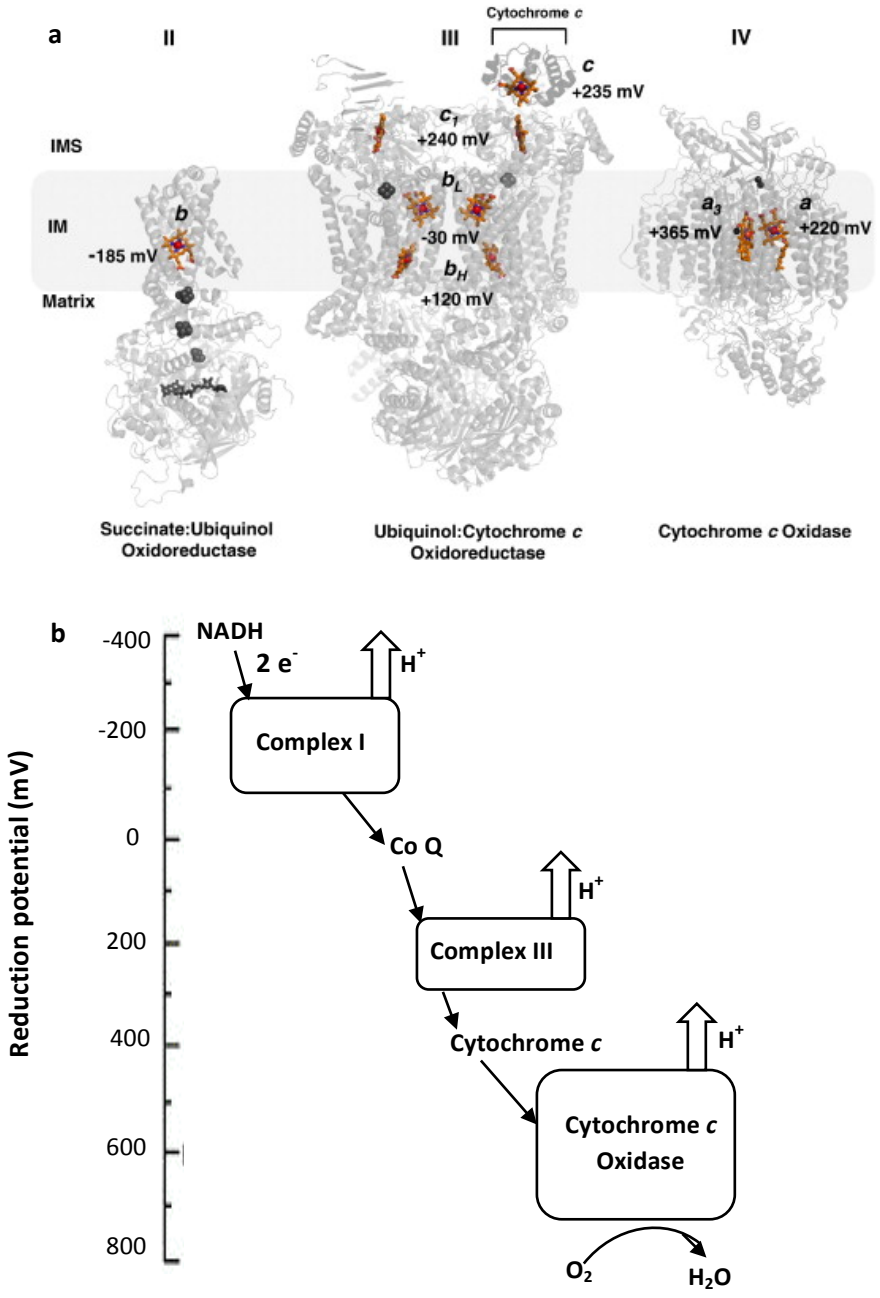

Figure 3.2. (a) Schematic representation of molecules involved in aerobic electron transport chain. Figure adapted from Ref. [11] Copyright © 2012 Elsevier B.V. (b) Associated redox potentials.

In addition to controlling rates of ET, tuning E° can regulate biological reactions. In several cases, the E° of a metalloprotein is changed upon binding to a substrate or to its cognate redox partner in a manner that facilitates the reactions. For example, cytochrome P450s are a class of

enzymes that catalyze activation of O_2 and then transfer the oxo group to many organic substrates. In the absence of the target, the enzyme has a low E° which prevents its reduction by its redox partner and is thus stable. The binding of the target substrate into active site, however, raises the E°, making the enzyme reducible by its redox partner, and allowing the reduced enzyme to bind O_2, activating it for oxo-transfer reactions such as epoxidation.[14-21]

Similarly, the reduction processes in cytochrome bc_1 are tightly regulated in order to avoid the formation of dead-end products. As a result, the system incorporates a way to ensure that cytochrome *c* is not reduced by the Rieske center before heme b_L is reduced. To achieve this goal, E° of the Rieske center is regulated by binding to quinone. The principle of regulation is based on the finding that semiquinone has a strong affinity for the reduced Rieske center and the strong binding increases the E° of Rieske center, due to presence of a cation radical (semiquinone). Before the ET reaction, deprotonated hydroquinone binds the oxidized Rieske center and reduces the Reiske center by giving an electron and changing to semiquinone in the first ET step. However, this reduction resulted in reduced Rieske that has a strong affinity for the semiquinone, and hence its redox potential will increase. The increase in E° does not allow the reduced Rieske center to transfer electrons to cytochrome *c*. In the second ET step, on the other hand, the heme b_L will oxidize the semiquinone to quinone, which has a lower affinity for Rieske protein Consequently, the E° of Rieske becomes low again, enough to transfer electrons to cytochrmome *c*.[22-24] Finally, interaction between plant-type ferredoxins and their redox partner ferredoxin/NADPH oxidoreductase (FNR) cause a change in E° of both proteins, facilitating ET between the two redox partners.[25,26]

3.1.2. Factors affecting redox potentials of ET centers and strategies to fine-tune them

In this section we will provide an in-depth review about the factors involved in tuning E°, as one of the most practical ways of designing tailor-made ET proteins.

3.1.2.1. Metal ions

The role of metal ions in determining the range of reduction potential of a metalloprotein is known to be very important. Depending on the metal ion and the valent states it's going through, the value of E° can vary substantially. Not all potentials are accessible to metal pairs and, especially in biology with the limited ligands offered, not all transitions are possible. In general,

copper is known to be on higher ends of redox potential range, while iron serves mostly as a low E° redox center.[27] The transitions that a metal center can go through are a major determinant of the overall range of E° for a metalloprotein. The main reason for the higher reduction potentials observed in the [4Fe-4S] clusters in high potential iron-sulfur proteins (HiPIPs) compared with those in ferredoxins (100-500 mV vs. -600-100 mV, respectively)[27] is the different transitions they go through ($[4Fe\text{-}4S]^{2+/3+}$ vs. $[4Fe\text{-}4S]^{1+/2+}$, respectively).[28-31]

The number of metal ions in the metal center is also an important determining factor for the redox potential of both ions. The presence of a positively charged metal ion will directly affect redox potentials of neighboring metals and more importantly, any changes in the redox state of one metal ion will influence overall redox state of the other ions. One such effect is observed in binuclear centers such as Cu_A or [2Fe-2S] clusters in which the orbitals of the metals are mixed, resulting in a spin paired system with half integer charges on each metal.[32-36]

Even in systems in which the metal centers are not as close, one can see cooperativity between metal centers. Cooperativity of the nearby hemes in multiheme cytochromes is one such example.[37-39] It has been suggested that interactions between the hemes in cytochrome c_3 around 28 Å for heme I and II in tetraheme c_{554} can change the values of E° of other hemes within the protein by 50-60 mV.[40-42] Electrostatic interactions and local aromatic groups are proposed to be the main mediators of such redox-dependent effects[43] (Figure 3.3). Spin state of a metal ion and the transitions it goes through also have effects on its redox potential. For example, low spin heme sites have shown to have lower redox potentials.[44] In cytochrome $P450_{cam}$, the low spin heme has a potential of -270 mV while the high spin state has a potential of -170 mV.[45]

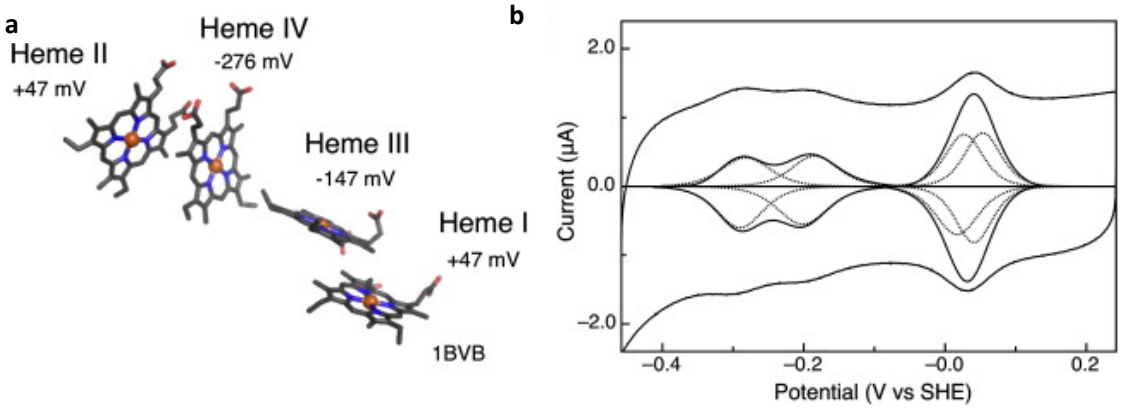

Figure 3.3. (a) The arrangement of hemes in tetraheme c_{554} with their corresponding redox potentials. (b) The redox potential windows of tetraheme c_{554}. Figures reprinted with permission from Ref. [46]. Copyright © 2013 Elsevier B.V.

3.1.2.2. Ligands in the primary coordination sphere

In addition to the identity of the metal ion and its valent states, the ligands coordinated to the metal ions are major contributors to E° of that ion, conferring their contribution through changes in geometry and electronic properties. While a combination of all these effects determine the E° of a site, some are more prevalent in specific proteins, and we use those as examples to better explain such effects. Some metal ions have different preferences for certain geometries in their different oxidation states. Cu is one example of a metal ion which accommodates a tetragonal or square pyramidal geometry in its oxidized Cu(II) form while preferring a tetrahedral or linear geometry in its reduced Cu(I) form.[47] If the active site of a protein has a ligand geometry more similar to the tetragonal form, Cu(II) is stabilized and a decrease in E° is observed.

A metal ion's preference for soft vs. hard ligands can also be used as a means to tune the E°. In general, higher oxidation states of a metal ion are considered to be harder, due to higher charge and lower radii. Thus, the presence of a hard ligand would preferentially stabilize higher oxidation states, resulting in a decrease in E° values. For example, the Fe(II) heme is softer than Fe(III) heme, therefore softer ligands such as His would favor the lower oxidation state in comparison with a harder ligand, ultimately increasing E°.[48]

Electron donating features of the primary ligands is also a major factor contributing to E° of the site. The proximal ligand of Tyr with high pKa is responsible for catalase to have a very low E° <-500 mV [49]. On the other hand, the proximal Cys with lower pKa than that of Tyr makes cyt P450 to have higher E° (E°= -170 mV in high spin and -270 mV in low spin p450 [45]). Finally the proximal His with even lower pKa caused the myoglobin to display even higher E° (E° = +50 mV)[50-52] (Figure 3.4). Mutation of the proximal His to either Cys or Tyr decreased the E° in Mb from +50 mV to -230 mV and -190 mV respectively, owing to the more electron donating ability of the new ligands.[50] Longer bond lengths between proximal His ligands and Fe in peroxidases is suggested to decrease electron density on heme, increasing the redox potential.[53,54] Similarly, it has been shown that one of the main reasons behind the higher potentials found in [2Fe-2S] Rieske centers compared to [2Fe-2S] ferredoxins is the replacement of Cys ligands in ferredoxin with less electron donating His ligands in Rieske proteins.[30,55] Mutation of Cys ligands in FeS proteins to less electron donating ligands such as Ser resulted in an increased E° in cases where the cluster remained intact.[23,56-58]

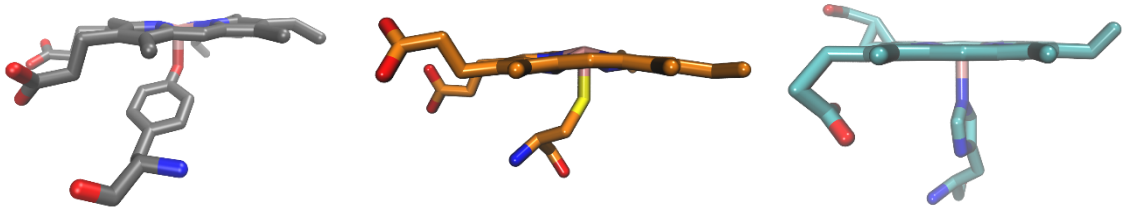

Catalase (E° <-500)

PDB ID: 4B7G

P450cam (E° =-170)

PDB ID: 3WRI

Myoglobin (E° = +50)

PDB ID: 1MBN

Figure 3.4. Effect of changing the proximal ligand in heme proteins. The more electron donating the proximal ligand is, the higher the redox potential will be.

Similar trends are observed with the electron donating nature of the distal ligand of heme proteins. In general, the more electron donating the distal ligand is, the more the higher redox states will be stabilized, increasing E°. Met ligation to heme results in an overall 100-150 mV increase in reduction potential compared with His ligation if all other factors remain the same[59-61] (Figure 3.5). Replacement of His with Met in cytochrome *c* results in an increased E°[62,63] while the Met to His replacement causes the reverse effect.[60]

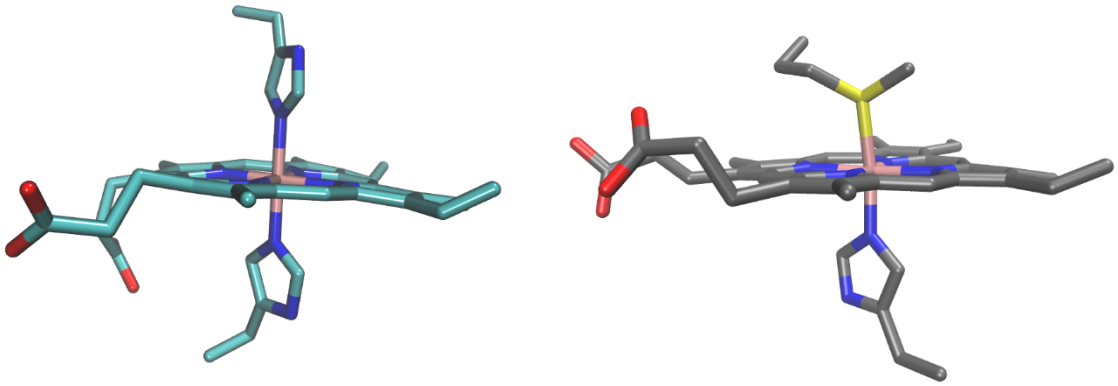

Cytochrome b_5 (E° = 3 mV)

PDB ID: 1CYO

Cytochrome b_{562} (E°= 168 mV)

PDB ID: 1QPU

Figure 3.5. Role of axial ligand in potential of cytochromes [64,65].

The electron donating or withdrawing features of the porphyrin functional groups also affect heme E° [48] due to delocalization of d orbitals into the π-system of the porphyrin ring [66]. Having more electron withdrawing groups on heme will create an electron poor Fe ion, hence increasing the E°.[51,52]

Heme distortion or ruffling can also contribute to E°. The degree of ruffling will influence the electronic structure of the porphyrin[67,68] and has been shown to decrease delocalization of π electrons.[69-75] Inducing heme distortion by protein changes have shown that the E° can be changed by 170 mV in heme-nitric oxide/oxygen protein[74] (Figure 3.6).

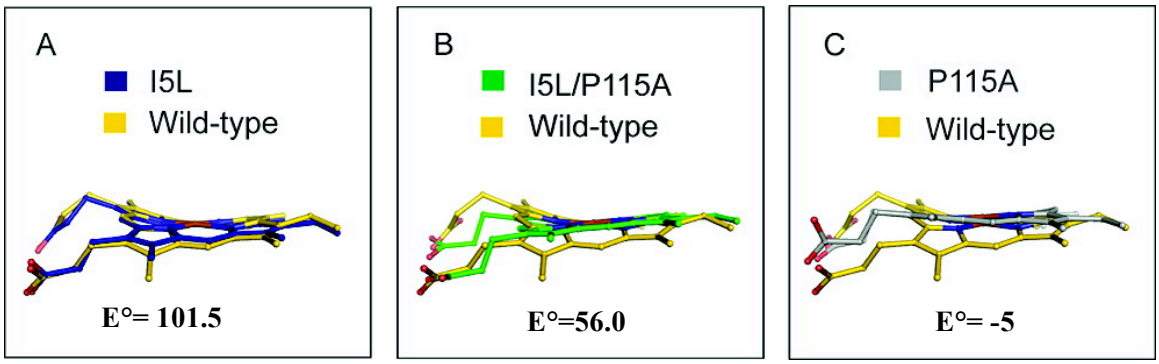

Figure 3.6. Changing the ruffling of the heme in H-NOX (heme nitric oxide-oxygen reductase) causes a change in the redox potential of the heme. Redox potential of the WT H-NOX is about 420 mV. (all values are reported vs. SHE). Figure is reprinted with permission from Ref. [74]. Copyright © 2010, American Chemical Society.

The presence of electron donating or withdrawing groups on the FeS proteins and the overall charge of the cluster have been shown to influence E° of the FeS proteins. The less negative overall charge of the [2Fe-2S] cluster in Rieske proteins (0/-1) vs. ferredoxins (-2/-3) is suggested as one of the main contributors to higher E° of former[27,76] (Figure 3.7). Slight changes in the structure of FeS clusters, such as differences in Fe-S-C_α-C_β bond angles[77-79] and distortions in the cuboidal structure of some 3Fe-4S centers can also cause E° changes.[80]

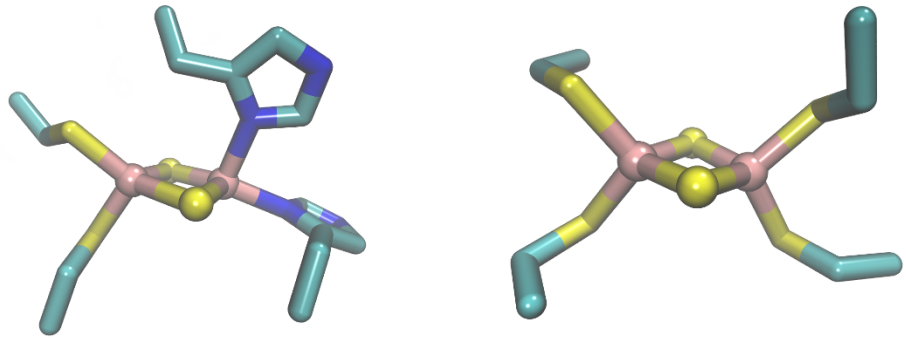

Figure 3.7. Structure of (a) Rieske center in complex bc_1 (PDB ID: 1BE3) and (b) a plant-type [2Fe-2S] ferredoxin (PDB ID: 3AV8). As shown in the figure, while the clusters look very similar, the Rieske center has replaced two of its thiolate ligands with imidazolate. Values for redox potential are obtained from Ref. [81] and [82], respectively.

3.1.2.3. Secondary coordination sphere interactions

While primary ligands are the major contributors to the overall range of E° of a given metal center, secondary coordination sphere (SCS) interactions can fine-tune the E° within proteins that share similar primary coordination spheres (PCS). A quick look at different classes of ET proteins can clarify the essential role of interactions beyond the PCS of metal ions in modulating the E° to match that of the redox partner to ensure efficient and specific ET and activity.[27]

As an example, cupredoxins share the same geometry of Cu binding sites with two His and one Cys ligating to the Cu ion in a distorted tetrahedral geometry (Figure 3.8).[27,83,84] Despite this similarity, their redox potentials span a range of over 500 mV.[27,83,85-88] Similar changes in range of E° are observed in cases of 2Fe-2S ferredoxins, and cytochromes. The nature of these interactions and how they affect reduction potential are discussed in more detail in chapter four.

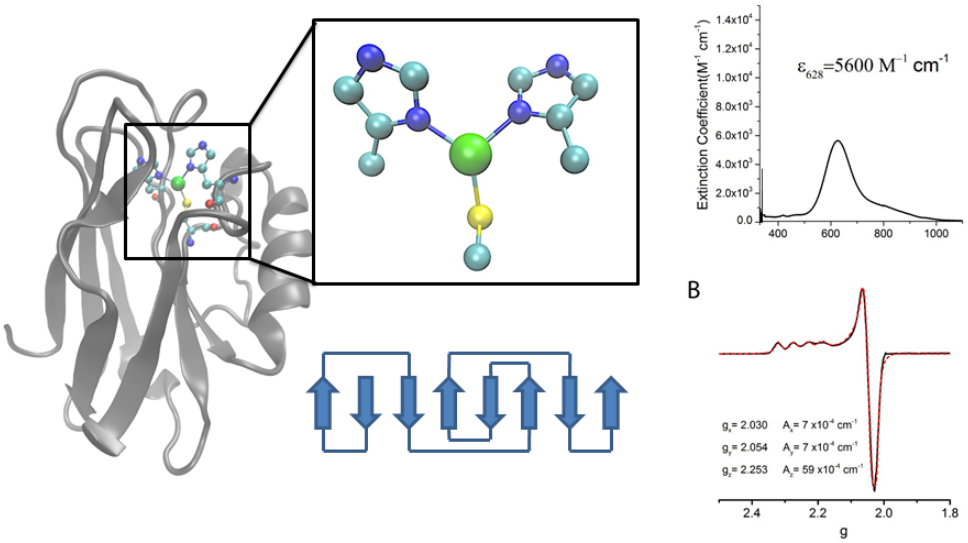

Figure 3.8. (a) Overall structure of a cupredoxins (azurin, PDB ID: 4AZU). (b) Representative active site structure of cupredoxins. (c) Overall scheme of Greek key β-barrel fold of cupredoxins (adapted from [117]). (d) , (e) Representative UV-vis and EPR spectra of cupredoxins, respectively. (adapted from [21])

3.1.2.4. Longer range interactions

While not as prominent as factors mentioned above, longer range interactions within proteins and the overall structural features of protein scaffolds in which metal ions are residing can also influence the E° of the metal center. Hydrophobic environments provided by protein around the metal will increase the reduction potential of metal centers by disfavoring higher redox states.[27] This desolvation is the reason that metal complexes in organic model systems usually have lower E° compared with those of proteins.[30] Exclusion of solvent from the site will change the

entropy and enthalpy of a redox transition. Solvent exclusion and heme burial is thought to be among the chief factors in controlling redox potential of cytochromes,[52,63,89-95] with an effect of up to 240 mV.[63]

In addition, there have been several reports of cases in which a change far away from metal site influences the overall arrangement of primary and secondary ligands, causing a shift in redox potential. This structural change is considered as one of the ways binding to a redox partner can change E° and facilitate ET. Surface charge mutations in cytochrome b_5[96] and C*c*P resulted in slight shifts in redox potential.[97] Net surface charges have been proposed to be important in determining E° of HiPIPs.[29,98,99]

3.1.3. Tuning E° using unnatural amino acids and non-native cofactors

While native cofactors and amino acids are very effective for designing ET centers, the repertoire of redox active molecules can be further expanded by the introduction of unnatural amino acids (UAAs) or non-native cofactors. These molecules enable the deconvolution of features that contribute to ET rates.

One successful example is the use of unnatural derivatives of Met in Az to study the role of hydrophobicity, specifically, in tuning the potential of the T1Cu center. Upon incorporation of a series of UAAs (shown in Figure 3.9), Lu and coworkers unambiguously demonstrated a linear relationship between hydrophobicity (logP) of the axial ligand and reduction potential of T1Cu center.[100]

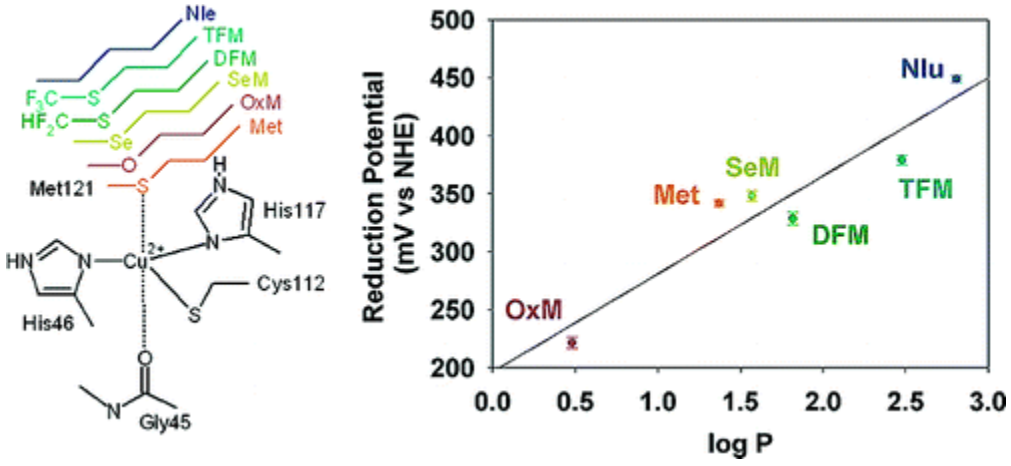

Figure 3.9. Unnatural Met derivatives that are incorporated into axial position of Az and their corresponding redox potentials. Figure is reprinted from Ref. [100].

Another example is the use of Tyr derivatives to probe ET. Tyr is a redox active amino acid that is shown to donate an electron and a proton during O_2 reduction by C*c*O. This Tyr is covalently attached to an adjacent His, which is a Cu ligand in the active site Cu_B center. In order to study the features of this Tyr that are important for ET and proton transfer, Lu and coworkers used derivatives of Tyr to study the role and function of this amino acid in the reaction mechanism of a functional model of C*c*O in myoglobin (Mb) (Figure 3.10). Using these derivatives, they showed the importance of the His-Tyr crosslink in increasing the activity and turnover of the enzyme.[101] They further confirmed the role of redox potential and pKa of the Tyr in the water production activity.[102,103]

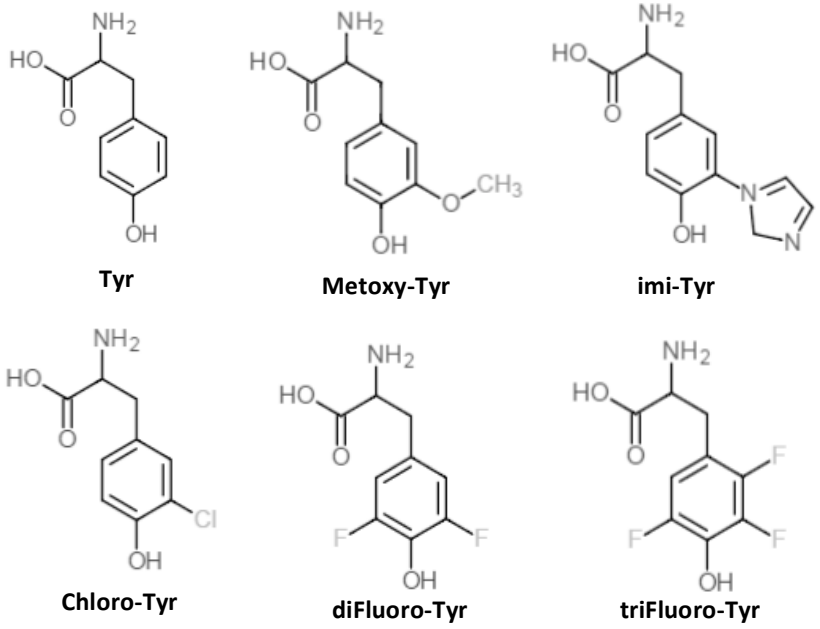

Figure 3.10. Redox active derivatives of Tyr used by Lu and coworkers to study water oxidation in mimics of C*c*O in Mb.

In order to study the role of H-bonds from backbone amide group in HiPIPs, Low and Hill used chemical synthesis to introduce O instead of N in the backbone of Val42 and Ala57 in *Rhodocyclus tenuis* HiPIP protein. They showed that removal of these H-bonds will result in a lower E° value as expected.[104]

One class of nonnative cofactors that are widely used in design and study of ET proteins are modified porphyrins. Porphyrins with modified electron withdrawing groups were used to change the redox potential and hence ET rate in a Mb model of C*c*O and it was shown that an

increase in ET rate corresponds to increase in activity[105] (Figure 3.11). Similarly, addition of a diacetyl group to the heme in horse radish peroxidase resulted in an increase in E°.[106]

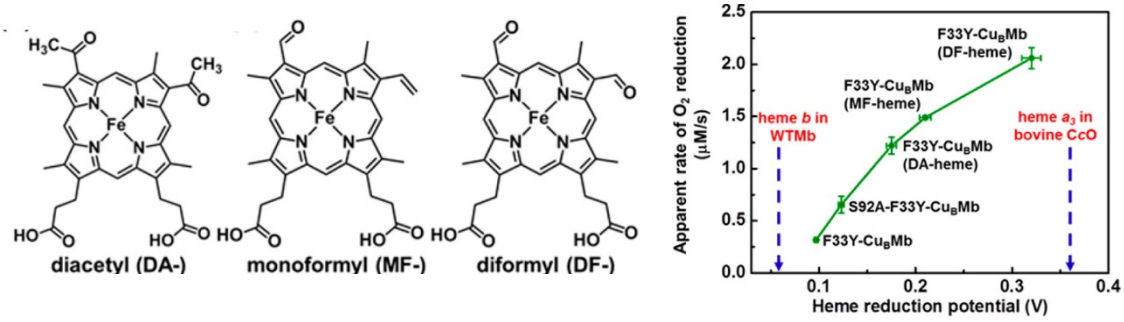

Figure 3.11. Addition of electron withdrawing groups to heme results in increase in reduction potential of the heme and in O_2 reduction activity in a Mb model of C*c*O. Figure adapted with permission from Ref. [105] Copyright © 2014, American Chemical Society.

3.1.4. An unaddressed question: how nature does this?

For millions of years, ET in biology has operated within the range of physiological E°′s, defined by the highest E°′ (~ +1 V vs. standard hydrogen electrode, SHE-all potentials mentioned in this study are vs. SHE) at which water is oxidized, and the lowest E°′ (~ -1V) at which protons are reduced to H_2.[27] Amazingly, nature has found a way to cover this wide range using a strikingly limited set of not only metal cofactors but also protein folds and metal center geometries, such as cupredoxins that cover 100 to 800 mV, cytochromes that cover -500 to 350 mV and Fe-S proteins that cover -700 to 500 mV (Figure 1).[27] Despite many years of research into these proteins and efforts to change the E°′,[107-111] how the E°′s can be tuned systematically in a wide range using the limited number of metal cofactors is still not well understood. An ultimate test of our understanding of this process is to design redox centers in a single protein, using a minimum number of metal cofactors and mutations that can cover the entire 2V range of physiological E°′. Furthermore, there are very few water-soluble/stable, chemical redox agents within the physiological E°′ range. Even for those redox agents that can cover a wide range of E°′ in non-aqueous solution, combining different redox agents with different scaffolds or surface properties makes it difficult to carry out systematic studies of the effect of E°′ on ET or catalytic functions, as it is difficult to deconvolute different factors in the redox process. In this chapter, I report the design of the ET protein azurin to cover a range from +970 ±20 mV to ~ -954 ±50 mV, by mutating only five residues and using two metal ions

3.2. Materials and methods

3.2.1. Design of constructs and molecular dynamics simulation

Before construction of HPAz, an *in silico* model of the protein was generated using VMD package.[112] The model was then energy minimized (5000 steps, 2 fsec/step) and simulated for a total of 1 ns, at 310 K with NPT condition using the NAMD software package.[113] The mutations were introduced into the Az gene containing a leader sequence to allow periplasmic expression in the pET-9a vector through QuickChange PCR (PfuUltraII, Agilent technologies) and confirmed by DNA sequencing at the CORE DNA sequencing facility (Urbana, IL).

3.2.2. Protein expression and purification

Expression and purification of HPAz was achieved through minor modifications of a previously reported method.[114] The HPAz plasmid was expressed in *E. coli* using BL21 (DE3)* chemical competent cells (NEB) transformed with the gene of interest using the standard heat shock method, plated on LB agar plates containing 50 μg/mL of kanamycin and incubated at 37°C overnight to produce single colonies. A single colony was then picked and inoculated in 50 mL LB culture media with 50 μg/mL kanamycin at 37°C overnight. The above 50 mL starter culture was then transferred to a 2 L culture of 2xYT media [16 g/L bactotryptone (BD), 10 g/L yeast extract (BD) and 5 g/L NaCl (Fisher)] containing 50 mg/L kanamycin. The 2 L cultures were incubated with shaking at 25°C until an OD_{600}~1.0-1.5 was reached. The cultures were then induced with 300 mg/L of IPTG (Gold Bio Technology Inc.) and incubation at 25°C was continued overnight.

After expression, the cells were harvested by centrifugation and re-suspended in 1/8 the original culture volume of a recovery solution consisting of 200 g/L sucrose, 50 mM Tris buffer at pH 8.0 and 1 mM EDTA. The cells were recovered by shaking for 45 minutes at room temperature, and then re-harvested. The periplasmic membrane was ruptured by re-suspending the cells in a solution of 4 mM NaCl and 1 mM DTT and shaking the cells vigorously at 4°C for 20 minutes. After centrifugation, the supernatant containing the Az variant was collected in a separate flask and further purified by adding 1/10 the volume of the supernatant of a 500 mM

sodium acetate solution at pH 4.0 to precipitate other components of the cells, which were then removed by centrifugation.

The above supernatant containing the Az variant was then applied to SP-sepharose resin (GE Healthcare) by adding the resin directly to the above supernatant and shaking the suspension at 4°C for at least 2 hours to allow the protein to bind to the resin. The mixture was then packed into a column and the Az variant was purified through a pH gradient from pH 4.1 to pH 6.4 using 50 mM ammonium acetate buffer at the appropriate pH for both washing and eluting. The Az variant was further purified by passing the protein through a Q-sepharose (GE Healthcare) column and a Sephadex S-100 gel filtration column (GE healthcare), both equilibrated in 50 mM ammonium acetate buffer at pH 6.0. The identity of the protein after purification was verified by electrospray ionization mass spectrometry (ESI-MS) (calculated: 13974; observed: 13978 Da). Typical protein yields ranged from 100-200 mg of pure protein per liter of culture and purity was >98 % based on SDS-PAGE.

Due to high affinity of the proteins for Cu, we used a slightly modified protocol for purification of samples for Ni addition. We treated the supernatant before SP column with 1mM EDTA to remove divalent cations. 1 mM EDTA was added to buffers as well. We then purified the protein on a size exclusion column that was previously washed with EDTA and then equilibrated with chelexed buffer. Chelexed buffer was used for running the column as well.

Met121Glu mutant was purified using a different procedure, described previously.[115] This is to ensure that the protein is purified in its apo form, since this protein has extremely high affinity for divalent metal ions and the procedure used for other variants is not effective to obtain metal-free form of this protein.

3.2.3. Copper and nickel reconstitution

The Az variant was expressed and purified as apo (metal-free) protein. To reconstitute the copper into the apo-protein, sub-saturating equivalents of either $CuSO_4$ or 5-10 mM $Cu(CH_3CN)_4PF_6$ in acetonitrile was added to the protein solution with stirring in order to minimize the chance that free copper in solution would precipitate the protein.

Ni^{2+} addition to the proteins was performed following a previously reported protocol.[116,117] Briefly, a 50 μM solution of protein in 100 mM phosphate buffer pH 8.0 was prepared. 10 eq. $NiCl_2$ was added to the solution and was stirred for two days at room temperature. As Met121Glu mutant was highly effective at binding to Ni^{2+}, we found that one hour was enough to obtain saturation of the LMCT peak from Ni^{2+} binding.

3.2.4. Mass spectrometry

Electrospray ionization mass spectroscopy (ESI-MS) were obtained on a Quattro II (Waters) ESI mass spectrometer maintained by the School of Chemical Sciences Mass Spectrometry Laboratory (Urbana, IL). For checking the mass of copper free proteins, formic acid was used to ionize the protein upon injection. For observing metal bound proteins, the formic acid was omitted and a solution of the copper bound protein in 5 mM ammonium acetate buffer pH 5.0 was injected as a continuous stream (5 μl/min) via syringe pump to build up sufficient signal to obtain an accurate mass.

3.2.5. Cyclic voltammetry (CV)

For CV on pyrolytic graphite electrodes (CH Instruments, Austin, TX), the electrode was first polished to a mirror finish and until no protein signal was visible. A 1 mM sample of either Cu(II)-1VAz or Cu(I)-1VAz (10 μL) in pH 6.35 ammonium acetate buffer (50 mM) was then added to the exposed carbon and immediately immersed in a solution of 50 mM ammonium acetate buffer at pH 5.0 and 500 mM NaCl. A scan from 0.6 V to 1.3 V vs. the standard hydrogen electrode, SHE, was then run at a scan rate of 0.1 V/sec. No signal was observed in different buffer solutions with carbon electrodes or below a scan rate of 0.1 V/sec. Using faster scan rate of 1V/sec increased the intensity of reductive peak significantly. The CV of Green-Cu(II)HPAz was obtained in 10 mM sodium phosphate buffer at pH 7.0 supplemented with 100 mM sodium formate.

To obtain the potential of Ni-loaded variants, CV was run at 100 mM phosphate buffer at pH 8.0 with 100 mM NaCl, with scan rate of 0.1 V/s. In addition to CV, differential pulse votammetry (DPV) was performed for Ni-loaded variants to check the accuracy of the peak positions. The DPV parameters are as follows: scan from 0.2 V to -1.2 V with increments of

0.004 V and amplitude of 0.05 V. Pulse width of o.o15 sec was applied with sampling width of 0.005 sec and sampling period of 0.02 sec. A sensitivity of 5e-006 was used.

Software SOAS and OriginPro9.0 were used for data process. Subtraction in SOAS was performed according to the manual. Subtractions in OriginPro were performed using the peak analysis tab. The presence of the peaks was confirmed by taking the first derivative of the voltammagram.

3.2.6. Stopped-flow UV-vis absorption spectroscopy

Stopped-flow UV-vis spectra were collected on an Applied Photophysics Ltd (Leatherhead, UK) SX18.MV stopped-flow spectrometer equipped with a 256-element photodiode array detector. HPAz was concentrated to 0.75 mM in an appropriate buffer and 0.5 mM $Cu(CH_3CN)_4PF_6$ was added by slow addition from a 50 mM stock of the salt in acetonitrile (the solution was sonicated to fully dissolve the Cu(I) salt before the experiment). Sub-saturating equivalents of Cu(I) were used to minimize the chance of free copper in solution to complicate interpretation of the results. Oxidant solutions were prepared in in the appropriate buffer at the appropriate concentrations to deliver the desired number of molar equivalents relative to the amount of Cu(I) in the protein solution upon mixing in the stopped flow chamber. Spectra were collected for up to 1000 seconds with 200 intervals spaced logarithmically with shorter intervals at the start of data collection. A series of chemical oxidants of varying redox potential were used to initially scan for oxidation of reduced HPAz, including $(NH_4)_2Ce(NO_3)_6$ (1.72 V),[118] Ce(IV)/EDTA (1.06 V),[119] Na_2IrCl_6 (0.892 V),[120] $K_2Mo(CN)_8$ (0.798 V),[121] and $K_3Fe(CN)_6$ (0.424 V vs. NHE).[121] In general, oxidants with redox potentials around 0.9 V or higher were able to oxidize Cu(I)-HPAz to varying degrees while lower redox potential oxidants could not. $(NH_4)_2Ce(NO_3)_6$ and Ce(IV)/EDTA only recovered about 10 % of the expected absorbance assuming 100 % oxidation of the protein. Significant scatter was also seen with these titrants, which suggests protein precipitation. Na_2IrCl_6 was seen to yield approximately 20 % of the expected visible absorbance intensity based upon the amount of Cu(I) in solution with one molar equivalent of oxidant. As such, it was used for further spectrochemical titrations. For pH dependent studies of copper oxidation with Na_2IrCl_6 only acetate and phosphate-based buffers were used because Na_2IrCl_6 was seen to react with several other buffering molecules. Cu(II)

incorporation was also monitored by stopped-flow by injecting a solution of apo-protein in buffer against a solution of $CuSO_4$.

Because of the instability of Cu(II)-HPAz, we can obtain its E°′ quantitatively using CV, as we can capture the state using a fast scan rate. While redox titrations using oxidants such as Na_2IrCl_6 can in principle obtain the E°′, because of the bimolecular redox reaction in solution is much slower, the Cu(II)-HPAz, once generated, can decompose within the time scale of the redox reaction. Therefore we can estimate the E°′ only semi-quantitatively. Nonetheless, these redox titrations confirm the E°′ obtained from CV is in the correct range.

3.2.7. Spectroscopic studies

Electronic absorption spectra in the UV-visible region (UV-vis) were collected on either an Agilent 8453 diode array (Agilent), a Carey 3E (Varian) or a Carey 5000 (Varian) UV-vis spectrometer. For the pH dependent studies, a buffer that is effective to maintain pH in a wide range (pH 4-11) without substantially altering the components in solution from sample to sample was used. This buffer (called UB buffer) contained 50 mM sodium acetate, 40 mM MES, 40 mM MOPS, 40 mM Tris, 40 mM CAPS and 100 mM NaCl.

Electron Paramagnetic Resonance (EPR) spectra were collected using an X-band Varian E-122 spectrometer at the Illinois EPR Research Center (IERC). Samples were prepared typically at a final concentration of copper loaded protein of about 0.5-1 mM in the appropriate buffer and frozen as a glass with 20 % glycerol. Spectra were obtained in a temperature independent buffer at pH 7.0 (TIP7)[122] as the effective pH of buffered solutions is known to change substantially when cooled to cryogenic temperatures, which can dramatically alter the observed spectra.

Freeze quench EPR was performed on a syringe-RAM controller freeze/chemical quench apparatus from Update Instrument, Inc., Madison, WI. Protein sample was prepared in 50 mM phosphate buffer, pH 6.5 with addition of 0.1 M NaCl to decrease the temperature-induced pH changes after freezing. Glycerol was mixed with the protein sample to a final concentration of 10% v/v. Concentrated protein sample loaded with Cu(I) was transferred to a 2 ml syringe and Na_2IrCl_6 to a 0.5 ml syringe at 4X the concentration of the protein. The samples were mixed with a ram speed of 1.6 cm/s using a reactor tube size of 6.4 with a calculated volume of 5.3 µL.

The displacement was set such that the reaction time is less than 20 msec and quenched by spraying into a pre-chilled EPR tube filled with iso-pentane cooled in an iso-pentane bath at -120°C. Calculating the time from the initial mixing in the reaction chamber and adding the time required to freeze, a sample time of 20 msec was attained. The frozen sample was packed into a compressed layer in an EPR tube.

Cryoreduction of the M121E-Ni sample was performed by Dr. Stoyan A. Tashkov in nuclear radiation laboratory, UIUC. In brief the samplew were radiated by gamma-rays for three hours under liquid nitrogen temperature.

Cu K-edge (8.9 keV) extended x-ray absorption fine structure (EXAFS) and x-ray absorption near edge (XANES) data were collected at the Stanford Synchrotron Radiation Lightsource operating at 3 GeV, with currents near 500 mA maintained by continuous top off. Samples were measured as aqueous glasses in 20% ethylene glycol at 10K. All edges were measured on beamline 7-3, using a Si[220] monochromator. All data were collected in fluorescence mode using a high-count rate Canberra 30-element Ge array detector with maximal count rates per array element of <120 kHz. For each edge, four to six scans of buffer blank were averaged and subtracted for all protein samples in order to remove the Z-1 filter Kβ fluorescence and produce a flat pre-edge baseline. A Cu foil was placed between the first and second ionization chamber in order to provide energy calibration. Cu K-edges were collected using an Rh-coated mirror upstream with a 12.5 KeV energy cutoff to reject harmonics, and a nickel oxide filter and Soller slit inserted in front of the detector in order to reduce elastic scattering relative to the Cu Kα fluorescence.

Data averaging, background subtraction, and normalization to the smoothly varying background atomic absorption were performed using EXAFSPAK[123]. For the experimental energy threshold energy (k=0), 8995 eV was selected. Spectral simulation was carried by least-squares curve fitting, utilizing full curved wave calculations as formulated by the SRS library program EXCURVE 9.2[124] as previously described.[125] We refined the parameters of the fit as follows: E_0, the photoelectron energy threshold, R_i the distance from the central metal atom (Cu, Se, or Ag) to atom *i* and $2\sigma_2^i$ the Debye-Waller (DW) term for atom *i*. Coordination numbers were fixed to those previously established from crystal structures whenever possible. The quality of the fits was determined using the least-squares fitting parameter, F, which is defined as:

$$F^2 = (1/N) \sum_i k^6(\chi_i^{theory} - \chi_i^{experiment})^2$$

and is hereafter referred to as the fit index or fit (FI).

3.3. Results and discussion

3.3.1. Protein design and purification

The type 1 (T1) Cu center in wild type azurin (WTAz) resides in a Greek key β-barrel fold (Figure 3.12a) commonly found in cupredoxins, such as rusticyanin and laccase. The active site consists of a $Cu(S_{Cys})(N_{His})_2$ core in a trigonal plane, common to all T1 Cu centers, with a thioether group from a Met residue (S_{Met}) in the axial position (Figure 3.12b,c).[27,85] This axial Met is found in most cupredoxins, except those with high E°'; rusticyanin and laccase contain a Leu residue at the axial position instead.[27,85] We have previously shown that the E°′ of Az can be predictably tuned from 90 mV to 640 mV at pH 7, by tuning hydrogen bonding interactions and the hydrophobicity of residues near the copper binding site (Figure 3.12c).[110] To our knowledge there is no report of a mononuclear cupredoxin with E°′s above or below this range.

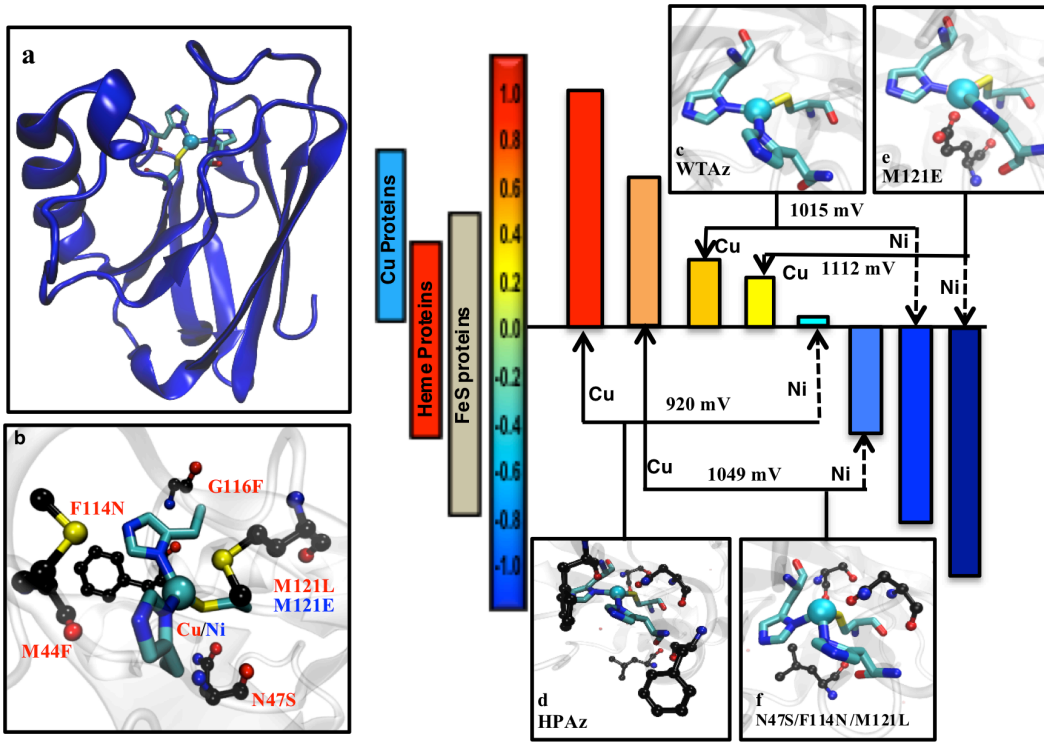

Figure 3.12. (a) Overall structure of Az. (b) Zoom-in of the metal binding site and the position of the residues mutated in this study. (c) WTAz active site structure, PDB ID: 4AZU, (d) Minimized structural model of HPAz, (e) Structure of M121E-Az, PDB ID: 4QLW, and (f) Minimized structural model of N47S/F114N/M121L-Az.

To tune the E°′ of the T1 Cu center in azurin to approach the highest E° under physiological conditions, we examined the T1 Cu centers in cupredoxins that exhibit extremely high E°′, such as those in multi-copper laccase (E°′ = 790 mV at pH 6- The E°′ for a multi-nuclear ceruplasmin has not been observed, but has been hypothesized to be > 1V, beyond the physiological E°′ range),[27,126] and found that these centers are highly desolvated and buried within the hydrophobic interior of the proteins.[126] The area surrounding the Cu center is also typically filled with bulky, hydrophobic residues like Phe.[126,127] Introducing such hydrophobic residues near the metal-binding sites or desolvating the site in several metalloproteins has resulted in increased E°′.[27,128-131] Based on these observations, we scanned the secondary coordination sphere of the T1 Cu center in Az for positions to introduce Phe residues, and found two such positions (Met44 and Gly116, see Figure 1b) that can be mutated to Phe with minimal structural perturbation (Figure 3.12d).

We combined the Met44Phe and Gly116Phe mutations with the Asn47Ser/Phe114Asn/Met121Leu mutations that had resulted in E°′ = 640 ± 1 mV at pH 7.0.[110] This quintuple variant of Az (Met44Phe/Asn47Ser/Phe114Asn/Gly116Phe/Met121Leu Az (Figure 3.12d), called HPAz hereafter) was constructed, expressed and purified to homogeneity as a metal-free apo protein using a procedure slightly modified from a previous study[110] and ESI results showed the correct protein. Syringe-pump ESI showed only one copper is bound to the protein (figure 3.13)

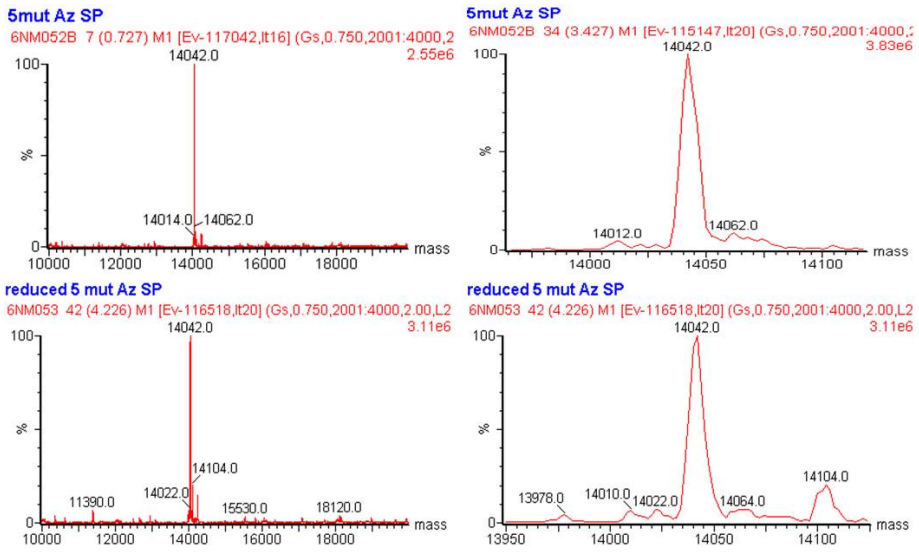

Figure 3.13. Syringe-pump ESI-MS of Cu(II)-HPAz (top) and Cu(I)-HPAz (bottom showing that one Cu is bound to the protein (MW= 14036 [13973 apo-HPAz+ 68 Cu])

3.3.2. Cyclic voltammetry experiments

After loading Cu(I) into the apo-HPAz, we employed cyclic voltammetry (CV) with a pyrolytic graphite "edge" plane electrode and observed a signal centered at 970 ±20 mV at pH 5.0 in 50 mM ammonium acetate buffer at a scan rate of 100 mV/s(Figure 3.14). Increasing the scan rate did not produce significant changes in the current or peak separation while at lower scan rates the signal disappeared. The faradaic current from the CV is much lower than those of inorganic complexes, due to much slower diffusion rates, and similar to those of other metalloproteins reported in the literature.[132-134] Attempts to obtain the potential in any other pH condition or buffer all failed. This failure maybe due to the low stability of the protein or impaired interaction with the electrode.

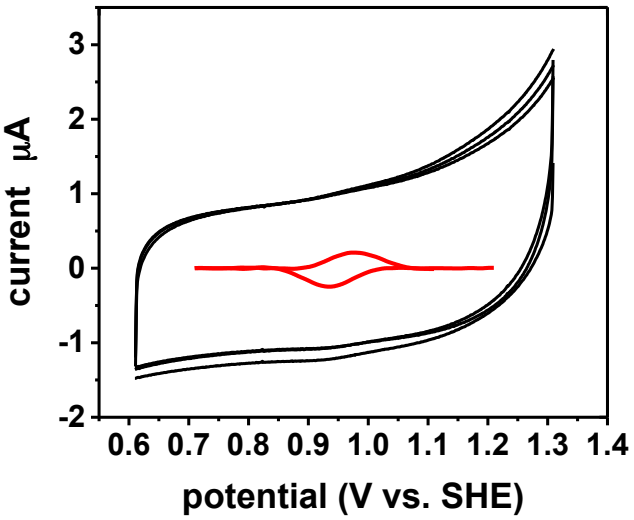

Figure 3.14. Cyclic voltammagram showing the reversible redox couple of HPAz. The potential obtained at scan rate of 0.1 V/sec at pH 5.0 in 50 mM ammonium acetate buffer, obtained at scan rate of 0.1 V/sec (black line). The signal with the capacitative current subtracted is shown as an inset in the middle (red line). (E_m= 0.97± 0.02 V vs. SHE).

To ensure that the observed CV signal is from the Cu-HPAz variant, we performed several control experiments, including repeating the CV experiment under the same conditions in the absence of any protein (Blank), in the presence of apo-HPAz (Figure 3.15a), and HPAz loaded with redox inactive Zn^{2+} (Zn(II)-HPAz, Figure 3.15b). None of these control experiments exhibited a signal near 970 mV, which strongly suggests that the CV signal is from the Cu(I)/Cu(II) redox couple of Cu-HPAz, instead of any other components present in the solution.

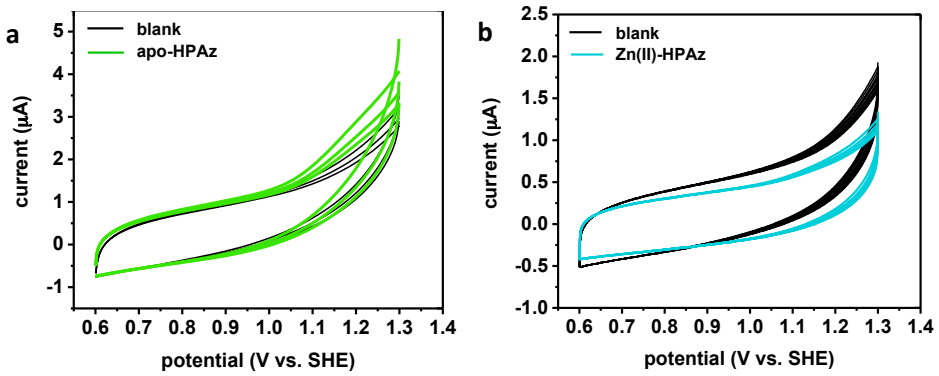

Figure 3.15. Cyclic voltammagram showing (a) electrode without protein (Blank) or in the presence of apo-HPAz , (b) Blank or Zn(II)-HPAz, at pH 5.0 in 50 mM ammonium acetate buffer, obtained at scan rate of 0.1 V/sec (black line).

Interestingly, the green Cu(II)HPAz displays a reductive peak around 650 mV vs. SHE at pH 7.0 (see Figure 3.16). Consistent with this is that the green-HPAz, which has a relatively lower E°′, is more stable than the blue HPAz.

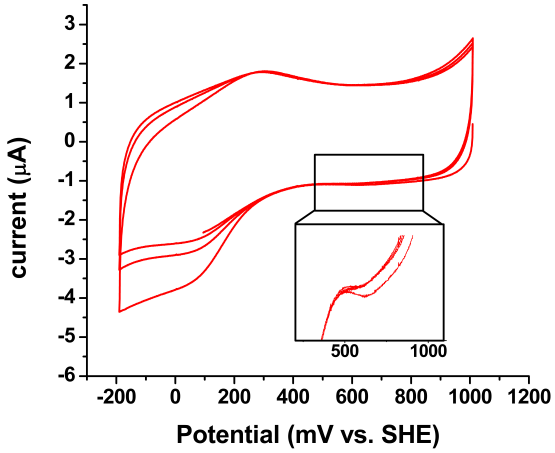

Figure 3.16. Cyclic voltammagram of Green-Cu(II)HPAz shows a weak reductive peak at 650 mV. CV performed in 10 mM sodium phosphate buffer pH 7 supplemented with 100 mM sodium formate. The reductive peak is small but it is reproducible. The peaks close to 200 mV are present in the blank electrode as well and are a result of some oxidized functionalities on the electrode surface.

3.3.3. Redox titration and stopped-flow experiments

To provide additional support to the E° value determined by the CV, we probed the ability of Cu-HPAz to react with other redox agents that have different potentials with little success in finding one that oxidize the protein. Among those, ferricyanide (E°′ = 0.424 V, pH 7.0), which is known to rapidly oxidize Cu(I)-WTAz (E°′ = 0.31 V at pH 7),[27,135] caused only minimal re-

oxidation (~2%) of 0.2 mM Cu(I)-HPAz under the same condition within the first 1 s, even when in the presence of a 10-fold molar excess of the oxidant (see Figure 3.17). At time scales longer than 1 s, a slower process similar to previously reported ferricyanide-induced protein unfolding and subsequent reacting with Cu(I) was observed (Figure 3.17). The inability of ferricyanide to oxidize Cu(I)-HPAz suggests that the E°′ of the T1 Cu center in HPAz is at least higher than 0.42 V.

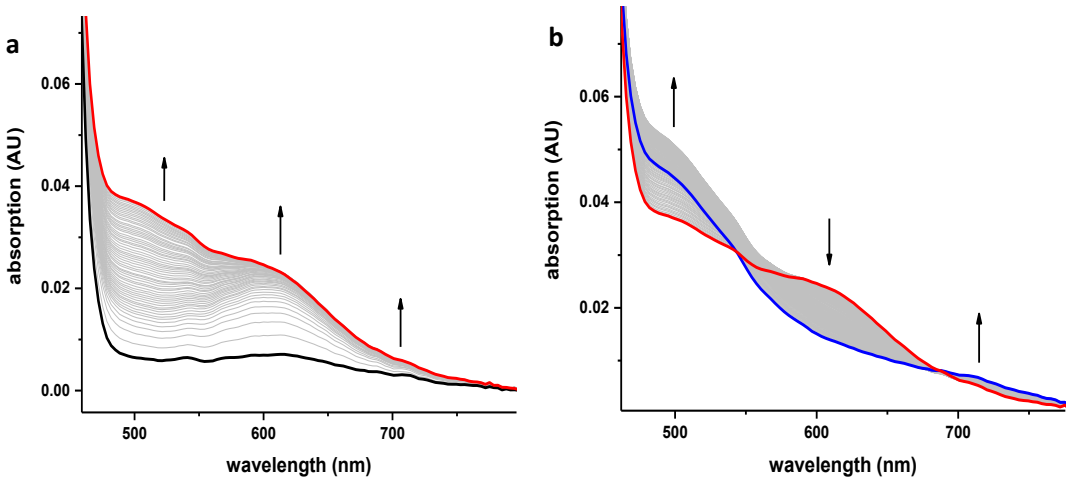

Figure 3.17. Stopped-flow UV-vis kinetic of Cu(I)-HPAz oxidation by ferricyanide. Reaction of reduced HPAz with 10 molar equivalents of ferricyanide for a) the 1st 20 s (black trace to red trace) and b) from 20 seconds to 1000 seconds (red to blue).

After trying several other oxidants of varying potentials to oxidize the HPAz, we found that 1 equivalent of Na_2IrCl_6 (E°′ = 0.96 V at pH 5, Figure 3.18) was able to oxidize 0.2 mM Cu(I)-HPAz at pH 5 with ~25 % loss of the Na_2IrCl_6 absorption bands (Figures 3.19 and 3.20). These results, together with the result obtained by replacing Cu with Ni on E°′ of the same protein (*vide infra*) indicate that the Cu-HPAz has an extremely high E°′.

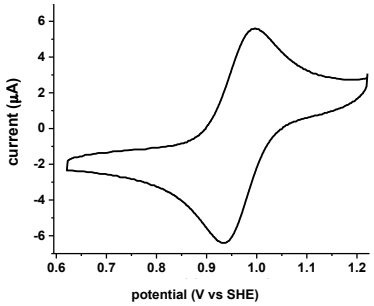

Figure 3.18. Sample voltammagram of $IrCl_6$. Spectrum taken in 50 mM NH_4OAc buffer pH=5.0 + 500 mM NaCl. $E_m = 0.96 \pm 0.0$.

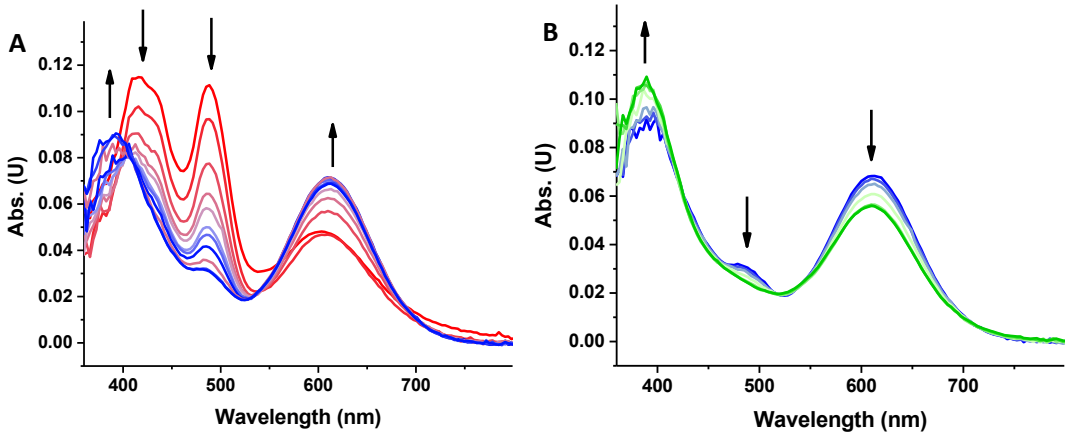

Figure 3.19. Stopped-flow UV-vis kinetics of oxidation of Cu(I)-HPAz by Na_2IrCl_6. (A) First 10 msec and (B) 10 msec to 10 s oxidation of Cu(I)-HPAz by Na_2IrCl_6 monitored by stopped-flow UV-vis at pH 5.0 ammonium acetate buffer.

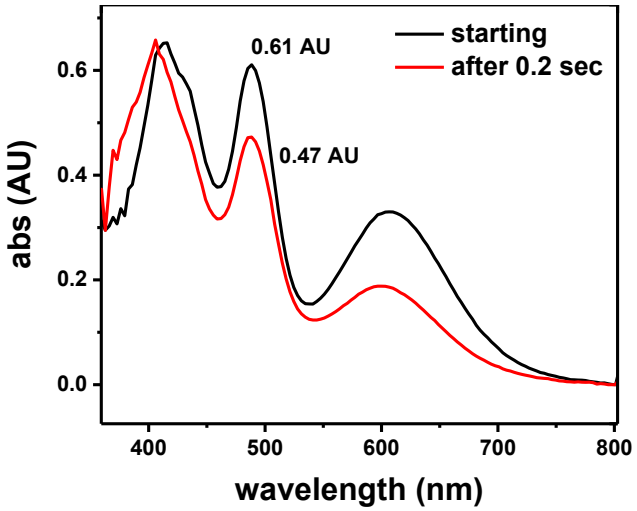

Figure 3.20. 1:1 reaction of Cu(I)-HPAz and Na_2IrCl_6 resulted in ~25% loss of $IrCl_6$ signal after 0.2 sec. The reaction was performed using stopped-flow. 0.2 sec was used as an end-point to measure the %loss of Na_2IrCl_6 for different reactions with a range of molar equivalent Na_2IrCl_6.

To characterize the reaction between Cu(I)-HPAz and Na_2IrCl_6, we used stopped-flow UV-Vis absorption spectroscopy (UV-Vis), aided by global spectral fit using the Specfit program (see Figure 3.21). Upon mixing 0.7 mM Cu(I)-HPAz with 1 equivalent of Na_2IrCl_6 at pH 6.5 in 50 mM phosphate buffer and 0.1 mM NaCl, the absorption bands at 420, 485 and 600 nm due to Na_2IrCl_6 (red line) rapidly decayed, while new absorbance bands at 404 and 610 nm (blue line), typical of a T1 Cu(II) center[136-139], grew in (Figure 3.21a,b). This species (henceforth referred to

as “Blue Cu(II)-HPAz”) reached a maximum at ~ 7 msec and then decreased (Figure 3.21a). As the Blue Cu(II)-HPAz started to decrease, a new species displaying absorption bands at 400 and 607 nm (green line, Figure 3.21a,b) concurrently increased in intensity with time (Figure 3.21c).

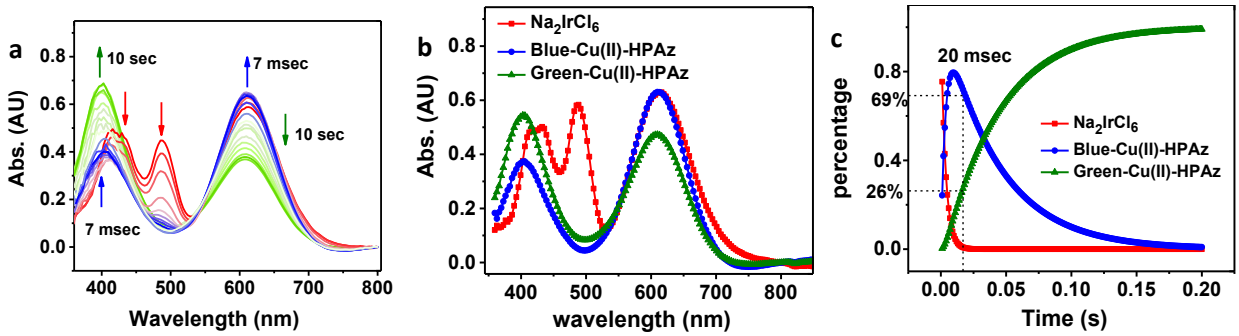

Figure 3.21. Stopped-flow UV-vis spectra of oxidation of 0.7 mM Cu(I)-HPAz by 1 eq Na_2IrCl_6 at pH 6.5 in 50 mM phosphate buffer and 100 mM NaCl. (a) Spectral changes in first 10 s of reaction; (b) Simulated spectra of individual species as determined by the Specfit program. (c) Time-dependent transitions of Na_2IrCl_6, Blue Cu(II)-HPAz and Green Cu(II)-HPAz, as simulated by the Specfit program.

The final spectrum is identical to that observed after direct addition of $CuSO_4$ to apo-HPAz (Figure 3.22), suggesting that it is the final product of the oxidation and the stable form of Cu(II)-HPAz (henceforth called “Green Cu(II)-HPAz”). Because the decay of Na_2IrCl_6 signal is concomitant with formation of Blue Cu(II)-HPAz, and the decay of Blue Cu(II)-HPAz results in growth of Green Cu(II)-HPAz, we used a global spectral fit to confirm the following kinetic process and obtained corresponding rate constants:

$$\text{Cu(I)-HPAz} \xrightarrow[175\ s^{-1}]{Na_2IrCl_6} \text{Blue Cu(II)-HPAz} \xrightarrow[5.3\ s^{-1}]{} \text{Green Cu(II)-HPAz}$$

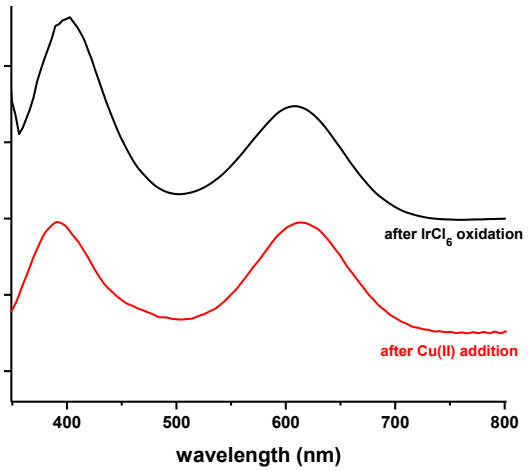

Figure 3.22. Comparison of final species after $IrCl_6$ oxidation of Cu(I)-HPAz and addition of Cu(II) to apo-HPAz.

In order to investigate the integrity of the protein, we re-reduced the green Cu(II)-HPAz and then re-oxidize it. The UV-vis spectrum of the resulting protein is almost identical to that of the starting protein (Figure 3.23), suggesting that there is little damage to the protein from such as redox process and thus making it possible to use the protein as a redox agent.

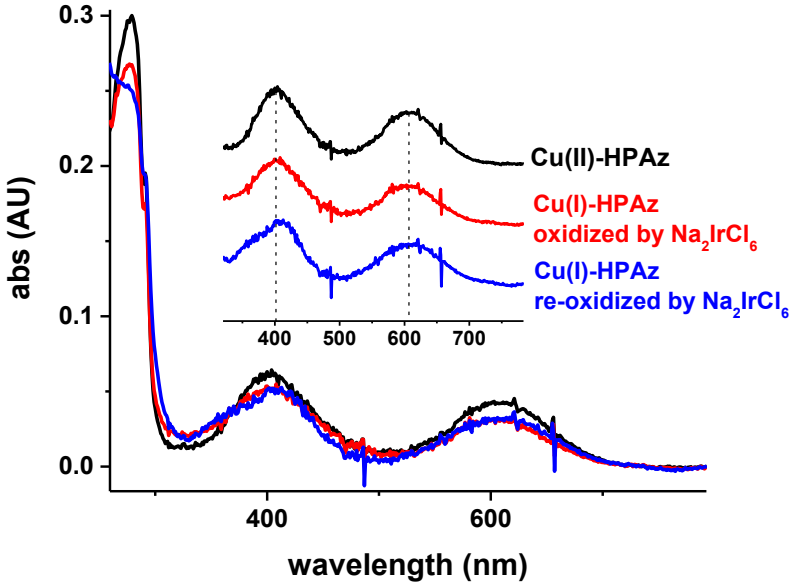

Figure 3.23. Oxidation and reduction studies of the Green-Cu(II)HPAz. The apo-protein loaded with Cu(I) and then oxidized by Na_2IrCl_6 (the red line) shows similar features to Cu(II)-HPAz at resting state (the black line). The protein can go back to the resting state after being reduced by ascorbate and then being oxidized back by Na_2IrCl_6 (the blue line).

3.3.4. Characterizing the intermediates of oxidation reaction

To further probe the nature of the products of the Na_2IrCl_6 oxidation found from the above study, we employed rapid freeze quench electron paramagnetic resonance (EPR) spectroscopy under the same conditions as those used in the stopped-flow UV-Vis study. The minimal achievable time of our freeze quench apparatus was 20 msec, which is slightly slower than the time necessary to form the maximal Blue Cu(II)-HPAz intermediate observed in the stopped-flow UV-Vis (7 msec). At 20 msec after addition of Na_2IrCl_6 to Cu(I)-HPAz, we observed an EPR spectrum (Figure 3.24, top) that can be best simulated as a mixture consisting of 60% T1Cu (g_z = 2.230 and Az = 65.19 cm^{-1}), 39% type 2 (T2) Cu (g_z = 2.309 and Az = 144.81 cm-1) and 1% radical (g_z = 1.992) (Table 3.1). The percentage values for the individual species observed in EPR are consistent with those obtained from stopped flow UV-Vis study (Figure 3.21c): at 20

msec in the stopped flow experiment, 69 % Blue Cu(II)-HPAz and 26 % Green Cu(II)-HPAz were formed.

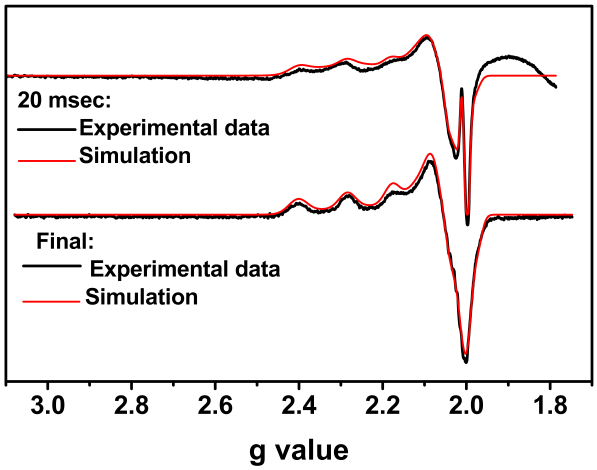

Figure 3.24. EPR spectra of Na_2IrCl_6 oxidation of Cu(I)-HPAz. The top spectra shows freeze-quenched after 20 msec of the reaction and the bottom spectra is the final product of the reaction. The broad feature at less than g = 2.0 in the 20 msec sample is due to packing of the tube during the freeze quench process. Black line: experimental spectra; Dotted red line: simulated spectra.

Table 3.1. EPR simulation parameters of 20 msec freeze quenched sample.

Species	**%**	**g_x, g_y, g_z**	**A_x, A_y, A_z (10^{-4} cm^{-1})**
Final species (T2 Cu like)	39	2.009, 2.079, 2.230	0.14, 11.46, 144.81
T1 Cu like	60	2.021, 2.069, 2.309	23.04, 25.23, 65.19
Free-radical like	1	2.011, 2.003, 1.992	0.00, 0.00, 0.00

At longer time scales, the percentage of the T1 Cu species decreased while that of the T2 Cu species increased. The final EPR spectrum is identical to that of addition of Cu(II) to apo-HPAz (Figure 3.24, bottom, Figure 3.25, and table 3.2). Based on the similar kinetic behavior between the UV-Vis and EPR studies, we assigned the Blue Cu(II)-HPAz to a T1 Cu center, and the Green Cu(II)-HPAz to a T2 Cu center.

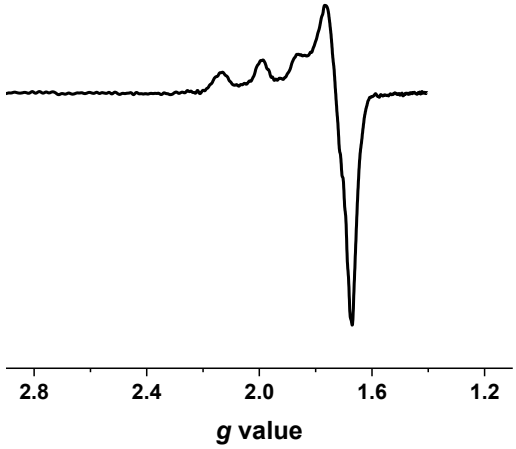

Figure 3.25. EPR spectrum of Cu(II)-HPAz. Sample is at 50 mM phosphate pH6.5 with 100 mM NaCl, recorded at 30 °K.

Table 3.2. Simulation paramters of EPR spectrum of the final product of Cu-HPAz oxidation at 50 mM phosphate pH6.5 with 100 mM NaCl, recorded at 30 °K.

Species	**%**	$\mathbf{g_x, g_y, g_z}$	$\mathbf{A_x, A_y, A_z}$ (10^{-4} cm^{-1})
Final species (T2 like)	74	2.009, 2.079, 2.230	0.14, 11.46, 144.81
T1 like	26	2.021, 2.069, 2.309	23.04, 25.23, 65.19

We have been, thus far, unable to crystalize the Cu(I) or Cu(II) form of the HPAz. Consequently, extended X-Ray absorption fine structure (EXAFS) was employed to obtain structural information. The spectra of the Cu(I)-HPAz and Cu(II)-HPAz species show a clear difference in their edges when overlaid, with the reduced HPAz exhibiting a strong feature at 8983.2 eV (Figure 3.26) that implicates Cu(I)-HPAz as a two-coordinate species, particularly when compared to the edge obtained for other biologically relevant sites, most notably that of the Cys to Ala mutant of *Bacillus subtilis* Sco.[140]

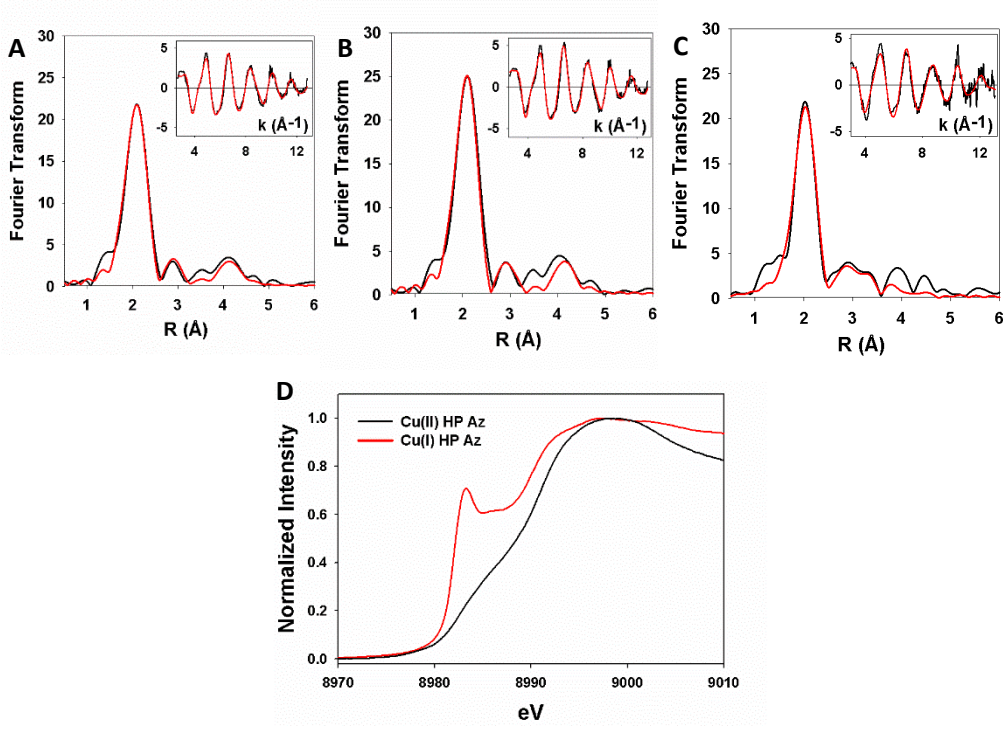

Figure 3.26. EXAFS and XANES analyses of different HpAz variants. Fourier transform and EXAFS (inset) for (a) Cu(I)-HPAz at phosphate buffer pH 6.5, (b) Cu(I)-HPAz at phosphate buffer pH 8, and (c) Cu(II)-HPAz at phosphate buffer pH 6.5. Experimental data are shown as solid black lines and simulation are shown as solid red lines. Parameters used to fit data were shown in Table 1. (c) Normalized edge spectra for (a) (red line) and (c) (black line).

The EXAFS spectrum of Cu(I)-HPAz (in Figure 3.26) was best simulated as one S_{Cys} at 2.17 Å, and one multiple scattering N_{His} at 1.92 Å (Table 3.3). The short Cu(I)-S_{Cys} and Cu-N distances are typical of 2-coordinate Cu(I) species.[140] In contrast, the EXAFS spectrum of Cu(II)-HPAz (Figure 3.26) required the addition of a second N_{His} at 1.98 Å, and the S_{Cys}–Cu bond was lengthened to 2.21 Å. This Cu(II)-S_{Cys} distance is significantly longer than that of Cu(II)-WTAz (2.17 Å), but similar to other thiolate-containing T2 Cu proteins such as nitrosocyanin[141] and Met121Hcy azurin.[125]

Table 3.3. EXAFS fitting parameters.

Sample/fit	F	Cu—S			Cu—N(His)			Cu—S(Met)			E_0
		N	R(Å)	DW(Å^2)	N	R(Å^2)	DW(Å)	N	R(Å^2)	DW(Å)	
Cu(I)-WTAz	0.0003 9	1	2.19	0.002	2	1.97	0.010	1	2.68	0.003	-0.231

Table 3.3 cont.

Cu(I)-HPAz	0.0002 2	1	2.17	0.004	1	1.92	0.010				-0.387
Cu(II)-WTAz	0.0005 1	1	2.17	0.003	2	1.93	0.008	1	2.70	0.006	-2.346
Cu(II)-HPAz	0.0005 6	1	2.23	0.010	2	1.98	0.005				-2.905

Interestingly, we observed that the EXAFS of Cu(I)-HPAz in phosphate buffer at pH 8 (Figure 3.26, Table 3.4) showed an increase in the His contribution to approximately 1.5. This change can be readily observed by comparing the intensity of the His peak in the Fourier transformed spectrum of Cu(I)-HPAz with that of Cu(I)-HPAz at pH 6.5 (Table 3.4). These results suggest that stronger binding of His ligand to the Cu center at high pH, due to deprotonation of the His ligand.

Table 3.4. EXAFS parameters of Cu(I)-HPAz in phosphate buffer pH 8:

Sample/fit	**F**	**Cu—S**			**Cu—N(His)**			**E_0**
		N	**R(Å)**	**DW($Å^2$)**	**N**	**R($Å^2$)**	**DW(Å)**	
Cu(I)-HPAz	0.23	1	2.17	0.003	1.3	1.93	0.003	-0.591

Putting these spectroscopic results together, we propose a scheme in which Cu(I)-HPAz exists as a bi-dentate copper center, with His117 no longer interacting with the copper, as it is the most solvent accessible copper ligand (Scheme 3.1). This result may also explain why the Cu-HPAz showed such a high E°′, because HPAz enforces a coordination sphere that is preferred by Cu(I). Upon oxidation by Na_2IrCl_6, the colorless Cu(I)-HPAz was rapidly oxidized, within the first 7 msec, to a blue species that exhibited UV-vis (Figure 3.21) and EPR (Figure 3.24) spectra that were are typical of a T1 Cu(II) center. To complete the T1 Cu(II) coordination sphere, the His117 rapidly bound to the Cu(II), as indicated by the combined stopped-flow, EPR and EXAFS data, however, because this Cu(II)-HPAz with E°′ of ~ 1V is so oxidizing, it became unstable under physiological conditions and changed its coordination sphere into a more stable green species whose UV-vis (Figure 3.22) and EPR (Figure 3.26) are typical of a T2 Cu(II) center.

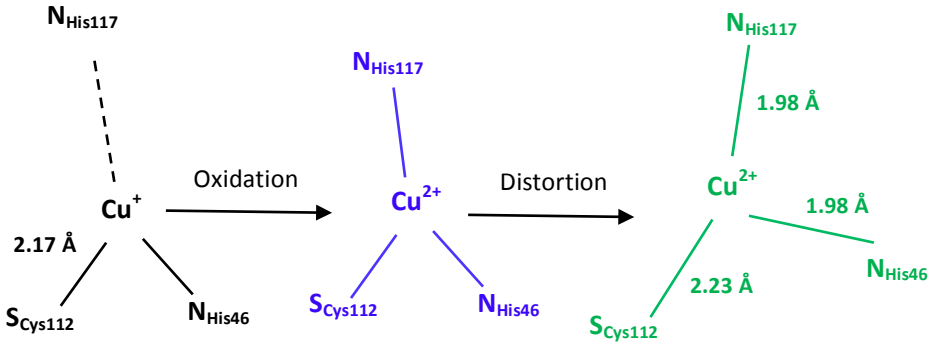

Scheme 3.1. Proposed mechanism for the oxidation of Cu(I)-HPAz with $IrCl_6$.

Although the CV results are obtained at pH 5.0, whereas other characterization are performed at pH 6.5, the similarity between intermediates observed upon reaction of Cu(I)-HPAz with Na_2IrCl_6 at pH 6.5 (Figure 3.21) and 5.0 (Figure 3.19) suggests that the scheme proposed applies to pH 5.0 as well.

3.3.5. Ni substitution in azurin variants and characterization of them

After tuning the T1Cu center in Az to reach the highest possible E°′ under physiological conditions (~ 1V), we explored the next challenge, which is to design azurin to reach the lowest E°′ under physiological conditions (~ -1V). To achieve this goal, we replaced the Cu ion in azurin with other physiologically available metal ions. Azurin, like other cupredoxins, has been shown to be amenable to metal substitutions with minimal perturbation of either the overall structure or the metal-binding site.[27,142] Among the transition metals previously used, the T1Cu in WTAz has been replaced with Ni(II);[116,117,143] the Ni(II)/Ni(I) redox pair has been shown to have much lower potential than the Cu(II)/Cu(I) pair within the same ligand set.[144] Therefore, we added Ni(II) to apo-HPAz. Successful incorporation of Ni(II) into HPAz was first confirmed by UV-vis, and was similar in features to those of Ni(II)-WTAz[143] (Figure 3.27).

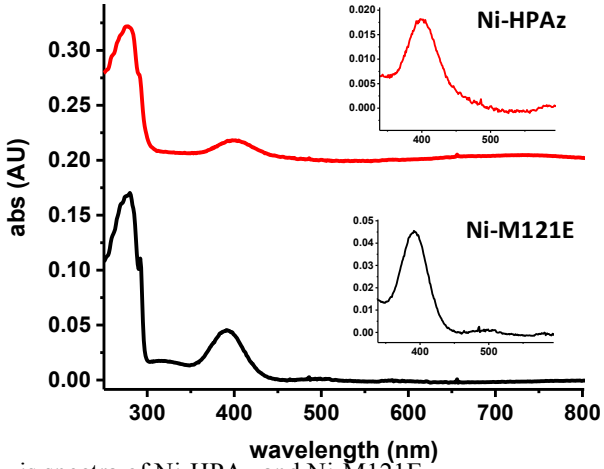

Figure 3.27. Representative UV-vis spectra of Ni-HPAz and Ni-M121E

The CV of this protein indicated an E°′ of 50 mV in pH 8.0 phosphate buffer (see Figure 3.28), which is ~ 900 mV lower than that of Cu(II)/Cu(I)-HPAz. Encouraged by the result, we added Ni(II) to an apo-azurin variant (Met121Glu-Az) whose Cu(II)/Cu(I) redox couple is at a low E°′ (184 mV at pH 8.0).[108] The E°′ of Ni(II)-M121EAz was observed to be -945 mV in pH 8.0 phosphate buffer, which is close to the lowest E°′ possible under physiological conditions.

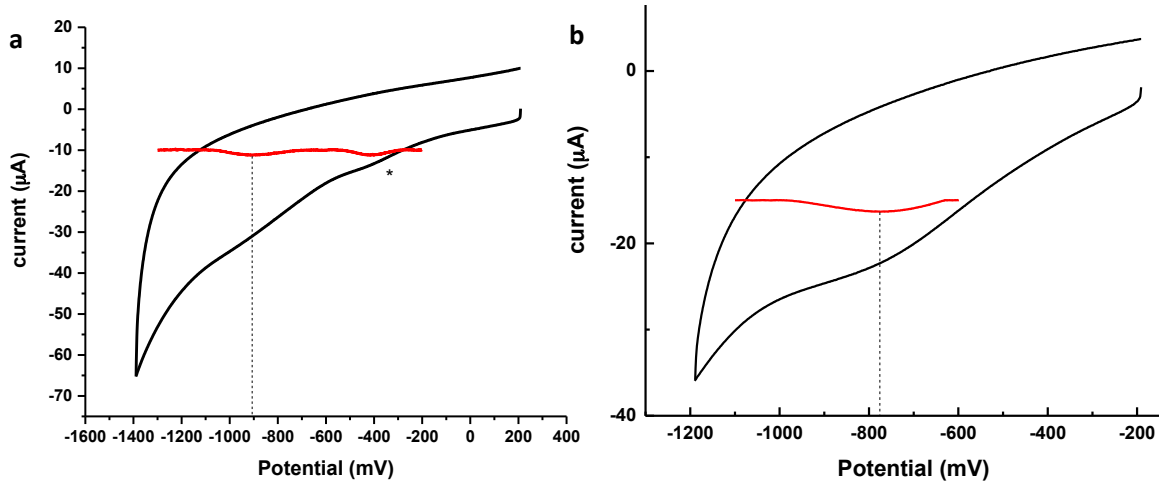

Figure3.28. Representative cyclic voltammagram Ni-Az variants. (a) Ni-Met121Glu and (b) Ni-WTAz, obtained at 100 mM phosphate buffer at pH 8.0 with 100 mM NaCl, at scan rate of 0.1 V/s. The red trace is after subtracting the capacitative current. As shown in the figure only a reductive peak is observable. The peak shown with * in Met121Glu spectra is observed in the blank as well. The values for Ni-loaded Az variants are based on the reductive peak position, as the Ni^{+} state is not stable.

Interestingly, replacing Cu ion with Ni ion in multiple variants of Az nearly always resulted in the lowering of E°′ by ~1000 mV, making the E°′ additive and predictable. In agreement with this trend, the E°′ of Ni-HPAz, measured at 50 mV, is similarly 900 mV below that of Cu-HPAz, providing additional support for the high E°′ of Cu-HPAz.

To confirm that the Ni(II)-Az variants indeed are going through the Ni(II)/Ni(I) transition, I radiated an EPR sample of Ni(II)-Met121Glu under liquid nitrogen temperature. The irradiation of the 20% glycerol in the sample by gamma-rays generated free electrons which then reduced the Ni(II)-Met121Glu. I hoped that since the sample is frozen, the Ni(I)-Met121Glu can be captured and as shown in figure 3.29, that is exactly what happened. The huge signal at g ~ 2 is due to free electrons.

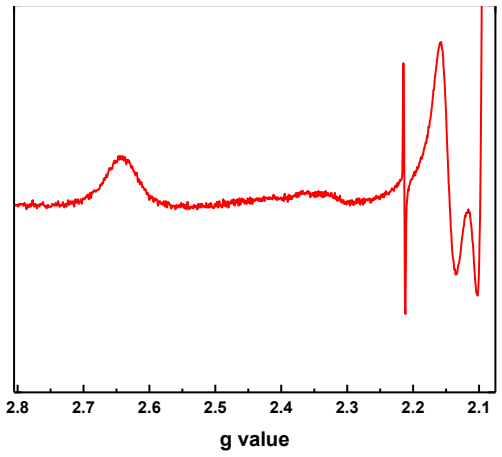

Figure 3.29. EPR of Ni-M121E after cryoreduction shows features of Ni(I). (power 20db, modulation 4, 15 K)

3.4. Summary and conclusion

In summary, by mutating only five residues in the secondary coordination sphere of the mononuclear T1 Cu center in Az and using two metal ions (Cu and Ni), we have achieved fine-tuning of a single protein, Az, whose potentials can expand the entire range of physiological E°′, from ~ +970 ±20 mV to ~ -954 ±50 mV. Before this work, the highest observed E°′ for a natural mononuclear metalloprotein is that of the T1 Cu center in rusticyanin (670 mV at pH7),[145,146] while the highest observed E°′ for a multi-nuclear metalloprotein is that of the T1 Cu center next to the tri-nuclear Cu cluster in laccase (E°′ = 790 mV at pH6).[126,147] The positive charge from the other Cu ions in the multi-copper cluster is known to play a role in raising the E°′ of the T1 Cu

center in laccase over that of mononuclear cupredoxins such as rusticyanin.[127] The E°′ of 970 mV represents the highest E°′ observed under physiological conditions, and approaches the theoretical limit of 1V, before water itself is oxidized. We achieved this goal by tuning hydrogen bonding networks near the Cu center (Asn47Ser and Phe114Asn), adding a hydrophobic residue in the axial position to the Cu center (Met121Leu) and desolvating the Cu center by adding Phe residues to surround it (Met44Phe and Gly116Phe). This result is remarkable, particularly when we consider that it has been accomplished on a mononuclear site without the aid of other positively charged metal ions nearby, as observed in the trinuclear copper center in laccase; such an E°′ exceeds the highest E°' of a natural mononuclear cupredoxin (rusticyanin) by ~ 300 mV. The spectroscopic studies indicate that the Cu(II)-HPAz displays an unusual geometric parameter from those of Az derivatives that has lower or more normal E°′. This is not unexpected for protein with such a high E°′ that is close to the physiological E°′limit at which H_2O can be oxidized. To capture and study metal complexes with very high or low E°′, very low temperature and non-aqueous solution were often employed to stabilize the unusual states. It is remarkable that such an unusually high E°′ can be captured in a protein at room temperature and under physiological condition. Furthermore, by replacing the Cu ion in the above azurin mutants with Ni ion, we can tune the E°′ to as low as -954 mV at pH 8.0, and anywhere in between the two extreme E°′s, by different combinations of these mutations and the metal ions.

In order to cover the entire range of physiological E°′, nature must use at least three different classes of proteins and metal ions (Figure 3.12). The ability to cover the entire physiological range of E°′, and even surpasses the observed E°′ range for all ET proteins combined, using two metal ions and mutating only five residues in a single protein scaffold (Figure 3.12) is a testimony of how much we now understand the structural features responsible for tuning E°′ of metalloproteins. Given the wide range of potentials attainable from a single protein possessing the same overall fold and surface properties, the azurin variants reported in this study may enable scientists and engineers to take advantage of these water-soluble redox agents for biochemical and biotechnological applications such as solar energy transfer and other alternative energy conversions. Since tuning the potentials of many inorganic, bioinorganic and organometallic catalysts can result in catalysts with different oxidation states with dramatically different catalytic efficiency for different substrates,[148] the knowledge gained from this study may also allow others to use the same principle to tune redox properties of numerous catalysts

for even wider applications, such as small molecule activation and synthesis of important intermediates or products for pharmaceutical applications.

3.5. References

(1) Zanello, P. *Inorganic Electrochemistry: Theory, Practice and Application*; Royal Society of Chemistry, 2003.
(2) Marcus, R. A. Electron-transfer reactions in chemistry: theory and experiment (Nobel lecture);*Angew. Chem. Int. Ed.* **1993**, *32*, 1111.
(3) Noy, D.; Moser, C. C.; Dutton, P. L. Design and engineering of photosynthetic light-harvesting and electron transfer using length, time, and energy scales;*Biochim. Biophys. Acta* **2006**, *1757*, 90.
(4) Kärkäs, M. D.; Verho, O.; Johnston, E. V.; Akermark, B. Artificial photosynthesis: molecular systems for catalytic water oxidation;*Chem. Rev.* **2014**, *114*, 11863.
(5) Nelson, N.; Ben-Shem, A. The complex architecture of oxygenic photosynthesis;*Nat. Rev. Mol. Cell. Biol.* **2004**, *5*, 971.
(6) Barber, J.; Tran, P. D. From natural to artificial photosynthesis;*J. R. Soc. Interface* **2013**, *10*, 20120984.
(7) Moser, C. C.; Keske, J. M.; Warncke, K.; Farid, R. S.; Dutton, P. L. Nature of Biological Electron-Transfer;*Nature* **1992**, *355*, 796.
(8) Blankenship, R. E. Origin and early evolution of photosynthesis;*Photosynth. Res.* **1992**, *33*, 91.
(9) Wraight, C. A. Chance and design--proton transfer in water, channels and bioenergetic proteins;*Biochim. Biophys. Acta* **2006**, *1757*, 886.
(10) Lenaz, G.; Genova, M. L. Structure and organization of mitochondrial respiratory complexes: a new understanding of an old subject;*Antioxid. Redox. Signal.* **2010**, *12*, 961.
(11) Kim, H. J.; Khalimonchuk, O.; Smith, P. M.; Winge, D. R. Structure, function, and assembly of heme centers in mitochondrial respiratory complexes;*Biochim. Biophys. Acta* **2012**, *1823*, 1604.
(12) Gunner, M. R.; Amin, M.; Zhu, X.; Lu, J. Molecular mechanisms for generating transmembrane proton gradients;*Biochim. Biophys. Acta* **2013**, *1827*, 892.
(13) Yoshikawa, S.; Shimada, A. Reaction Mechanism of Cytochrome c Oxidase;*Chem. Rev.* **2015**, *115*, 1936.
(14) Murray, R. I.; Fisher, M. T.; Debrunner, P. G.; Sligar, S. G. Structure and chemistry of cytochrome P-450;*Top. Mol. Struct. Biol.* **1985**, *6*, 157.
(15) Sligar, S. G. Nature's universal oxygenases: the cytochromes P450;*Essays Biochem.* **1999**, *34*, 71.
(16) Coon, M. J. Cytochrome P450: nature's most versatile biological catalyst;*Annu. Rev. Pharmacol. Toxicol.* **2005**, *45*, 1.
(17) Denisov, I. G.; Makris, T. M.; Sligar, S. G.; Schlichting, I. Structure and chemistry of cytochrome P 450;*Chem. Rev.* **2005**, *105*, 2253.
(18) Schuler, M. A.; Sligar, S. G. Diversities and similarities in P450 systems: an introduction;*Met. Ions Life Sci.* **2007**, *3*, 1.
(19) Denisov, I. G.; Sligar, S. G. In *Handbook of Porphyrin Science*; Kadish, K. M., Smith, K. M., Guilard, R., Eds.; World Scientific Publishing Co. Pte. Ltd.: 2010; Vol. 5, p 165.
(20) Jung, S. T.; Lauchli, R.; Arnold, F. H. Cytochrome P 450: taming a wild type enzyme;*Curr. Opin. Biotechnol.* **2011**, *22*, 809.
(21) Poulos, T. L. Heme Enzyme Structure and Function;*Chem. Rev.* **2014**, *114*, 3919.
(22) Link, T. A. The role of the 'Rieske' iron sulfur protein in the hydroquinone oxidation (QP) site of the cytochrome bc1 complex. The 'proton-gated affinity change' mechanism;*FEBS Lett.* **1997**, *412*, 257.
(23) Link, T. A. The structures of Rieske and Rieske-type proteins.;*Adv. Inorg. Chem.* **1999**, *47*, 83.
(24) Hsueh, K. L.; Tonelli, M.; Cai, K.; Westler, W. M.; Markley, J. L. Electron transfer mechanism of the Rieske protein from Thermus thermophilus from solution nuclear magnetic resonance investigations;*Biochemistry* **2013**, *52*, 2862.
(25) De, P., Antonio R.; Jelesarov, I.; Ackermann, F.; Koppenol, W. H.; Hirasawa, M.; Knaff, D. B.; Bosshard, H. R. Binding of ferredoxin to ferredoxin:NADP+ oxidoreductase: The role of carboxyl groups, electrostatic surface potential, and molecular dipole moment.;*Protein Sci.* **1993**, *2*, 1126.
(26) Hase, T.; Schurmann, P.; Knaff, D. B. The interaction of ferredoxin with ferredoxin-dependent enzymes.;*Adv. Photosynth. Respir.* **2006**, *24*, 477.
(27) Liu, J.; Chakraborty, S.; Hosseinzadeh, P.; Yu, Y.; Tian, S.; Petrik, I.; Bhagi, A.; Lu, Y. Metalloproteins containing cytochrome, iron-sulfur, or copper redox centers;*Chem. Rev.* **2014**, *114*, 4366.
(28) Langen, R.; Jensen, G. M.; Jacob, U.; Stephens, P. J.; Warshel, A. Protein control of iron-sulfur cluster redox potentials.;*J. Biol. Chem.* **1992**, *267*, 25625.
(29) Cowan, J. A.; Lui, S. M. Structure-function correlations in high-potential iron proteins;*Adv. Inorg. Chem.* **1998**, *45*, 313.
(30) Venkateswara, R. P.; Holm, R. H. Synthetic analogues of the active sites of iron-sulfur proteins;*Chem. Rev.* **2004**, *104*, 527.
(31) Carter, C. W. In *Handbook of Metalloproteins*; John Wiley & Sons, Ltd: 2006.
(32) Holden, H. M.; Jacobson, B. L.; Hurley, J. K.; Tollin, G.; Oh, B. H.; Skjeldal, L.; Chae, Y. K.; Cheng, H.; Xia, B.; Markley, J. L. Structure-function studies of [2Fe-2S] ferredoxins.;*J. Bioenerg. Biomembr.* **1994**, *26*, 67.
(33) Meyer, J. Ferredoxins of the third kind.;*FEBS Lett.* **2001**, *509*, 1.
(34) Meyer, J.; Andrade, S. L.; Einsle, O. In *Handbook of Metalloproteins*; John Wiley & Sons, Ltd: 2006.

(35) Binda, C.; Aliverti, A. In *Encyclopedia of Inorganic and Bioinorganic Chemistry*; John Wiley & Sons, Ltd: 2011.
(36) Wilson, T. D.; Yu, Y.; Lu, Y. Understanding Copper-thiolate Containing Electron Transfer Centers by Incorporation of Unnatural Amino Acids and the CuA Center into the Type 1 Copper Protein Azurin;*Coord. Chem. Rev.* **2012**, *257*, 260.
(37) Park, J.-S.; Ohmura, T.; Kano, K.; Sagara, T.; Niki, K.; Kyogoku, Y.; Akutsu, H. Regulation of the redox order of four hemes by pH in cytochrome C3 from D. vulgaris Miyazaki F;*Biochim. Biophys. Acta* **1996**, *1293*, 45.
(38) Chapman, S.; Daff, S.; Munro, A. In *Metal Sites in Proteins and Models*; Hill, H. A. O., Sadler, P. J., Thomson, A. J., Eds.; Springer Berlin Heidelberg: 1997; Vol. 88, p 39.
(39) Martel, P. J.; Soares, C. M.; Baptista, A. M.; Fuxreiter, M.; Náray-Szabó, G.; Louro, R. O.; Carrondo, M. A. Comparative redox and pK a calculations on cytochrome c 3 from several Desulfovibrio species using continuum electrostatic methods;*J. Biol. Inorg. Chem.* **1999**, *4*, 73.
(40) Santos, H.; Moura, J. J. G.; Moura, I.; LeGall, J.; Xavier, A. V. NMR studies of electron transfer mechanisms in a protein with interacting redox centres: Desulfovibrio gigas cytochrome c3;*Eur. J. Biochem.* **1984**, *141*, 283.
(41) Fan, K. J.; Akutsu, H.; Kyogoku, Y.; Niki, K. Estimation of microscopic redox potentials of a tetraheme protein, cytochrome c3 of Desulfovibrio vulgaris, Miyazaki F, and partial assignments of heme groups;*Biochemistry* **1990**, *29*, 2257.
(42) Coletta, M.; Catarino, T.; LeGall, J.; Xavier, A. V. A thermodynamic model for the cooperative functional properties of the tetraheme cytochrome c3 from Desulfovibrio gigas;*Eur. J. Biochem.* **1991**, *202*, 1101.
(43) Takayama, Y.; Taketa-Sato, M.; Komori, H.; Morita, K.; Kang, S.-J.; Higuchi, Y.; Akutsu, H. Role of π-Electron Systems in Stabilization of the Oxidized Tetraheme Architecture in Cytochrome c₃;*Bull. Chem. Soc. Jpn.* **2011**, *84*, 1096.
(44) Sligar, S. G.; Egeberg, K. D.; Sage, J. T.; Morikis, D.; Champion, P. M. Alteration of heme axial ligands by site-directed mutagenesis: a cytochrome becomes a catalytic demethylase;*J. Am. Chem. Soc.* **1987**, *109*, 7896.
(45) Gunsalus, I. C.; Meeks, J. R.; Lipscomb, J. D.; Debrunner, P.; Muenck, E. In *molecular mechanism of oxygen activation*; Academic: 1974, p 559.
(46) Bewley, K. D.; Ellis, K. E.; Firer-Sherwood, M. A.; Elliott, S. J. Multi-heme proteins: nature's electronic multi-purpose tool;*Biochim Biophys Acta* **2013**, *1827*, 938.
(47) Lu, Y. In *Comprehensive Coordination Chemistry II*; McCleverty, J. A., Meyer, T. J., Eds.; Elsevier: Pergamon: Oxford, 2003; Vol. 8, p 91.
(48) Battistuzzi, G.; Bellei, M.; Bortolotti, C. A.; Sola, M. Redox properties of heme peroxidases;*Arch. Biochem. Biophys.* **2010**, *500*, 21.
(49) Williams, R. J. P. In *Iron in Biochemistry and medicine*; Jacobs, A., Warwood, M., Eds.; Academic: 1974, p 183.
(50) Adachi, S.; Nagano, S.; Watanabe, Y.; Ishimori, K.; Morishima, I. Alteration of human myoglobin proximal histidine to cysteine or tyrosine by site-directed mutagenesis: characterization and their catalytic activities;*Biochem. Biophys. Res. Commun.* **1991**, *180*, 138.
(51) Reedy, C. J.; Elvekrog, M. M.; Gibney, B. R. Development of a heme protein structure-electrochemical function database;*Nucleic Acids Res.* **2008**, *36*, D307.
(52) Zheng, Z.; Gunner, M. R. Analysis of the electrochemistry of hemes with E(m)s spanning 800 mV;*Proteins* **2009**, *75*, 719.
(53) Piontek, K.; Glumoff, T.; Winterhalter, K. Low pH crystal structure of glycosylated lignin peroxidase from Phanerochaete chrysosporium at 2.5 Ã… resolution;*FEBS Lett.* **1993**, *315*, 119.
(54) Banci, L. Structural properties of peroxidases;*J. Biotechnol.* **1997**, *53*, 253.
(55) Balk, J.; Lill, R. The Cell's Cookbook For Iron–Sulfur Clusters: Recipes For Fool's Gold?;*ChemBioChem* **2004**, *5*, 1044.
(56) Werth, M. T.; Cecchini, G.; Manodori, A.; Ackrell, B. A.; Schroder, I.; Gunsalus, R. P.; Johnson, M. K. Site-directed mutagenesis of conserved cysteine residues in Escherichia coli fumarate reductase: modification of the spectroscopic and electrochemical properties of the [2Fe-2S] cluster;*Proc Natl Acad Sci U S A* **1990**, *87*, 8965.
(57) Iismaa, S. E.; Vazquez, A. E.; Jensen, G. M.; Stephens, P. J.; Butt, J. N.; Armstrong, F. A.; Burgess, B. K. Site-directed mutagenesis of Azotobacter vinelandii ferredoxin I. Changes in [4Fe-4S] cluster reduction potential and reactivity;*J. Biol. Chem.* **1991**, *266*, 21563.
(58) Cheng, H.; Xia, B.; Reed, G. H.; Markley, J. L. Optical, EPR, and 1H NMR spectroscopy of serine-ligated [2Fe-2S] ferredoxins produced by site-directed mutagenesis of cysteine residues in recombinant Anabaena 7120 vegetative ferredoxin;*Biochemistry* **1994**, *33*, 3155.
(59) Raphael, A. L.; Gray, H. B. Axial ligand replacement in horse heart cytochrome c by semisynthesis;*Proteins Struct. Funct. Bioinformat.* **1989**, *6*, 338.
(60) Miller, G. T.; Zhang, B.; Hardman, J. K.; Timkovich, R. Converting a c-type to a b-type cytochrome: Met61 to His61 mutant of Pseudomonas cytochrome c-551;*Biochemistry* **2000**, *39*, 9010.
(61) Hay, S.; Wydrzynski, T. Conversion of the Escherichia coli Cytochrome b562 to an Archetype Cytochrome b: A Mutant with Bis-Histidine Ligation of Heme Iron†;*Biochemistry* **2004**, *44*, 431.
(62) Dolla, A.; Blanchard, L.; Guerlesquin, F.; Bruschi, M. The protein moiety modulates the redox potential in cytochromes c;*Biochimie* **1994**, *76*, 471.
(63) Tezcan, F. A.; Winkler, J. R.; Gray, H. B. Effects of Ligation and Folding on Reduction Potentials of Heme Proteins;*J. Am. Chem. Soc.* **1998**, *120*, 13383.
(64) Funk, W. D.; Lo, T. P.; Mauk, M. R.; Brayer, G. D.; MacGillivray, R. T.; Mauk, A. G. Mutagenic, electrochemical, and crystallographic investigation of the cytochrome b5 oxidation-reduction equilibrium: involvement of asparagine-57, serine-64, and heme propionate-7;*Biochemistry* **1990**, *29*, 5500.

(65) Springs, S. L.; Bass, S. E.; McLendon, G. L. Cytochrome b562 variants: a library for examining redox potential evolution;*Biochemistry* **2000**, *39*, 6075.
(66) Holm, R. H.; Kennepohl, P.; Solomon, E. I. Structural and Functional Aspects of Metal Sites in Biology;*Chem. Rev.* **1996**, *96*, 2239.
(67) Senge, M. O. Exercises in molecular gymnastics-bending, stretching and twisting porphyrins.;*Chem. Commun.* **2006**, 243.
(68) Roder, B.; Buchner, M.; Ruckmann, I.; Senge, M. O. Correlation of photophysical parameters with macrocycle distortion in porphyrins with graded degree of saddle distortion;*Photochem. Photobiol. Sci.* **2010**, *9*, 1152.
(69) Senge, M. O. The conformational flexibility of tetrapyrroles - current model studies and photobiological relevance.;*J. Photochem. Photobiol., B* **1992**, *16*, 3.
(70) Hobbs, J.; Shelnutt, J. Conserved nonplanar heme distortions in cytochromesc;*J. Protein Chem.* **1995**, *14*, 19.
(71) Jentzen, W.; Ma, J.-G.; Shelnutt, J. A. Conservation of the conformation of the porphyrin macrocycle in hemoproteins.;*Biophys. J.* **1998**, *74*, 753.
(72) Ma, J. G.; Laberge, M.; Song, X. Z.; Jentzen, W.; Jia, S. L.; Zhang, J.; Vanderkooi, J. M.; Shelnutt, J. A. Protein-induced changes in nonplanarity of the porphyrin in nickel cytochrome *c* probed by resonance Raman spectroscopy;*Biochemistry* **1998**, *37*, 5118.
(73) Todd, L. N.; Zimmer, M. Moderating influence of proteins on nonplanar tetrapyrrole deformations: coenzyme F430 in methyl-coenzyme-M reductase;*Inorg. Chem.* **2002**, *41*, 6831.
(74) Olea, C., Jr.; Kuriyan, J.; Marletta, M. A. Modulating heme redox potential through protein-induced porphyrin distortion;*J. Am. Chem. Soc.* **2010**, *132*, 12794.
(75) Can, M.; Zoppellaro, G.; Andersson, K. K.; Bren, K. L. Modulation of ligand-field parameters by heme ruffling in cytochromes *c* revealed by EPR spectroscopy;*Inorg. Chem.* **2011**, *50*, 12018.
(76) Link, T. A. In *Adv. Inorg. Chem.*; Sykes, A. G., Ed.; Academic Press: 1999; Vol. Volume 47, p 83.
(77) Backes, G.; Mino, Y.; Loehr, T. M.; Meyer, T. E.; Cusanovich, M. A.; Sweeney, W. V.; Adman, E. T.; Sanders-Loehr, J. The environment of Fe4S4 clusters in ferredoxins and high-potential iron proteins. New information from x-ray crystallography and resonance Raman spectroscopy;*J. Am. Chem. Soc.* **1991**, *113*, 2055.
(78) Duee, E. D.; Fanchon, E.; Vicat, J.; Sieker, L. C.; Meyer, J.; Moulis, J. M. Refined crystal structure of the 2[4Fe-4S] ferredoxin from Clostridium acidurici at 1.84 Å resolution;*J Mol Biol* **1994**, *243*, 683.
(79) Dauter, Z.; Wilson, K. S.; Sieker, L. C.; Meyer, J.; Moulis, J. M. Atomic resolution (0.94 Å) structure of Clostridium acidurici ferredoxin. Detailed geometry of [4Fe-4S] clusters in a protein;*Biochemistry* **1997**, *36*, 16065.
(80) Stout, C. D.; Stura, E. A.; McRee, D. E. Structure of Azotobacter vinelandii 7Fe ferredoxin at 1.35 Å resolution and determination of the [Fe-S] bonds with 0.01 Å accuracy;*J. Mol. Biol.* **1998**, *278*, 629.
(81) Link, T. A.; Hagen, W. R.; Pierik, A. J.; Assmann, C.; Von Jagow, G. Determination of the redox properties of the Rieske [2Fe-2S] cluster of bovine heart bc1 complex by direct electrochemistry of a water-soluble fragment;*Eur. J. Biochem.* **1992**, *208*, 685.
(82) Cammack, R.; Rao, K. K.; Bargeron, C. P.; Hutson, K. G.; Andrew, P. W.; Rogers, L. J. Midpoint redox potentials of plant and algal ferredoxins;*Biochem. J.* **1977**, *168*, 205.
(83) Lu, Y. In *Biocoordination Chemistry*; Que, J. L., Tolman, W. B., Meyer, T. J., Eds.; Elsevier: Oxford, UK, 2004; Vol. 8; 8, p 91.
(84) Choi, M.; Davidson, V. L. Cupredoxins-a study of how proteins may evolve to use metals for bioenergetic processes.;*Metallomics* **2011**, *3*, 140.
(85) Gray, H. B.; Malmstrom, B. G.; Williams, R. J. Copper coordination in blue proteins;*J. Biol. Inorg. Chem.* **2000**, *5*, 551.
(86) Vila, A. J.; Fernandez, C. O. In *Handbook on Metalloproteins*; Bertini, I., Sigel, A., Sigel, H., Eds.; Marcel Dekker: New York, NY, 2001, p 813.
(87) Solomon, E. I.; Szilagyi, R. K.; DeBeer George, S.; Basumallick, L. Electronic Structures of Metal Sites in Proteins and Models: Contributions to Function in Blue Copper Proteins;*Chem. Rev.* **2004**, *104*, 419.
(88) Dennison, C. Investigating the structure and function of cupredoxins.;*Coord. Chem. Rev.* **2005**, *249*, 3025.
(89) Kassner, R. J. Effects of nonpolar environments on the redox potentials of heme complexes;*Proc. Natl. Acad. Sci. U S A* **1972**, *69*, 2263.
(90) Stellwagen, E. Haem exposure as the determinate of oxidation-reduction potential of haem proteins;*Nature* **1978**, *275*, 73.
(91) Churg, A. K.; Warshel, A. Control of the redox potential of cytochrome c and microscopic dielectric effects in proteins;*Biochemistry* **1986**, *25*, 1675.
(92) Rivera, M.; Seetharaman, R.; Girdhar, D.; Wirtz, M.; Zhang, X.; Wang, X.; White, S. The reduction potential of cytochrome b5 is modulated by its exposed heme edge;*Biochemistry* **1998**, *37*, 1485.
(93) Fantuzzi, A.; Sadeghi, S.; Valetti, F.; Rossi, G. L.; Gilardi, G. Tuning the reduction potential of engineered cytochrome c-553;*Biochemistry* **2002**, *41*, 8718.
(94) Battistuzzi, G.; Borsari, M.; Canters, G. W.; de Waal, E.; Leonardi, A.; Ranieri, A.; Sola, M. Thermodynamics of the Acid Transition in Blue Copper Proteins;*Section Title: General Biochemistry* **2002**, *41*, 14293.
(95) Paoli, M.; Marles-Wright, J.; Smith, A. Structure-function relationships in heme-proteins;*DNA Cell Biol.* **2002**, *21*, 271.
(96) Rodgers, K. K.; Sligar, S. G. Surface electrostatics, reduction potentials, and the internal dielectric constant of proteins;*J. Am. Chem. Soc.* **1991**, *113*, 9419.
(97) DiCarlo, C. M.; Vitello, L. B.; Erman, J. E. Reduction potential shifts due to active site and surface mutations of yeast cytochrome *c* peroxidase;*ECS Trans.* **2007**, *6*, 27.

(98) Jensen, G. M.; Warshel, A.; Stephens, P. J. Calculation of the redox potentials of iron-sulfur proteins: the 2-/3-couple of [Fe4S*4Cys4] clusters in Peptococcus aerogenes ferredoxin, Azotobacter vinelandii ferredoxin I, and Chromatium vinosum high-potential iron protein;*Biochemistry* **1994**, *33*, 10911.
(99) Banci, L.; Bertini, I.; Ciurli, S.; Luchinat, C.; Pierattelli, R. Rationalization of the reduction potentials within the series of the high potential iron-sulfur proteins;*Inorg. Chim. Acta* **1995**, *240*, 251.
(100) Garner, D. K.; Vaughan, M. D.; Hwang, H. J.; Savelieff, M. G.; Berry, S. M.; Honek, J. F.; Lu, Y. Reduction potential tuning of the blue copper center in Pseudomonas aeruginosa azurin by the axial Methionine as probed by unnatural amino acids;*J. Am. Chem. Soc.* **2006**, *128*, 15608.
(101) Liu, X.; Yu, Y.; Hu, C.; Zhang, W.; Lu, Y.; Wang, J. Significant Increase of Oxidase Activity through the Genetic Incorporation of a Tyrosine-Histidine Cross-Link in a Myoglobin Model of Heme-Copper Oxidase.;*Angew. Chem. Int. Ed.* **2012**, *51*, 4312.
(102) Yu, Y.; Lv, X.; Li, J.; Zhou, Q.; Cui, C.; Hosseinzadeh, P.; Mukherjee, A.; Nilges, M. J.; Wang, J.; Lu, Y. Defining the role of tyrosine and rational tuning of oxidase activity by genetic incorporation of unnatural tyrosine analogs;*J. Am. Chem. Soc.* **2015**, *137*, 4594.
(103) Yu, Y.; Zhou, Q.; Wang, L.; Liu, X.; Zhang, W.; Hu, M.; Dong, J.; Li, J.; Lv, X.; Ouyang, H.; Li, H.; Gao, F.; Gong, W.; Lu, Y.; Wang, J. Significant improvement of oxidase activity through the genetic incorporation of a redox-active unnatural amino acid;*Chem. Sci.* **2015**.
(104) Low, D. W.; Hill, M. G. Backbone-Engineered High-Potential Iron Proteins: Effects of Active-Site Hydrogen Bonding on Reduction Potential;*J. Am. Chem. Soc.* **2000**, *122*, 11039.
(105) Bhagi-Damodaran, A.; Petrik, I. D.; Marshall, N. M.; Robinson, H.; Lu, Y. Systematic Tuning of Heme Redox Potentials and Its Effects on O2 Reduction Rates in a Designed Oxidase in Myoglobin;*J. Am. Chem. Soc.* **2014**, *136*, 11882.
(106) He, B.; Sinclair, R.; Copeland, B. R.; Makino, R.; Powers, L. S.; Yamazaki, I. The structure-function relationship and reduction potentials of high oxidation states of myoglobin and peroxidase;*Biochemistry* **1996**, *35*, 2413.
(107) Varadarajan, R.; Zewert, T. E.; Gray, H. B.; Boxer, S. G. Effects of buried ionizable amino acids on the reduction potential of recombinant myoglobin;*Science* **1989**, *243*, 69.
(108) Pascher, T.; Karlsson, B. G.; Nordling, M.; Malmström, B. G.; Vänngård, T. Reduction potentials and their pH dependence in site-directed-mutant forms of azurin from Pseudomonas aeruginosa;*Eur. J. Biochem.* **1993**, *212*, 289.
(109) Miller, A.-F. Redox tuning over almost 1 V in a structurally conserved active site: lessons from Fe-containing superoxide dismutase;*Acc. Chem. Res.* **2008**, *41*, 501.
(110) Marshall, N. M.; Garner, D. K.; Wilson, T. D.; Gao, Y.-G.; Robinson, H.; Nilges, M. J.; Lu, Y. Rationally tuning the reduction potential of a single cupredoxin beyond the natural range;*Nature* **2009**, *462*, 113.
(111) Zuris, J. A.; Halim, D. A.; Conlan, A. R.; Abresch, E. C.; Nechushtai, R.; Paddock, M. L.; Jennings, P. A. Engineering the redox potential over a wide range within a new Class of FeS proteins;*J. Am. Chem. Soc.* **2010**, *132*, 13120.
(112) Humphrey, W.; Dalke, A.; Schulten, K. VMD: Visual molecular dynamics;*Journal of Molecular Graphics* **1996**, *14*, 33.
(113) Phillips, J. C.; Braun, R.; Wang, W.; Gumbart, J.; Tajkhorshid, E.; Villa, E.; Chipot, C.; Skeel, R. D.; Kale, L.; Schulten, K. Scalable molecular dynamics with NAMD;*J. Comput. Chem.* **2005**, *26*, 1781.
(114) Hay, M.; Richards, J. H.; Lu, Y. Construction and characterization of an azurin analog for the purple copper site in cytochrome c oxidase;*Proc. Natl. Acad. Sci. U S A* **1996**, *93*, 461.
(115) Lancaster, K. M.; DeBeer George, S.; Yokoyama, K.; Richards, J. H.; Gray, H. B. Type-zero copper proteins;*Nat Chem* **2009**, *1*, 711.
(116) Czernuszewicz, R. S.; Fraczkiewicz, G.; Zareba, A. A. A detailed resonance Raman spectrum of Nickel(II)-substituted Pseudomonas aeruginosa azurin;*Inorg Chem* **2005**, *44*, 5745.
(117) Moratal, J. M.; Romero, A.; Salgado, J.; Perales-Alarcon, A.; Jimenez, H. R. The crystal structure of nickel(II)-azurin;*Eur. J. Biochem.* **1995**, *228*, 653.
(118) Lide, D. R.; Frederikse, H. P. R. *Handbook of Chemistry and Physics*; CRC Press, 1997.
(119) Abbaspour, A.; Mehrgardi, M. A. Electrocatalytic activity of Ce(III)-EDTA complex toward the oxidation of nitrite ion;*Talanta* **2005**, *67*, 579.
(120) Bossu, F. P.; Chellappa, K. L.; Margerum, D. W. Ligand effects on the thermodynamic stabilization of copper(III)-peptide complexes;*J. Am. Chem. Soc.* **1977**, *99*, 2195.
(121) Robert, S.; Peter, Y. E. H.; Theodore, K. In *Electrochemical Studies of Biological Systems*; AMERICAN CHEMICAL SOCIETY: 1977; Vol. 38, p 143.
(122) Sieracki, N. A.; Hwang, H. J.; Lee, M. K.; Garner, D. K.; Lu, Y. A temperature independent pH (TIP) buffer for biomedical biophysical applications at low temperatures;*Chem Commun (Camb)* **2008**, 823.
(123) George, G. N.; Stanford Synchrotron Radiation Laboratory: Menlo Park, CA, 1990.
(124) Binsted, N.; Gurman, S. J.; Campbell, J. W.; Laboratory, D., Ed. Warrington, UK, 1998; Vol. 9.2.
(125) Clark, K. M.; Yu, Y.; Marshall, N. M.; Sieracki, N. A.; Nilges, M. J.; Blackburn, N. J.; van, d. D. W. A.; Lu, Y. Transforming a blue copper into a red copper protein: engineering cysteine and homocysteine into the axial position of azurin using site-directed mutagenesis and expressed protein ligation;*J. Am. Chem. Soc.* **2010**, *132*, 10093.
(126) Davies, G. J.; Ducros, V. In *Handbook of Metalloproteins*; Messerschmid, A., Huber, R., Poulos, T., Wieghardt, K., Eds.; Wiley: Chichester, 2001; Vol. 2; 2, p 1359.
(127) Solomon, E. I.; Sundaram, U. M.; Machonkin, T. E. Multicopper Oxidases and Oxygenases;*Chem. Rev.* **1996**, *96*, 2563.
(128) Kennedy, M. L.; Gibney, B. R. Metalloprotein and redox protein design;*Curr. Opin. Struct. Biol.* **2001**, *11*, 485.

(129) Dey, A.; Jenney, F. E. J.; Adams, M. W. W.; Babini, E.; Takahashi, Y.; Fukuyama, K.; Hodgson, K. O.; Hedman, B.; Solomon, E. I. Solvent tuning of electrochemical potentials in the active sites of HiPIP versus ferredoxin;*Science* **2007**, *318*, 1464.
(130) Berry, S. M.; Baker, M. H.; Reardon, N. J. Reduction potential variations in azurin through secondary coordination sphere phenylalanine incorporations.;*J. Inorg. Biochem.* **2010**, *104*, 1071.
(131) Hong, G.; Ivnitski, D. M.; Johnson, G. R.; Atanassov, P.; Pachter, R. Design Parameters for Tuning the Type 1 Cu Multicopper Oxidase Redox Potential: Insight from a Combination of First Principles and Empirical Molecular Dynamics Simulations;*J. Am. Chem. Soc.* **2011**, *133*, 4802.
(132) Dryhurst, G.; Kadish, K. M.; Scheller, f.; Renneberg, R. In *Biological electrochemistry*; Academic Press, Inc.: New York, 1982; Vol. 1, p 398.
(133) Elliott, S. J.; Leger, C.; Pershad, H. R.; Hirst, J.; Heffron, K.; Ginet, N.; Blasco, F.; Rothery, R. A.; Weiner, J. H.; Armstrong, F. A. Detection and interpretation of redox potential optima in the catalytic activity of enzymes;*Biochim Biophys Acta* **2002**, *1555*, 54.
(134) Hudson, J. M.; Heffron, K.; Kotlyar, V.; Sher, Y.; Maklashina, E.; Cecchini, G.; Armstrong, F. A. Electron transfer and catalytic control by the iron-sulfur clusters in a respiratory enzyme, E. coli fumarate reductase;*J. Am. Chem. Soc.* **2005**, *127*, 6977.
(135) Hwang, H. J.; Ang, M.; Lu, Y. Determination of reduction potential of an engineered CuA azurin by cyclic voltammetry and spectrochemical titrations;*J. Biol. Inorg. Chem.* **2004**, *9*, 489.
(136) Solomon, E. I. Spectroscopic Methods in Bioinorganic Chemistry: Blue to Green to Red Copper Sites;*Inorg. Chem.* **2006**, *45*, 8012.
(137) Solomon, E. I.; Hadt, R. G. Recent advances in understanding blue copper proteins;*Coord. Chem. Rev.* **2011**, *255*, 774.
(138) Warren, J. J.; Ener, M. E.; Vlcek, A.; Winkler, J. R.; Gray, H. B. Electron hopping through proteins.;*Coord. Chem. Rev.* **2012**, *256*, 2478.
(139) Solomon, E. I.; Heppner, D. E.; Johnston, E. M.; Ginsbach, J. W.; Cirera, J.; Qayyum, M.; Kieber-Emmons, M. T.; Kjaergaard, C. H.; Hadt, R. G.; Tian, L. Copper active sites in biology;*Chem Rev* **2014**, *114*, 3659.
(140) Siluvai, G. S.; Mayfield, M.; Nilges, M. J.; Debeer George, S.; Blackburn, N. J. Anatomy of a red copper center: spectroscopic identification and reactivity of the copper centers of Bacillus subtilis Sco and its Cys-to-Ala variants;*J Am Chem Soc* **2010**, *132*, 5215.
(141) Lieberman, R. L.; Arciero, D. M.; Hooper, A. B.; Rosenzweig, A. C. Crystal structure of a novel red copper protein from Nitrosomonas europaea;*Biochemistry* **2001**, *40*, 5674.
(142) Hauenstein, B. L., Jr.; McMillin, D. R. In *Met. Ions Biol. Syst.*; Sigel, H., Ed.; Marcel Dekker, Inc: New York, 1981; Vol. 13; 13, p 319.
(143) Di Bilio, A. J.; Chang, T. K.; Malmström, B. G.; Gray, H. B.; Karlsson, B. G.; Nordling, M.; Pascher, T.; Lundberg, L. G. Electronic absorption spectra of M(II)(Met121X) azurins (M=Co, Ni, Cu; X=Leu, Gly, Asp, Glu): charge-transfer energies and reduction potentials;*Inorg. Chim. Acta* **1992**, *198-200*, 145.
(144) Pragathi, M.; Reddy, K. H. Synthesis, spectral characterization and DNA interactions of copper(II) and nickel(II) complexes with unsymmetrical Schiff base ligands;*Indian J. Chem., Sect. A: Inorg., Bio-inorg., Phys., Theor. Anal. Chem.* **2013**, *52A*, 845.
(145) Hall, J. F.; Kanbi, L. D.; Harvey, I.; Murphy, L. M.; Hasnain, S. S. Modulating the redox potential and acid stability of Rusticyanin by site-directed mutagenesis of Ser86.;*Biochemistry* **1998**, *37*, 11451.
(146) Shoham, M. In *Handbook of Metalloproteins*; Messerschmidt, A., Ed.; John Wiley & Sons Ltd.: 2001; Vol. 2, p 1235.
(147) Xu, F.; Berka, R. M.; Wahleithner, J. A.; Nelson, B. A.; Shuster, J. R.; Brown, S. H.; Palmer, A. E.; Solomon, E. I. Site-directed mutations in fungal laccase: effect on redox potential, activity and pH profile;*Biochem J* **1998**, *334 (Pt 1)*, 63.
(148) Camasso, N. M.; Sanford, M. S. Design, synthesis, and carbon-heteroatom coupling reactions of organometallic nickel(IV) complexes;*Science* **2015**, *347*, 1218.

CHAPTER 4

ROLE OF RESIDUE 114 IN TUNING REDUCTION POTENTIAL OF AZURIN

* Portions of this chapter are going to be in a manuscript to be submitted as "The effect of hydrogen-bonding residues at position 114 on the redox properties of cupredoxins azurin" (Marshall N.M.*, Hosseinadeh P.*, Petrik I.D., Robinson H., Gao Y-G., Nilges M.J., Lu Y.). Marshall N.M. performed EPR and UV-vis and designed the mutants. Petrik I.D. helped in confirming refinements.
* Portions of the introduction are from a review submitted to Biophys. Biochim. Acta as "Designed and fine-tuning redox potentials of metalloproteins involved in electron transfer in biology" (Hosseinzadeh P., Lu Y.)

4.1. Introduction

A significant portion of biological processes are involved with providing vital energy sources such as ATP, and controlling the flow of energy through living systems. These bioenergetics processes, the most important of which are photosynthesis and respiration, require electron transfer (ET) between different redox partners. Metalloproteins are one of the most widely used ET centers in biology. They can be classified into three major classes: cupredoxins, which include type 1 copper (T1Cu) proteins and Cu_A centers,[1-10] cytochromes,[10-17] and iron-sulfur (FeS) proteins.[10,18-24] Each class of ET proteins transfer electrons between different redox partners which possess different reduction potentials (E°) (Figure 4.1). Therefore, the ET centers need to adjust their E° in a way that matches those of their redox partners. Cupredoxins usually function at the high end of the E°, while FeS proteins are mostly involved in ET reactions possessing relatively low E°.[10] The E°'s of FeS proteins overlap significantly with those of cytochromes that often have intermediate E° among the three classes of ET proteins. How reduction potential is tuned in a wide range within each class of proteins despite sharing similar metal geometries and protein scaffolds is a question that remained to be fully understood

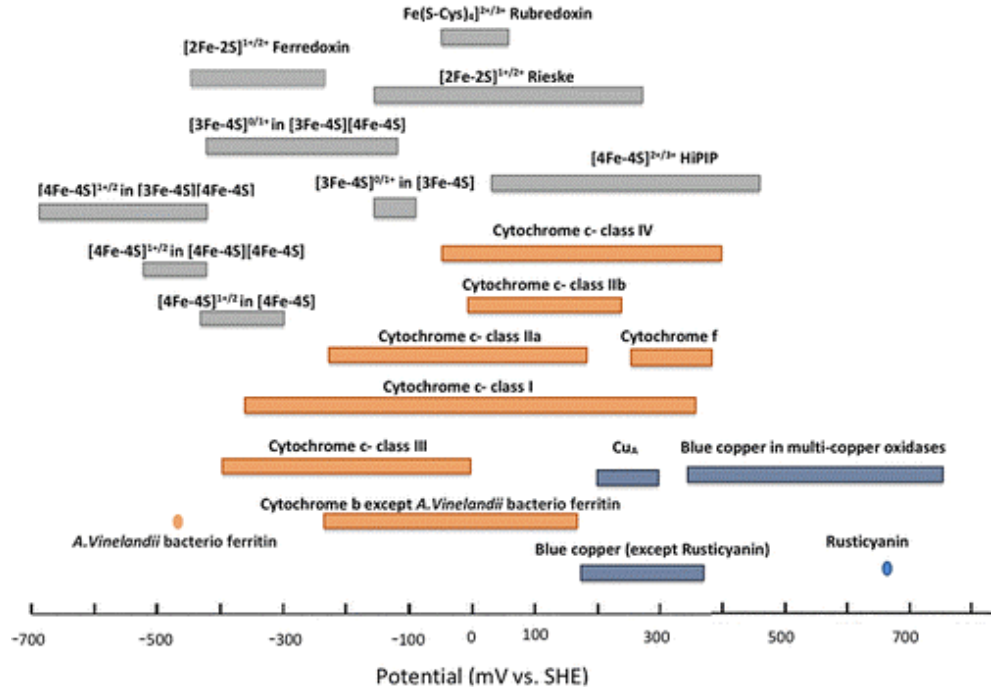

Figure 4.1. Reduction potential range of metal centers in electron transfer metalloprotein. Adapted from ref. [10]

Although metal ions and their primary ligands are the main contributors to the E°, these factors are highly evolved and optimized in natural ET proteins to ensure the lowest reorganization energy required for the rapid transfer of electrons. Such factors usually remain unchanged in different classes of ET proteins to avoid the need to re-optimize the sites, so accordingly most changes are exerted through SCS modifications. In this section, we will go through the ways by which nature tunes the ET proteins without changing the primary ligands.

4.1.1. Role of axial interactions

Axial interactions can have a great effect on the E° of the metal center. They are among the strongest SCS interactions and are usually closer to the metal center than the rest. Their effects can usually be directly transferred to the metal site. Several homology studies between proteins with the same metal center have sparked interest in investigating the role of the axial residue, showing a correlation between the nature of this ligand and the redox potential of the metal center. These observations further encouraged researchers to replace axial residues in several metalloproteins with other natural and unnatural amino acids.

Hydrophobicity of the axial residue has been shown to modify the metal center potential in different proteins. The more hydrophobic it is, the higher the E° of the site (Figure 4.2).

Cupredoxins are the best demonstration of such an effect. While a Met is present in the majority of cupredoxins, there is a Gln in stellacyanin, which has a very low E° (190 mV).[10] A Leu or Phe is found in laccase and ceruloplasmin, cupredoxins that are known to be in the higher extremes of the reduction potentials (790 mV for laccase).[10] Replacement of the axial residue in several cupredoxins has confirmed that the hydrophobicity of this residue is directly related to E° values.[25-27]

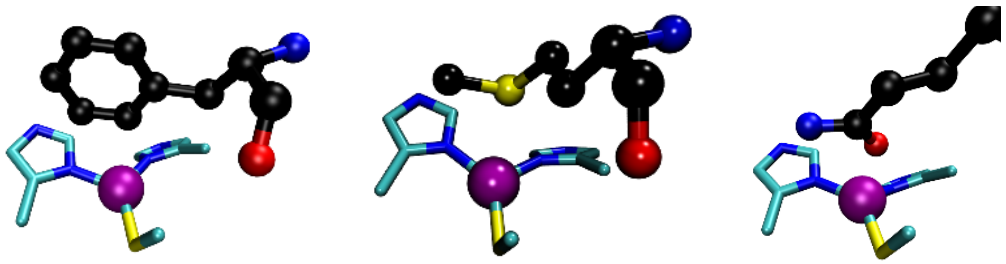

Figure 4.2. Role of hydrophobicity of the axial ligand in redox potential of cupredoxins. Moving from more hydrophobic to more hydrophilic (a to c), the redox potential will decrease [4,26,28]. Cu ion is shown as a purple ball, the primary ligands are shown in cyan and the axial ligand is shown in black stick and balls.

The presence of a carbonyl oxygen in azurin in a distal site of Cu is proposed to lower the redox potential of the site by stabilizing the Cu(II) form through increased electron density at the site.[7,29]

4.1.2. Role of hydrogen bonding interactions

Despite the important role of the axial residue, it is not the sole contributor to E° fine-tuning as evidenced by cytochromes with similar primary and axial ligands, yet display a variety of E° values. There are known cases of cupredoxins with the same Met axial residues yet significantly different potentials, and FeS proteins with a range of E° values despite sharing similar Cys and inorganic S ligands.[10] In both these cases a prominent factor in tuning the E° is the hydrogen-bonding (H-bonding) network around the metal center. H-bonding interactions can lock the ligands in the proper position required for the redox activity, however, this is not the only role they play. H-bonding to primary ligands can alter their chemical properties resulting in altered reduction potentials.

H-bonding to the Cys ligand of cupredoxin is shown to decrease the electron-donating features of this residue. Removal of just one of these H-bond interactions from the backbone amide of Phe114 residue through a Phe114Pro mutation in azurin resulted in a decrease of 100 mV in the E°.[30,31] Asn to Ser mutation removes a H-bond between loops and has been shown to cause a 131 mV increase in E° in azurin,[32] while changing Ser to Asn in rusticyanin decreases E° by 77 mV.[33] Decreasing the electron density on the Cu site by adding an H-bond to distal carbonyl of Gly45 through Phe114Asn mutation resulted in an increase in E° of azurin.[34]

Another example can be found in the case of peroxidases. Heme *b* is found both in peroxidases and Mb, and both proteins have a His residue as their proximal ligand. However, peroxidases have significantly lower E°, as is required for their activity. This lowering of E° is mainly attributed to the presence of an Asp residue that H-bonds to a metal coordinated His ligand (Figure 4.3). This strong H-bond can partially deprotonate His, giving more imidazolate character to it.[35,36] Electrostatic stabilization of the positive charges in Fe(III) will lower the E°.[37,38] Removal of this bond will increase the reduction potential, drastically decreasing peroxidase activity. The presence of such H-bonds are indeed important, but they also require proper orientation to fully convey their role. Interestingly, strengthening the H-bond to the proximal His ligand of cytochrome *c* resulted in a 100 mV decrease in redox potential.[39] Disruption of H-bonds from Tyr to the Met axial ligand in yeast iso-1 cytochrome *c* resulted in a decrease of up to 56 mV in E°. This change in the E° was attributed to the increase in electron density on Met, stabilizing Fe(III) state.[40,41]

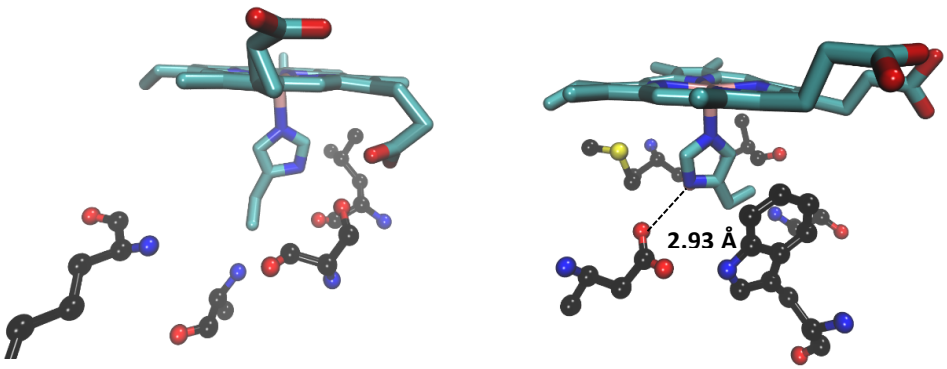

Mb (E° = 50 mV)

PDB ID: 1MBN

CcP (E° = -190 mV)

PDB ID: 2CYP

Figure 4.3. Comparison of the heme binding pocket of Mb and C*c*P. C*c*P has an Asp ligand that H-bonds to its proximal His and lowers the redox potential (potentials from Ref. [42] and [43], respectively)

H-bonding from backbone amides of SCS residues to FeS cluster ligands are shown to be an important feature in determining E° of FeS proteins.[44,45] More $NH_{amide}\cdots S$ H-bonds increase the E° by decreasing electron density on the sulfur ligand, thereby selectively stabilizing the reduced state. While ferredoxins have 11 conserved H-bonds, only 8 are observed in HiPIP proteins. This difference results in two distinct oxidation states of the cluster ($[4Fe\text{-}4S]^{1+/2+}$ for ferredoxins and $[4Fe\text{-}4S]^{2+/3+}$ for HiPIPs).[44,46-49] Altering these H-bonds by replacing them with Pro residues resulted in a decrease in E°.[50,51] In Rieske proteins, several H-bonding interactions to Cys ligands are present from either main chain nitrogens or conserved residues such as Tyr or Ser. Mutagenesis studies have shown the importance of these H-bonds in maintaining high to Cys ligands of the Rieske center.[50,52]. Interestingly, Rieske-type proteins have significantly lower E° values (between -150 to -100 mV)[50,51,53] than Rieske proteins (-100 to +490 mV)[50] despite their similarities in their primary ligands (Figure 4.4). This lower E° is partially attributed to lack of the H-bonds from conserved Tyr and Ser residues to the Cys ligands of FeS cluster.[52]

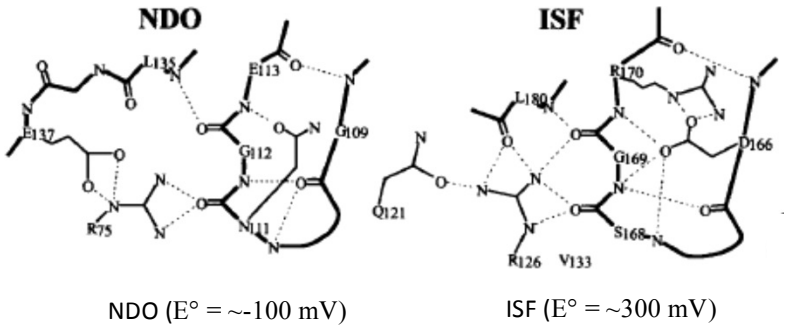

Figure 4.4. Comparison of H-bonding network between a Rieske-type protein (naphthalene dioxygenase-NDO) and a Rieske protein (water soluble fragment of complex bc_1- ISF). The figure is reprinted with permission from Ref. [50].

4.1.3. Role of hydrophobicity and solvent exposure

In general, placing the metal center in a more hydrophobic environment and less exposure to water will result in an increase in E° due to greater destabilization of higher oxidation states compared with lower ones. The Cu sites in laccase and ceruloplasmin are surrounded by hydrophobic residues.[28] Placing Phe at several positions in SCS of Cu site in Az resulted in an overall increase in redox potential.[54] Increased hydrophobicity around the heme pocket is also shown to increase the redox potential in various heme proteins.[55-58] The most significant example of such hydrophobicity effect is seen in the case of HiPIPs and [4Fe-4S] ferredoxins. While the

cluster is very similar between the two, the cluster's buried location resulted in a much higher E° in HiPIPs[47,59,60] (Figures 4.5). Furthermore, the covalency of Fe-S bond can be altered by hydration, hence influencing the redox potential.[61]

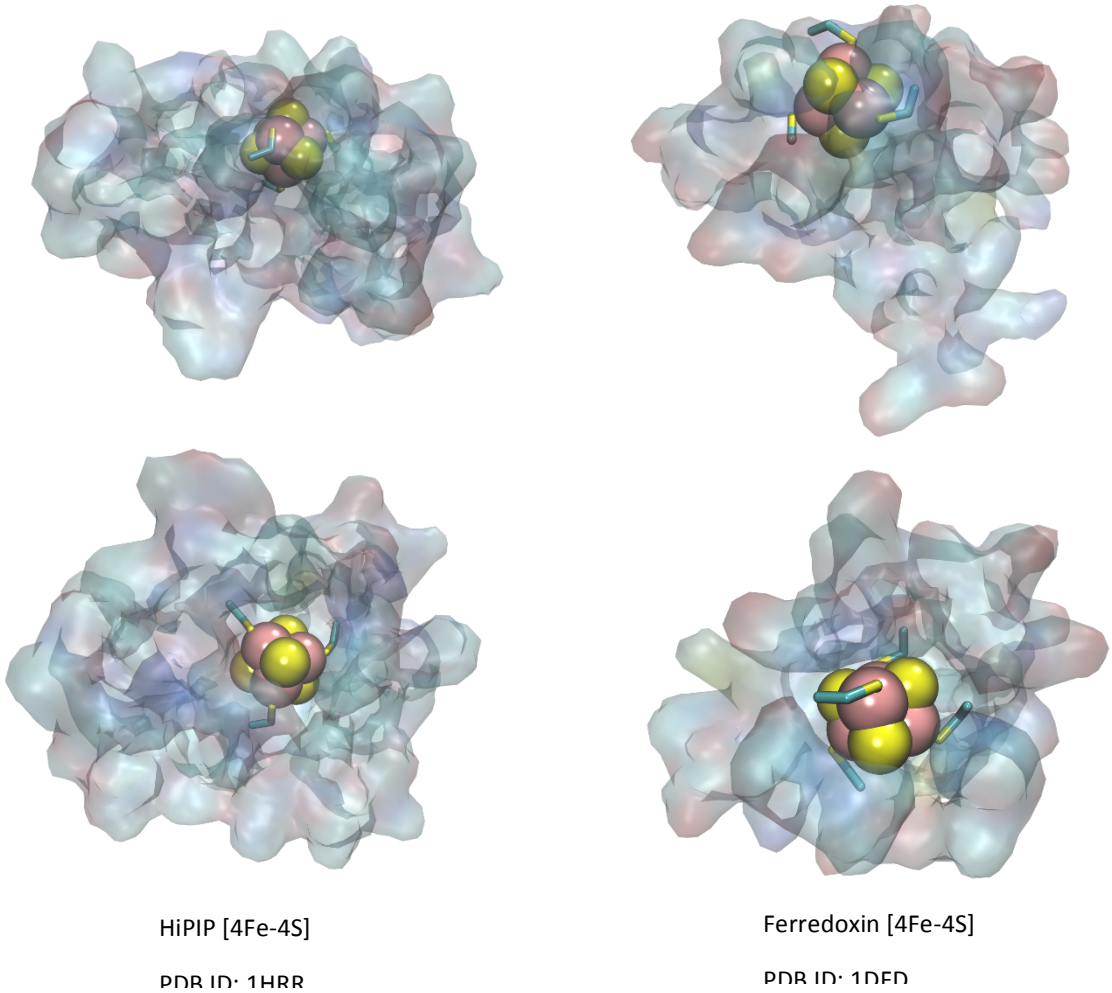

Figure 4.5. The [4Fe-4S] cluster is more buried in HiPIPS (PDB ID: 1HRR) vs. ferredoxins (PDB ID: 1DFD). One of the ligands in ferredoxin is completely exposed to water.

4.1.4. Role of the net charge of the protein

While controversial in some cases, a net charge in the SCS of a metal center can influence the E°. Presence of a negative charge, or even a negative dipole, can stabilize higher oxidation states and decrease the E°. Precise positioning of Gln and the interaction of its dipole with heme in cytochromes c_6 and c_{6a} has been shown to raise the potential by 100 mV.[62] Mutation of Tyr to

a Lys in cytochrome *c* resulted in 117 mV increase in the reduction potential, due to neutralization of negative charges in propionates by the positively charges Lys, resulting in less negative heme ring and hence destabilizing higher oxidation state of Fe.[63] Placement of polar or negative residues close to heme in Mb reduced the reduction potential by up to 200 mV.[64] Replacement of Leu by Glu in a *de novo* designed heme protein lowers the E° by 40 mV while introducing a Gln increased it from -156 to -104 mV.[57] Positive charges, on the other hand, will increase the E° by destabilizing these higher oxidation states. The presence of net positive amide dipoles is suggested to account for the differences between redox potentials of HiPIPs and ferredoxins.[59,65,66]

4.1.5. Role of the aromatic interactions and pi stacking

Although to a much lesser extent, aromatic interactions and π-stacking are known to influence the redox potential of certain metal centers. The majority of observed effects resulting from mutagenesis of aromatic residues are on the stability, rather than directly on the E° of the site.[67-70] However, there are cases in which an aromatic residue is shown to play a role in determining the E° of a metalloprotein, mostly through π–interactions. Effects due to increased hydrophobicity or H-bonding have been already discussed. Aromatic π-interactions between Tyr and proximal His in tetraheme cytochrome c_3 results in a 34-45 mV decrease in E°.[71] An aromatic residue is present in cyt b_6f that is in contact with heme *f* at position four. In algea cytochromes, there is a Trp present in this position, while a Phe in seen in cyanobacteria. Swapping these residues can result in a 70mV difference between the E° of the two proteins.[72] Another example is the Phe in cytochrome c_3 that is shown to be in contact with heme I, and is suggested to lower its E° through π-π interactions with porphyrin π system.[73]

4.1.6. Other factors in the secondary coordination sphere

The overall composition of SCS ligands and the length of the loop between ligands have also been shown to be important in determining the E° of the metalloprotein. An interesting example of such effects is seen in a series of loop-directed mutagenesis studies performed on blue copper proteins, in which the ligand loop of different cupredoxins were swapped with one another.[74-77] The E° of the chimeric proteins were in between those of the loop donor and acceptor. A loop from a lower E° protein would decrease the E° of the acceptor and vice versa.[75-78]

4.1.7. Blue copper protein azurin as a platform for tuning reduction potential

Azurin (Az) from *Pseudomonas aeruginosa* is one of the most well studied blue copper proteins. Several studies have been performed in order to understand the underlying role of different residues in determining the redox potential of Az and the ET rates in this protein.[79-91] Table 4.1 provides one of the studies in which E° of several Az variants were investigated under different pH conditions.[26] As shown in the table, replacement of the axial Met with hydrophobic ligands resulted in an increase in E° while addition of polar or charged ligands decreased it.

Table 4.1. Reduction potential of different Az variants. Reprinted from ref. [26]. Copyright © 2005, John Wiley and Sons under license number 3636610216032.

Protein	**pH**				
	4	5	6	7	8
Wild-type		346	333	310	293
His35Lys		344	337	317	296
Met44Phe	434	428	412	384	373
Gly45Ala		333	314	300	292
Asn47Asp				333	
Trp48Leu		352	345	323	306
Trp48Met		352	340	312	299
Lys85Glu		340	335	321	299
Ser89Gly	354	339	312	294	288
Glu91Gln		352	340	314	298
Phe114Ala		377	372	358	343
Phe114Val		346	340	324	314
Met121Ala				373	
Met121Asn				348	
Met121Asp			333	319	287
Met121Glu					184
Met121End				205	
Met121His				310	
Met121Ile				448	
Met121Leu			433	412	392
Met121Leu+Asn47Leu				510	
Met121Lys				318	
Met121Val				445	

In order to understand the role of different factors in SCS of T1Cu sites and their interplay in determining the E°, Marshall *et al*. used Az to incorporate several mutations in the SCS. As a result several variants were obtained that could span a range of ~700 mV in redox potential, never before reported in the cupredoxin superfamily (Figure 4.6).[34] With only 3 mutations (Asn47Ser/Phe114Ans/Met121Leu) it was deomonstrated that the E° can increase beyond any reported E° values of mononuclear T1Cu sites. The mutant with the lowest E°, Phe114Pro/Met121Gln, had a redox potential very close to 0 at pH=9, never reported before in any natural cupredoxins or their variants.[34] The authors further demonstrated that the effects of these specific mutations are additive in nature.[34] Replacement of the Met axial ligand with a more hydrophobic residue is accompanied with an increase in E°, while placing a more polar Gln residue at the same position decreased the redox potential, as explained in section 5.1. An Asn47Ser mutation also resulted in an increase in the reduction potential due to strengthening the H-bonds to a Cys ligand and rigidifying the site. The role of Phe114 is more complicated. Mutation of this residue to a Pro slightly disrupted the site, removing a H-bond to the Cys ligand, and hence decreased the E°. Mutation of Phe114 to Asn introduced an H-bond to backbone carbonyl of Gly45, and increased E°.[34]

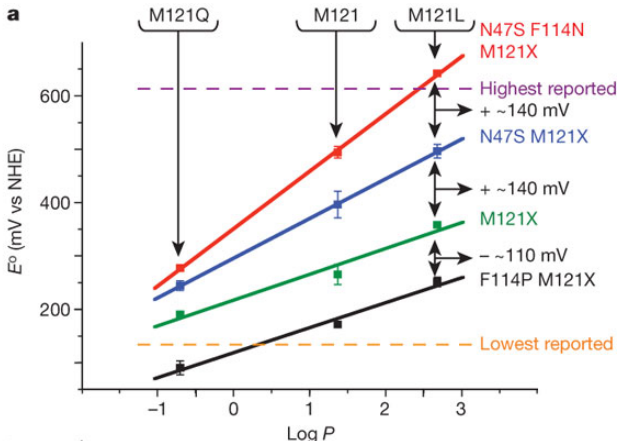

Figure 4.6. SCS mutants of azurin span a range of reduction potential never reported before. The effect of these mutations is additive. Adapted from [34]

A more in depth study on some of these mutants, Phe114Pro, Phe114Asn, and Asn47Ser, was performed to understand the underlying reason for their observed effects on E°.[92] Based on the experimental data that was obtained, Hadt *et al*. performed density functional theory (DFT) calculations on the mutants, and showed that the effects could be divided into covalent and nonlocal electrostatic contributions (Figure 4.7a).[92] The covalent component arises from the

changes in metal-ligand covalency, which can in turn influence the molecular orbitals. This component can be measured using S K-edge x-ray absorption spectroscopy studies. Active H-bonds (Figure 4.7b) within 5 Å of the metal site and carbonyl dipoles with a specific orientation towards the site, are the main SCS contributors to the covalent component. Nonlocal electrostatic interactions are another contributor to the changes observed in redox potential through affecting the enthalpy of the reaction. The effect of active H-bonds is additive. On the other hand, the effect of dipoles can be additive or oppose on other. The combination of these effects contribute to the fine-tuning of E° in azurin.[92]

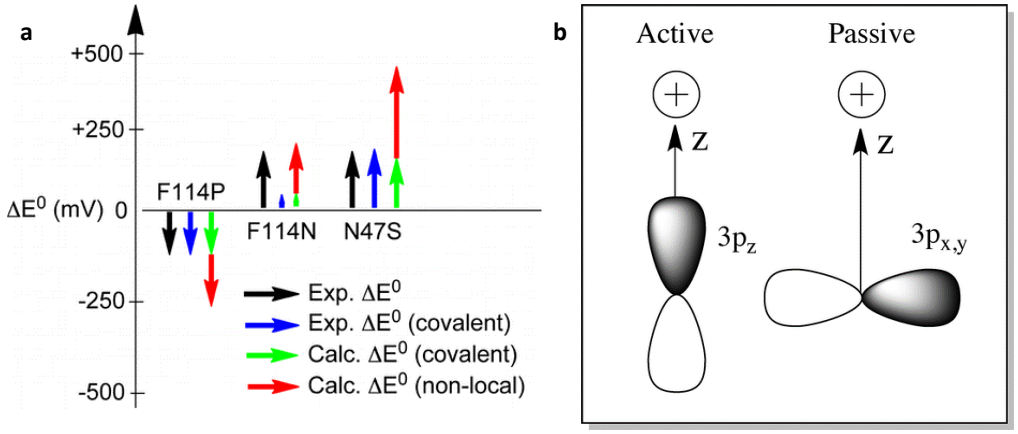

Figure 4.7. (a) Contribution of different factors in determining the E° in azurin mutants. (b) Active vs. passive H-bond. Reprinted with permission from [92]. Copyright © 2012, American Chemical Society.

4.1.8. Goals of the study:

Previously, we reported that the redox potential of Az could be altered over the entirety of this range by altering intraprotein hydrogen bonding and hydrophobic interactions near the copper binding site. Along the path towards finding which interactions could be changed to give the desired effects to the redox potential, we noticed several interesting interactions, or trends that always resulted in a change in redox potential. Chief among these is the effect of adding hydrogen bonding groups at position 114 in Az.

Phe114 in Az is directly adjacent to the copper binding site and across from the backbone carbonyl oxygen of Gly45 that has been proposed to have a strong ionic interaction with the copper in Az. Position 114 was initially investigated for its effects on redox potential because the similarly positioned amino acid in another cupredoxin, rusticyanin, was known to be crucial for maintaining the high reduction potential (E_m) of that copper site. Furthermore, it was known that one of the copper sites in the protein ceruloplasmin that has an estimated E_m of higher than 1

V naturally has an Asn residue at this position. This Asn in ceruloplasmin hydrogen bonds to the aforementioned carbonyl oxygen in that protein, forming a hydrogen bonding bridge between the copper ligand containing loops of ceruloplasmin.

Initial computer aided modeling of potential hydrogen bonding residues at position 114 showed that residues the size of Gln or Glu were too long to remain close to the copper binding site. We therefore were limited to shorter hydrogen bonding residues like Asn, Asp and Ser. Here we report the redox potentials of Phe114Asn, Phe114Asp and Phe114Ser Az, the spectral characteristics of each variant and the crystal structures of each. The changes in redox potential of Phe114Xxx Az variants are correlated to subtle but significant structural changes near the copper binding site.

4.2. Materials and methods

4.2.1. Protein expression and purification

The proteins were expressed using our previously reported method of azurin purification. In brief, the BL21 (DE3) cells that were transformed by the plasmids were grown in 5ml LB media for 8 hours at 37 C. 1ml of the starter culture will then be used to inoculate 2L of 2xYT media. The proteins are then extracted from the periplasm using osmotic shock procedure. Reconstitution of the apo proteins with copper, the variants were purified using a 5 mL HiTrap HP Q-sepharose column (GE Healthcare, Piscataway, NJ, USA) equilibrated in 50 mM ammonium acetate buffer at pH 6.0 on an AKTA basic FPLC system (GE Healthcare, Piscataway, NJ, USA). The electrospray mass spectrometry (ESI-MS) confirms that the molecular weights of the variants match those predicted from calculations, within the experimental errors (Phe114Asn: calculated 13192.72; Phe114Asp: calculated 13913.72; and Phe114Ser Az: calculated 13885.71.

4.2.2. Spectroscopic characterization of Az variants

UV-visible spectra of Az and its variants were collected on a Varian Cary 5000 UV-visible spectrometer in TIP7 buffer.[93] Electron paramagnetic resonance spectra were collected on Varian E-line 12” Century Series X-Band CW spectrometer at 30 °K in the same buffer. The parameters for each EPR spectrum were determined by simulation with the Simpower 6 program.[94,95]

Extinction coefficients were determined by spin counting using EPR spectroscopy, in which several $CuSO_4$ standards in the concentration range from 0.125 mM to 2.0 mM were prepared in deionized water. The EPR spectra of the samples were then collected and the total area of the integrated EPR absorption spectra were plotted vs. $[Cu^{2+}]$ to build a standard curve. The protein samples were then exchanged into the TIP7 buffer and concentrated to ~0.5 mM. The UV-vis spectra were obtained and then EPR of the same samples were collected. The total area of EPR signal in the protein samples was then used to determine the $[Cu^{2+}]$ in each sample, which was, in turn, used to calculate the extinction coefficient of the LMCT band of the protein *via* Beer's Law.

4.2.3. Cyclic voltammetry

Redox potential values of Az variants were measured *via* cyclic voltammetry (CV) as thin films on pyrolytic graphite edge (PGE) electrodes, assembled according to previous procedures,[96] with a platinum wire as an auxiliary electrode and a Ag/AgCl electrode as a reference electrode. Protein solution (typically 5 μL of 2 mM) was applied to the graphite and allowed to incubate at 4°C for 10 minutes. The working electrode, auxiliary wire and reference electrode were then immersed in a mixed buffer solution consisting of 50 mM ammonium acetate, 40 mM MOPS, 40 mM MES, 40 mM Tris, 40 mM CAPS and 100 mM NaCl at either pH 4.0 or 7.0. The potential range was then scanned at a rate of 0.2 V/s, typically with a total of 6 scans (3 in each direction). No dependence of the E_m upon the scan rate was observed in the range from 0.01 to 1 V/s, as is typical for Az and most Az variants.[97] Redox potential values were calculated by averaging the positions of the oxidation and reduction waves. Peak separations were typically less than 0.1 V indicating the reversibility of the redox cycle for each variant. The values obtained were then corrected to be reported vs. the standard hydrogen electrode (SHE) by adding 210 mV to the observed E_m. The correction factor was determined by testing the redox potential of ferrocene with the reference electrode used.

4.2.4. Protein crystallization and diffraction

The holo, copper bound version of Phe114Ser was crystallized by hanging drop vapor diffusion from a mixture of protein (6 mM) in pH 6.0 ammonium acetate mixed 1:1 with a solution of 50 mM ammonium acetate buffer, 260 mM $CaCl_2$, 280 mM $LiNO_3$ and 30 % w/w

polyethylene glycol (PEG) M.W. = 8000 Da. Crystals typically formed after about 1 month time at 4°C and the highest quality crystals formed after as much as 6 months.

The holo, copper bound form of Phe114Asp was crystallized using hanging drop vapor diffusion method from a 1:1 mixture of 1mM protein in pH 6.0 ammonium acetate with a solution of 100 mM Tris buffer at pH 8.0, 100 mM $LiNO_3$, 10 mM $CuSO_4$ and 25% w/w PEG M.W. =10000 Da. Rectangular-shape crystals were formed in about a mount of incubating the drop against the described solution at 4°C and were mounted after 2 months incubation using 100 mM Tris buffer at pH 8.0, 100 mM $LiNO_3$, 10 mM $CuSO_4$ and 50% PEG M.W.=400 Da as cryoprotectant.

The holo, copper bound form of Phe114Asn was crystallized using hanging drop vapor diffusion method from a 1:1 mixture of 2mM protein in pH 6.0 ammonium acetate with a solution of 100 mM Tris buffer at pH 8.0, 100 mM $LiNO_3$, and 30% w/w PEG M.W. =10000 Da. Rectangular-shape crystals were formed in about a mount of incubating the drop against the described solution at 4°C and were mounted after 2 months incubation using 100 mM Tris buffer at pH 8.0, 100 mM $LiNO_3$, and 50% PEG M.W.=400 Da as cryoprotectant.

Diffraction patterns were collected at Brookhaven National Laboratory (Upton, NY, USA). The data for Phe114Asn and Phe114Asp was refined and solved using PHENIX program version 1.8.4.

4.3. Results and discussion

4.3.1. Electronic Absorption (UV-vis) and Electron Paramagnetic Resonance (EPR) Spectroscopic studies

As shown in Figure 4.8A, all three Az variants display a strong absorption band around 625 nm (Table 4.2), similar to that in WT Az. This absorption band has been assigned to Cys sulfur to Cu(II) charge transfer, typical of the cupredoxin family. Similarly, the three Az variants also show axial EPR spectra with narrow hyperfine coupling constants, again very similar to that of WT Az and typical of other T1 Cu proteins. The only significant change to the EPR signals is that Phe114Ser has a slightly smaller g_z value as compared to the other variants (table 4.2), which may indicate some slight effect to the Cu-S interaction. The similarity in UV-vis and EPR characteristics of the investigated Az variants indicates minimal perturbation of the copper binding site from the mutations.[87,89,98-100]

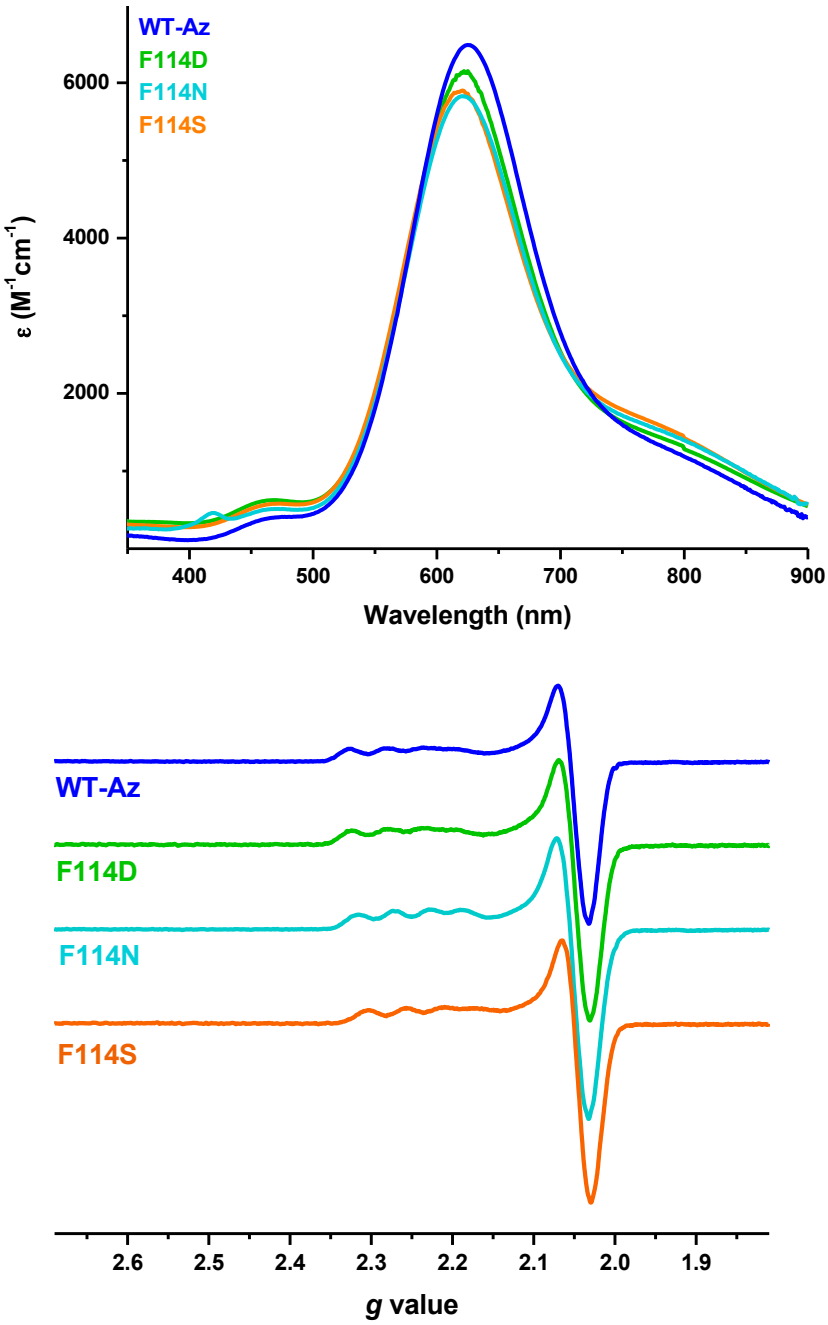

Figure 4.8. A) UV-visible spectra and B) EPR for (–) F114D Az, (–) F114N Az, (–) F114S Az, and (–) WT Az.

In all cases, when a hydrogen bond donor was added to Az at position 114, very little change to the UV-vis and EPR parameters were seen. Even when added to other mutations, these hydrogen bond altering mutations generally had little effect on these spectroscopic signatures. This retention of the spectroscopic signatures suggests that Phe114Asn, Phe114Asp and Phe114Ser alone have only subtle effects on the geometry of the copper binding site,[87,89,98-100] at

least as far as can be observed with UV-vis and EPR. The exception to this is the Asn47Ser/Phe114Asp/Met121Leu variant, which was observed to be green in color, as opposed to blue. Combining Phe114Asp with other mutations was clearly destabilize, which is not surprising as it introduces a negatively charged residue to a highly hydrophobic region of the protein. Significant decrease in bond length between Cu ligands and Cu is observed in Phe114Ser structure.

Table 4.2. Spectroscopic parameters for Az variants from this study.

Variant	λ_{max} (nm), ε ($M^{-1}cm^{-1}$)	g_x	g_y	g_z	A_x (cm^{-1})	A_y (cm^{-1})	A_z (cm^{-1})
WT	625, 6487	2.028	2.055	2.262	9	9	50
F114N	621, 5829	2.030	2.058	2.252	8	8	57
F114D	622, 6150	2.027	2.054	2.264	9	9	47
F114S	621, 5900	2.028	2.052	2.245	8	8	48

4.3.2. Reduction potentials of Az variants

While the spectroscopic properties of each Az variant studied here vary little from protein to protein, the E_m values were observed to vary by a wide range. Table 4.3 gives the observed E_m values for each Az variant in this study. The values obtained for WT Az at each pH are close to previously reported values, indicating that our method of measurement is consistent with previous studies. Figure 4.9 shows representative CV for all variants. Of the previously unreported residue 114 variants of Az, Phe114Asp has the identical effect to the E_m as compared to Phe114Asn at pH 4.0. The inflation of the E_m in Phe114Asp is, however, lessened slightly at pH 7.0. Phe114Ser also increases the E_m of Az at each pH, although to a lesser degree than Phe114Asn or Phe114Asp.

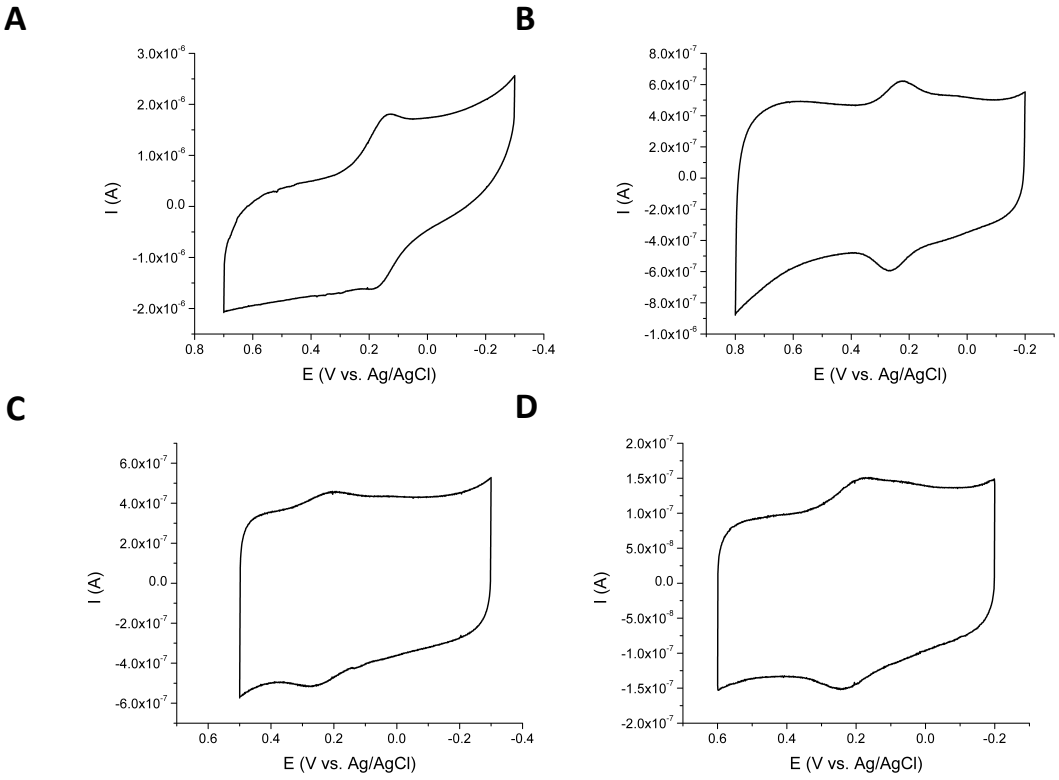

Figure 4.9. CV of A) WT, B) Phe114Asn, C) Phe114Asp and D) Phe114Ser Az

In previous publications, others and we have shown that the effect of individual mutations in Az can be additive in regards to E_m.[26,34,54] We had previously shown that Phe114Asn, Asn47Ser and Met121Leu can be combined to raise the E_m of Az beyond the upper range of E_m values known for mononuclear cupredoxins.[34] We decided to investigate whether Phe114Ser and Phe114Asp mutations also show such additive effects when combined with Asn47Ser and Met121Leu. Table 2 gives a summary of the E_m values of the individual mutations and shows the additive effect when mutations are combined. In the case of both Phe114Asp and Phe114Ser, a similar total increase in E_m upon combination of mutations was seen. Both Asn47Ser/Phe114Asp/Met121Leu Az and Asn47Ser/Phe114Ser/Met121Leu Az also have similar, although slightly lower, E_m values as compared to Asn47Ser/Phe114Asn/Met121Leu Az. As is denoted in the table, the Asn47Ser/Phe114Asp/Met121Leu variant was exceptionally unstable and exhibited multiple species in the potential range scanned.

Table 4.3. Observed E_m values for different Az variants studied in this paper.

Variant	Redox Potential at pH 4.0 (mV vs. SHE)	Deviation from WT (mV)	Redox Potential at pH 7.0 (mV vs. SHE)	Deviation from WT (mV)
WT	359 ± 8	-	286 ± 8	-
F114N	446 ± 7	+87	376 ± 4	+90
F114D	446 ± 17	+87	364 ± 8	+78
F114S	414 ± 7	+55	331 ± 3	+45
N47S	462 ± 3	+103	385 ± 4	+99
M121L	420 ± 12	+61	388 ± 5	+102
N47S/F114N/M121L	707 ± 3	+348	641 ± 9	+355
N47S/F114D/M121L*	668 ± 14	+309	-	-
N47S/F114S/M121L	665 ± 7	+306	608 ± 2	+322

* This combination of mutations was seen to result is significant changes to the visible spectrum of the protein with strong absorbance around 400 nm indicating significant perturbation of the copper binding site. The visible spectrum was also seen to be pH dependent in both cases.

4.3.3. Structural studies of the mutants

Table 4.4 gives a list of relevant atom-to-atom distances seen in the crystal structure of Phe114Ser/Asn/Asp Az. For comparison, several distances from previously reported WT structure are also shown.

Table 4.4. Selected crystallographically observed bond lengths and the change in the length from the WT protein.

Variant (PDB Code if deposited, resolution Å)	Atoms of Interest	Molecule in the Asymmetric Unit	Distance (Å)	Average Distance (Å)	Deviation from WT Distance (Å)
WT (4AZU,[30] 1.90)	S_{Cys112}-Cu	A	2.27	2.24	-
		B	2.27		
		C	2.24		
		D	2.17		
	N^{δ}_{His46}-Cu	A	1.99	2.08	-
		B	2.06		
		C	2.13		
		D	2.12		
	N^{δ}_{His117}-Cu	A	2.11	2.01	-
		B	1.98		
		C	1.96		
		D	2.00		
	S_{Met121}-Cu	A	3.18	3.15	-
		B	3.16		
		C	3.21		
		D	3.05		
	O_{Gly45}-Cu	A	2.84	2.97	-
		B	2.95		
		C	3.05		
		D	3.03		
		B	3.60		

Table 4.4 cont.

F114S (2.39)	S_{Cys112}-Cu	A	2.38	2.39	+0.15
		B	2.54		
		C	2.33		
		D	2.32		
	N^{δ}_{His46}-Cu	A	2.09	2.10	+0.02
		B	2.08		
		C	2.24		
		D	2.01		
	N^{δ}_{His117}-Cu	A	2.12	2.36	+0.35
		B	2.20		
		C	2.63		
		D	2.49		
	S_{Met121}-Cu	A	3.19	2.87	-0.28
		B	2.84		
		C	2.66		
		D	2.80		
	O_{Gly45}-Cu	A	2.86	3.03	+0.06
		B	2.75		
		C	3.29		
		D	3.20		
	O^{γ}_{Ser114}-O_{Gly45}	A	2.50	2.80	-
		B	2.72		
		C	3.27		
		D	2.72		
F114N (1.95)	S_{Cys112}-Cu	A	2.19	2.26	+0.02
		B	2.29		
		C	2.33		
		D	2.23		
	N^{δ}_{His46}-Cu	A	2.06	2.05	-0.03
		B	2.02		
		C	2.04		
		D	2.09		
	N^{δ}_{His117}-Cu	A	2.07	2.10	+0.09
		B	2.05		
		C	2.16		
		D	2.11		
	S_{Met121}-Cu	A	3.10	3.07	+0.02
		B	3.15		
		C	2.86		
		D	3.15		
	O_{Gly45}-Cu	A	3.23	3.21	+0.24
		B	3.16		
		C	3.28		
		D	3.18		
	N^{δ}_{Asn114}-O_{Gly45}	A	2.70	2.79	-
		B	2.78		
		C	2.91		
		D	2.77		
F114D (2.20)	S_{Cys112}-Cu	A	2.26	2.22	-0.02
		B	2.18		
	N^{δ}_{His46}-Cu	A	2.10	2.09	+0.01
		B	2.09		
	N^{δ}_{His117}-Cu	A	2.19	2.15	+0.14
		B	2.01		
	S_{Met121}-Cu	A	2.83	2.93	-0.22
		B	3.04		
	O_{Gly45}-Cu	A	2.96	2.99	+0.02

Table 4.4 cont.

		B	3.02		
	O^{δ}_{Asp114}-O_{Gly45}	A	3.53	3.36	-
		B	3.19		

Of the distances shown above, most are within the error of atom positions as determined by calculation of the average uncertainty in the position of atoms using the resolution of each structure, the refinement parameters and the empirical methods published by Freeman.[101] However, there are several significant changes in the structure of these variants. In the structure of Phe114Asn and Phe114Asp, the N^{δ}_{His117}-Cu distance is longer by 0.09 and 0.14 Å, respectively. Also in the structure of Phe114Asp, the S_{Met121}-Cu distance was seen to be shorter than average by 0.22 Å. In the Phe114Ser and Phe114Asn structure, the average distance between hydrogen bond donors from Ser or Asn and the carbonyl O_{Gly45} is 3.07 and 2.27 Å, respectively, which is sufficiently short to be considered a hydrogen bond. The same distance on Phe114Asp is longer, 3.36 Å, suggesting a weaker hydrogen bond if present. Also, a significant elongation of O_{Gly45}-Cu distance is observed in Phe114Asn. The overall structures and important distances are shown in figure 4.10.

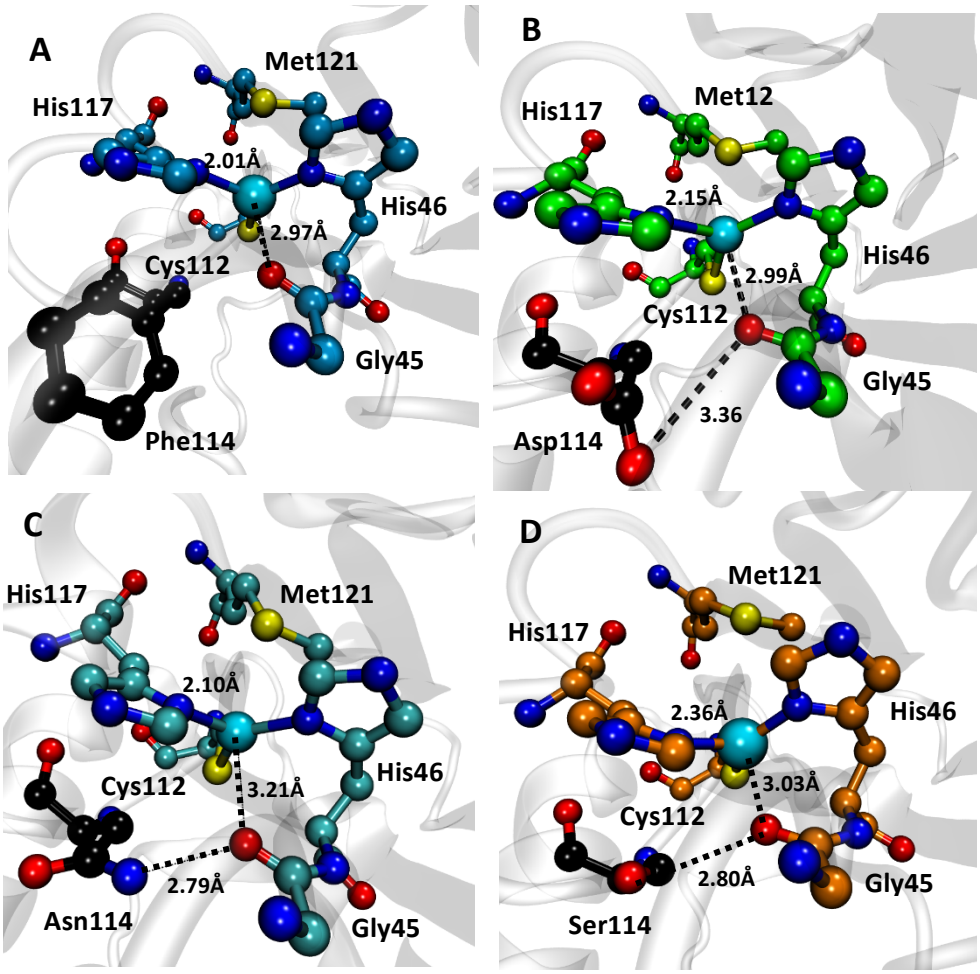

Figure 4.10. Comparison of the crystal structures of A) WT Az and C) Phe114Ser Az showing the hydrogen bonds formed to Gly45 upon mutation. In all panels nitrogen atoms are shown in blue, sulfur atoms in yellow and copper is shown in green. To differentiate between structures, the backbone in Panel A is shown in blue with carbon atoms in cyan, while the backbone and carbon atoms are orange in panel B and green in panel C. Average atom-to-atom distances are shown as dashed lines with the average distance listed for each interaction.

4.3.4. Structural effects of F114S

Table 4.5 shows the crystallographic parameters for the Phe114Ser Az variant. The slight decrease in g_z in Phe114Ser (table 4.2) can be explained by observed decrease in Cys-Cu distance in crystal structure (table 4.5).

Table 4.5. Crystallographic parameters for F114S-Az.

Crystal Data	F114S
Space Group	$P1_211$
Unit Cell	
***a* (Å)**	49.771
***b* (Å)**	83.155
***c* (Å)**	63.237
α *(o)*	90.00
β (o)	108.93
γ (o)	90.00
Data collection statistics	
Wavelength (Å)	1.1
Resolution (Å)	2.39
Number of unique reflections	19118
Completeness (%)	98.52
Refinement statistics	
Resolution (Å)	10.0 - 2.39
R-all (%)	30.26
R-work (%)	22.39
RMS Bond lengths (Å)	0.009
RMS Bond angles (°)	1.25
Metal Ion	4
No. of water molecules	82

The structure of Phe114Ser Az clearly shows that the desired hydrogen bond does form, which can be directly correlated to the increase in E_m of this variant as well (Figure 4.10D and Table 2). However, the crystal structure also shows that the hydrogen bond between Ser114 and Gly45 is fluxional to some extent. In two of four molecules in the asymmetric unit, the oxygen-oxygen distance is about 3 Å or less, which can be considered a strong hydrogen bond. In the other 2 molecules, this distance is between 3 Å and 3.5 Å, indicating a weaker interaction. Given the resolution of the structure, the average Cu-O_{Gly45} distance for all the molecules in the asymmetric unit was effectively unchanged. The inherently weaker nature of the hydrogen bond between Ser and O_{Gly45} can explain the fact that O_{Gly45}-Cu distance is almost unchanged in Phe114Ser structure while it significantly increases in Phe114Asn structure in which a strong hydrogen bond is formed between N^{δ} of Asn114 and O_{Gly45}.

Similar to other variants discussed, elongation of $N^{\delta}{}_{His117}$-Cu distance is also observed for Phe114Ser. Interestingly, Phe114Ser also shows a significant increase in S_{Cys112}-Cu distance in

the structure. Such movement of the Cu ligands away from the Cu site results in a more electron deficient site, destabilizing Cu(II) state and increasing the E_m.

In this same structure of Phe114Ser Az, it is also seen that the methyl group on the end of Met121 has significantly more conformational freedom. The increase conformational freedom of Met121 observed in the crystal structure was also apparent in the EXAFS data of F114N Az where a large DW factor was seen. This structural effect is likely also due to the destabilization of the loop containing Asn114 and His117, as Met121 is also a part of this loop. In these structures, the axial Met came closer to the Cu site. This lower distance can be justified by the movement of two of the Cu ligands away from the Cu site and the need to compensate for the charges to hold the Cu in place. This compensation of electron deficiency on the site by the Met residue in Phe114Ser variant can explain the lower increase in E_m in this protein compared to Phe114Asp and Phe114Asn variants.

4.3.5. Structural effects of F114N

Table 4.6 shows the structural parameters for Phe114Asn mutant. Phe114Asn was designed to form a hydrogen bond directly to the backbone carbonyl of Gly45 in order to mimic the aforementioned hydrogen bonding interaction seen in ceruloplasmin. Analysis of the crystal structure shows that this hydrogen bond is indeed forming between the N^{δ} of Asn and the O of Gly45, with an average distance of 2.79 Å. Formation of this hydrogen bond resulted in a concomitant elongation of O_{Gly45}-Cu distance probably due to the carbonyl atom being pulled by N^{δ} of Asn114 (figure 4.10A,C). this in turn will remove the electron density donated to the Cu, hence increasing the redox potential (table 4.3).

Table 4.6. Crystallographic parameters for F114N-Az.

Crystal Data	**F114N**
Space Group	$P12_11$
Unit Cell	
***a* (Å)**	61.24
***b* (Å)**	49.29
***c* (Å)**	80.38
α (o)	90.00
β (o)	108.437
γ (o)	90.00

Table 4.6 cont.

Data collection statistics	
Wavelength (Å)	1.1
Resolution (Å)	1.95
Number of unique reflections	33388
Completeness (%)	99.53
Refinement statistics	
Resolution (Å)	41.39-1.95
R-all (%)	24.8
R-work (%)	20.5
RMS Bond lengths (Å)	0.007
RMS Bond angles (°)	1.083
Metal Ion	4
No. of water molecules	374

Another observed effect is the elongation of N^{δ}_{His117}-Cu distance (figure 3A,C). This structural effect is likely also due to the destabilization of the loop containing Asn114 and His117. Weakening the N^{δ}_{His}-Cu bond in Az has been previously shown to result in a higher E_m both experimentally and computationally.[82,102-105] When His117 was mutated to a Gly residue, thereby completely removing the ligand all together, the E_m of Az increased by 300 mV.[102] Upon addition of exogenous imidazole, the E_m returned to nearly the WT value.[102] However, it is unclear if the dramatic changes seen in the previous study are due to the absence of the His ligand, or the possible binding of other exogenous ligands to the copper, such as water or chloride, when the His ligand is not present.

As further proof of the importance of N^{δ}_{His}-Cu length in tuning the E_m of cupredoxins, a recent computational study showed that the crystallographic N^{δ}_{His}-Cu length can be correlated to the electron affinity of the copper site in several cupredoxins when the rest of the ligand set is the same. This effect also correlates to the E_m of the proteins, with higher E_m cupredoxins exhibiting longer N^{δ}_{His}-Cu distances on average. Weakening the N^{δ}_{His}-Cu interaction in

cupredoxins removes the strong σ-donating His from the coordination sphere of the copper, resulting in a more electron deficient metal and, in turn, preferentially stabilizing the Cu(I) state. Thus, the significant lengthening of this bond seen in the Phe114Asn structure can explain the increase in E_m.

Another observed effect is a slight change in the orientation of His117 residue compared with that of WT and other variants studied (figure 3). Increased conformational freedom for His117, as the Phe114Asn mutation also removes steric bulk from the vicinity of His117 allows His117 to twist towards residue 114, away from its position in WT Az (Figure 3A,C). Even if the distance between the Cu and the N of His117 is not lengthened, the rotation of the imidazole ring away from the position in WT will affect the orbital overlap between the Cu and His117 and, thereby, the redox potential of the site. A similar structural effect was seen in the previously reported Phe114Ala variant, along with a concomitant increase in redox potential of the copper site.[106]

4.3.6. Structural effects of F114D

Table 4.7. shows structural parameters for Phe114Asp. While it was initially expected that Phe114Asp would lower the redox potential of Az due to stabilization of the Cu(II) state by adding a full negative charge in close proximity to the copper binding site,[107] experimental results show that this mutation actually causes an identical increase in the E_m as compared to Phe114Asn at pH 4.0. As these residues, Asn and Asp, are isostructural to one another, they will have similar capacities to hydrogen bond and presumably cause similar structural perturbations at pH 4.0.

Table 4.7. Crystallographic parameters for F114D-Az.

Crystal Data	**F114D**
Space Group	$P2_12_12_1$
Unit Cell	
***a* (Å)**	48.109
***b* (Å)**	56.606
***c* (Å)**	83.638
α (o)	90.00
β (o)	90.00
γ (o)	90.00

Table 4.7 cont.

Data collection statistics	
Wavelength (Å)	1.1
Resolution (Å)	2.39
Number of unique reflections	11973
Completeness (%)	99.35
Refinement statistics	
Resolution (Å)	46.88-2.20
R-all (%)	24.7
R-work (%)	19.0
RMS Bond lengths (Å)	0.008
RMS Bond angles (°)	1.074
Metal Ion	4
No. of water molecules	137

At pH 7.0, Phe114Asp has less of an inflating effect, which is likely due to deprotonation of the side chain of the Asp residue. Upon deprotonation, the capacity of Asp to donate a hydrogen bond is lost, which suggests that the hydrogen bonding effects of the side chain are actually more important than both the loss of steric bulk at position 114 and the introduction of ionic interactions. This

The structure of Phe114Asp, prepared at pH 8.0, shows the possibility of a weak hydrogen bond, if any, between Asp and O_{Gly45} (figure 4.10B). This observation is consistent with the dampening of the increased in E_m at pH 7.0 (table 4.2) due to the probable deprotonation of Asp.

Interestingly, the crystal structure of Phe114Asp shows two deviations from the WT structure (figure 3A,B) that work in opposite directions, both resulted from the increased flexibility of the loop containing residues 114, 117 and 121, and removal of the steric hindrence from Phe114. On one hand significant elongation of the N^{δ}_{His}-Cu distance results in an increase in E_m for reasons similar to those explained for Phe114Asn. On the other hand, S_{Met}-Cu distance in Phe114Asp is shorter than other Az variants. A stronger S_{Met}-Cu interaction can decrease the E_m.

4.4. Summary and conclusion

In general, addition of hydrogen bond donors at position 114 produced a large effect on E_m (+50 to +100 mV at pH 4.0) with little apparent disruption to the copper binding site based on EPR and UV-vis. Although all the hydrogen bond donating residues introduced at this position were initially designed to hydrogen bond directly to the carbonyl oxygen of Gly45 to mimic a similar interaction found in ceruloplasmin, crystal structures of these variants show that the relative length of the residue at this position determines the exact molecular effect of the mutation. Structural analysis of variants that contain an Asn or Asp residue at position 114 shows that this mutation destabilizes the loop of Az that contains both of the copper ligands His117 and Met121. This destabilization weakens the interactions between the copper and these ligands, which raises redox potential. Moreover, the strong hydrogen bond formed between Asn and O_{Gly45} moves this carbonyl away from the Cu site. Due to the structural similarity between Asn and Asp, it is likely that the F114D mutation has a similar effect. The key to these mutations is that, while the ligand-metal interactions are weakened, the destabilization is not large enough to completely abolish ligand binding. In this way, the copper site maintains most of the features of WT Az, but exhibits a higher redox potential.

A hydrogen bond to Gly45 via Phe114Asn or Phe114Ser mutation is observed. It is difficult to determine whether the effect of withdrawing electron density from the copper-oxygen interaction by forcing a hydrogen bond to form has the greatest effect on E_m, or, if adding a hydrogen bond in this way, between the two ligand containing loops in Az, causes some other effect, such as rigidifying other hydrogen bonds to Cys112[26,33,108-111] or having a similar destabilizing effect as the Phe114Asn mutation. It is, however, exceptionally clear that the identity of the amino acid at position 114 in Az has a strong influence on the redox tuning of Az and that adding hydrogen bond donors at this position can be used to raise the E_m, although through different mechanisms.

4.5. References

(1) Farver, O.; Pecht, I. Electron transfer processes of blue copper proteins;*Met. Ions Biol.* **1981**, *3*, 151.
(2) Stevens, T. H.; Martin, C. T.; Wang, H.; Brudvig, G. W.; Scholes, C. P.; Chan, S. I. The nature of copperA in cytochrome c oxidase;*J. Biol. Chem.* **1982**, *257*, 12106.
(3) Dennison, C.; Canters, G. W. The CuA site of cytochrome c oxidase;*Receuil des Travaux Chimiques des Pays-Bas* **1996**, *115*, 345.
(4) Battistuzzi, G.; Borsari, M.; Loschi, L.; Righi, F.; Sola, M. Redox Thermodynamics of Blue Copper Proteins;*J. Am. Chem. Soc.* **1999**, *121*, 501.

(5) De Rienzo, F.; Gabdoulline, R. R.; Menziani, M. C.; Wade, R. C. Blue copper proteins: A comparative analysis of their molecular interaction properties;*Protein Sci.* **2000**, *9*, 1439.
(6) Gray, H. B.; Malmstrom, B. G.; Williams, R. J. Copper coordination in blue proteins;*J. Biol. Inorg. Chem.* **2000**, *5*, 551.
(7) Lu, Y. In *Biocoordination Chemistry*; Que, J. L., Tolman, W. B., Meyer, T. J., Eds.; Elsevier: Oxford, UK, 2004; Vol. 8; 8, p 91.
(8) Rorabacher, D. B. Electron Transfer by Copper Centers;*Chem. Rev.* **2004**, *104*, 651.
(9) Wilson, T. D.; Yu, Y.; Lu, Y. Understanding Copper-thiolate Containing Electron Transfer Centers by Incorporation of Unnatural Amino Acids and the CuA Center into the Type 1 Copper Protein Azurin;*Coord. Chem. Rev.* **2012**, *257*, 260.
(10) Liu, J.; Chakraborty, S.; Hosseinzadeh, P.; Yu, Y.; Tian, S.; Petrik, I.; Bhagi, A.; Lu, Y. Metalloproteins containing cytochrome, iron-sulfur, or copper redox centers;*Chem. Rev.* **2014**, *114*, 4366.
(11) Keilin, D.; Hartree, E. F. Cytochrome and cytochrome oxidase;*Proc. R. Soc. London, Ser. B* **1939**, *127*, 167.
(12) Lember, R.; Barrett, J. *Cytochromes*; Academic Press: London, 1973.
(13) Vonjagow, G.; Sebald, W. B-Type Cytochromes;*Annu. Rev. Biochem* **1980**, *49*, 281.
(14) Meyer, T. E.; Kamen, M. D. New Perspectives on C-Type Cytochromes;*Adv. Protein Chem.* **1982**, *35*, 105.
(15) Pettigrew, G. W.; Moore, G. R. *Cytochromes C: Biological Aspects*; Springer: Berlin, 1987.
(16) Coutinho, I. B.; Xavier, A. V. Tetraheme cytochromes;*Methods Enzymol.* **1994**, *243*, 119.
(17) Rodgers, K. R.; Lukat-Rodgers, G. S. In *Comprehensive Coordination Chemistry II*; McCleverty, J. A., Meyer, T. J., Eds.; Elsevier Ltd.: Amsterdam, 2004; Vol. 8, p 17.
(18) Tsibris, J. C. M.; Woody, R. W. Structural studies of iron-sulfur proteins.;*Coord. Chem. Rev.* **1970**, *5*, 417.
(19) Beinert, H.; Holm, R. H.; Munck, E. Iron-sulfur clusters: nature's modular, multipurpose structures;*Science* **1997**, *277*, 653.
(20) Sticht, H.; Rosch, P. The structure of iron-sulfur proteins.;*Prog. Biophys. Mol. Biol.* **1998**, *70*, 95.
(21) Anand, B. N. Iron-sulfur proteins and their synthetic analogs: structure, reactivity and redox properties.;*Resonance* **1998**, *3*, 52.
(22) Kummerle, R.; Kyritsis, P.; Gaillard, J.; Moulis, J.-M. Electron transfer properties of iron-sulfur proteins.;*J. Inorg. Biochem.* **2000**, *79*, 83.
(23) Meyer, J. Iron-sulfur protein folds, iron-sulfur chemistry, and evolution.;*J. Biol. Inorg. Chem.* **2008**, *13*, 157.
(24) Lill, R. Function and biogenesis of iron-sulfur proteins.;*Nature* **2009**, *460*, 831.
(25) Romero, A.; Hoitink, C. W. G.; Nar, H.; Huber, R.; Messerschmidt, A.; Canters, G. W. X-ray analysis and spectroscopic characterization of M121Q azurin. A copper site model for stellacyanin;*J. Mol. Biol.* **1993**, *229*, 1007.
(26) Pascher, T.; Karlsson, B. G.; Nordling, M.; Malmström, B. G.; Vänngård, T. Reduction potentials and their pH dependence in site-directed-mutant forms of azurin from Pseudomonas aeruginosa;*Eur. J. Biochem.* **1993**, *212*, 289.
(27) Yanagisawa, S.; Dennison, C. Reduction potential tuning at a type 1 copper site does not compromise electron transfer reactivity;*J. Am. Chem. Soc.* **2005**, *127*, 16453.
(28) Davies, G. J.; Ducros, V. In *Handbook of metalloproteins*; Messerschmidt, A., Huber, R., Poulos, T., Wieghardt, K., Eds.; Wiley: Chichester, 2001; Vol. 2, p 1359.
(29) Lowery, M. D.; Solomon, E. I. Axial ligand bonding in blue copper proteins;*Inorg. Chim. Acta* **1992**, *198–200*, 233.
(30) Nar, H.; Messerschmidt, A.; Huber, R.; van de Kamp, M.; Canters, G. W. Crystal structure analysis of oxidized Pseudomonas aeruginosa azurin at pH 5.5 and pH 9.0. A pH-induced conformational transition involves a peptide bond flip;*J. Mol. Biol.* **1991**, *221*, 765.
(31) Yanagisawa, S.; Banfield, M. J.; Dennison, C. The role of hydrogen bonding at the active site of a Cupredoxin: The Phe114Pro azurin variant.;*Biochemistry* **2006**, *45*, 8812.
(32) Clark, K. M.; Yu, Y.; Marshall, N. M.; Sieracki, N. A.; Nilges, M. J.; Blackburn, N. J.; van, d. D. W. A.; Lu, Y. Transforming a blue copper into a red copper protein: engineering cysteine and homocysteine into the axial position of azurin using site-directed mutagenesis and expressed protein ligation;*J. Am. Chem. Soc.* **2010**, *132*, 10093.
(33) Kanbi, L. D.; Antonyuk, S.; Hough, M. A.; Hall, J. F.; Dodd, F. E.; Hasnain, S. S. Crystal structures of the Met148Leu and Ser86Asp mutants of rusticyanin from Thiobacillus ferrooxidans: insights into the structural relationship with the cupredoxins and the multi copper proteins;*J. Mol. Biol.* **2002**, *320*, 263.
(34) Marshall, N. M.; Garner, D. K.; Wilson, T. D.; Gao, Y.-G.; Robinson, H.; Nilges, M. J.; Lu, Y. Rationally tuning the reduction potential of a single cupredoxin beyond the natural range;*Nature* **2009**, *462*, 113.
(35) Poulos, T. L. Heme enzyme crystal structures;*Adv. Inorg. Biochem.* **1988**, *7*, 1.
(36) Dawson, J. H. Probing structure-function relations in heme-containing oxygenases and peroxidases;*Science* **1988**, *240*, 433.
(37) Poulos, T. L.; Kraut, J. The stereochemistry of peroxidase catalysis;*J. Biol. Chem.* **1980**, *255*, 8199.
(38) Banci, L.; Bertini, I.; Turano, P.; Tien, M.; Kirk, T. K. Proton NMR investigation into the basis for the relatively high redox potential of lignin peroxidase;*Proc. Natl. Acad. Sci. U S A* **1991**, *88*, 6956.
(39) Bowman, S. E.; Bren, K. L. Variation and analysis of second-sphere interactions and axial histidinate character in c-type cytochromes;*Inorg. Chem.* **2010**, *49*, 7890.
(40) Berghuis, A. M.; Brayer, G. D. Oxidation state-dependent conformational changes in cytochrome *c*;*J. Mol. Biol.* **1992**, *223*, 959.
(41) Berghuis, A. M.; Guillemette, J. G.; Smith, M.; Brayer, G. D. Mutation of tyrosine-67 to phenylalanine in cytochrome *c* significantly alters the local heme environment;*J. Mol. Biol.* **1994**, *235*, 1326.

(42) Adachi, S.; Nagano, S.; Watanabe, Y.; Ishimori, K.; Morishima, I. Alteration of human myoglobin proximal histidine to cysteine or tyrosine by site-directed mutagenesis: characterization and their catalytic activities;*Biochem. Biophys. Res. Commun.* **1991**, *180*, 138.
(43) Conroy, C. W.; Tyma, P.; Daum, P. H.; Erman, J. E. Oxidation-reduction potential measurements of cytochrome c peroxidase and pH dependent spectral transitions in the ferrous enzyme;*Biochim. Biophys. Acta, Protein Struct.* **1978**, *537*, 62.
(44) Langen, R.; Jensen, G. M.; Jacob, U.; Stephens, P. J.; Warshel, A. Protein control of iron-sulfur cluster redox potentials.;*J. Biol. Chem.* **1992**, *267*, 25625.
(45) Chen, K.; Tilley, G. J.; Sridhar, V.; Prasad, G. S.; Stout, C. D.; Armstrong, F. A.; Burgess, B. K. Alteration of the reduction potential of the [4Fe-4S](2+/+) cluster of Azotobacter vinelandii ferredoxin I;*J. Biol. Chem.* **1999**, *274*, 36479.
(46) Adman, E.; Watenpaugh, K. D.; Jensen, L. H. NH---S hydrogen bonds in *Peptococcus aerogenes* ferredoxin, *Clostridium pasteurianum* rubredoxin, and *Chromatium* high potential iron protein;*Proc. Natl. Acad. Sci. U S A* **1975**, *72*, 4854.
(47) Backes, G.; Mino, Y.; Loehr, T. M.; Meyer, T. E.; Cusanovich, M. A.; Sweeney, W. V.; Adman, E. T.; Sanders-Loehr, J. The environment of Fe4S4 clusters in ferredoxins and high-potential iron proteins. New information from x-ray crystallography and resonance Raman spectroscopy;*J. Am. Chem. Soc.* **1991**, *113*, 2055.
(48) Ichiye, T. Computational studies o redox properties of electron transfer proteins;*AIP Conf. Proc.* **1999**, *492*.
(49) Noodleman, L.; Pique, M. E.; Roberts, V. A.; John Wiley & Sons, Inc.: 2009; Vol. 2, p 458.
(50) Link, T. A. The structures of Rieske and Rieske-type proteins.;*Adv. Inorg. Chem.* **1999**, *47*, 83.
(51) Brown, E. N.; Friemann, R.; Karlsson, A.; Parales, J. V.; Couture, M. M.; Eltis, L. D.; Ramaswamy, S. Determining Rieske cluster reduction potentials;*J. Biol. Inorg. Chem.* **2008**, *13*, 1301.
(52) Denke, E.; Merbitz-Zahradnik, T.; Hatzfeld, O. M.; Snyder, C. H.; Link, T. A.; Trumpower, B. L. Alteration of the midpoint potential and catalytic activity of the Rieske iron-sulfur protein by changes of amino acids forming hydrogen bonds to the iron-sulfur cluster;*J. Biol. Chem.* **1998**, *273*, 9085.
(53) Mason, J. R.; Cammack, R. The electron-transport proteins of hydroxylating bacterial dioxygenases;*Annu. Rev. Microbiol.* **1992**, *46*, 277.
(54) Berry, S. M.; Baker, M. H.; Reardon, N. J. Reduction potential variations in azurin through secondary coordination sphere phenylalanine incorporations.;*J. Inorg. Biochem.* **2010**, *104*, 1071.
(55) Benson, D. R.; Hart, B. R.; Zhu, X.; Doughty, M. B. Design, Synthesis, and Circular Dichroism Investigation of a Peptide-Sandwiched Mesoheme;*J. Am. Chem. Soc.* **1995**, *117*, 8502.
(56) Holm, R. H.; Kennepohl, P.; Solomon, E. I. Structural and Functional Aspects of Metal Sites in Biology;*Chem. Rev.* **1996**, *96*, 2239.
(57) Shifman, J. M.; Gibney, B. R.; Sharp, R. E.; Dutton, P. L. Heme redox potential control in de novo designed four-alpha-helix bundle proteins;*Biochemistry* **2000**, *39*, 14813.
(58) Gibney, B. R.; Isogai, Y.; Rabanal, F.; Reddy, K. S.; Grosset, A. M.; Moser, C. C.; Dutton, P. L. Self-assembly of heme *a* and heme *b* in a designed four-helix bundle: implications for a cytochrome *c* oxidase maquette;*Biochemistry* **2000**, *39*, 11041.
(59) Jensen, G. M.; Warshel, A.; Stephens, P. J. Calculation of the redox potentials of iron-sulfur proteins: the 2-/3-couple of [Fe4S*4Cys4] clusters in Peptococcus aerogenes ferredoxin, Azotobacter vinelandii ferredoxin I, and Chromatium vinosum high-potential iron protein;*Biochemistry* **1994**, *33*, 10911.
(60) Shen, B.; Jollie, D. R.; Stout, C. D.; Diller, T. C.; Armstrong, F. A.; Gorst, C. M.; La Mar, G. N.; Stephens, P. J.; Burgess, B. K. Azotobacter vinelandii ferredoxin I. Alteration of individual surface charges and the [4FE-4S]2+/+ cluster reduction potential;*J. Biol. Chem.* **1994**, *269*, 8564.
(61) Dey, A.; Jenney, F. E., Jr.; Adams, M. W.; Babini, E.; Takahashi, Y.; Fukuyama, K.; Hodgson, K. O.; Hedman, B.; Solomon, E. I. Solvent tuning of electrochemical potentials in the active sites of HiPIP versus ferredoxin;*Science* **2007**, *318*, 1464.
(62) Worrall, J. A. R.; Schlarb-Ridley, B. G.; Reda, T.; Marcaida, M. J.; Moorlen, R. J.; Wastl, J.; Hirst, J.; Bendall, D. S.; Luisi, B. F.; Howe, C. J. Modulation of Heme Redox Potential in the Cytochrome c6 Family;*J. Am. Chem. Soc.* **2007**, *129*, 9468.
(63) Lett, C. M.; Guillemette, J. G. Increasing the redox potential of isoform 1 of yeast cytochrome c through the modification of select haem interactions;*Biochem. J.* **2002**, *362*, 281.
(64) Varadarajan, R.; Zewert, T. E.; Gray, H. B.; Boxer, S. G. Effects of buried ionizable amino acids on the reduction potential of recombinant myoglobin;*Science* **1989**, *243*, 69.
(65) Wilson, D. F.; Erecinska, M.; Brocklehurst, E. S. Chemical properties of cytochrome c oxidase in intact mitochondria.;*Arch. Biochem. Biophys.* **1972**, *151*, 180.
(66) Banci, L.; Bertini, I.; Ciurli, S.; Luchinat, C.; Pierattelli, R. Rationalization of the reduction potentials within the series of the high potential iron-sulfur proteins;*Inorg. Chim. Acta* **1995**, *240*, 251.
(67) Soriano, A.; Li, D.; Bian, S.; Agarwal, A.; Cowan, J. A. Factors influencing redox thermodynamics and electron self-exchange for the [Fe4S4] cluster in Chromatium vinosum high potential iron protein: the role of core aromatic residues in defining cluster redox chemistry;*Biochemistry* **1996**, *35*, 12479.
(68) Liu, D.; Williamson, D. A.; Kennedy, M. L.; Williams, T. D.; Morton, M. M.; Benson, D. R. Aromatic side chain-porphyrin interactions in designed hemoproteins;*J. Am. Chem. Soc.* **1999**, *121*, 11798.
(69) Vondrasek, J.; Bendova, L.; Klusak, V.; Hobza, P. Unexpectedly Strong Energy Stabilization Inside the Hydrophobic Core of Small Protein Rubredoxin Mediated by Aromatic Residues: Correlated Ab Initio Quantum Chemical Calculations;*J. Am. Chem. Soc.* **2005**, *127*, 2615.

(70) Riley, K. E.; Merz, K. M., Jr. Role of solvation in the energy stabilization inside the hydrophobic core of the protein rubredoxin;*J. Phys. Chem. B* **2006**, *110*, 15650.
(71) Ozawa, K.; Takayama, Y.; Yasukawa, F.; Ohmura, T.; Cusanovich, M. A.; Tomimoto, Y.; Ogata, H.; Higuchi, Y.; Akutsu, H. Role of the Aromatic Ring of Tyr43 in Tetraheme Cytochrome c3 from Desulfovibrio vulgaris Miyazaki F;*Biophys. J.* **2003**, *85*, 3367.
(72) Ponamarev, M. V.; Schlarb, B. G.; Howe, C. J.; Carrell, C. J.; Smith, J. L.; Bendall, D. S.; Cramer, W. A. Tryptophan-heme pi-electrostatic interactions in cytochrome f of oxygenic photosynthesis;*Biochemistry* **2000**, *39*, 5971.
(73) Takayama, Y.; Taketa-Sato, M.; Komori, H.; Morita, K.; Kang, S.-J.; Higuchi, Y.; Akutsu, H. Role of π-Electron Systems in Stabilization of the Oxidized Tetraheme Architecture in Cytochrome c₃;*Bull. Chem. Soc. Jpn.* **2011**, *84*, 1096.
(74) Dennison, C.; Vijgenboom, E.; Hagen, W. R.; Canters, G. W. Loop-Directed Mutagenesis Converts Amicyanin from Thiobacillus versutus into a Novel Blue Copper Protein;*J. Am. Chem. Soc.* **1996**, *118*, 7406.
(75) Buning, C.; Canters, G. W.; Comba, P.; Dennison, C.; Jeuken, L.; Melter, M.; Sanders-Loehr, J. Loop-Directed Mutagenesis of the Blue Copper Protein Amicyanin from Paracoccus versutus and Its Effect on the Structure and the Activity of the Type-1 Copper Site;*J. Am. Chem. Soc.* **1999**, *122*, 204.
(76) Remenyi, R.; Jeuken, L. J.; Comba, P.; Canters, G. W. An amicyanin C-terminal loop mutant where the active-site histidine donor cannot be protonated;*J. Biol. Inorg. Chem.* **2001**, *6*, 23.
(77) Battistuzzi, G.; Borsari, M.; Canters, G. W.; di Rocco, G.; de Waal, E.; Arendsen, Y.; Leonardi, A.; Ranieri, A.; Sola, M. Ligand loop effects on the free energy change of redox and pH-dependent equilibria in cupredoxins probed on amicyanin variants;*Biochemistry* **2005**, *44*, 9944.
(78) Yanagisawa, S.; Dennison, C. Loop-Contraction Mutagenesis of Type 1 Copper Sites;*J. Am. Chem. Soc.* **2004**, *126*, 15711.
(79) Farver, O.; Pecht, I. Long-range intramolecular electron transfer in azurins;*Proc. Natl. Acad. Sci. U S A* **1989**, *86*, 6968.
(80) Mizoguchi, T. J.; Di Bilio, A. J.; Gray, H. B.; Richards, J. H. Blue to type 2 binding. Copper(II) and cobalt(II) derivatives of a Cys112Asp mutant of Pseudomonas aeruginosa azurin;*J. Am. Chem. Soc.* **1992**, *114*, 10076.
(81) Karlsson, B. G.; Nordling, M.; Pascher, T.; Tsai, L.-C.; Sjolin, L.; Lundberg, L. G. Cassette mutagenesis of Met121 in azurin from Pseudomonas aeruginosa;*Protein Eng.* **1991**, *4*, 343.
(82) Den Blaauwen, T.; Canters, G. W. Creation of type-1 and type-2 copper sites by addition of exogenous ligands to the Pseudomonas aeruginosa azurin His117Gly mutant;*J. Am. Chem. Soc.* **1993**, *115*, 1121.
(83) Messerschmidt, A.; Prade, L.; Kroes, S. J.; Sanders-Loehr, J.; Huber, R.; Canters, G. W. Rack-induced metal binding vs. flexibility: Met121His azurin crystal structures at different pH;*Proc. Natl. Acad. Sci. U S A* **1998**, *95*, 3443.
(84) Skov, L. K.; Pascher, T.; Winkler, J. R.; Gray, H. B. Rates of Intramolecular Electron Transfer in Ru(bpy)2(im)(His83)-Modified Azurin Increase below 220 K;*J. Am. Chem. Soc.* **1998**, *120*, 1102.
(85) Baker, E. N.; Anderson, B. F.; Blackwell, K. E.; Kingston, R. L.; Norris, G. E.; Shepard, W. E. B. The relative rigidity of the type 1 copper site in azurin, as seen in high resolution X-ray analyses of various forms of the protein;*J. Inorg. Biochem.* **1991**, *43*, 162.
(86) Bjerrum, M. J.; Casimiro, D. R.; Chang, I. J.; Di Bilio, A. J.; Gray, H. B.; Hill, M. G.; Langen, R.; Mines, G. A.; Skov, L. K.; Winkler, J. R.; et al. Electron transfer in ruthenium-modified proteins;*J. Bioenerg. Biomembr.* **1995**, *27*, 295.
(87) Berry, S. M.; Gieselman, M. D.; Nilges, M. J.; Van der Donk, W. A.; Lu, Y. An engineered azurin variant containing a selenocysteine copper ligand;*J. Am. Chem. Soc.* **2002**, *124*, 2084.
(88) Farver, O.; Canters, G. W.; van Amsterdam, I.; Pecht, I. Intramolecular Electron Transfer in a Covalently Linked Mutated Azurin Dimer;*J. Phys. Chem. A* **2003**, *107*, 6757.
(89) Berry, S. M.; Ralle, M.; Low, D. W.; Blackburn, N. J.; Lu, Y. Probing the role of axial methionine in the blue copper center of azurin with unnatural amino acids;*J. Am. Chem. Soc.* **2003**, *125*, 8760.
(90) Cascella, M.; Magistrato, A.; Tavernelli, I.; Carloni, P.; Rothlisberger, U. Role of protein frame and solvent for the redox properties of azurin from Pseudomonas aeruginosa;*Proc. Natl. Acad. Sci. U S A* **2006**, *103*, 19641.
(91) Lancaster, K. M.; Sproules, S.; Palmer, J. H.; Richards, J. H.; Gray, H. B. Outer-sphere effects on reduction potentials of copper sites in proteins: the curious case of high potential type 2 C112D/M121E Pseudomonas aeruginosa azurin;*J. Am. Chem. Soc.* **2010**, *132*, 14590.
(92) Hadt, R. G.; Sun, N.; Marshall, N. M.; Hodgson, K. O.; Hedman, B.; Lu, Y.; Solomon, E. I. Spectroscopic and DFT studies of second-sphere variants of the type 1 copper site in azurin: Covalent and nonlocal electrostatic contributions to reduction potentials;*J. Am. Chem. Soc.* **2012**, *134*, 16701.
(93) Sieracki, N. A.; Hwang, H. J.; Lee, M. K.; Garner, D. K.; Lu, Y. A temperature independent pH (TIP) buffer for biomedical biophysical applications at low temperatures;*Chem Commun (Camb)* **2008**, 823.
(94) Nilges, M. J., 1979.
(95) Chang, H. R.; Diril, H.; Nilges, M. J.; Zhang, X.; Potenza, J. A.; Schugar, H. J.; Hendrickson, D. N.; Isied, S. S. An unusually stable manganese(II)manganese(III) complex with novel EPR spectra: synthesis, structure, magnetism, and EPR analysis;*J. Am. Chem. Soc.* **1988**, *110*, 625.
(96) Jeuken, L. J. C.; Ubbink, M.; Bitter, J. H.; van Vliet, P.; Meyer-Klaucke, W.; Canters, G. W. The Structural Role of the Copper-coordinating and Surface-exposed Histidine Residue in the Blue Copper Protein Azurin;*J.Mol.Biol.* **2000**, *299*, 737.
(97) Jeuken, L. J. C.; Armstrong, F. A. Electrochemical Origin of Hysteresis in the Electron-Transfer Reactions of Adsorbed Proteins: Contrasting Behavior of the "Blue" Copper Protein, Azurin, Adsorbed on Pyrolytic Graphite and Modified Gold Electrodes;*J. Phys. Chem. B* **2001**, *105*, 5271.

(98) Garner, D. K.; Vaughan, M. D.; Hwang, H. J.; Savelieff, M. G.; Berry, S. M.; Honek, J. F.; Lu, Y. Reduction potential tuning of the blue copper center in Pseudomonas aeruginosa azurin by the axial Methionine as probed by unnatural amino acids;*J. Am. Chem. Soc.* **2006**, *128*, 15608.
(99) Solomon, E. I.; Baldwin, M. J.; Lowery, M. D. Electronic Structures of Active Sites in Copper Proteins: Contributions to Reactivity;*Chem. Rev.* **1992**, *92*, 521.
(100) Solomon, E. I. Spectroscopic Methods in Bioinorganic Chemistry: Blue to Green to Red Copper Sites;*Inorg. Chem.* **2006**, *45*, 8012.
(101) Freeman, H. C. Metalloprotein crystallography;*ACS Symp. Ser.* **1998**, *692*, 62.
(102) Hammann, C.; van Pouderoyen, G.; Nar, H.; Rüth, F.-X. G.; Messerschmidt, A.; Huber, R.; den Blaauwen, T.; Canters, G. W. Crystal structures of modified apo-His117Gly and apo-His46Gly mutants of Pseudomonas aeruginosa azurin;*J. Mol. Biol.* **1997**, *266*, 357.
(103) Den Blaauwen, T.; Van, d. K.; Canters, G. W. Type I and II copper sites obtained by external addition of ligands to a His117Gly azurin mutant;*J. Am. Chem. Soc.* **1991**, *113*, 5050.
(104) van Pouderoyen, G.; Andrew, C. R.; Loehr, T. M.; Sanders-Loehr, J.; Mazumdar, S.; Hill, H. A.; Canters, G. W. Spectroscopic and Mechanistic Studies of Type-1 and Type-2 Copper Sites in Pseudomonas aeruginosa Azurin As Obtained by Addition of External Ligands to Mutant His46Gly;*Biochemistry* **1996**, *35*, 1397.
(105) Hong, G.; Ivnitski, D. M.; Johnson, G. R.; Atanassov, P.; Pachter, R. Design Parameters for Tuning the Type 1 Cu Multicopper Oxidase Redox Potential: Insight from a Combination of First Principles and Empirical Molecular Dynamics Simulations;*J. Am. Chem. Soc.* **2011**, *133*, 4802.
(106) Tsai, B. L. C.; Sjolin, L.; Langer, V.; Bonander, N.; Karlsson, G.; Vänngård, T.; Hammann, C.; Nar, H. Structure of the Azurin Mutant Nickel-Trp48Met from Pseudomonas aeruginosa at 2.2A Resolution;*Acta Crystallographica* **1995**, *D51*, 711.
(107) Hoffman, B.; Nocek, J. M.; Liang, Z.-X.; Leesch, V. W.; Kurnikov, I. V.; Beratan, D. N. Electrostatic control of electron transfer within protein complexes;*Abstr.Pap.- Am.Chem.Soc.* **2000**, *220th*, INOR.
(108) Hoitink, C. W. G.; Canters, G. W. The importance of Asn47 for structure and reactivity of azurin from Alcaligenes denitrificans as studied by site-directed mutagenesis and spectroscopy;*J. Biol. Chem.* **1992**, *267*, 13836.
(109) Hall, J. F.; Kanbi, L. D.; Harvey, I.; Murphy, L. M.; Hasnain, S. S. Modulating the redox potential and acid stability of Rusticyanin by site-directed mutagenesis of Ser86.;*Biochemistry* **1998**, *37*, 11451.
(110) Machczynski, M. C.; Gray, H. B.; Richards, J. H. An outer-sphere hydrogen-bond network constrains copper coordination in blue proteins;*J. Inorg. Biochem.* **2002**, *88*, 375.
(111) Regan, J. J.; Di Bilio, A. J.; Langen, R.; Skov, L. K.; Winkler, J. R.; Gray, H. B.; Onuchic, J. N. Electron tunneling in azurin: the coupling across a b-sheet;*Chemistry & biology* **1995**, *2*, 489.

CHAPTER 5

INVESTIGATING MARCUS INVERTED REGION IN A NON-DERIVATIZED PROTEIN SYSTEM USING A SERIES OF AZURIN VARIANTS

* Portions of this chapter are from the manuscript published in *J. Phys. Chem. Let.* "Long-range electron transferred in engineered Azurins exhibits Marcus inverted region behavior" (Farver O., Hosseinzadeh P., Marshall N.M., Wherland S., Lu Y., Pecht I.). Farver O., Wherland S., and Pecht I. performed the electron transfer studies and generated the related figures.

5.1. Introduction

5.1.1. Marcus theory of ET

Marcus theory of electron transfer was first developed by Rudolph Marcus to describe ET rates in a non-adiabatic system in which electrons are transferred between two molecules without any perturbation of the structures or reorganization of ligands, i.e. outer-sphere ET.[1] The main assumption behind the theory is that such ET reaction happens through reorganization of solvent molecules that are shielding the two redox centers. During ET, the two reactants more or less keep their individuality. Hence, the electron can jump as a whole. Since the rate of electron jump is faster than the reorganization of the solvent molecules, the nuclear positions of solvent molecules remain constant before and after the reaction (Frank-Condon principle). Therefore, the electron jump is only possible when the energy of ET system doesn't change during the jump. A visual representation of what stated above is provided in Figure 5.1a. As shown in the figure, electron transfer can happen only and only when the energy diagrams of the system of two reactants before and after ET overlap. The basic equation of Marcus theory is shown in equation 5.1:

$$k_{ET} = \frac{2\pi}{\hbar} |H_{AB}|^2 \frac{1}{\sqrt{4\pi\lambda k_b T}} \exp\left(-\frac{(\lambda+\Delta G^\circ)^2}{4\lambda k_b T}\right) \qquad \text{Eq. 5.1}$$

where k_{ET} is the rate of electron transfer, H_{AB} is the electron coupling constant. The higher H_{AB}, the higher the coupling between the two systems, hence higher probability of electron jumps. λ is the reorganization energy, a term that is an indicative of changes in the system before

and after ET event. The smaller the λ, the lower the rearrangement of molecules between molecules of solvent in the system during ET. ΔG° is the driving force of the reaction.[1]

One counterintuitive prediction of Marcus equation is that by moving towards more negative free energies, which is known to increase the reaction rates, after a certain point, which is called reorganization energy, the rate of ET would decrease. This regime is also known as Marcus inverted region (Figure 5.1b). Later, unambiguous experimental results confirmed the presence of Marcus inverted region in several organic and inorganic small molecules,[2,3] and derivatized[4,5] and non-derivatized protein systems.[6] Although the equation predicts a hyperbolic shape for the rate, the rates at inverted region usually reach a plateau due to generation of electronically excited products.[7]

Marcus theory has been widely used to explain ET processes in biology including photosynthesis, charge separation, some types of chemiluminescence and corrosion.[7]

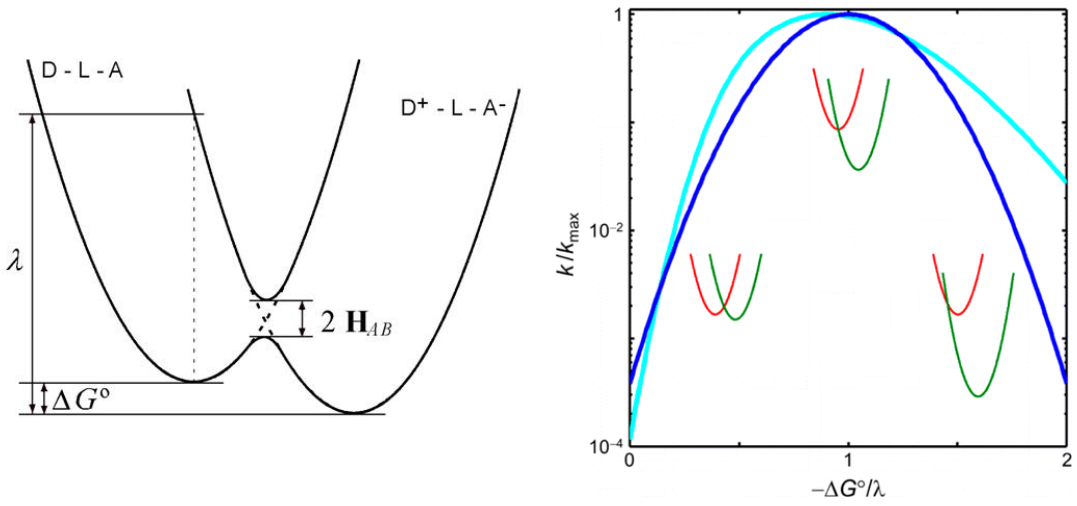

Figure 5.1. (a) Schematic representation of energy diagrams of the ET system before and after ET (figure from Wikipedia). (b) Effects of changes in rate based on changes in driving force and visual representation of Marcus inverted region (Adapted from 7).

5.1.2. Ways to measure ET rates

Direct measurement of ET rates in metalloprotiens is of prime importance for understanding the kinetics of the process and obtaining the experimental values for ET. There are several ways to measure intermolecular and intramolecular rate constants of ET. We will briefly give some examples of such ways without going into details since it is not within the scope of this review.

A very common classic way of measuring the rates of intermolecular ET (i.e. between two molecules) is through using stopped-flow kinetics and monitoring the accumulation or decay of species using UV-vis. This method is particularly useful for heme-containing proteins as they have very strong soret band that is distinct between reduced and oxidized forms and has been widely used to study ET rates in heme proteins.[8] The data will then fit into rate equations, most of the times first order or second order rate equations, and rate constants will be deduced.

Pulse radiolysis is another very common technique to measure ET rates. In this technique, a single pulse of high-energy radiation will be delivered to sample. The pulse should be powerful enough to generate sufficient amount of reactive intermediates that can be detected by some means such as UV-vis, EPR, or fluorescent. Fast electrons with 2-15 MeV energy are a common source of such pulses. A high-energy irradiation will be applied to the protein sample and will generate both oxidizing ($OH^{-\square}$) and reducing ($H^{\square}$) reactive species. Based on the molecules in the solution, these reactive species will later generate some reactive intermediates in the proteins that can transfer electrons to the metal center. For biological studies, reactions are performed in formate buffer, interaction of which with $OH^{-\square}$ anion radical will result in a powerful reducing agent, $CO_2^{-\square}$ anion radical.[9,10] As an example, $CO_2^{-\square}$ anion radicals have been used to later generate disulfide anion radicals in Azurin. Electrons will then transfer from this anion radical (decay can be tracked by monitoring 410 nm peak, ε_{410}=10,000 $M^{-1}cm^{-1}$) to the reduced metal center and the production of oxidized metal will be monitored at the right wavelength. At any given temperature, k_{ET} is:[6,11,12]

$$k_{ET} = k(r)v\ exp\left\{-\frac{E_a}{RT}\right\} \qquad \text{Eq. 5.2}$$

where k(r) is the electronic transmission coefficient at a distance r between two reactants, v is the nuclear frequency factor, and E_a is the activation free energy.

Flash photolysis is another way of measuring ET rates in biological samples. This technique is very similar to pulse radiolysis, but with a lower energy. In flash photolysis, samples are irradiated with highly focused laser beams. Upon irradiation, a chemical reaction would happen that cause a certain molecule in the sample to go to an excited state. This molecule will then transfer electrons to the metal site and the rates can be measured by fitting the curves obtained from monitoring the formation of final products or decay of initial reactive species. One example

of molecules that can get excited by laser is flavin cofactor.[13] The most commonly used so-called photosensitive molecule is probably trisbipyridine Ru(II) ($[Ru(bpy)_3]^{2+}$ hereafter). Upon irradiation, $Ru(bpy)_3$ will go to the $[Ru(bpy)_3]^{2+*}$ excited state. This molecule can either accept or donate an electron. In the presence of sacrificial oxidants in the solution such as peroxodisulfate or chloropentamine cobalt chloride, $[Ru(bpy)_3]^{2+*}$ will transfer an electron and turn into $[Ru(bpy)_3]^{3+}$, which is a strong oxidant. Conversely, $[Ru(bpy)_3]^{2+*}$ can be a reductant and donates electrons directly. In order for the process to be catalytic, presence of sacrificial reductants such as $EDTA^{4-}$ or triethanolamine is required. ($[Ru(bpy)_3]^{2+}$ have been widely used by multiple groups to study ET rates in several proteins such as Az, Mb, and cytochrome *c*.[14-21]

Cyclic voltammetry (CV) is another way to obtain ET rate constants. While CV is mostly known for its ability to measure reduction potential, ET rates can be deduced using the peak separation at different scan rate and applying Marcus theory.[22-25] The common way of modeling the rate is to fit the data by Butler-Volmer equation:

$$k_{ox}^{BV} = k_0 \exp\left(\frac{-\alpha n F (E - E^\circ)}{RT}\right) \qquad \text{Eq. 5.3}$$

$$k_{red}^{BV} = k_0 \exp\left(\frac{(1-\alpha) n F (E - E^\circ)}{RT}\right) \qquad \text{Eq. 5.4}$$

Where E is the applied potential, E° is the formal reduction potential of the couple, n is the number of transferred electrons, α is the transfer coefficient showing the degree of symmetry of the rate constant for oxidation and reduction and k_0 is the rate at zero overpotential.

5.1.3. Long-range ET

Perhaps the most intriguing feature of ET in biology is the fact that in many biological systems electrons can transfer over long distances. In order to explain long-range ET in respiratory chain, it was proposed initially that electrons move in energy bands, like what is observed in semiconductors [26]. It is now clear that long-range ET in biology is achieved through two main mechanisms, electron tunneling, mostly, and electron hopping.[7,27,28] A thermally activated model of tunneling was first postulated by Hopfield[29] and was then experimentally proved by Gray and coworkers using Ru modified cytochrome *c*.[30] Later several studies were

performed on understanding the electron tunneling and rules governing it. In general, electron tunneling is distant-dependent as the coupling constant (H_{AB}) decrease exponentially with distance. Figure 5.2 shows the dependence of tunneling time with distance in several media.

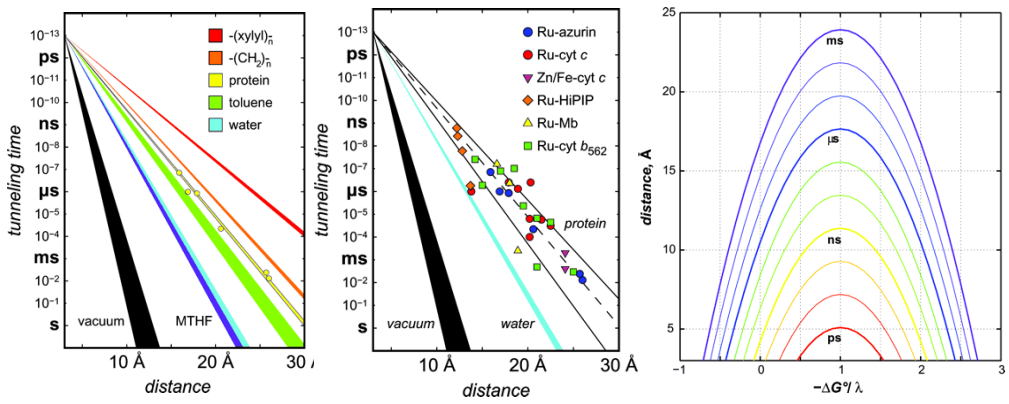

Figure 5.2. (a) and (b) show how the tunneling time increase rapidly by increase in the distance between electron donor and acceptor. (a) shows a comparison between different media and (b) shows a more detailed results in different protein systems. (c) shows the contour diagram of dependence of rates to distance. Figures are adapted with permission from Ref. 28

Electrons can tunnel effectively up to a distance of 2.5 nm in proteins due to their small mass.[28,31,32] For transfers after this range, multiple electronic tunneling steps are required, a process called hopping. In order for hopping to be efficient, the sites should be arranged in a favorable manner with low reorganization energies, i.e. the free energy changes of endergonic reactions between intermediates steps being less than 0.2 eV.[28] Multiple electron tunneling steps happen through redox active cofactors, including metal centers and also amino acids. In general, covalent bonds are preferred to van der Waals interactions (through-bond *vs*. through-space) and aromatic residues are preferred over non-aromatic residues. Interestingly, a sequence analysis of different classes of proteins in databank showed that the frequency of aromatic residues in oxidoreductases (enzymes performing reactions that require ET) is significantly higher than others and above the average [7].

5.1.4. Previous studies on Marcus inverted region-the need for a protein-only system

It was not until 1984 when Miller, Calcaterra and Closs provided the first experimental observation of the Marcus inverted region, three decades after Marcus coined it. They measured the intramolecular ET rates anions of bifunctional steroids (Figure 5.3) and showed that in 2-methyltetrahydrophuran (MTHF) solution, inverted region can be observed at 296 K.[2]

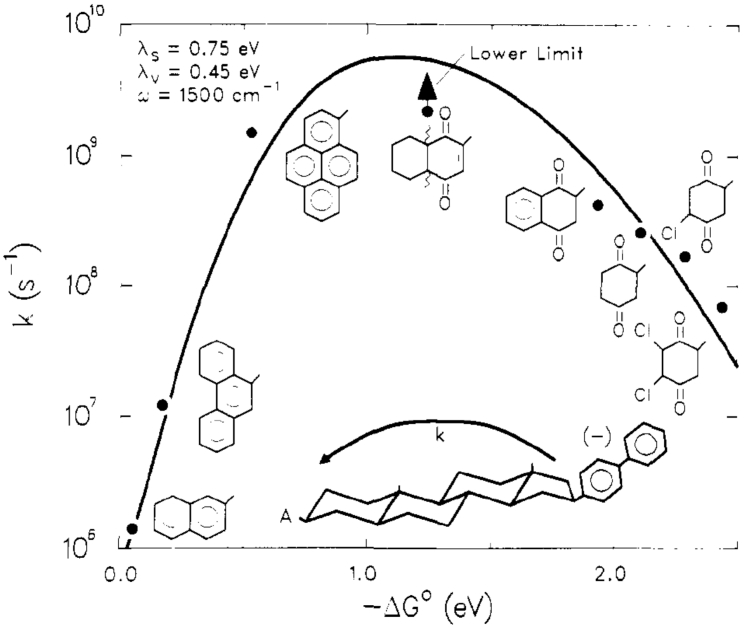

Figure 5.3. Inverted region can be observed in intramolecular ET rates between anions of bifunctional steroids in MTHF solution, measured at 296 K. Figure from ref. [2]

Later, more and more experiments described the observation of the inverted region in different systems. Gray and coworkers reported the observation of a Gaussian free-energy dependence in photoinduced ET rates in a series of synthetic electron donor-acceptors, as predicted by Marcus theory.[3] In these series, the electron donors were excited Iridium dimers and the acceptors were *N*-alkylpyridinium groups covalently linked to the phosphinite ligands of Ir_2.

A series of studies later showed that Marcus inverted region can be observed in derivatized protein systems as well. A classic example of such observation is reported by Millett and coworkers.[4] They measured the rates of ET in a cytochrome b_5 system that was labeled by Ruthenium(II) polypyridine complexes.

While several reports are available in which the Marcus inverted region is observed in a synthetic or derivatized protein systems, reports of observation of such system in protein-only systems are rare. We only found two examples of such observation. The first is reported by Gunner and Dutton in the reaction center from *Rhodobacter spheroids*.[33] They measured the ET rates from bacteriopheophytin to different quinones in a series of temperatures and in some they observed the inverted region and Gaussian dependence of the rates to the free energy. It is worth noting that while the study was performed in a native protein, the rates of ET were between two cofactors. The other example was recently provided by Boussac *et. Al.*[34] They studied the kinetics of charge recombination in the Tyr-qunione radical pair in photosystem II of

Thermosynechococcus elongates in cryogenic temperatures using EPR and showed that this recombination occurred in Marcus inverted region.

In this chapter I report our studies to demonstrate Marcus inverted region in a non-derivatzied protein system. This study is built upon our previous investigation of the intramolecular ET rates in a series of azurin variants with different reduction potentials.[12] In that paper we observed lower reorganization energy in our variants compared to the WT-Az, which was contributed to a more flexible Cu binding site. We also observed a plateau in the free energy dependence plot of the rates. These observations gave us hope that we are close to reach the Marcus inverted region and we should be able to observe that region by using variants with higher reduction potential. Indeed, we observed, for the first time, the Marcus inverted region within a system consisting of only protein at room temperature.

5.2. Materials and methods

5.2.1. Preparation, purification and characterization of azurin (Az) mutants

The Az mutants were constructed, expressed and purified following the previously reported protocols.[12,16,35] Correct mutations were verified by DNA sequencing. To ensure higher purity, a gel filtration chromatography step was added to the last step of the purification process. Such a protocol resulted in a low yield for N47S/F114S/M121L Az. To obtain this protein with a higher yield, the procedure of induction and growth of cells were revised as follows: Two litres of 2xYT media was inoculated by 50 ml of an overnight starter culture and grew to optical density (OD) = 0.6 at 25 °C. Expression was then induced at 25 °C by addition of 1mM IPTG and expression continued overnight. The identity of proteins were again confirmed by electrospray ionization (ESI) mass spectrometry using ZMD (Waters) ESI mass spectrometer at the School of Chemical Sciences Mass Spectrometry Laboratory (Urbana, IL). To check the mass of copper-free proteins, formic acid was used to ionize the protein upon injection.

5.2.2. Electrochemical measurements

Redox potentials of the proteins were measured on a CH instruments electrochemical analyzer equipped with Chi620a software, using a previously reported protein film voltammetry technique.[12,35-37] All the measurements were performed in 10 mM sodium phosphate buffer at pH

7 with 100 mM sodium formate in order to reproduce the conditions employed in the pulse radiolysis experiments. To increase the electrochemical signal for some of the mutants, a dodecyldimethyl ammonium bromide (DDAB)-coated electrode was used to collect the CV results in protein solutions as reported before.[38]

5.2.3. Spectroscopic analysis

UV-vis spectra were collected on an Agilent 8453 diode array spectrometer. The buffer used for these studies was 50 mM ammonium acetate at pH 6.35. EPR spectra were collected using an X-band Varian E-122 spectrometer at the Illinois EPR Research Center. Most of the samples were prepared by exchanging the protein into TIP7 buffer since the effective pH of this buffer is known to remain about the same at cryogenic temperatures as that at room temperature.[39] 50 mM potassium phosphate buffer at pH 6.5 with 100 mM NaCl was used to obtain the data for N47S/F114S/M121L mutant. The spectra were simulated using the Simpow program.[40,41] The observed spectral parameters for all the Az mutants in this study are in good agreement with reported values for type 1 copper, electron transfer proteins.

5.2.4. Kinetic measurements

The pulse radiolysis experiments were carried out using the Varian V-7715 linear accelerator at the Hebrew University in Jerusalem. 5 MeV pulses of accelerated electrons at pulse lengths in the range from 0.4 to 1.0 μs were applied. All kinetic measurements were carried out anaerobically in N_2O saturated solutions contained in a 1 cm quartz cuvette using three light passes which results in an overall optical path-length of 3 cm. A 150 W xenon lamp produced the analysing light beam. In order to avoid photochemistry and light scattering, an optical filter with a cut-off at 385 nm was used. The data acquisition system consisted of a Tektronix 390 A/D digitizer connected to a PC. The temperature range employed in the kinetic studies, from 4 to 45 ^{o}C, was controlled by a thermostat, and continuously monitored by a thermocouple attached to the cuvette holder. The protein concentration was varied between 75 and 200 μM. All reactions were performed under pseudo-first order conditions, with typically a 10-fold excess of oxidized protein over reductant. The concentration of Cu(II) was monitored at 600 - 635 nm ($\varepsilon_{625} \sim 5{,}000$ M^{-1} cm^{-1}) while formation and decay of the $RSS^{*}R^{-}$ radical were followed at 410 nm

(ε_{410} = 10,000 M^{-1} cm^{-1}). Data collection was performed in aqueous solutions containing 0.10 M in sodium formate and 10 mM sodium phosphate at pH 7.0, deaerated and saturated with N_2O by bubbling directly in the cuvette. Afterwards, an appropriate small volume of concentrated protein stock solution was added to the cuvette, and N_2O bubbling was continued for another 5-10 minutes before starting the kinetic measurements. Each individual kinetic measurement was repeated at least three times at each temperature. Spectra of the samples were taken prior, during, and after the kinetic measurements to monitor the state of the protein throughout the kinetic measurements. Two reaction phases were observed following the introduction of a pulse into the solutions when monitored by absorption changes at either 410 nm (disulfide radical) or at ~625 nm [Cu(II)]. The first step is the bimolecular reduction of disulfide (monitored at 410nm) and Cu(II) (at ~625nm) by the CO_2^- radicals, followed by the second phase shown to be the intramolecular ($RSS^{\bullet}R^-$ to Cu(II)) ET which is the process of interest (*cf.* reaction scheme and Fig. 2). All the kinetic traces were analysed by fitting to a sum of exponentials using a non-linear least squares program written in MATLAB® (The MathWorks, Natick, MA)

5.2.5. Molecular dynamics simulations

Molecular dynamics were performed using VMD and NAMD software.[42,43] The structure of mutants was modelled based on PDBs reported in Table S2. PSF files were generated using the PSFGEN suite in VMD. Proteins were solvated in a water box with a size 15 Å, and the overall structure was neutralized by 0.1 M NaCl. Molecular dynamics simulations were performed using 1000 or 2000 steps of minimization followed by 1 ns of equilibration (2 fs/step) in a PVT format.

5.3. Results and discussion

5.3.1. Mutant design and reduction potentials

In order to enable a quantitative examination of the relationship between the ET driving force and the rate constant in a protein-only system without any ancillary foreign donor or acceptor, we have now expanded this series and prepared several other mutants (F114N, N47S/F114S/M121L, and M44F/N47S/F114N/G116F) with higher potentials than that of WT Az (Figure 5.4 and Table 5.1).

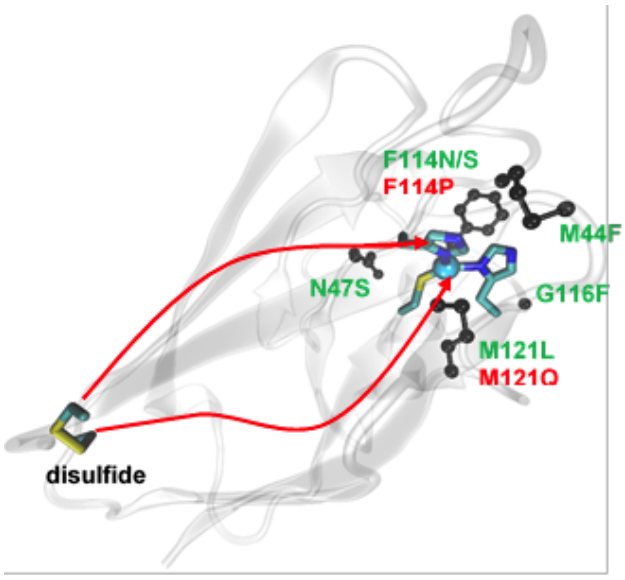

Figure 5.4. Schematic presentation of Az and the designed mutants. Calculated paths (see below) of electron transfer from the disulfide to Cu are illustrated by the red arrows. The mutated residues are shown in black stick and ball. The green mutations cause increase in reduction potential while the red ones decrease it.

Table 5.1. Rate constants, activation parameters of the intramolecular ET reactions, and the potentials of the copper site.

	Azurin Mutant	k_{ET} (s^{-1}) at 298 K	E° (mV)	$\Delta H^{\ddagger}$ (kJ/mol)	$\Delta S^{\ddagger}$ (J/K·mol)
1.	**F114P/M121Q***	81 ± 11	122 ± 6	36.6 ± 7.5	-86 ± 14
2.	**F114P***	191 ± 26	220 ± 18	~29	-106
3.	**F114N****	198 ± 14	381 ± 8	29.9 ± 0.2	-101 ± 1
4.	**N47S/F114N***	387 ± 59	499 ± 3	33.7 ± 2.5	-82 ± 4
5.	**N47S/M121L***	355 ± 51	503 ± 5	44.0 ± 2.1	-48 ± 1
6.	**F114N/M121L***	287 ± 34	513 ± 4	~ 39	~ -66
7.	**M44F/N47S/ F114N/G116F****	220 ± 13	588 ± 20	26.8 ± 2.3	-110 ± 7
8.	**N47S/F114S/ M121L****	44 ± 5	604 ± 14	30.4 ± 4.3	-110 ± 12
9.	**N47S/F114N/ M121L***	78 ± 12	614 ± 11	41.7 ± 5.9	-71 ± 8

*Data from Ref.[12]. **This study.

5.3.2. Kinetic measurements of the electron transfer rates

Kinetic measurements of the intramolecular ET in these nine different Az mutants, including three previously unreported ones with reduction potentials from 0.39 to 0.61 V vs. NHE have

been investigated. Pulse radiolytically produced CO_2^- radicals reduce both the disulfide bridge (Cys3-Cys26) and the Cu(II) site in Az with similar, essentially diffusion controlled rate constants ($k_1 \approx 10^9$ $M^{-1}s^{-1}$), (Figure 2). Since an excess of protein is employed over the reducing CO_2^- radicals, only a fraction of either disulfide or Cu(II) is reduced, allowing for the disulfide radical produced ($RSS^{\bullet}R^-$) to transfer an electron to the Cu(II) center in a second, slower and concentration independent, intramolecular ET process (Figure 5.5):

$$\text{Az[Cu(II)RSS}^{\bullet}\text{R}^-] \xrightarrow{k_{ET}} \text{Az[Cu(I)RSSR]}$$

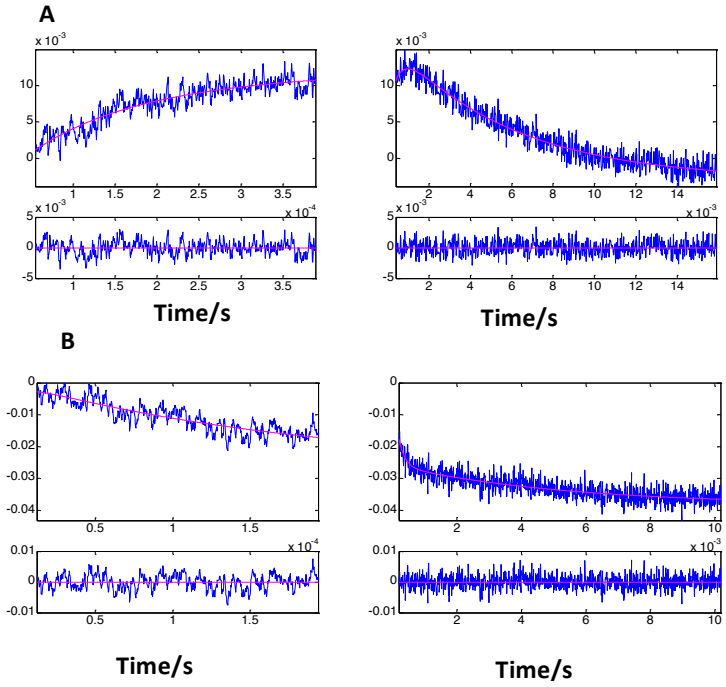

Figure 5.5. (A). Time resolved absorption changes at 410 nm of the F114N azurin mutant, monitoring formation and decay of the $RSS^{\bullet}R^-$ radical ions. (B) Time resolved absorption changes (625 nm) of the F114N Az mutant monitoring reduction of Cu(II). The protein concentration was 93 μM in an N_2O saturated solution; temperature 25 ^oC. All other technical details are described in the Experimental methods section.

The rate constants, k_{ET} at 25^{o}C, were determined by monitoring both the oxidation of the radical (410 nm, Figure 5.5A) and reduction of Cu(II) (600-635 nm, depending on the mutant's absorption maximum). The k_{ET} values and calculated activation parameters are presented in Table 1 together with earlier results.

Calculations of ET pathways between the $RSS^{\bullet}R^-$ radical ion and Cu(II) in these mutants showed that the same two pathways are operating in them and in the WT. Neither pathway involves the mutated residues.

The semi-classical Marcus theory for ET reactions between spatially fixed and oriented donors and acceptors provides a framework for analysis of rate constants in the non-adiabatic regime, Eq. 5.5:[44]

$$k_{ET} = \kappa(r)\nu \exp(-\Delta G^* / RT) \qquad \text{Eq 5.5}$$

where

$$\Delta G^* = \frac{\lambda_{TOT}}{4}\left[1 + \frac{\Delta G^0}{\lambda_{TOT}}\right]^2 \qquad \text{Eq 5.6}$$

In Eq. 5.5, κ(r) is the transmission coefficient at a separation distance, r, while ν is the frequency of nuclear motions. (In the non-adiabatic regime, κ(r)ν is independent of this frequency). R and T are the gas constant and temperature (in K) respectively. ΔG^* and ΔG^0 (cf. Eq. 5.6) are the activation free energy and standard free energy of reaction, respectively, and λ_{TOT} is the total reorganization free energies of both the ET donor and acceptor. When the driving force of the reaction equals the total reorganization energy, the rate constant reaches a maximum value, k_{MAX}. Since κ(r)ν decays exponentially with the separation distance, we can calculate k_{MAX} by Eq. 5.7 below:

$$k_{MAX} = \frac{k_B T}{h}\exp\left[-\beta(r - r_0)\right] \qquad \text{Eq. 5.7}$$

where k_B and h, respectively are Boltzmann's and Planck's constants, r is the donor-acceptor separation distance and r_0 is the value of r for direct (van der Waals) contact; the generally accepted value for r_0 is 0.3 nm. The timetable for activationless electron tunneling in β-sheet proteins of Gray *et al*. provides a decay constant of $\beta = 10\ nm^{-1}$.[45]

Attempts to experimentally determine the reduction potential for the formation of the RSS$^{\bullet}$R$^-$ radical in azurin have failed so far. Since the cystine is partly solvent exposed, we have been using a value of -0.41 V vs. NHE, determined from hybrid disulfide between a nitroaromatic and a protein cysteine thiol.[46] It is noteworthy that any change in the value for the reduction potential of the disulfide primarily adds or subtracts a constant from the abscissa values of the plot in Figure 5.5, and thus the reorganization energy by the same value.

The activation free energies, ΔG^* of the ET reactions in each mutant can be calculated from the activation parameters presented in Table 5.1. However, the experimentally determined activation entropy, $\Delta S^{\ddagger}$, includes a contribution from the electronic coupling:[44]

$$\Delta S^{\ddagger} = \Delta S^* + R\ln(\kappa\nu / 10^{13}) = \Delta S^* - R\beta(r - r_0) \qquad \text{Eq. 5.8}$$

where the symbols have already been defined above.

5.3.3. Investigating the Marcus plot in azurin variants

Figure 5.6 shows a plot of the ET rate constants, k_{ET}, vs. driving force, for the nine Az mutants fitted to the theoretical curve calculated using Eqs. 5.5 and 5.6 above. A non-linear least squares analysis of the data yields a value of k_{MAX} = 249(+56/-44) s^{-1} and a reorganization free energy of λ_{TOT} = 0.78(+0.04/-0.04) eV. The broken lines result from using the method of support planes,[47] the limit of each parameter that produces a 10% change in chi squared while the other parameter is allowed to optimize. The two broken lines represent the limits of k_{MAX}. In this analysis, k_{MAX} is the pre-exponential term in Eq. 5.5, treated as a constant, and is consistent with a k_{MAX} = 286 s^{-1} calculated directly from Eq. 5.7.

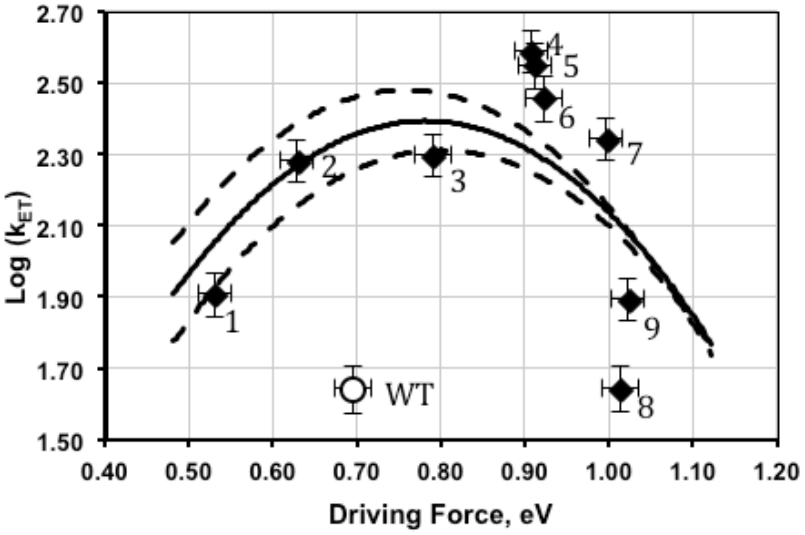

Figure 5.6. The Marcus plot of log(k_{ET}) of intramolecular ET in the Az mutants as function of the driving force. The fitted line is calculated using k_{MAX} = 249 (+56/-44) s^{-1} and λ_{TOT} = 0.78 (+0.04/-0.04 eV. The points are labelled 1 – 9, as in Tables 1 & 2. WT Az is the open circle symbol.

Also, the reorganization free energies of the individual mutants were calculated independently using the experimental activation parameters, $\Delta H^{\ddagger}$ and $\Delta S^{\ddagger}$. Using $\beta(r\text{-}r_0)$ = 23.8 (*cf.* Eq. 3) we obtain $R\beta$ (r- r_0) = 198 $JK^{-1}mol^{-1}$ (or 2.05 meV K^{-1}). We then calculate ΔG^* using

the activation enthalpy and the corrected activation entropy values. Finally, the reorganization free energy, λ_{calc} is calculated from Eq. 2. The results are presented in Table 5.2.

Table 5.2. Reorganization free energies, $\lambda_{calc.}$ for the Az mutants.

Azurin Mutant	$-\Delta G^0$ (eV)	ΔG^* (eV)	$\lambda_{calc.}$ (eV)
1. F114P/M121Q*	0.532 ± 0.006	0.033 ± 0.007	0.87
2. F114P*	0.630 ± 0.023	~0.016	0.87
3. F114N**	0.791 ± 0.008	0.009 ± 0.001	0.98
4. N47S/F114N*	0.909 ± 0.003	-0.009 ± 0.001	0.91
5. N47S/M121L*	0.913 ± 0.005	-0.007 ± 0.006	0.91
6. 114N/M121L*	0.923 ± 0.004	~ -0.003	0.92
7. M44F/N47S/F114S/G116F**	0.998 ± 0.020	0.006 ± 0.001	0.85
8. N47S/F114S/M121L**	1.014 ± 0.014	0.043 ± 0.005	0.67
9. N47S/F114N/M121L*	1.024 ± 0.011	0.040 ± 0.006	0.69

*Data from (Ref.12). **This study.

As illustrated in Figure 5.6, the experimentally determined rate constant values of the intramolecular ET in the Az mutants fit the theoretical parabola calculated using Marcus theory in the above plot of the ET rate constants vs. their driving force reasonably well, considering the redox potential range of mutants studied and the requirement of k_{MAX} and λ_{TOT} being constant for the entire set of examined mutants. The reorganization energy includes contributions from both the T1 Cu site and the disulfide-radical ion. From previous pulse radiolysis studies, we have calculated a λ_{SS} = 1.2 eV[48,49] which yields a λ_{Cu} = 0.4 eV, a significantly lower value than that (λ_{Cu} = 0.82 eV) previously determined for WT *Pseudomonas aeruginosa* Az.[49,50] In a previous study, we have attributed such lowering of the reorganization energy to increased flexibility of the T1 copper center caused by changes in non-covalent interactions such as hydrogen bonding and hydrophobicity in the secondary coordination sphere of the T1 copper site.[12] It has been shown before that changing hydrogen bonds and collective perturbation of the protein dynamics

can affect the λ values.[51] The deviations from the fit line at the highest driving force would, if attributed only to variation in the reorganization energy, correspond to a variation of up to 0.25 eV from the average or fit value.

5.3.4. Discussion

The exponential decay constant, β (*cf.* Eqs. 5.7 and 5.8) is another important parameter determining the ET rates. Differences in β would affect both the ET rates and activation entropies even when a common ET pathway is operating. These differences may be due to subtle changes in the electronic coupling between the copper ion and its ligands, particularly upon slight differences in the covalency of the Cu^{2+}–S(Cys) bond. Calculations of the Fermi contact term presented in table 5.3 show only small differences in the anisotropic covalency, suggesting that the mutations have only a minor effect on the total electronic coupling along the ET pathway (Figure 5.7).

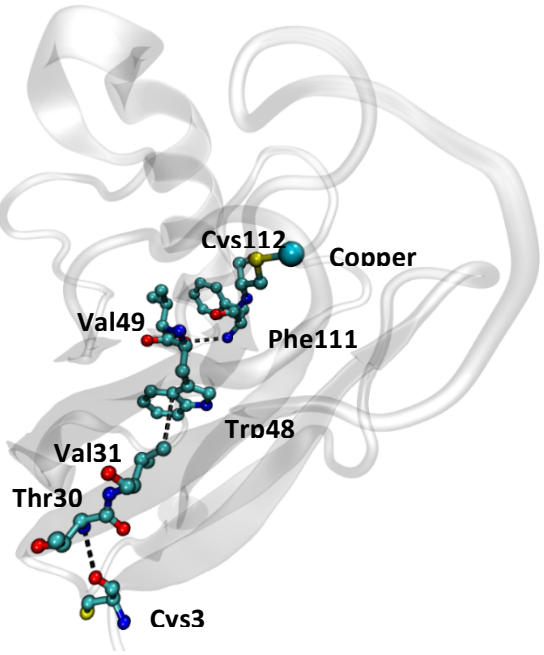

Figure 5.7. Major residues along the ET pathway in azurin (WT-Az, PDB ID: 4AZU)

Table 5.3. EPR parameters of the Az mutants and calculated Fermi contact terms. The EPR spectra were measured under conditions identical to those of the ET measurements.

	g_x	g_y	g_z	A_x/cm^{-1}	A_y/cm^{-1}	A_z/cm^{-1}	Fermi contact term
WT	2.028	2.055	2.262	8.5 x10^{-4}	8.6 x10^{-4}	5.3 x10^{-3}	0.414
F114P/M121Q	2.03	2.054	2.257	7.9 x10^{-4}	7.9 x10^{-4}	4.5 x10^{-3}	0.389
F114P	2.028	2.049	2.205	7.0 x10^{-4}	7.0 x10^{-4}	6.5 x10^{-3}	0.386

Table 5.3 cont.

N47S/F114N	2.028	2.056	2.28	$8.9x10^{-4}$	$8.9x10^{-4}$	$5.0x10^{-3}$	0.424
N47S/M121L	2.026	2.062	2.298	$9.6x10^{-4}$	$9.6x10^{-4}$	$3.9x10^{-3}$	0.415
F114N/M121L	2.028	2.057	2.263	$8.7x10^{-4}$	$8.7x10^{-4}$	$5.3x10^{-3}$	0.415
N47S/F114N/M121L	2.021	2.058	2.31	$9.2 x10^{-4}$	$9.2 x10^{-4}$	$4.2 x10^{-3}$	0.433
F114N	2.057	2.028	2.248	$8.45x10^{-4}$	$8.45x10^{-4}$	$5.92x10^{-3}$	0.400
M44F/N47S/F114N/G116F	2.054	2.03	2.258	$7.78 x10^{-4}$	$7.78 x10^{-4}$	$6.18x10^{-3}$	0.410
N47S/F114S/M121L	2.047	2.025	2.234	$14.05x10^{-4}$	$14.05x10^{-4}$	$6.31x10^{-3}$	0.383

Furthermore, the electronic coupling between electron donor and acceptor does not change significantly as a result of the mutations (an average $\beta = 10.0 +/- 0.2$ nm^{-1}) and is unlikely to cause the observed steep decrease in rate constants in mutants with the highest driving force illustrated in Figure 5.6. Comparing mutants 7 and 8, the five-fold decrease in rate constant would require an unlikely change in the decay constant, β, from 10.0 to 10.7. However, minor changes in the electronic coupling could be responsible for the scatter of the points in Figure 5.5 (beside experimental errors). Examination of the distances in the ET pathways of the different mutants using their crystal structure or molecular dynamics (MD) simulations showed minor differences that do not correlate with the observed rate constants (Table 5.4).

Table 5.4. Calculated distances between major residues along the ET pathways in azurin mutants (based on either crystal structures when available or molecular dynamic (MD) simulation models)

Mutant	**Cys3 (O) –Thr 30 (N)**	**Val 31 (CG1) –Trp 48 (CD2)**	**Val 49 (O)— Phe111(N)**
WT-Az (4AZU)	3.06	3.83	2.88
F114P/M121Q (3IN0)	3.15	4.09	2.83
F114P (2GHZ)	2.98	3.91	2.91
F114N[#]	3.00	3.88	3.00
N47S/F114N (3JTB)	3.20	3.89	3.01
N47S/M121L (3JT2)	3.05	3.93	2.96
F114N/M121L*	3.04	4.06	3.16
M44F/N47S/F114N/G116F*	3.43	3.83	3.17
N47S/F114S/M121L*	3.08	4.05	3.01
N47S/F11N/M121L*	3.20	3.94	2.99

data from unpublished x-ray structure
* from MD models

5.4. Summary and conclusion

Taken together the present results provide rare[34] and compelling evidence that, in this set of Az mutants, the Marcus inverted region has been reached at driving forces greater than ~0.8 eV (Figure 5.6). However, the ET rates observed for mutants with the highest driving force lie considerably below the calculated curve. Marcus theory in its semi-classical form attributes the inverted region to an increasing activation energy in the exponential term of the rate equation, but nuclear tunneling may cause a decrease in the pre-exponential factor leading to the considerably lower rates observed.[52]

These mutants reach the "inverted region" in the internal ET process, since they possess a lower reorganization energy than most other Az mutants. When the reorganization energy is higher, as in the case of WT Az (cf. Figure 5.6), even greater driving force would be required to reach the "inverted region", a rather difficult task to fulfill with modifications of the copper environment. Moreover, the inverted region could be achieved in this system because both ET products, Cu(I) and disulfide, have closed shells and their electronic excited states are too high to be populated after the long range ET. The inverted region in a bimolecular ET reaction with closed shell products has indeed been demonstrated before.[53] The present results provide the first demonstration of the Marcus inverted region in a non-derivatized protein-only system. It has been hypothesized that the dramatically different ET rates in the photosynthetic reaction center are due to the lower reorganization free energy and large activation barrier for the reverse processes that result from the inverted region.[1] The inverted region, therefore, allows for the charge separation required for unidirectional ET through that system and is critical for efficient energy conversion processes.

5.5. References

(1) Marcus, R. A. Electron-transfer reactions in chemistry: theory and experiment (Nobel lecture);*Angew. Chem. Int. Ed.* **1993**, *32*, 1111.
(2) Miller, J. R.; Calcaterra, L. T.; Closs, G. L. Intramolecular long-distance electron transfer in radical anions. The effects of free energy and solvent on the reaction rates;*J. Am. Chem. Soc.* **1984**, *106*, 3047.
(3) Fox, L. S.; Kozik, M.; Winkler, J. R.; Gray, H. B. Gaussian free-energy dependence of electron-transfer rates in iridium complexes;*Science* **1990**, *247*, 1069.
(4) Scott, J. R.; Willie, A.; McLean, M.; Stayton, P. S.; Sligar, S. G.; Durham, B.; Millett, F. Intramolecular electron transfer in cytochrome b5 labeled with ruthenium(II) polypyridine complexes: rate measurements in the Marcus inverted region;*J. Am. Chem. Soc.* **1993**, *115*, 6820.
(5) Winkler, J. R.; Malmstrom, B. G.; Gray, H. B. Rapid electron injection into multisite metalloproteins: intramolecular electron transfer in cytochrome oxidase;*Biophys. Chem.* **1995**, *54*, 199.

(6) Farver, O.; Hosseinzadeh, P.; Marshall, N. M.; Wherland, S.; Lu, Y.; Pecht, I. Long-Range Electron Transfer in Engineered Azurins Exhibits Marcus Inverted Region Behavior;*J. Phys. Chem. Lett.* **2015**, *6*, 100.
(7) Winkler, J. R.; Gray, H. B. Long-Range Electron Tunneling;*J. Am. Chem. Soc.* **2014**, *136*, 2930.
(8) Cheung, E.; Taylor, K.; Kornblatt, J. A.; English, A. M.; McLendon, G.; Miller, J. R. Direct measurements of intramolecular electron transfer rates between cytochrome c and cytochrome c peroxidase: effects of exothermicity and primary sequence on rate;*Proc. Natl. Acad. Sci. U S A* **1986**, *83*, 1330.
(9) Swallow, A. J. Recent Results from Pulse Radiolysis;*Photochem. Photobiol.* **1968**, *7*, 683.
(10) Truscott, T. G. In *Photosensitisation*; Moreno, G., Pottier, R., Truscott, T., Eds.; Springer Berlin Heidelberg: 1988; Vol. 15, p 39.
(11) Farver, O.; Hwang, H. J.; Lu, Y.; Pecht, I. Reorganization energy of the CuA center in purple azurin: Impact of the mixed valence-to-trapped valence state transition;*J. Phys. Chem. B* **2007**, *111*, 6690.
(12) Farver, O.; Marshall, N. M.; Wherland, S.; Lu, Y.; Pecht, I. Designed azurins show lower reorganization free energies for intraprotein electron transfer.;*Proc. Natl. Acad. Sci. U S A* **2013**, *110*, 10536.
(13) Hazzard, J. T.; Marchesini, A.; Curir, P.; Tollin, G. Direct measurement by laser flash photolysis of intramolecular electron transfer in the three-electron reduced form of ascorbate oxidase from zucchini;*Biochim. Biophys. Acta* **1994**, *1208*, 166.
(14) Berkoff, R.; Krist, K.; Gafney, H. D. Measurement of the rates of the electron-transfer reactions between tris(2,2'-bipyridine)ruthenium(3+) and tris(1,10-phenanthroline)cobalt(2+) or tris(2,2'-bipyridine)cobalt(2+) by flash photolysis techniques;*Inorg. Chem.* **1980**, *19*, 1.
(15) Bechtold, R.; Kuehn, C.; Lepre, C.; Isied, S. S. Directional electron transfer in ruthenium-modified horse heart cytochrome c;*Nature* **1986**, *322*, 286.
(16) Chang, I. J.; Gray, H. B.; Winkler, J. R. High-driving-force electron transfer in metalloproteins: intramolecular oxidation of ferrocytochrome c by Ru(2,2'-bpy)2(im)(his-33)3+;*J. Am. Chem. Soc.* **1991**, *113*, 7056.
(17) Skov, L. K.; Pascher, T.; Winkler, J. R.; Gray, H. B. Rates of Intramolecular Electron Transfer in Ru(bpy)2(im)(His83)-Modified Azurin Increase below 220 K;*J. Am. Chem. Soc.* **1998**, *120*, 1102.
(18) Immoos, C. E.; Di, B. A. J.; Cohen, M. S.; Van, d. V. W.; Gray, H. B.; Farmer, P. J. Electron-transfer chemistry of Ru-linker-(Heme)-modified myoglobin: Rapid intraprotein reduction of a photogenerated porphyrin cation radical;*Inorg. Chem.* **2004**, *43*, 3593.
(19) Warren, J. J.; Herrera, N.; Hill, M. G.; Winkler, J. R.; Gray, H. B. Electron Flow through Nitrotyrosinate in Pseudomonas aeruginosa Azurin;*J. Am. Chem. Soc.* **2013**, *135*, 11151.
(20) Winkler, J. R.; Gray, H. B. Electron transfer in ruthenium-modified proteins;*Chem. Rev.* **1992**, *92*, 369.
(21) Miller, J. E.; Di Bilio, A. J.; Wehbi, W. A.; Green, M. T.; Museth, A. K.; Richards, J. R.; Winkler, J. R.; Gray, H. B. Electron tunneling in rhenium-modified Pseudomonas aeruginosa azurins;*Biochim. Biophys. Acta* **2004**, *1655*, 59.
(22) Gaigalas, A. K.; Niaura, G. Measurement of electron transfer rates between adsorbed azurin and a gold electrode modified with a hexanethiol layer;*J.Colloid Interface Sci.* **1997**, *193*, 60.
(23) Heering, H. A.; Weiner, J. H.; Armstrong, F. A. Direct Detection and Measurement of Electron Relays in a Multicentered Enzyme: Voltammetry of Electrode-Surface Films of E. coli Fumarate Reductase, an Iron−Sulfur Flavoprotein;*J. Am. Chem. Soc.* **1997**, *119*, 11628.
(24) Jeuken, L. J. C.; Jones, A. K.; Chapman, S. K.; Cecchini, G.; Armstrong, F. A. Electron-Transfer Mechanisms through Biological Redox Chains in Multicenter Enzymes;*J. Am. Chem. Soc.* **2002**, *124*, 5702.
(25) Hirst, J. Elucidating the mechanisms of coupled electron transfer and catalytic reactions by protein film voltammetry;*Biochim. Biophys. Acta* **2006**, *1757*, 225.
(26) Szent-GyÖRgyi, A. Towards a New Biochemistry?;*Science* **1941**, *93*, 609.
(27) Moser, C. C.; Page, C. C.; Chen, X.; Dutton, P. L. Electron transfer in natural proteins: theory and design.;*Subcellular Biochemistry* **2000**, *35*, 1.
(28) Gray, H. B.; Winkler, J. R. Long-range electron transfer;*Proc. Natl. Acad. Sci. U S A* **2005**, *102*, 3534.
(29) Hopfield, J. J. Electron transfer between biological molecules by thermally activated tunneling;*Proc. Natl. Acad. Sci. U S A* **1974**, *71*, 3640.
(30) Winkler, J. R.; Nocera, D. G.; Yocom, K. M.; Bordignon, E.; Gray, H. B. Electron-transfer kinetics of pentaammineruthenium(III)(histidine-33)-ferricytochrome c. Measurement of the rate of intramolecular electron transfer between redox centers separated by 15Å in a protein;*J. Am. Chem. Soc.* **1982**, *104*, 5798.
(31) Mayo, S. L.; Ellis, W. R., Jr.; Crutchley, R. J.; Gray, H. B. Long-range electron transfer in heme proteins;*Science* **1986**, *233*, 948.
(32) Voityuk, A. A. Long-range electron transfer in biomolecules. Tunneling or hopping?;*J. Phys. Chem. B* **2011**, *115*, 12202.
(33) Gunner, M. R.; Dutton, P. L. Temperature and -.DELTA.G.degree. dependence of the electron transfer from BPh.cntdot.- to QA in reaction center protein from Rhodobacter sphaeroides with different quinones as QA;*J. Am. Chem. Soc.* **1989**, *111*, 3400.
(34) Boussac, A.; Rappaport, F.; Brettel, K.; Sugiura, M. Charge recombination in SnTyrZ•QA-• radical pairs in D1 protein variants of photosystem II: long range electron transfer in the Marcus inverted region.;*J. Phys. Chem. B* **2013**, *117*, 3308.
(35) Marshall, N. M.; Garner, D. K.; Wilson, T. D.; Gao, Y.-G.; Robinson, H.; Nilges, M. J.; Lu, Y. Rationally tuning the reduction potential of a single cupredoxin beyond the natural range;*Nature* **2009**, *462*, 113.
(36) Armstrong, F. A. Insights from protein film voltammetry into mechanisms of complex biological electron-transfer reactions;*J. Chem. Soc., Dalton Trans.* **2002**, 661.

(37) Leger, C.; Elliott, S. J.; Hoke, K. R.; Jeuken, L. J. C.; Jones, A. K.; Armstrong, F. A. Enzyme electrokinetics: using protein film voltammetry to investigate redox enzymes and their mechanisms;*Biochemistry* **2003**, *42*, 8653.
(38) Hwang, H. J.; Ang, M.; Lu, Y. Determination of reduction potential of an engineered CuA azurin by cyclic voltammetry and spectrochemical titrations;*J. Biol. Inorg. Chem.* **2004**, *9*, 489.
(39) Sieracki, N. A.; Hwang, H. J.; Lee, M. K.; Garner, D. K.; Lu, Y. A temperature independent pH (TIP) buffer for biomedical biophysical applications at low temperatures;*Chem Commun (Camb)* **2008**, 823.
(40) Nilges, M. J.;*Ph.D. Thesis, University of Illinois* **1979**.
(41) Chang, H. R.; Diril, H.; Nilges, M. J.; Zhang, X.; Potenza, J. A.; Schugar, H. J.; Hendrickson, D. N.; Isied, S. S. An unusually stable manganese(II)manganese(III) complex with novel EPR spectra: synthesis, structure, magnetism, and EPR analysis;*J. Am. Chem. Soc.* **1988**, *110*, 625.
(42) Humphrey, W.; Dalke, A.; Schulten, K. VMD: Visual molecular dynamics;*Journal of Molecular Graphics* **1996**, *14*, 33.
(43) Phillips, J. C.; Braun, R.; Wang, W.; Gumbart, J.; Tajkhorshid, E.; Villa, E.; Chipot, C.; Skeel, R. D.; Kale, L.; Schulten, K. Scalable molecular dynamics with NAMD;*J. Comput. Chem.* **2005**, *26*, 1781.
(44) Marcus, R. A.; Sutin, N. Electron transfers in chemistry and biology;*Biochim. Biophys. Acta* **1985**, *811*, 265.
(45) Gray, H. B.; Winkler, J. R. Electron transfer in proteins;*Annu. Rev. Biochem* **1996**, *65*, 537.
(46) Faraggi, M.; Klapper, M. H. Intramolecular long-range electron transfer in the .alpha.-hemoglobin subunit;*J. Am. Chem. Soc.* **1988**, *110*, 5753.
(47) Duggleby, R. G. Estimation of the reliability of parameters obtained by non-linear regression;*Eur. J. Biochem.* **1980**, *109*, 93.
(48) Farver, O.; Lu, Y.; Ang, M. C.; Pecht, I. Enhanced rate of intramolecular electron transfer in an engineered purple CuA azurin;*Proc. Natl. Acad. Sci. U S A* **1999**, *96*, 899.
(49) Farver, O.; Pecht, I. Electron transfer in blue copper proteins;*Coord. Chem. Rev.* **2011**, *255*, 757.
(50) Di Bilio, A. J.; Hill, M. G.; Bonander, N.; Karlsson, B. G.; Villahermosa, R. M.; Malmström, B. G.; Winkler, J. R.; Gray, H. B. Reorganization Energy of Blue Copper: Effects of Temperature and Driving Force on the Rates of Electron Transfer in Ruthenium- and Osmium-Modified Azurins;*J. Am. Chem. Soc.* **1997**, *119*, 9921.
(51) Alvarez-Paggi, D.; Castro, M. A.; Tórtora, V.; Castro, L.; Radi, R.; Murgida, D. H. Electrostatically Driven Second-Sphere Ligand Switch between High and Low Reorganization Energy Forms of Native Cytochrome c;*J. Am. Chem. Soc.* **2013**, *135*, 4389.
(52) Liang, N.; Miller, J. R.; Closs, G. L. Temperature-independent long-range electron transfer reactions in the Marcus inverted region;*J. Am. Chem. Soc.* **1990**, *112*, 5353.
(53) McCleskey, T. M.; Winkler, J. R.; Gray, H. B. Driving-force effects on the rates of bimolecular electron-transfer reactions;*J. Am. Chem. Soc.* **1992**, *114*, 6935.

CHAPTER 6

ATTEMPTS TO DESIGN A HIGH-THROUGHPUT SCREENING PLATFORM TO OBTAIN AZURIN VARIANTS WITH DESIRED POTENTIAL

6.1. Introduction:

Three chapters of this thesis were dedicated to rationally tuning the reduction potential of the protein azurin, understanding the factors that contribute to the reduction potential, and application of such systematically tuned protein variants. While the rational design approach has been very successful in achieving a protein that spans the entire 2V range of biological reduction potentials and a great deal is learnt by studying the detailed spectroscopic and crystallographic features of those mutants, some issues still remain. Proteins at the high extreme are usually not very stable. Moreover, the Ni-Az variants (see chapter 3) are not stable at their desired reducing state, the Ni(I) state.

Proven to be a powerful method regarding primary and secondary sphere interactions,[1-3] rational design is not promising beyond that regime. It is usually very difficult to predict the effect of mutations far from the active site and there are always unexpected interactions that can be transferred via protein motions or more complicated networks of interactions. In addition, stabilizing mutations are very difficult to be designed and predicted rationally. Directed evolution is the method of choice in such cases. In this method random mutations are introduced to proteins and the created library is then screened for desired activity to select the best mutants and the library generation and selection process continues until no further enhancement is observed.[4-19]

Oxidized azurin has a strong absorption at 625 nm due to ligand to metal charge transfer, while reduced form lacks this absorption.[20-23] This change is obvious *in vitro*; however, such it is very hard to detect absorption changes under physiological conditions due to strong background. Fluorescent signal usually has the advantage of low background and bio-compatibility. The idea is to couple oxidation-reduction process to a change in fluorescence so that we can use flow-cytometry to sort our library of mutants.[24] Paramagnetic quenching of a nearby fluorophore

(either a protein or a small molecule) by Cu(II) can be restored upon reduction of the Cu(II), providing a means to distinguish lower potential variants from higher potential ones.

In this chapter, I will describe several attempts to design and test this system. Due to the variety of techniques tested, I broke down the chapter first by the approach used. Then, I further sub-categorized each section into a brief introduction, materials and methods, and results. An overall summary and future direction is presented at the end of this chapter.

6.2. Conjugation to Alexa-fluor 688 dye

6.2.1. Introduction

Alexa dyes are a class of fluorophores available through several companies with a range of emissions and different modalities for conjugation. We chose Alexa fluor 610 (Figure 6.1) which has an emission close to Cu(II) absorption in azurin to enhance the efficiency of quenching. This dye is conjugated via a maleimide labeling conjugation. In order to attach the dye, Yang Yu designed N42C-Az variant, which has a Cys close to the Cu binding site.

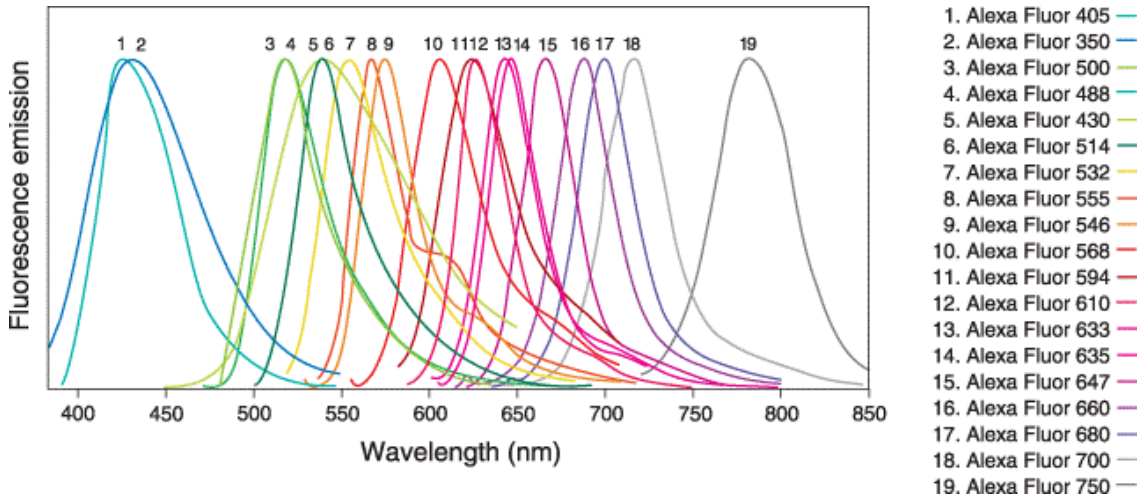

Figure 6.1. Spectra of emission of different Alexa Fluor dyes. Adapted from life technologies website/

6.2.2. Materials and methods

Alexa Fluor dye was purchased from Fluka Analytical. The labeling was performed first according to the manual as follows. The protein was exchanged using PD-10 columns into 50 mM Tris-HCl buffer pH= 7.0. The reduction of disulfides was skipped, as the Cys42 is surface exposed and not linked to any other Cys resideus. A 10-20 mM stock of the dye was prepared in

DMSO. As a control, a 20 mM stock of maleimide was used. 10-20 moles excess of the dye was added dropwise to the stirring solution of the protein and was stirred for two hours at room temperature (or overnight at 4 C). Instead of adding thiols to stop the reaction, we passed the protein down a PD-10 column to remove unreacted dye and to exchange the protein to the buffer required for mass spectroscopy. To optimize the condition, different concentrations of protein was used (less than 50 μM, between 50-100 μM and more than 100 μM). We also tested different ratios of maleimide to protein (20, 250, 1000). To label with the dye, we used 200 μl of 180 μM protein and added about 5 molar excess dye and stir overnight at 4C. We also tried using both fresh dye and the dye that came out of the PD-10 and was not reacting in order to save the dye.

Expression and purification of N42C-Az variant was performed as described previously.[1] In brief the cells are subjected to osmotic shock to release the protein from periplasmic space. A precipitation step via acidifying the culture is used to precipitate other proteins. The apo-protein is purified via a cation exchange SP-sepharose column. After addition of Cu, the holo-protein is separated from the apo-protein using an anion exchange Q-sepharose column. The protein content was confirmed using a QuatroII-waters electrospray ionization mass spectroscopy machine (ESI-MS)

MALDI mass spectroscopy was performed by the university mass-spec facility.

Fluorescent studies were performed on a HORIBA Jobin Yvon Fuoromax-P using an excitation of 610 nm, scanning from 600-750 nm with slit opening of 2 nm.

6.2.3. Results and discussion

6.2.3.1. Protein purification

N42C-Az protein was purified with comparable yields to the WT-Az. The mass obtained by ESI (13931 ± 5) was very close to the estimated mass (13934.3) as shown in figure 6.2.

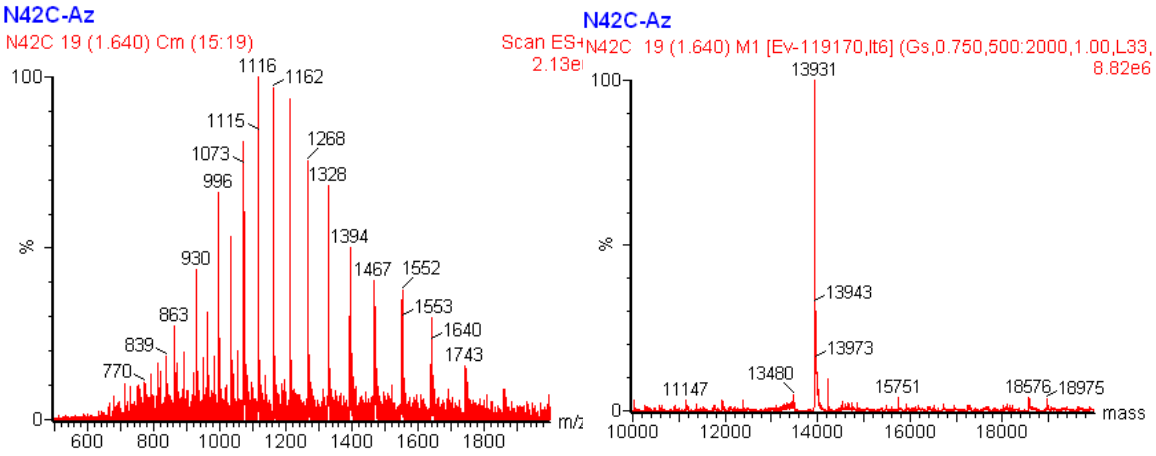

Figure 6.2. ESI mass spectrum of N42C-Az.

6.2.3.2. Maleimide labeling

Upon reaction with maleimide (control) using the Fluka Analytical protocol (described in the materials section), no significant maleimide labeling (expected mass around 14904) was observed by ESI-MS as shown in figure 6.3.

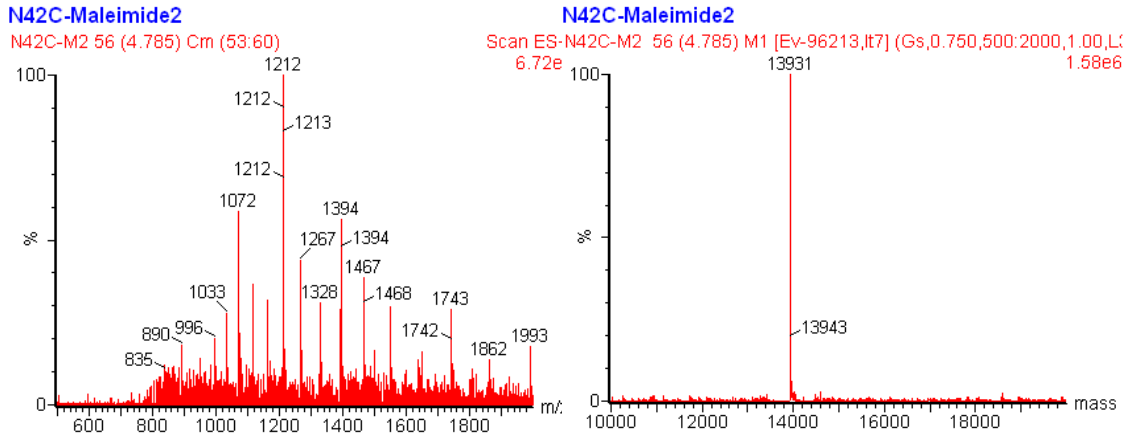

Figure 6.3. ESI of initial attempts of maleimide labeling of N42C.

MALDI mass spectroscopy showed about 40% labeling with maleimide and an enhancement of the labeling efficiency upon addition of more protein. The labeling for overnight at 4 C didn't increase the efficiency. Labeling efficiency was greatly enhanced using increased maleimide to protein ratio as shown in figure 6.4.

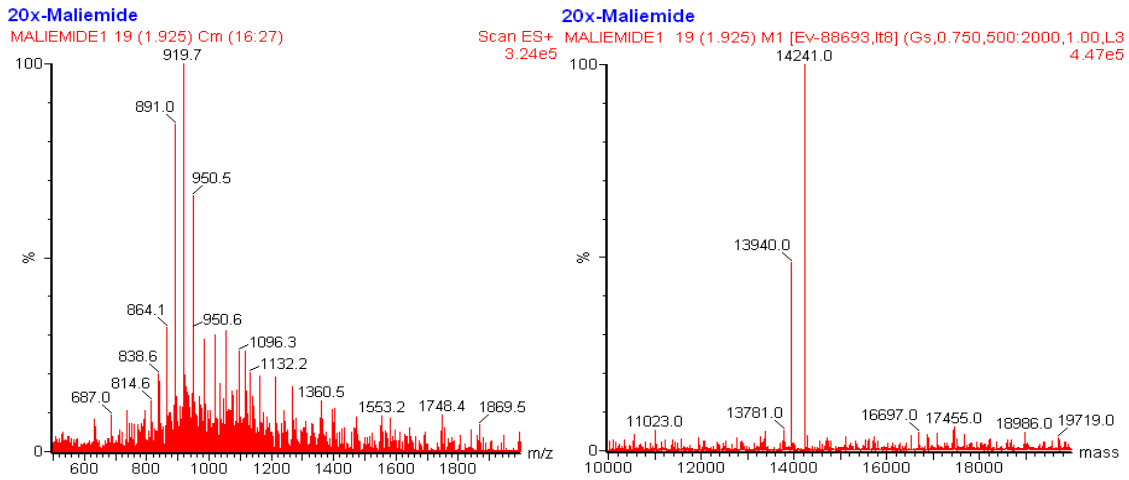

Figure 6.4. Increasing maleimide labeling results in an enhanced labeling efficiency.

N42C-Az labeled with Alexa came out of PD-10 column as a pink band with UV-vis features of both Alexa and Cu(II)-Az (see figure 6.5). MALDI results also confirmed the labeling (figure 6.5b). We noticed that labeling with fresh or old dye did not affect the yield as observed by MALDI (data for the old one is not shown but is similar to the one in figure 6.5).

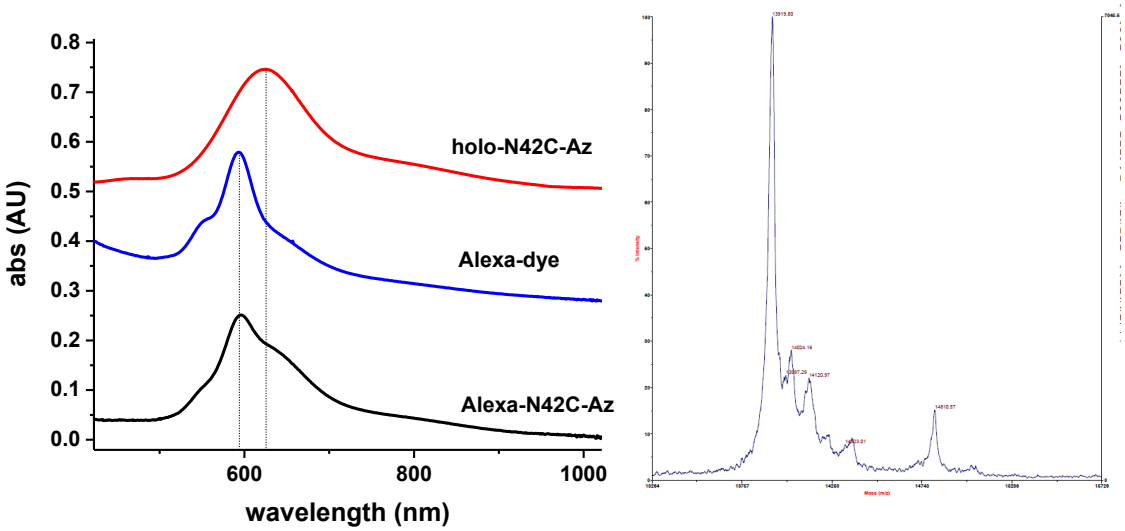

Figure 6.5. UV-vis of labeled N42C with Alexa is shown on the left. The right figure shows MALDI result of the same sample.

6.2.3.3. Fluorescence studies

In contrast to labeling studies, fluorescent studies were very successful. As shown in figure 6.6, we observed significantly better quenching of the emission with our labeled dye compared to the control in which free azurin was added to the Alexa Fluor sample. The emission signal was

restored upon quenching of the Cu(II) by addition of ascorbate (75% increase in intensity in labels compared to only 8% in the control).

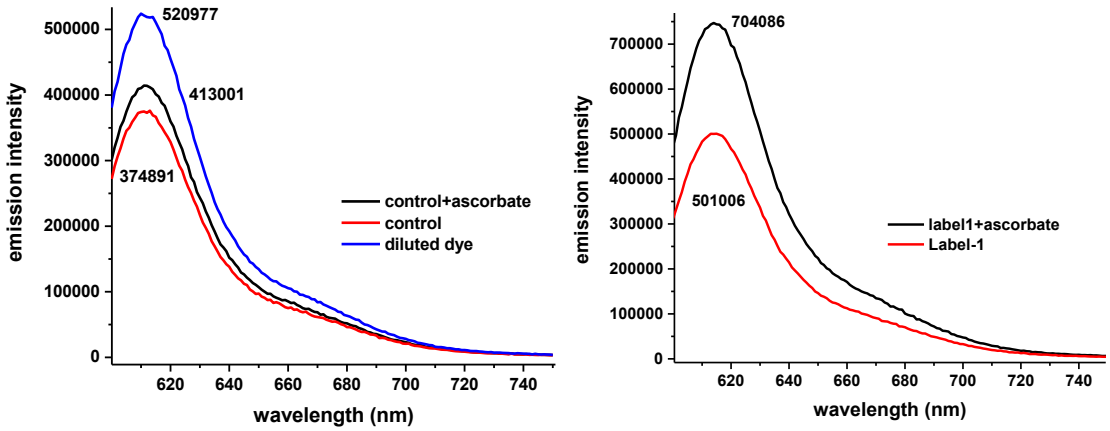

Figure 6.6. Fluorescent studies on the Alexa-N42C-Az show efficient quenching and later restoration of the fluorescent upon reduction of Cu.

Fluorescent studies on the reactions treated with cell culture showed no fluorescent signals.

6.3. Fusion to mCherry

6.3.1. Introduction

The discovery of fluorescent proteins opened new avenues in the field of protein science and especially *in vivo* studies of protein dynamics and localization [25-27] as evident by dedication of the Nobel prize in Chemistry, 2008, for the discovery of GFP.[28] One big advantage of using fluorescent proteins compared to conjugation techniques is the ability to genetically encode them and hence avoiding the post-purification processes. To take advantage of these properties, Yang Yu and I decided to design a series of constructs in which mCherry is fused to azurin (mCh-Az) and to use that system for our directed evolution set up.

6.3.2. Materials and methods

Some of the proteins used in this study were designed by Yang Yu. Detailed information of those constructs is not provided in here and readers are referred to Yang's thesis or his progress reports.

6.3.2.1. Preparation of fragments for Yeast display vector

Yeast display was performed with the help of Tong Si from Huimin Zhao lab, using a method previously reported[29] and then later developed by their group.[30] The experimental details of the technique are provided here.

PRS416 vector was used as the yeast display vector. Azurin fragment was inserted between V5 and GS linkers that connect α-hemmaglutinin gene to TEF. To design vectors, adjacent fragments had 40 nucleotides overhang with each other so that we could use yeast homologous recombination system. Primers are listed below:

PRS423-seq-f: 5'-gtgctgcaaggcgattaag (primer to get TEF)

V5-Az-r: 5'-gcatctgatcattaccctggatatcaacggagcattcagccgtagaatcgagaccgagg (primer to get TEF with overlapping region of Azurin)

V5-Az-f: 5'-ggtaagcctatccctaaccctctcctcggtctcgattctacggctgaatgctccgttgatatcc (primer to get Azurin with overlapping region of V5)

GS-Az-f: 5'-ggtcactccgcactgatgaaaggtaccctgactctgaaagagggtggaggcggtagtggcgg (primer to get Azurin with overlapping region to GS)

GS-Az-r: 5'-gcttttggcgctaacctccaccgccactaccgcctccaccctctttcagagtcagggtacc (primer to get GS with overlapping region to Azurin)

ADH2t-Seq-r: 5'-caattaatgtgagttacctc (primer to get Gs from vector)

Gal10 was extracted from yeast genomic DNA using following primers: (genomic DNA of yeast was isolated using zymolase kit from Huimin Zhao lab)

Gal10-r: 5'- GTA GAA TCG AGA CCG AGG AGA GGG TTA GGG ATA GGC TTA CCA CCT GCA GCT AAT GCG GAG GAT GCT GCG AAT AAA ACT GCA GTA AAA ATT GAA GGA AAT CTC ATT TTC AAA AAT TCT TAC TTT TTT TTT GGA TGG ACG C

Gal10-f: 5'- CCC AGT CAC GAC GTT GTA AAA CGA CGG CCA GTG AGC GCG CGT AAT ACG GTC AAT ATA GCA ATG AGC AGT TAA GCG

Forward primer for mCherry-Azurin construct, since the reverse is the same:

Mch-Az-f: 5'- TCC GCA TTA GCT GCA GGT GGT AAG CCT ATC CCT AAC CCT CTC CTC GGT CTC GAT TCT ACG GCT GAA TGC TTT CCC GGG ATG GTG AGC AAG GGC GAG GAG G

To make the construct polymerase chain reaction (PCR) was performed on each of the fragments. Source for TEF and Aga was PRS416 plasmid and Azurin was purified from the stock plasmid in pET9a vector. PCR reaction was performed as follow: an initial cycle of denaturation at 95 for 1 min, followed by 34 cycles of 30 sec denaturation at 95, annealing for 30 sec at 53 and elongation at 72 for 40 sec. the final product was finally elongated for 2 min at 72. For most genes Phusion polymerase from NEB was used except for mCherry containing

genes and Aga that worked better with Platinum Taq from Invitrogen. PCR products were then loaded onto a 1% agarose gel and ran for 20 min at 127 V. Fragments then gel extracted using Qiagen minimprep gel extraction kit according to the user guide.

PRS416 fragment was prepared by double digestion of the vector with BamHI and EcoRI, based on NEB protocol. The fragment then gel extracted as described previously.

6.3.2.2. Yeast recombination

To generate the construct using yeast homologous recombination system, the fragments should first be uptaken by yeast. Yeast competent cells were prepared as follows for one shot transformation: a single colony of yeast strain (EYB100 or CPNK) was grown in 2-3 ml yPAD media overnight at 30. Inoculate 5 ml (times number of shots) yPAD media with overnight culture to get OD~ 0.7. Let grow for 3-4 hours. Centrifuge 5 minutes at 4000 rpm using Eppendorf centrifuge. The pellet was then resuspended in 25 mL water and centrifuged again. Cells resuspended in 1ml of 0.1 M $LiNO_3$ and centrifuged again. Finally cells were resuspended in 100 µL (per shot) of 0.1 M $LiNO_3$. For transformation, 240 µL filtered 30% PEG was gently added to the top of cell containing vials. After that 50 µL of preheated salmon sperm DNA (5 min at 100), 36 µL 1M $LiNO_3$ and 200 ng of each fragment were added respectively. The concentrations of fragments were calculated based on 260 absorption using HP diod array spectrometer. Cells were then placed in 42 water bath for 40 minutes. After this heat shock period, 1 mL SC-Ura media was added to cells and 50 µl is plated on SC-Ura plates. The plates are incubated at 30 for 2 days. To validate colonies, they are grown in 5 mL SC-Ura for 2 days and plasmids are extracted by zymoprep yeast plasmid extraction kit based on manual. All constructs are validated by sequencing at ACGT Inc.

yPAD media: (600 mL)

0.6 gr Difco yeast extract

12.0 gr Difco peptone

12.0 gr glucose

60 mg adenine hemisulfate

(+10 gr bacto agar for solid media)

SC-Ura: (600ml)

1.0 gr difco yeast nitrogen base

3.0 gr ammonium sulfate

12.0 gr dextrose

0.5 gr SC-Ura

60 mg Adenine hemisulfate

(+10 gr bacto agar for solid media)

6.3.2.3. Construction of bacterial surface display

The pAPEX vector for bacterial surface display was a kind gift from Dr. George Georgiou lab, University of Texas, Austin. The vector was constructed as described before.[31] The vector sequence is shown below. Regions with yellow highlight and red text are the SfiI restriction sites.

1 ACCCGCCACC ATCGAATGGC GCAAAACCTT TCGCGGTATG GCATGATAGC GCCCGGAAGA

61 GAGTCAATTC AGGGTGGTGA ATGTGAAACC AGTAACGTTA TACGATGTCG CAGAGTATGC

121 CGGTGTCTCT TATCAGACCG TTTCCCGCGT GGTGAACCAG GCCAGCCACG TTTCTGCGAA

181 AACGCGGGAA AAAGTGGAAG CGGCGATGGC GGAGCTGAAT TACATTCCCA ACCGCGTGGC

241 ACAACAACTG GCGGGCAAAC AGTCGTTGCT GATTGGCGTT GCCACCTCCA GTCTGGCCCT

301 GCACGCGCCG TCGCAAATTG TCGCGGCGAT TAAATCTCGC GCCGATCAAC TGGGTGCCAG

361 CGTGGTGGTG TCGATGGTAG AACGAAGCGG CGTCGAAGCC TGTAAAGCGG CGGTGCACAA

421 TCTTCTCGCG CAACGCGTCA GTGGGCTGAT CATTAACTAT CCGCTGGATG ACCAGGATGC

481 CATTGCTGTG GAAGCTGCCT GCACTAATGT TCCGGCGTTA TTTCTTGATG TCTCTGACCA

541 GACACCCATC AACAGTATTA TTTTCTCCCA TGAAGACGGT ACGCGACTGG GCGTGGAGCA

601 TCTGGTCGCA TTGGGTCACC AGCAAATCGC GCTGTTAGCG GGCCCATTAA GTTCTGTCTC

661 GGCGCGTCTG CGTCTGGCTG GCTGGCATAA ATATCTCACT CGCAATCAAA TTCAGCCGAT

721 AGCGGAACGG GAAGGCGACT GGAGTGCCAT GTCCGGTTTT CAACAAACCA TGCAAATGCT

781 GAATGAGGGC ATCGTTCCCA CTGCGATGCT GGTTGCCAAC GATCAGATGG CGCTGGGCGC

841 AATGCGCGCC ATTACCGAGT CCGGGCTGCG CGTTGGTGCG GACATCTCGG TAGTGGGATA

901 CGACGATACC GAAGACAGCT CATGTTATAT CCCGCCGTTA ACCACCATCA AACAGGATTT

961 TCGCCTGCTG GGGCAAACCA GCGTGGACCG CTTGCTGCAA CTCTCTCAGG GCCAGGCGGT

1021 GAAGGGCAAT CAGCTGTTGC CCGTCTCACT GGTGAAAAGA AAAACCACCC TGGCGCCCAA

1081 TACGCAAACC GCCTCTCCCC GCGCGTTGGC CGATTCATTA ATGCAGCTGG CACGACAGGT

1141 TTCCCGACTG GAAAGCGGGC AGTGAGCGGT ACCCGATAAA AGCGGCTTCC TGACAGGAGG

1201 CCGTTTTGTT TTGCAGCCCA CCTCAACGCA ATTAATGTGA GTTAGCTCAC TCATTAGGCA

1261 CCCCAGGCTT TACACTTTAT GCTTCCGGCT CGTATGTTGT GTGGAATTGT GAGCGGATAA

1321 CAATTTCACA CAGGAAACAG CTATGACCAT GATTACGAAT TTCTAGAGAA GGAGATATAC

1381 ATATGAAACT GACAACACAT CATCTACGGA CAGGGGCCGC ATTATTGCTG GCCGGAATTC

1441 TGCTGGCAGG TTGCGACCAG AGTAGCAGCG AGGCCCAGCC GGCCATGGCG GATCCTTGCT

1501 ATTTACCGCG GCTTTTTATT GAGCTTGAAA GATAAATAAA ATAGATAGGT TTTATTTGAA

1561 ACTAAATCTT CTTTATCGTA AAAAATGCCC TCTTGGGTTA TCAAGAGGGT CATTATATTT

1621 CGCGGAATAA CATCATTTGG TGACGAAATA ACTAAGCACT TGTCTCCTGT TTACTCCCCT

1681 GAGCTTGAGG GGTTAACATG AAGGTCATCG ATAGCAGGAT AATAATACAG TAAAACGCTA

1741 AACCAATAAT CCAAATCCAG CCATCCCAAA TTGGTAGTGA ATGATTATAA ATAACAGTAA

1801 ACAGTAATGG GCCAATAACA CCGGTTGCAT TGGTAAGGCT CACCAATAAT CCCTGTAAAG

1861 CACCTTGCTC ATGACTCTTT GTTTGGATAG ACATCACTCC CTGTAATGCA GGTAAAGCGA

1921 TCCCACCACC AGCCAATAAA ATTAAAACAG GGAAATCTAA CCAACCTTCA GATATAAACG

1981 CTAAAAAGGC AAATGCACTA CTATCTGCAA TAAATTCGAG CAGTACTGCC GTTTTTTCGC

2041 CCCATTTAGT GGCTATTCTT CCTGCCACAA AGGCTTGGAA TACTGAGTGT AAAAGACCAA

2101 GACCCGCTAA TGAAAAGCCA ACCATCATGC TATTCCATCC AAAACGATTT TCGGTAAATA

2161 GCACCCACAC CGTTGCGGGA ATTTGGCCTA TCAATTGCGC TGAAAAATAA ATAATCAACA

2221 AAATGGGCAT CGTTTTAAAT AAAGTGATGT ATACCGAATT CGATTGCGTC TCAACCCCTA

2281 CTTCGGTATC TGTATTATCA CGTGTATTTT TGGTTTCACG GAACCAAAAC ATAACCACAA

2341 GGAAAGTGAC AATATTTAGC AACGCAGCGA TAAAAAAGGG ACTATGCGGT GAAATCTCTC

2401 CTGCAAAACC ACCAATAATA GGCCCCGCTA TTAAACCAAG CCCAAAACTT GCCCCTAACC

2461 AACCGAACCA CTTCACGCGT TGAGAAGCTG AGGTGGTATC GGCAATGACC GATGCCGCGA

2521 CAGCCCCAGT AGCTCCTGTG ATCCCTGAAA GCAAACGGCC TAAATACAGC ATCCAAAGCG

2581 CACTTGAAAA AGCCAGCAAT AAGTAATCCA GCGATGCGCC TATTAATGAC AACAACAGCA

2641 CTGGGCGCCG ACCAAATCGG TCAGACATTT TTCCAAGCCA AGGAGCAAAG ATAACCTGCA

2701 TTAACGCATA AAGTGCAAGC AATACGCCAA AGTGGTTAGC GATATCTTCC GAAGCAATAA

2761 ATTCACGTAA TAACGTTGGC AAGACTGGCA TGATAAGGCC AATCCCCATG GCATCGAGTA

2821 ACGTAATTAC CAATGCGATC TTTGTCGAAC TATTCATTTC ACTTTTCTCT ATCACTGATA

2881 GGGAGTGGTA AAATAACTCT ATCAATGATA GAGTGTCAAC AAAAATTAGG AATTAATGAT

2941 GTCTAGATTA GATAAAAGTA AAGTGATTAA CAGCGCATTA GAGCTGCTTA ATGAGGTCGG

3001 AATCGAAGGT TTAACAACCC GTAAACTCGC CCAGAAGCTA GGTGTAGAGC AGCCTACATT

3061 GTATTGGCAT GTAAAAAATA AGCGGGCTTT GCTCGACGCC TTAGCCATTG AGATGTTAGA

3121 TAGGCACCAT ACTCACTTTT GCCCTTTAGA AGGGGAAAGC TGGCAAGATT TTTTACGTAA

3181 TAACGCTAAA AGTTTTAGAT GTGCTTTACT AAGTCATCGC GATGGAGCAA AAGTACATTT

3241 AGGTACACGG CCTACAGAAA AACAGTATGA AACTCTCGAA AATCAATTAG CCTTTTTATG

3301 CCAACAAGGT TTTTCACTAG AGAATGCATT ATATGCACTC AGCGCTGTGG GGCATTTTAC

3361 TTTAGGTTGC GTATTGGAAG ATCAAGAGCA TCAAGTCGCT AAAGAAGAAA GGGAAACACC

3421 TACTACTGAT AGTATGCCGC CATTATTACG ACAAGCTATC GAATTATTTG ATCACCAAGG

3481 TGCAGAGCCA GCCTTCTTAT TCGGCCTTGA ATTGATCATA TGCGGATTAG AAAAACAACT

3541 TAAATGTGAA AGTGGGTCTT AAAAGCCCCA TCGGCCTCGG GGGCCGAATT CGCGGCCGCA

3601 GTCGACCATC ATCATCACCA TCACGGGGCC GCAGAACAAA AACTCATCTC AGAAGAGGAT

3661 CTGAATGGGC GCGCCGCATA GTGATATCGC AAGCTTGACC TGTGAAGTGA AAAATGGCGC

3721 ACATTGTGCG ACATTTTTTT TGTCTGCCGT TTACCGCTAC TGCGTCACGG ATCCCCACGC

3781 GCCCTGTAGC GGCGCATTAA GCGCGGCGGG TGTGGTGGTT ACGCGCAGCG TGACCGCTAC

3841 ACTTGCCAGC GCCCTAGCGC CCGCTCCTTT CGCTTTCTTC CCTTCCTTTC TCGCCACGTT

3901 CGCCGGCTTT CCCCGTCAAG CTCTAAATCG GGGCATCCCT TTAGGGTTCC GATTTAGTGC

3961 TTTACGGCAC CTCGACCCCA AAAAACTTGA TTAGGGTGAT GGTTCACGTA GTGGGCCATC

4021 GCCCTGATAG ACGGTTTTTC GCCCTTTGAC GTTGGAGTCC ACGTTCTTTA ATAGTGGACT

4081 CTTGTTCCAA ACTGGAACAA CACTCAACCC TATCTCGGTC TATTCTTTTG ATTTATAAGG

4141 GATTTTGCCG ATTTCGGCCT ATTGGTTAAA AAATGAGCTG ATTTAACAAA AATTTAACGC

4201 GAATTTTAAC AAAATATTAA CGTTTACAAT TTCAGGTGGC ACTTTTCGGG GAAATGTGCG

4261 CGGAACCCCT ATTTGTTTAT TTTTCTAAAT ACATTCAAAT ATGTATCCGC TCATGTCGAG

4321 ACGTTGGGTG AGGTTCCAAC TTTCACCATA ATGAAATAAG ATCACTACCG GGCGTATTTT

4381 TTGAGTTATC GAGATTTTCA GGAGCTAAGG AAGCTAAAAT GGAGAAAAAA ATCACTGGAT

4441 ATACCACCGT TGATATATCC CAATGGCATC GTAAAGAACA TTTTGAGGCA TTTCAGTCAG

4501 TTGCTCAATG TACCTATAAC CAGACCGTTC AGCTGGATAT TACGGCCTTT TTAAAGACCG

4561 TAAAGAAAAA TAAGCACAAG TTTTATCCGG CCTTTATTCA CATTCTTGCC CGCCTGATGA

4621 ATGCTCATCC GGAGTTCCGT ATGGCAATGA AAGACGGTGA GCTGGTGATA TGGGATAGTG

4681 TTCACCCTTG TTACACCGTT TTCCATGAGC AAACTGAAAC GTTTTCATCG CTCTGGAGTG

4741 AATACCACGA CGATTTCCGG CAGTTTCTAC ACATATATTC GCAAGATGTG GCGTGTTACG

4801 GTGAAAACCT GGCCTATTTC CCTAAAGGGT TTATTGAGAA TATGTTTTTC GTCTCAGCCA

4861 ATCCCTGGGT GAGTTTCACC AGTTTTGATT TAAACGTGGC CAATATGGAC AACTTCTTCG

4921 CCCCCGTTTT CACCATGGGC AAATATTATA CGCAAGGCGA CAAGGTGCTG ATGCCGCTGG

4981 CGATTCAGGT TCATCATGCC GTCTGTGATG GCTTCCATGT CGGCAGAATG CTTAATGAAT

5041 TACAACAGTA CTGCGATGAG TGGCAGGGCG GGGCGTAATT TTTTTAAGGC AGTTATTGGT

5101 GCCCTTAAAC GCCTGGTGCT ACGCCTGAAT AAGTGATAAT AAGCGGATGA ATGGCAGAAA

5161 TTCGAAAGCA AATTCGACCC GGTCGTCGGT TCAGGGCAGG GTCGTTAAAT AGCCGCTTAT

5221 GTCTATTGCT GGTTTACCGG TTTATTGACT ACCGGAAGCA GTGTGACCGT GTGCTTCTCA

5281 AATGCCTGAG GCCAGTTTGC TCAGGCTCTC CCCGTGGAGG TAATAATTGC TCGACATGAC

5341 CAAAATCCCT TAACGTGAGT TTTCGTTCCA CTGAGCGTCA GACCCCGTAG AAAAGATCAA

5401 AGGATCTTCT TGAGATCCTT TTTTTCTGCG CGTAATCTGC TGCTTGCAAA CAAAAAAACC

5461 ACCGCTACCA GCGGTGGTTT GTTTGCCGGA TCAAGAGCTA CCAACTCTTT TTCCGAAGGT

5521 AACTGGCTTC AGCAGAGCGC AGATACCAAA TACTGTCCTT CTAGTGTAGC CGTAGTTAGG

5581 CCACCACTTC AAGAACTCTG TAGCACCGCC TACATACCTC GCTCTGCTAA TCCTGTTACC

5641 AGTGGCTGCT GCCAGTGGCG ATAAGTCGTG TCTTACCGGG TTGGACTCAA GACGATAGTT

5701 ACCGGATAAG GCGCAGCGGT CGGGCTGAAC GGGGGGTTCG TGCACACAGC CCAGCTTGGA

5761 GCGAACGACC TACACCGAAC TGAGATACCT ACAGCGTGAG CTATGAGAAA GCGCCACGCT

5821 TCCCGAAGGG AGAAAGGCGG ACAGGTATCC GGTAAGCGGC AGGGTCGGAA CAGGAGAGCG

5881 CACGAGGGAG CTTCCAGGGG GAAACGCCTG GTATCTTTAT AGTCCTGTCG GGTTTCGCCA

5941 CCTCTGACTT GAGCGTCGAT TTTTGTGATG CTCGTCAGGG GGGCGGAGCC TATGGAAAAA

6001 CGCCAGCAAC GCGGCCTTTT TACGGTTCCT GGCCTTTTGC TGGCCTTTTG CTCACATG

//

The vector was a periplasmic anchor vector with chloramphenicol (CM) resistance, so I had to make my own CM plates: 200 ml LB and 15 g/L bacto agar were mixed and autoclaved. After cooling down the autoclaved media and before pouring the plates, a final concentration of 34 μg/ml was added.

The SfiI enzyme is an enzyme that generates non-compatible ends so one can use it to directly insert fragments without being worried about the vector self-ligation. The designed primers to incorporate fragments into vector:

pAPEX-rev	5'- GGC CGG CTG GGC CTC GCT GCT ACT CTG GTC GC
pAPEX-for	5'- GGC CTC GGG GGC CGA ATT CGC GGC CGC
Az-APEX-for	5'- GCA GCG AGG CCC AGC CGG CCG CTG AAT GCT CCG TTG ATA TCC
Az-APEX-rev	5'- CGC GAA TTC GGC CCC CGA GGC CCT ATT TCA GAG TCA GGG TAC CTT TCA TCA G
mCh-APEX-for	5'- GCA GCG AGG CCC AGC CGG CCA TGG TGA GCA AGG GCG AGG AGG
mCh-APEX-rev	5'- CGC GAA TTC GGC CCC CGA GGC CTT ACT ACT TGT ACA GCT CGT CCA TGC C
mCh-APEX-long-f	5'- GGC AGG TTG CGA CCA GAG TAG CAG CGA GGC CCA GCC GGC CAT GGT GAG CAA GGG CGA GGA GG
mCh-APEX-long-r	5'- GGT GAT GAT GAT GGT CGA CTG CGG CCG CGA ATT CGG CCC CCG AGG CCC TTG TAC AGC TCG TCC ATG CCG CC

To obtain mCh-Az fragment, I used mCh-APEX-for and Az-APEX-rev. to obtain mCh, I had to use the mCh-APEX-long pair. I obtained the fragments using PCR. The PCR of the vector wasn't successful, so I digested it using SfiI enzyme. The construct preparation was formed

using Gibson assembly kit from NEB. The constructs were confirmed through sequencing by ACGT-inc Company.

The surface expression was performed similar to what reported by Georgiou's group with slight modifications.[31] The plasmid was transformed into TOP10 cells to enable arabinose induction. The cells were induced when they reached O.D. 0.6 by addition of 0.5-1% Ara and then let expressed overnight at 30 C. Purification is similar to azurin, but I keep the cells after osmatic shock. To incorporate Cu *in vivo*, I tried adding 1mM Cu together with arabinose.

6.3.2.4. Construction of mCherry fusion to circularly permutated proteins

Yang Yu designed two versions of circularly permutated azurin (cp-Az1/2) and I designed primers to get the pET28-cpAz-mCh construct. The primer sequences are shown below:

CP-Az1-EcoRI-f: 5'-GCGGATCCGATGGAGTTCAACACCAA

CP-Az1-SacI-r: 5'-CGAGCTCCTGATCATTACCCTGGATA

CP-Az2-EcoRI-f: 5'-GCGGATCCGATGGGCGTTATGGGTC

CP-Az2-SacI-r: 5'-CGAGCTCCTTCGGCAGGTTACCTGG

mCh-SacI-f: 5'-CGAGCTCATGGTGAGCAAGGGCG

mCh-NotI-r: 5'- ATAAGAATGCGGCCGCTTACTACTTG

I built the constructs in two ways. In the first method, I ran PCR and obtained the fragments as shown above. I PCR-purified the fragments and confirm them by running them on 1% agarose gel, 120 V, 20 min. I then digested both the fragments and the pET28b vector with the proper restriction enzyme, PCR-purified them following the protocol provided by Qiagen kit and set the ligation reaction using Roche quick ligation kit. The final constructs were confirmed through sequencing by DNA-inc, UIUC.

In the other method, to obtain the cpAz1/2-mCh fragment, I performed an overlap extension PCR. In this method I first run few PCR cycles to obtain small fragments of cp-Az and mCh. I then used those fragments and the forward primer from cpAz and the reverse primer from mCh to extend the cp-Az-mCh fragment. After obtaining that fragment and confirming that by running on a gel, I performed the digestion and ligation as explained above.

6.3.2.5. Protein purification

Plasmids were transformed into BL21(DE3) competent cells. Single colonies were picked and inoculated into start culture of 5 mL LB with corresponding antibiotics. After 8 hours, start culture was inoculated 1:1000 into large LB culture with corresponding antibiotics. It was shaken at 37 °C overnight. IPTG was added to final concentration of 0.3 mM and culture was inducted for 4 hours before harvesting. Cells were harvested by centrifuge at 8000 rpm for 10 min. Pellet was resolubilized in 25mM HEPES, 250 mM NaCl, pH 7 and sonicated for 6 min at 70 W. After sonication, cells were centrifuged for 30 min at 13000rpm to separate supernatant and pellet.

Proteins without His-tag(mCherry-linker-Azurin) were exchanged to 50mM Tris, pH9, then loaded on HiTrap Q column(GE healthcare), desired protein were eluted with salt gradient and with 590nm absorbance monitored on AKTA.

Proteins with His-tag were loaded on a Ni-NTA(NEB) column. Following washing with 10mM imidazole, protein was eluted by 500mM imidazole or an imidazole gradient. Protein identity and purity were verified by SDS-PAGE.

To purify the proteins without His-tag, the purification protocol for GFP was adopted. Briefly, after sonication of cells, ammonium sulfate is added to the supernatant to reach 40% ammonium sulfate in total. This will precipitate most proteins. After stirring for an hour at 4 C, the protein is subjected to centrifugation. The supernatant contains the proteins. To pellet the protein, ammonium sulfate is added to the protein solution to reach a final of 80%. After centrifugation, the pellet is dissolved in lysis buffer and is dialyzed against 20 mM HEPES buffer at pH 7.5. The protein will then be loaded onto a size exclusion column.

To purify mCh-Az in membrane form, I adapted a protocol from Gennis lab. After 4 hours of induction with 0.5 % arabinose at 37 C, I harvested the cells and resuspended them in 200 mM potassium phosphate buffer, pH 7.5. I then sonicated the cells for 3 times using Misonix ultrasonic liquid processor. The process time was 6:00 min with 6 s pulses on and 12 s pulses off and amplitude of 70. I then used the ultracentrifuge instrument. The vacuum was first turned on until the instrument was cooled down to 4 C. Cells were then poured ultracentrifuge tubes and carefully adjusted for weight. The vacuum was stopped and the protein samples were placed in ultracentrifuge. After sealing the door, the vacuum was turned on again. When the pressure was below 200 I started the centrifugation at 40000 rpm for four hours. The pellet had the membrane proteins. It was then resuspended in buffer with 1% DDM (a detergent). I first resuspended the cells in the buffer and then added DDM dropwise while stirring. I stirred for three hours at 4 C.

Cells were then centrifuged in the ultracentrifuge for one hour at 40000 rpm (or half an hour at 42000). All other purification steps should be performed with buffers that contain 0.5% DDM.

6.3.2.6. Fluorescence spectrometry

Fluorescent studies were performed on a HORIBA Jobin Yvon Fuoromax-P using an excitation wavelength of 590 nm, a scan range from 600-750 nm, slit width of 1.5 nm in excitation and 2 nm at emission, integration time of 0.01 s with 0.5 nm increments. About 200µL of 0.1mM protein was used for fluorescence measurement. $CuSO_4$ or ascorbate acid were added into protein solution in cuvette and mixed by vortex. Every spectrum was taken in triplicate. The concentration of the proteins when fused to mCherry was estimated based on mCh absorption (ε_{590} = 41000) and for azurin variants using ε_{280} = 9000 $M^{-1}cm^{-1}$. For cpAz-mCh studies, excitation at 587 was used with slit opening of 3 and 3 nm.

6.3.2.7. Spectroscopies

Electronic absorption was taken on an HP diode array spectrometer or a Cary 5000 spectrometer. X-band EPR spectra were collected on a Varian E-122 spectrometer at the Illinois EPR Research Center (IERC). Proteins were exchanged to TIP7 buffer[32] by a short Sephadex G-25 column and 25% of glycerol was added. The samples were run at ~30 K using liquid He and an Air Products Helitran cryostat with 20% glycerol. Magnetic fields were calibrated with a Varian NMR gaussmeter, and the frequencies were measured with an EIP frequency counter.

6.3.2.8. Flow cytometry analysis

To make sure the protein is displayed on the surface of yeast, flow cytometry studies was performed. Cells were first grown on 2 ml media at 30 overnight. The density of cells was checked by measuring absorption at 600 nm. A volume of OD=0.1(initial OD=x, volume to be added=X/0.1) was added to v-shape 96 well plates (highest density that instrument can handle). Centrifuge the pellet for 2 min at 4000 rpm. Cells were resuspended in 200 µl PBS-BSA 5% and then centrifuged again. Supernatant was taken out using vacuum and this washing step was repeated at least for 3 more times. Then 25 ml of 1x antibody (antiV5-mouse antibody) was added to the wells and incubated 1 hour at 4. 190 µl PBS-BSA was added and centrifuged and

the supernatant was removed by vacuum. This washing step was repeated one more time. 25 µl of 1x second antibody which is biotin-anti mouse was added to pellet and incubated 1 hour at 4. Cells were washed twice with 190 µl PBS-BSA.25 µl of third tag, streptavidin-PE, was added next and plate was incubated for 40 minutes at 4 covered with aluminum foil. Plates were washed three times with 190 µl PBS-BSA and if washing is good, one should see pink color in plates. Pellets were resuspended in 280 µl PBS-BSAand were transferred to flow cytometry tubes and analyzed by flow cytometry instrument as suggested by operator on PE channel.

To perform flow cytometry on bacterial display variant, I resuspended the pellet after osmatic shock in PBS buffer and used those to run the flow cytometry. I used to use an old program using PE-A and perCy5 dyes before but then I realized it is wrong and I changed it with the help of Barbara Pilas in flow-cytometry lab. The SCS threshold was set to 1000 due to small size of the cells and cells were run at low rate. We also changed the instrument so that I can get yellow laser for better results.I used Forresta flow cytometer in MNTL and used PE-Texas Red to excite my samples. The instrument also has a photomultiplier tube that enhances the signal. The method was written by Barbara.

PBS buffer was prepared as follows:

8 gr NaCl, 0.2 gr KCl, 1.44 gr Na_2HPO_4, 0.24 gr KH_2PO_4 in 20 ml water

6.3.2.9. Construction of domain insertion variants

I used Gibson assembly to build these constructs. The general design is vector_mCh-part1_cpAz_mCh-part2_vector. I designed to types of primers: primers to PCR the vector and primers to add NdeI and XhoI to mCh to insert mCh into vector if the vector PCR didn't work. Below are the sequences of the primers. The constructs were confirmed through sequencing by ACGT-inc.

mCh-pET28b-NdeI-f	5'- GGG AAT TCC ATA TGG TGA GCA AGG GCG AGG AGG ATA AC
mCh-pET28b-XhoI-r	5'- GGC GCT CGA GTT ACT ACT TGT ACA GCT CGT CCA TGC CGC C
pET28b-mCh-gr-2	5'- GGC GGC ATG GAC GAG CTG TAC AAG CAC CAC CAC CAC CAC CAC TGA GAT CCG GCT GCT AAC AAA GCC C
pET28b-mCh-gf	5'-GGC GGC ATG GAC GAG CTG TAC AAG CAC CAC CAC CAC CAC CAC TGA
mCh-pET28b-gf-2	5'- CCC CTC TAG AAA TAA TTT TGT TTA ACT TTA AGA AGG AGA TAT ACC ATG GTG AGC AAG GGC GAG GAG GAT AAC

mCh-pET28b-gr-2	5'- GGG CTT TGT TAG CAG CCG GAT CTC AGT GGT GGT GGT GGT GGT GCT TGT ACA GCT CGT CCA TGC CGC C
mCh189-190_r	5'- CTT GGC CTT GTA GGT GGT CTT GAC C
mCh189-190_f	5'- AAG CCC GTG CAG CTG CCC
mCh193-194_r	5'- CTG CAC GGG CTT CTT GGC CTT G
mCh193-194_f	5'- CTG CCC GGC GCC TAC AAC G
cpAz1_mCh189-190_linker_f	5'- GGT CAA GAC CAC CTA CAA GGC CAA GTC GGG CGG CTC CAT GGA GTT CAA CAC CAA CGC C
cpAz1_mCh189-190_linker_r	5'- GGG CAG CTG CAC GGG CTT GGA GCC GCC CGA CTG ATC ATT ACC CTG GAT ATC AAC GG
cpAz1_mCh193-194_linker_f	5'- CAA GGC CAA GAA GCC CGT GCA GTC GGG CGG CTC CAT GGA GTT CAA CAC CAA CGC C
cpAz1_mCh193-194_linker_r	5'- CGT TGT AGG CGC CGG GCA G GGA GCC GCC CGA CTG ATC ATT ACC CTG GAT ATC AAC GG
cpAz2_mCh189-190_linker_f	5'- GGT CAA GAC CAC CTA CAA GGC CAA GTC GGG CGG CTC CAT GGG CGT TAT GGG TCA CAA CTG GG
cpAz2_mCh189-190_linker_r	5'- GGG CAG CTG CAC GGG CTT GGA GCC GCC CGA CTT CGG CAG GTT ACC TGG GTG AG
cpAz2_mCh193-194_linker_f	5'- CAA GGC CAA GAA GCC CGT GCA GTC GGG CGG CTC CAT GGG CGT TAT GGG TCA CAA CTG GG
cpAz2_mCh193-194_linker_r	5'- CGT TGT AGG CGC CGG GCA G GGA GCC GCC CGA CTT CGG CAG GTT ACC TGG GTG AG

6.3.3. Results and discussion

6.3.3.1. Construction of Azurin-mCherry fusion protein

We used overlap extension PCR to fuse Azurin to mCherry and put the fragment into pET22b vector using standard digestion and ligation protocol. Azurin and mCherry attached to each other via different types of linkers and also without linker and the constructs were validated by sequencing.

6.3.3.2. Fluorescence analysis of Azurin-mCherry fusion proteins

Since all the fusion proteins have His tag, they were purified according to Ni-NTA protocol by passing through a Nickel column. The quenching efficiency of each protein was assessed by measuring mCherry fluorescence using a fluorometer. Results are shown in figure 1. Construct

mCherry-SGGS-azurin gave the best quenching over other constructs (~30% at 1Eq of Cu^{2+}, Figure 6.7, generated by Yang Yu)

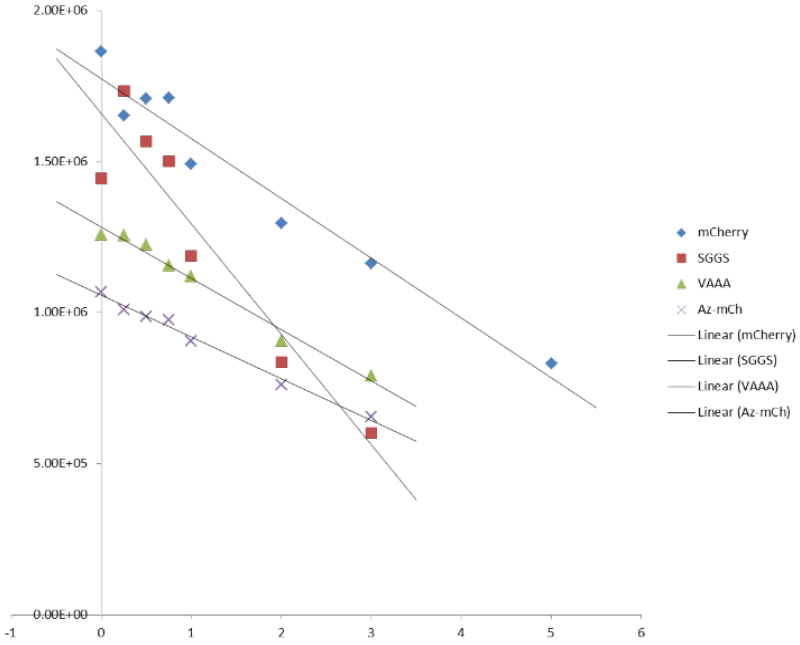

Figure 6.7. Results of Fluorescent quenching upon Cu addition in different mCh-Az variants.

6.3.3.3. Yeast surface display of Azurin-mCherry

We chose the commonly used method of α-agglutinin fusion for displaying the fusion protein on the surface of the yeast.[29,30] To evaluate the method, we started to display azurin alone first. The construct was made using homologous recombination of yeast, by a method called DNA Assembler.[33] Although sequencing has confirmed the proper placement of Azurin gene inside the vector, we couldn't see protein expression using antibodies against a-agglutinin and TEF (figure 6.8).

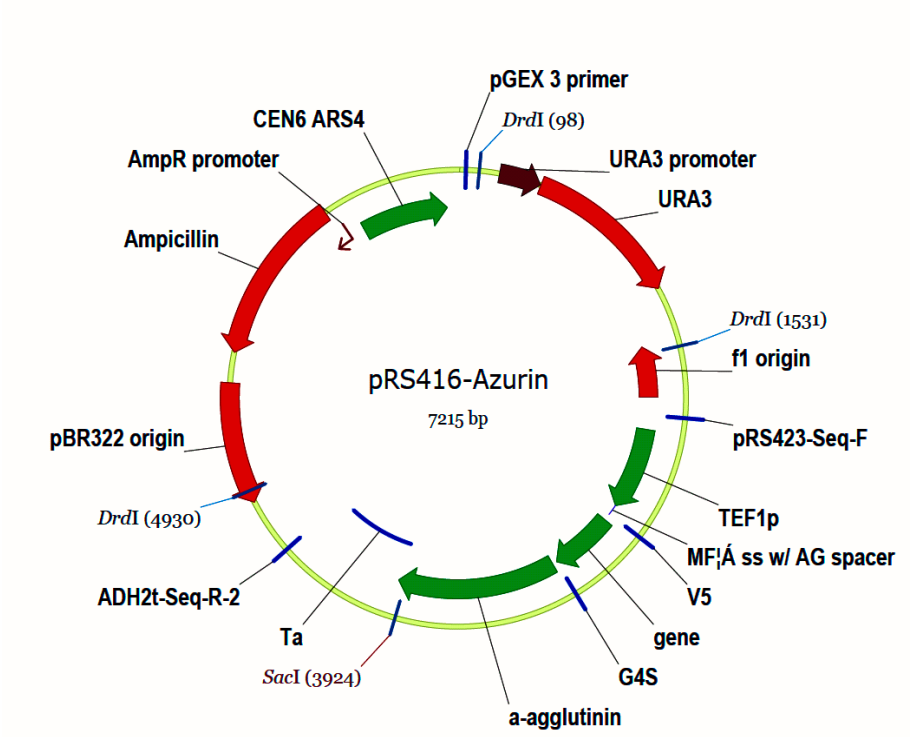

Figure 6.8. Aschematic representation of the vector for yeast display of Az generated by Tong Si from Huimin Zhao lab using Vector-NTI program.

The expression failed in multiple trials, so we hypothesized that Azurin cannot be folded properly inside yeast, which prevents its display on surface. To circumvent this problem, we repeated the experiment with Azurin-mCherry fusion based on the fact that mCherry has a very stable fold that can mediate azurin folding. However, we couldn't see any expression. To overcome the obstacle, we put Azurin-mCherry gene in front of inducible Gal10 promoter because it has higher expression levels than the constitutive promoter we were using. The expression failed again for this construct. We tested the expression using flow cytometry (data not shown but is presented in page 140 of PH notebook III).

6.3.3.4. Bacterial surface display of Azurin-mCherry and flow cytometry

Since azurin could not be displayed on the surface of yeast, we decided to change our display system from yeast to bacteria. We adapted the anchored periplasmic expression (APEx) method reported by George Georgiou group (figure 6.9). Visual inspection of the mCh color confirmed that the majority of the protein is expressed on cell surface. This observation was confirmed by

running the cells on flow cytometry and observing a shift in cell population compared to Az-pAPEX control that has no fluorescent.[31]

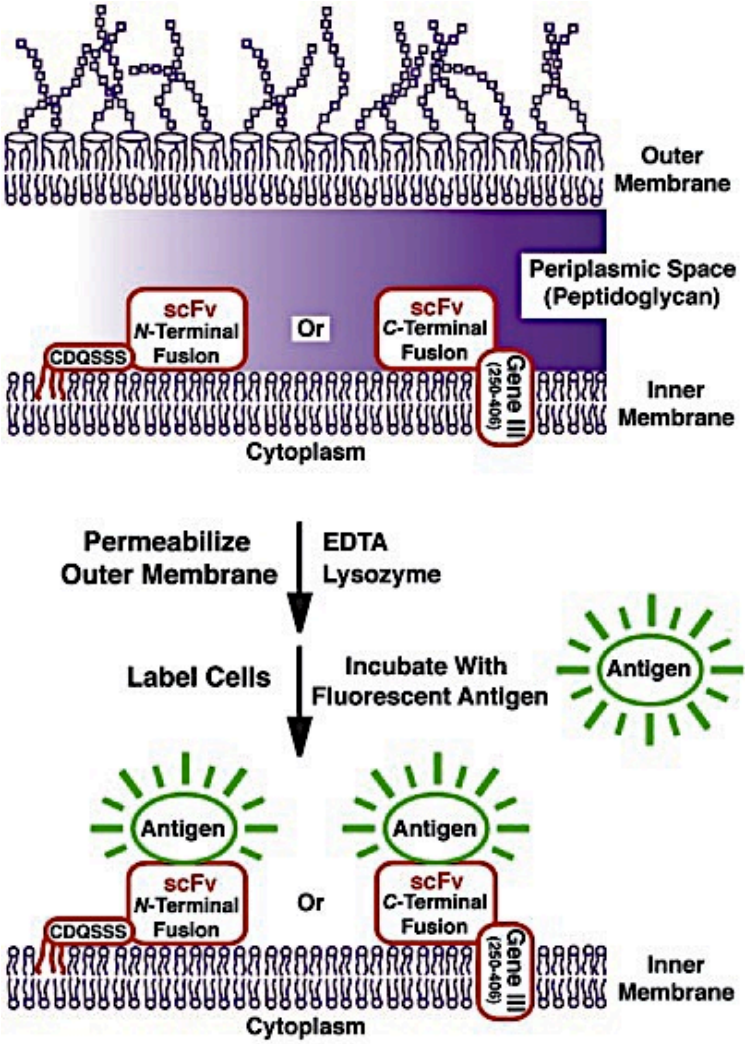

Figure 6.9. Overall scheme of bacterial surface display, adapted from ref .[31]

Using the old method, I could only see aggregates of cell and a small signal due to the laser not exciting the mCh at right wavelength. Using the machine with yellow laser and the new set up, I obtained clear results showing that cells expressed the fluorescent protein (figure 6.10).

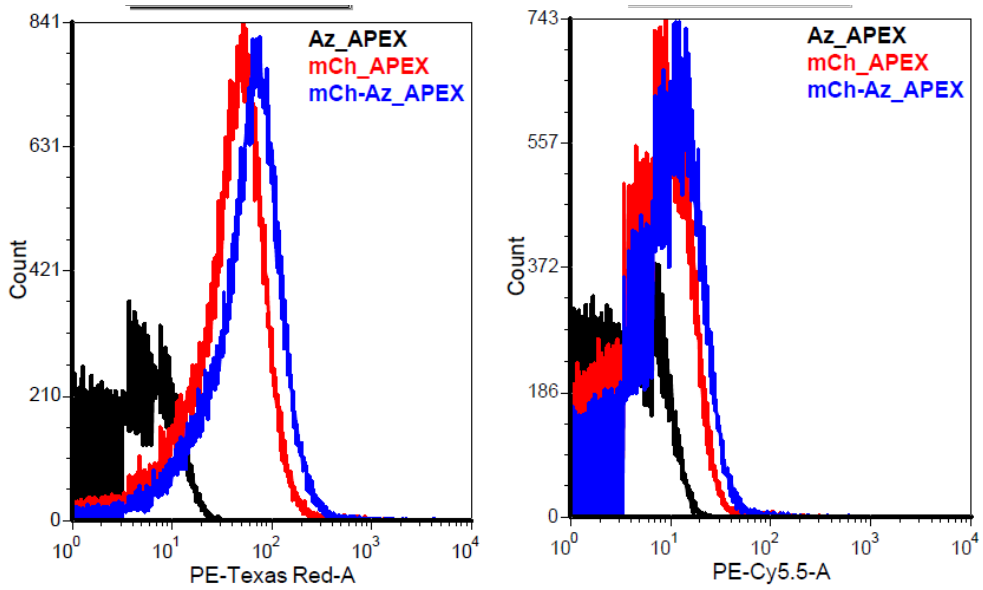

Figure 6.10. Flow cytometry of cells expressing mCh, mCh-Az, or Az on surface. The left figure is shown the result upon excitation with yellow laser. Results from excitation with an improper laser are shown on the right.

The Cu quenching experiments resulted in inconsistent outputs. Sometimes Cu seemed to quench the fluorescent and sometimes not and even when it quenched, according to Barbara Pilas, it was not enough to sort the cells. Since the Cu was effective at quenching mCh alone, unfolding of Az on the surface was one of the possible scenarios that came into mind (figure 6.11).

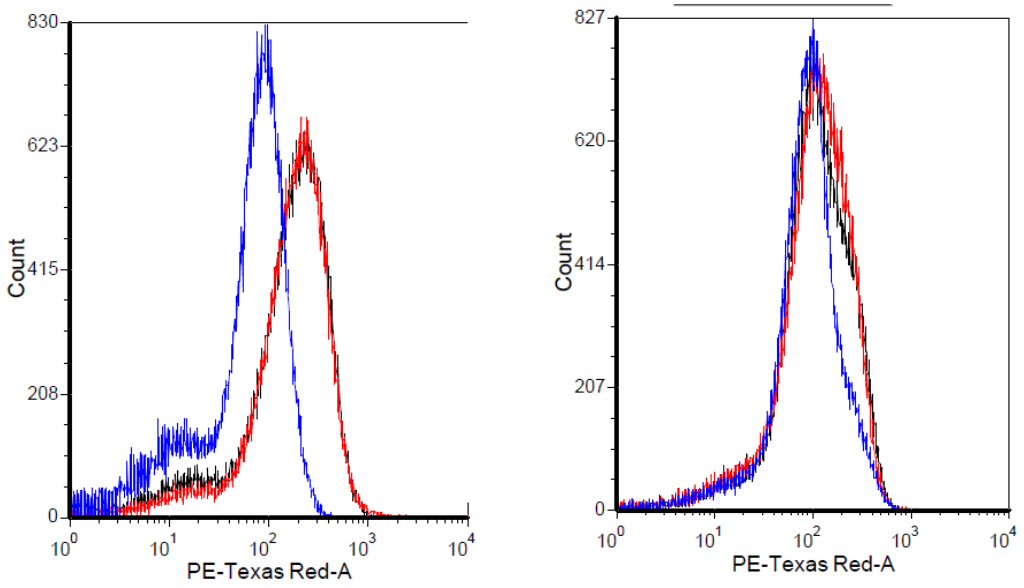

Figure 6.11. Flow cytometry results of Cu quenching.

In order to test the possibility, I purified the mCh-Az in its membrane-bound form. Presence of a pink color in final supernatant is another indicator of the protein being membrane-associated as designed. Attempts to incorporate Cu into the protein was not successful, which is an indicator of improper Cu incorporation due to maybe wrong folding (figure 6.12).

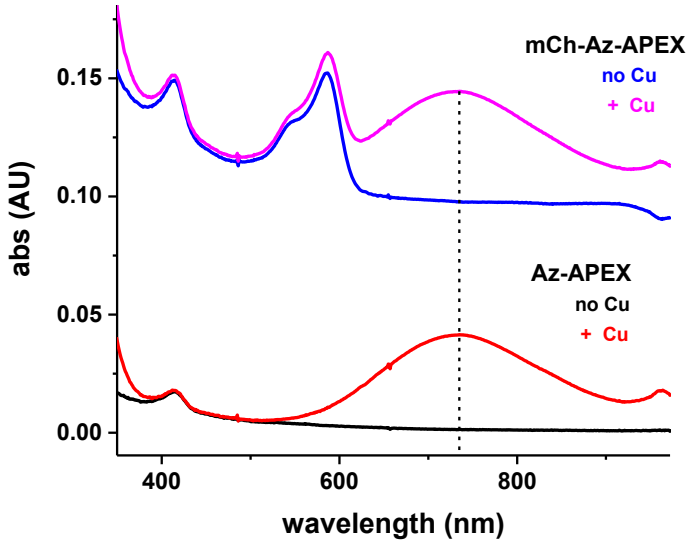

Figure 6.12. UV-vis of membranous Az and mCh-Az protein, before and after Cu incorporation. The peak at 700 nm corresponds to free-Cu(II) absorption. The peak around 580 is due to mCherry.

6.3.3.5. In vitro studies of cpAz variants

The cpAz-mCh variants were designed with the hope that having the mCh closer to the Cu site (now at terminals) would increase the quenching efficiency (figure 6.13, generated by Yang Yu). The protein was expressed in decent yield and the ESI showed mass values (43042 ± 5) close to the expected mass (43194). However, initial fluorescent investigations of the cpAz-mCh constructs showed that the quenching by Cu is nominal in Cu equivalents less than two and that the observed quenching cannot be restored by reducing the Cu using ascorbate (data not shown but available in PH notebook II, page 187).

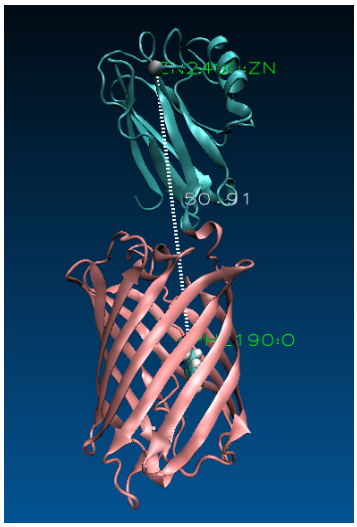

Figure 6.13. Schematic representation of cpAz-mCh construct.

Cu titration into the purified protein showed detectable Cu incorporation (figure 6.14) but the levels are much lower than the normal azurin variants.

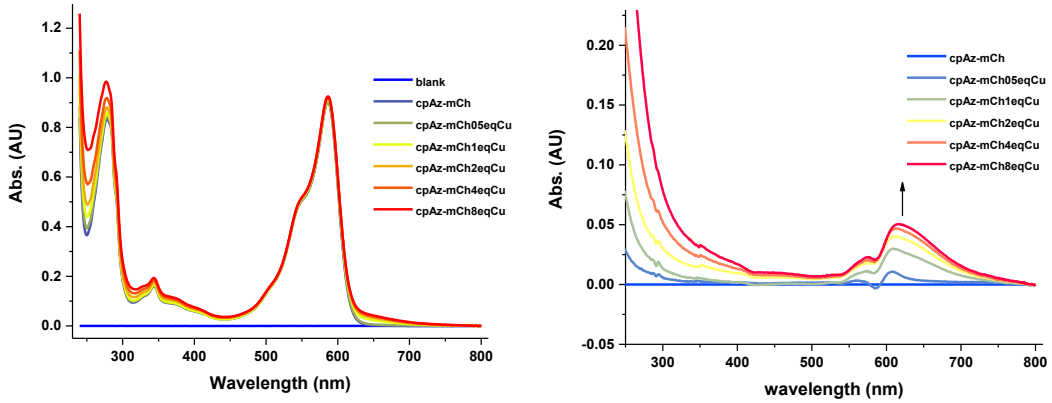

Figure 6.14. Cu incorporation into cpAz1-mCh.

The EPR studies of the Cu loaded protein (the protein concentration was estimated using ε_{587}= 78000 $M^{-1}cm^{-1}$) showed a distorted Cu binding site that is more similar to a type 2 Cu center as shown in figure 6.15.

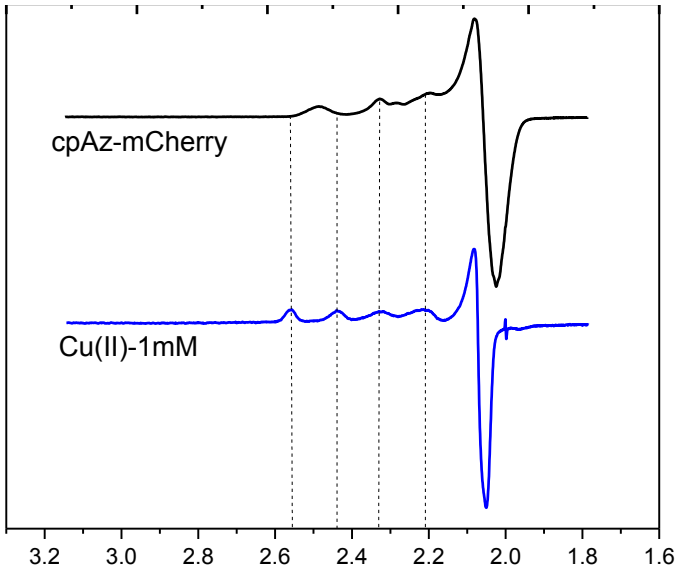

Figure 6.15. EPR of cpAz-mCherry in a Cu-loaded form. (30 mW, 30 K, 4 g modulation)

Fluorescent studies showed that although a decrease in fluorescent signal is observed upon Cu addition, the decrease is about the same as what one will see with just Cu and mCh (figure 6.16).

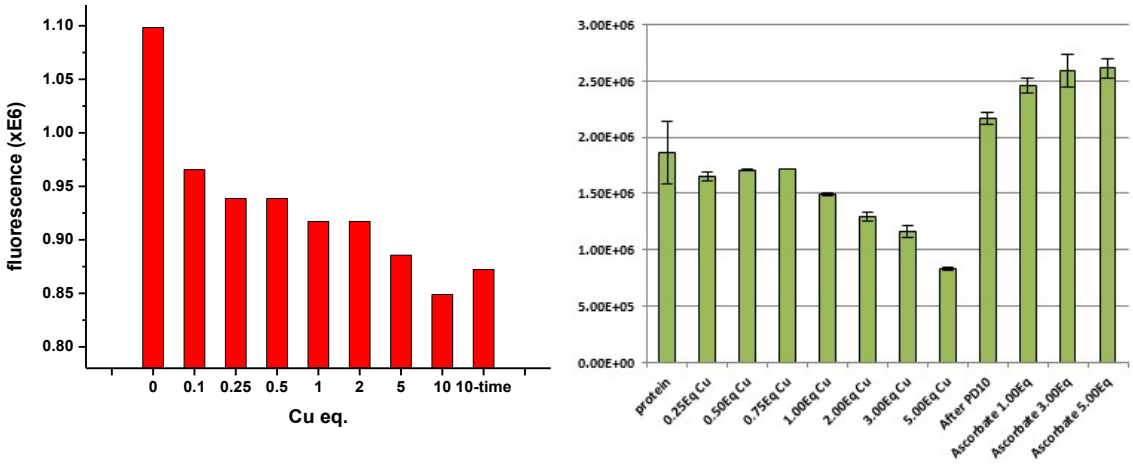

Figure 6.16. The left figure shows the effects of Cu titration in quenching the fluorescent from cpAz-mCh. The right figure, generated by Yang Yu, shows the same experiment but with mCh alone.

To make sure that the free mCh and the one fused to azurin have similar properties, I measured the quantum yield of the protein in my cpAz-mCh construct using the equation below:

Qy= # photons emitted/ # of photons absorbed

# of photons emitted can be estimated by the area under emission when you excite the sample and the # of photons absorbed depends on the concentration and the extinction coefficient which I assumed to be the same for mCh and cpAz-mCh.

The calculated quantum yield for the cpAz-mCh is about 0.359 close to the one from mCh, 0.22. Interestingly, keeping the sample in -80 decreased the quantum yield (maybe because it was exposed to light).

6.3.3.6. Attempts for domain insertion

One way to decrease the distance between the two proteins is to insert one of them in the loops of another. Yang Yu tried some positions in mCh that were structurally analogous to the successful insertion positions in GFP. However, that failed. I picked positions 189-190 and 193-194 (figure 6.17) that were known to retain mCherry fluorescent after being cut in the circularly permutated variants.[34,35]

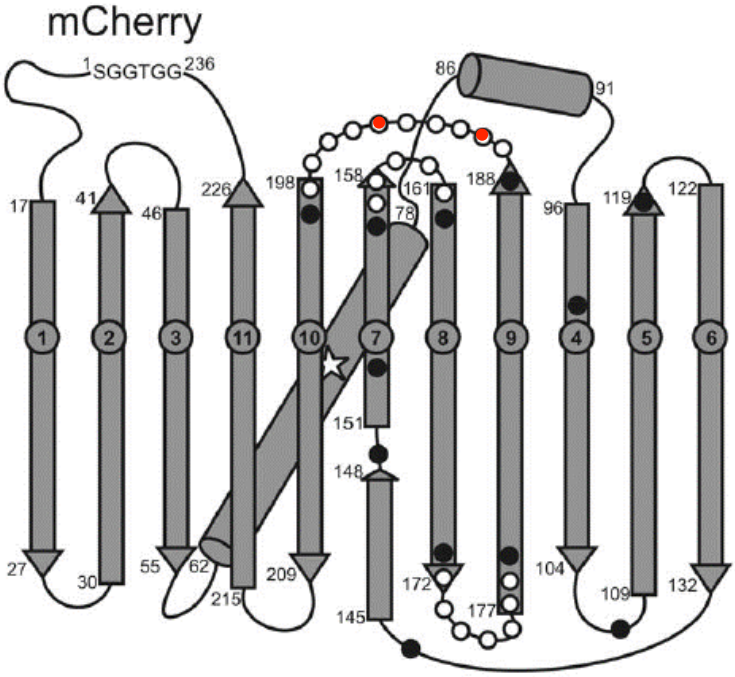

Figure 6.17. Positions of mCh that were tried to generate circularly permutated variants. The one in white retained fluorescence. The red dots show the positions I tried. Figure from ref [35]

The variants however failed to express functional mCh as observed by lack of color despite being expressed based on SDS-PAGE (figure 6.18).

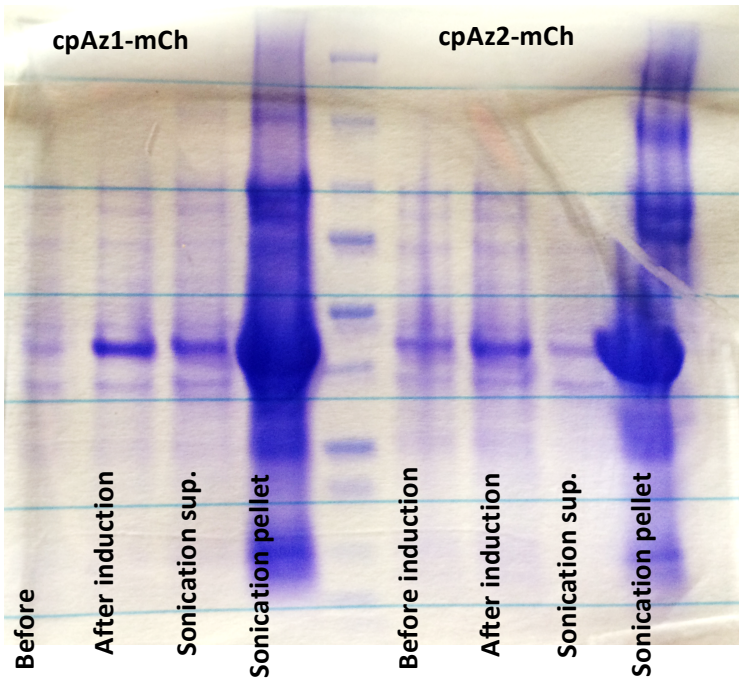

Figure 6.18. 4-20% SDS gel, monitoring expression of domain inserted mCh-Az. The protein band is clearly visible, indicating that the protein is expressed. The lower band in the ladder is 10 kDa.

6.4. Use of noncanonical amino acid, hydroxycoumarin

6.4.1. Introduction

The ability to incorporate noncanonical amino acids (ncAAs) into a protein greatly expanded the repertoire of available functional groups to study proteins and add new modalities to them. While a large number of ncAAs can be incorporated into peptides using chemical synthesis,[36] most proteins are much bigger than the upper limits of the chemical synthesis, about 50 to 100 amino acids.[37] Expressed protein ligation (EPL) was a leap in incorporating ncAAs into proteins, combining the power of chemical synthesis and the ability to express the bigger part of the protein by homologous recombination (see figure 6.19).[38-42] Despite the progress made in the possible ways the peptide can be linked to the protein, there are still limitations on the positions in proteins into which one can incorporate the ncAA of interest.

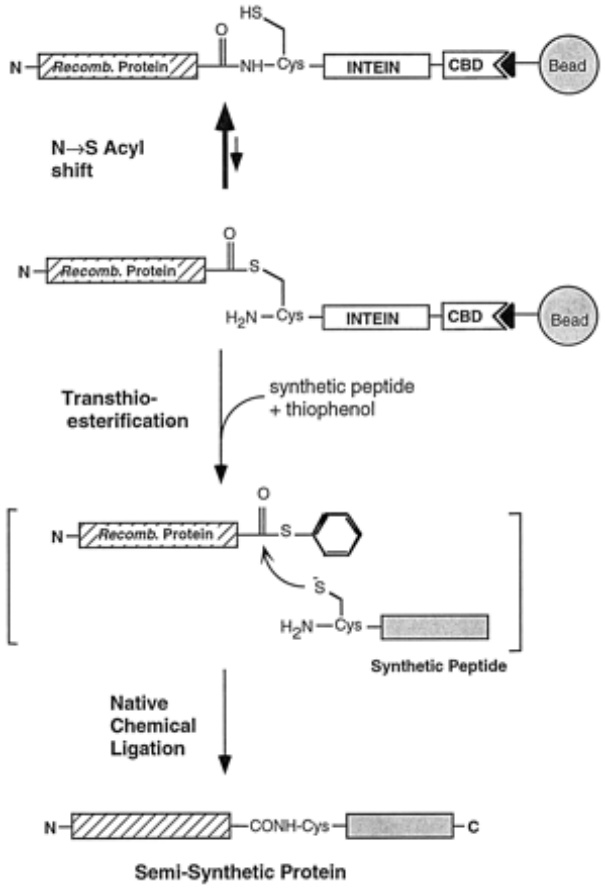

Figure 6.19. Schematic of a common EPL technique, adapted from Ref [39]

The emergence of an orthogonal tRNA-tRNA synthase method for incorporation of ncAAs developed by Peter Schulz opened new avenues in ncAA incorporation.[43] This method enables scientists to incorporate the ncAA in a completely *in vivo* set up and express the protein with the ncAA incorporated in a stop codon that is placed in the position of interest, usually Amber stop codon.[44-49] In order for the method to work, one need to evolve an unnatural pair of tRNA and tRNA synthetase that can recognize and incorporate the ncAA and not recognize other amino acids. The most common way of carrying out the selection is shown in figure 6.20.

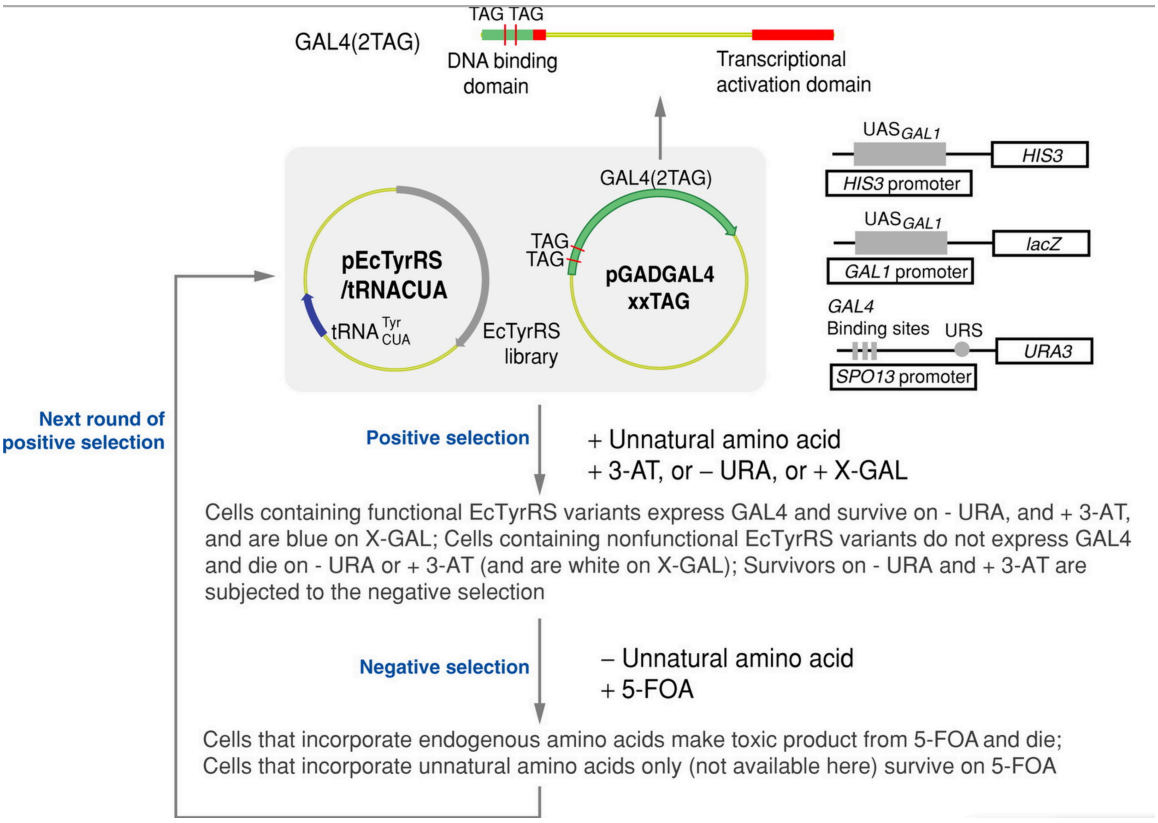

Figure 6.20. General method of evolution of tRNA-tRNA synthase pair. Figure from Ref [44]

We used the same method to incorporate a fluorescent amino acid, hydroxycoumarin, into our protein as the fluorescent probe. The ncAA was designed and developed by our collaborator. Figure 6.21 shows some of the properties of this ncAA.[50]

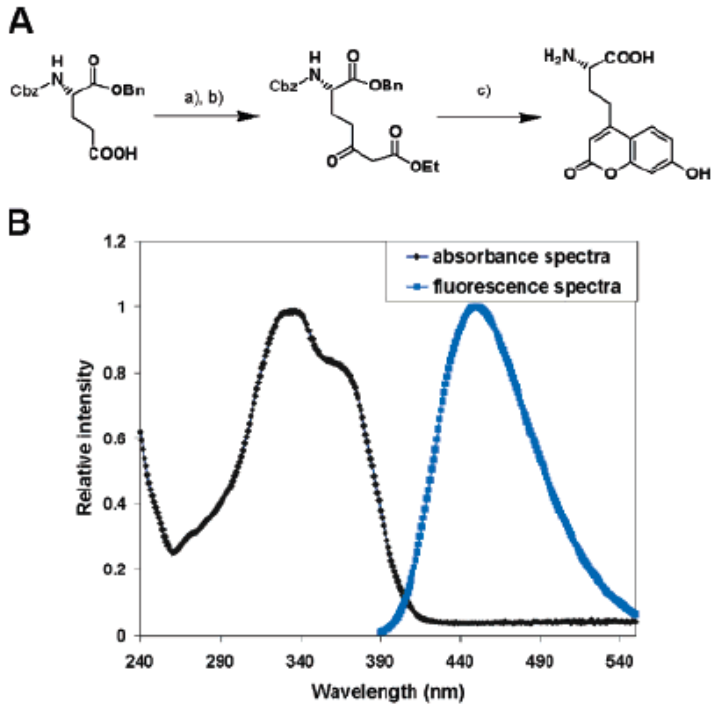

Figure 6.21. Synthesis and UV-vis spectroscopy of hydroxycoumarin. Figure from Ref [50]

6.4.2. Materials and methods

6.4.2.1. Protein expression and purification

The F114TAG (pET vector, kan^r) and pEVol-Hq (CM^r) were transformed into BL21 (DE3) cells from NEB using normal transformation protocol. However, the cells were plated on a plate containing both kanamycin and chloramphenicol. Protein expression was induced by addition of 1 mM IPTG and 0.2 % arabinose. At the same time 12 mg/50 ml of the hydroxycoumarin was also added. Protein was purified as normal azurin but I skipped the precipitation step to avoid precipitating the protein. The purification was performed in a small scale.

6.4.2.2. Fluorescent studies

Fluorescent studies were performed on a HORIBA Jobin Yvon Fuoromax-P using an excitation wavelength of 340 nm, a scan range from 390-450 nm, slit width of 2 nm in excitation and 2 nm at emission, integration time of 0.01 s with 0.5 nm increments. About 200µL of 10 µM protein was used for fluorescence measurements.

6.4.2.3. VMD analysis

I wrote the topology file for the hydroxycoumarin myself based on provided topologies in VMD. Below you may find the topology file:

```
RESI COU          0.00
GROUP
ATOM N    NH1    -0.47  !      |               H1   O2
ATOM HN   H       0.31  !  HN-N                |  ||
ATOM CA   CT1     0.07  !      |   HB1 HG1     C1--C2
ATOM HA   HB      0.09  !      |   |    |     //     \
GROUP                   !  HA-CA--CB---CG--CD       O3
ATOM CB   CT2    -0.26  !      |   |    |     \       /
ATOM HB1  HA      0.13  !      |   HB2  HG2    C3==C4
ATOM HB2  HA      0.13  !    O=C              /     \
ATOM CG   CT2    -0.26  !      |         H5--C5      C6—H6
ATOM HG1  HA      0.13  !                      \\    //
ATOM HG2  HA      0.13  !                       C7--C8
GROUP                   !                       |      \
ATOM C    C       0.51  !                       H7     O4--H4
ATOM O    O      -0.51  !
GROUP
ATOM CD   CA      0.00
ATOM C1   CA     -0.115
ATOM H1   HP      0.115
ATOM C2   CA      0.5
ATOM O2   O      -0.5
ATOM O3   OS   -0.04
ATOM C4   CT2     0.04
GROUP
ATOM C3   CT2    -0.03
ATOM C5   CA     -0.085
ATOM H5   HP      0.115
ATOM C6   CA     -0.115
ATOM H6   HP      0.115
ATOM C7   CA     -0.115
ATOM H7   HP      0.115
ATOM C8   CA      0.11
ATOM O4   OH1    -0.54
ATOM H4   H       0.43
BOND CB CA  N  HN  N  CA
BOND C  CA  C  +N  CA HA  CB HB1  CB HB2
BOND CB CG CG HG1 CG HG2 CG CD
BOND CD C3  C3 C5  C5 H5
BOND C1 C2  C1 H1  C2 O3
BOND O3 C4  C4 C6 C6 H6
BOND C6 C8  C8 O4 O4 H4 C7 C8  C7 H7
DOUBLE O  C  CD C1 C3 C4 C5 C7  C6 C8  C2  O2
IMPR N -C CA HN  C CA +N O
CMAP -C  N  CA  C   N  CA  C  +N
DONOR HN N  H4 O4
ACCEPTOR O C O2 C2
```

I couldn't generate a good parameters file for the molecule, so I never ran simulations with the ncAA. For my simulations, I just used Trp.

6.4.3. Results and discussion

6.4.3.1. Purification

I have designed three positions as candidates for incorporating hydroxycoumarin. Figure 6.22 shows the designs. Residue Tyr72 seems the best position to me. Although it is not as close to the Cu site as Phe114, it has a lower chance to interfere with Cu binding. Met13 position was suggested by Yang Yu but I didn't try it because it was very flexible. Since Chang Cui had already made the mutation for Phe114Hq, I went ahead with that one.

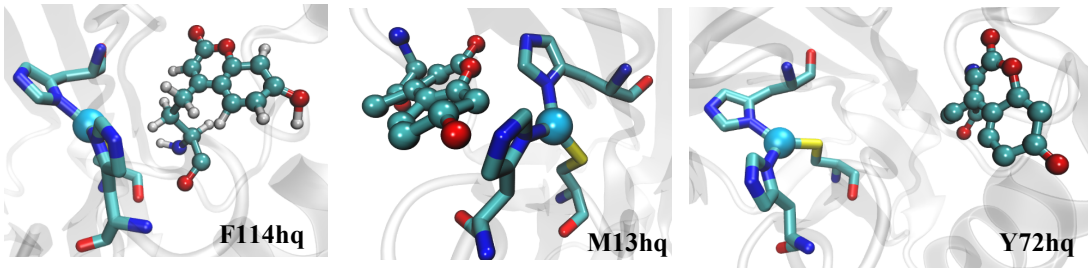

Figure 6.22. VMD representation of hydroxycoumarin in different positions in Az.

The expression yield was as expected for a ncAA-containing protein, poor. As shown in figure 6.23, both SDS-PAGE and the UV-vis are indicative of expression of the protein. The UV-vis data also shows the peak from hydroxycoumarin, suggesting the incorporation of the ncAA.

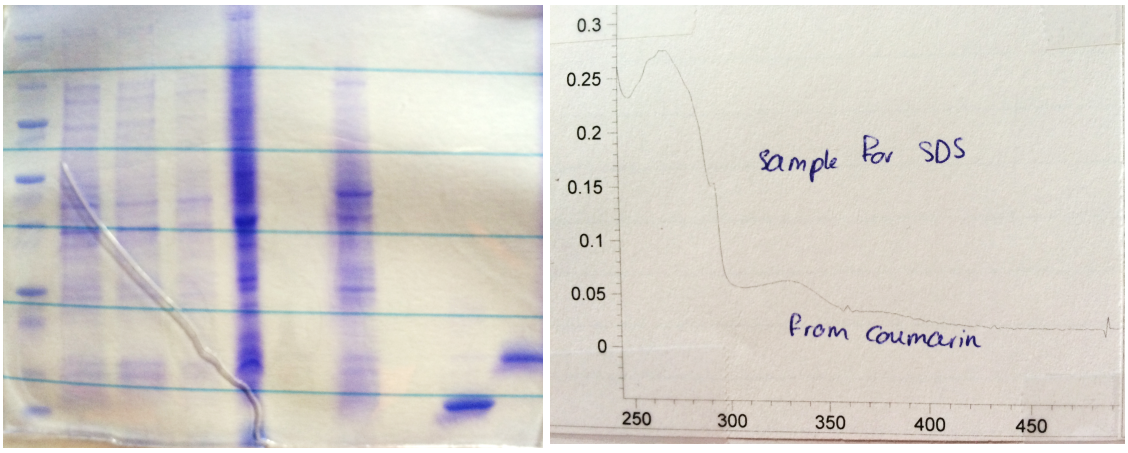

Figure 6.23. SDS-PAGE of F114Hq shows clear expression band corresponding to molecular weight of the protein in the right-most lane. UV-vis features of the protein are also consistent with the presence of the fluorescent hydroxycoumarin.

The Cu titration showed successful incorporation of Cu into the protein. The 635 nm peak however, looked different from other azurin variants, suggesting a possible rearrangement in the Cu site (figure 6.24).

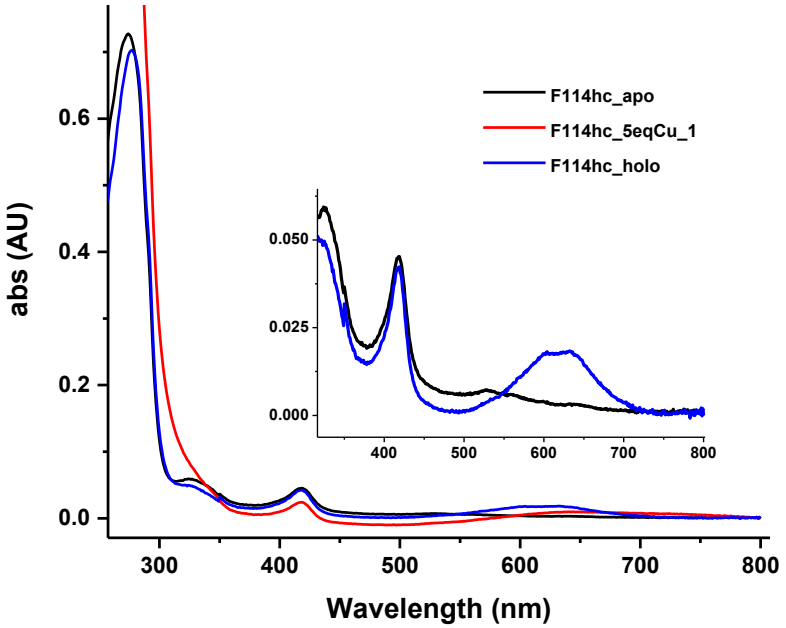

Figure 6.24. Cu titration into F114Hq. The blue spectrum is obtained after removing excess Cu by PD-10.

6.4.3.2. Fluorescent studies

The fluorescent studies on the F114Hq-Az showed that the quenching upon Cu titration into F114Hq-Az is more than the quenching resulted by adding holo-WTAz. Addition of Asc or dithionite however, did not restore the fluorescent. Adding more reducing equivalents just decreased the fluorescence even more. Figure 6.25 summarizes the results.

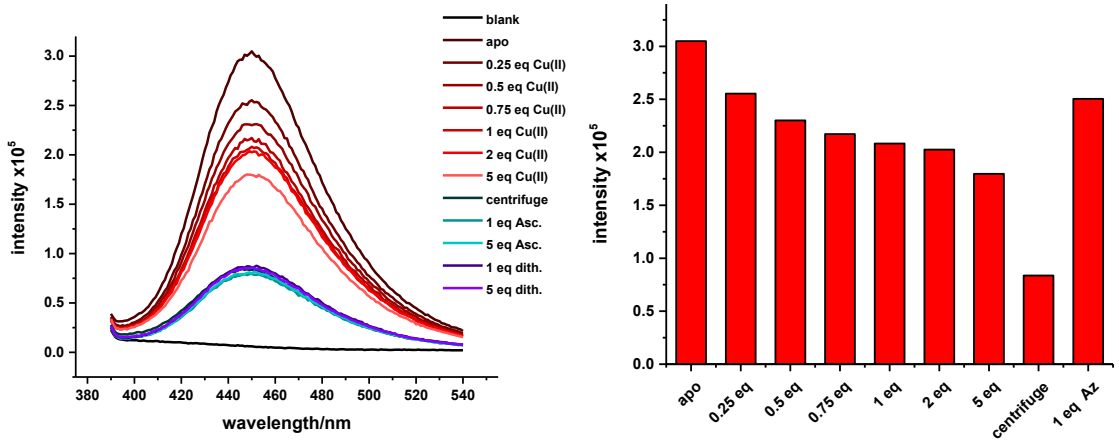

Figure 6.25. Summary of fluorescent studies on F114Hq-Az.

6.5. FlAsH dye

6.5.1. Introduction and rationale

Recent years has witnessed a significant progress in the field of small molecule sensors that can bind to specific sequences or motifs and can be detected by a signal, usually fluorescent read out. One such sensor is FlAsH. FlAsH is a bi-arsenate molecule designed by Roger Tsien and coworkers and was shown to have fluorescent signal upon binding to a special peptide motif, Cys-Cys-Xxx-Xxx-Cys-Cys, usually as a part of small helix (figure 6.26).[51] This motif is very rare in natural proteins, hence by tagging a protein with this peptide, one can selectively monitor it inside a cell. The probe is shown to work very well in cellular conditions with bright fluorescence.[51] The FlAsH molecule itself is also very stable and relatively easy to synthesize.[52] Later, the Schepartz group showed that FlAsH and its red analogue ReAsH are able to bind to loop regions as well as to two different proteins each of which has a di-Cys motif in them.[53-55] They used this property of the molecule to monitor binding of two proteins.[53-55] Due to the high affinity of FlAsH to bind the motif and our previous success of fluorescent studies with Alexa Fluor, I decided to use FlAsH as a bright fluorophore that only fluoresce upon binding and can be quenched by Cu(II). Lack of other FlAsH binding motif will give binding specificity and since it is not covalent, the conjugation/binding may be more efficient than its covalent counterparts, such as Alexa Fluor.

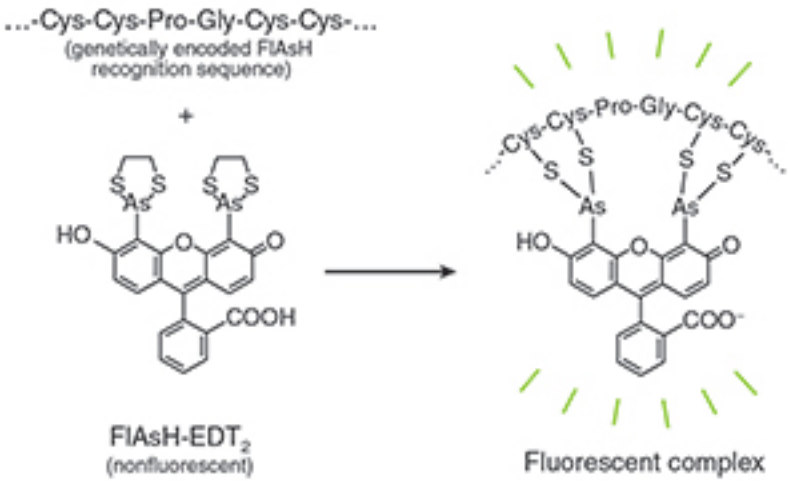

Figure 6.26. FlAsH and schematic representation of its mode of action. Figure from Life technologies website.

6.5.2. Materials and methods

6.5.2.1. Construct design, molecular dynamics simulations, and purification

The constructs were designed for three different positions in azurin and are called Az-FlAsH-1to3. The rationale behind each design is described in results and discussion section. Below you may find the designed primers for each site and the protein sequence for each of them. I used Gibson assembly to obtain the constructs. For FlAsH1 and FlAsH2, the primers were first designed for site directed mutagenesis but that didn't work, so I mixed the two together and let anneal at room temperature for 2 hours and used that as the Gibson fragment. For FlAsH3, a separate Gibson fragment was ordered:

Az_FlAsH_1:

AECSVDIQGCCPGCCGQFNTNAITVDKSCKQFTVNLSHPGNLPKNVMGHNWVLSTAADMQGVVTDGMASGLDK
DYLKPDDSRVIAHTKLIGSGEKDSVTFDVSKLKEGEQYMFFCTFPGHSALMKGTLTLK

FlAsH-1_Az_r	5'- GCC GCA GCA GCC CGG GCA GCA ACC CTG GAT ATC AAC GGA GC
FlAsH-1_Az_f	5'- TGC TGC CCG GGC TGC TGC GGC CAG TTC AAC ACC AAC GCC
FlAsH-1_f	5'- GCT CCG TTG ATA TCC AGG GTT GCT GCC CGG GCT GCT GCG GCC AGT TCA ACA CCA ACG CC
FlAsH-1_r	5'- GGC GTT GGT GTT GAA CTG GCC GCA GCA GCC CGG GCA GCA ACC CTG GAT ATC AAC GGA GC

Az_FlAsH_2:

AECSVDIQGQFNTNAITVDKSCKQFTVNLSHPGNCCPGCCSGHNWVLSTAADMQGVVTDGMASGLDKDYLKPDD
SRVIAHTKLIGSGEKDSVTFDVSKLKEGEQYMFFCTFPGHSALMKGTLTLK

FlAsH-2_Az_r	5'- GCT GCA GCA GCC CGG GCA GCA GTT ACC TGG GTG AGA CAG G
FlAsH-2_Az_f	5'- TGC TGC CCG GGC TGC TGC AGC GGT CAC AAC TGG GTT CTG TCC
FlAsH-2_f	5'- CCT GTC TCA CCC AGG TAA CTG CTG CCC GGG CTG CTG CAG CGG TCA CAA CTG GGT TCT GTC C
FlAsH-2_r	5'- GGA CAG AAC CCA GTT GTG ACC GCT GCA GCA GCC CGG GCA GCA GTT ACC TGG GTG AGA CAG G

Az_FlAsH_3:

AECSVDIQGPGCCGSQFNTNAITVDKSCKQFTVNLSHPGCCPKNVMGHNWVLSTAADMQGVVTDGMASGLDKD
YLKPDDSRVIAHTKLIGSGEKDSVTFDVSKLKEGEQYMFFCTFPGHSALMKGTLTLK

FlAsH-3_site1_r	5'- GAT GGC GTT GGT GTT GAA CTG GCT GCC GCA GCA GCC CGG ACC CTG GAT ATC AAC GGA GCA TTC
FlAsH-3_site2_f	5'- CCT GTC TCA CCC AGG TTG CTG CCC GAA GAA CGT TAT GGG TC
Az_FlAsH3_Gibson	5'- GAA TGC TCC GTT GAT ATC CAG GGT CCG GGC TGC TGC GGC AGC CAG TTC AAC ACC AAC GCC ATC ACC GTC GAC AAG AGC TGC AAG CAG TTC ACT GTT AAC CTG TCT CAC CCA GGT TGC TGC CCG AAG AAC GTT ATG GGT C

The primers were synthesized by IDT, Inc. and the constructs were confirmed through sequencing by ACGT, Inc.

In order to make sure the constructs are well folded, molecular dynamics simulations on the designed proteins were performed. Since the constructs were not a result of simple mutagenesis, I used I-TASSER server[56-58] to predict the structure of the given amino acid sequence first and then used that structure as initial point for PSF generation and molecular dynamics simulations. PVT cell was used with 10000 steps of minimization (2 fs/step) and 1 ns of simulation.[59]

Proteins were expressed in small scale using common azurin purification protocol but the precipitation step was skipped. The purification was stopped after collecting fractions of a small SP-sepharose column due to small scale. The presence of samples was confirmed by running SDS-PAGE, 4-20%, 120 V, one hour.

6.5.2.2. Labeling method

The FlAsH dye was purchased from Santa Cruz Biotech (sc-363644). The dye stock was prepared by dissolving a small amount of the dye in DMSO in a black tube to avoid light. The concentration of the stock was calculated using ε_{508}= 41000 $M^{-1}cm^{-1}$.

The labeling was performed using the method reported by Schepartz group with some modifications.[53,54] In brief, 100 µl of 100 nM dye, diluted from the stock in 100 mM Tris-HCl pH 8 + 75 mM NaCl+ 3.5 mM TCEP was mixed with 100 µl of protein exchanged into the same buffer in different concentrations. The reaction was kept at room temperature, in dark, for 90 min to complete. I avoided adding EDT and EDTA due to making the condition more stringent for dye binding and Cu binding, respectively. Later different concentrations of TCEP and different buffers were used as well.

6.5.2.3. Spectroscopic studies

Spectroscopic studies were performed either on a photo diode array HP instrument or on a Cary 5E spectrophotometer. Cu was titrated in an Eppendorf tube while stirring.

6.5.2.4. Fluorescent studies

Fluorescent studies were performed on a HORIBA Jobin Yvon Fuoromax-P using an excitation wavelength of 508 nm, a scan range from 500-650 nm, slit width of 3 nm in excitation and 3 nm at emission, integration tume of 0.01 s with 0.5 nm increments. The time course measurements were performed using the "time" option in the experiment type subdirectory of the instrument. The sample was excited at 508 nm and the 524 nm emission was monitored during a course of 300 sec with 1 sec intervals.

6.5.2.5. NMR

NMR samples were prepared by weighting the dry compounds and dissolving them in deuterated DMSO. The final concentration of the dye was about 3 mM and Cu and Zn salt were added to final of 5 molar equivalent to the dye. NMR tubes were covered with foil to protect the samples from light.

6.5.3. Results and discussion

6.5.3.1. Construct design and expression

Three different designs were used to add the FlAsH binding motif to azurin. In the first design, Az_FlAsH_1 (figure 6.27), I inserted the binding motif in azurin loop 12 (the loop containing residue 12). This length of this loop varies the most among cupredoxins and is the one that is extended in nitrosocyanin so I thought that it would be more resistant to insertions. Molecular dynamics simulation showed that disulfide bond formation is not very likely with this design, however, there is a chance of the loop flipping outwards to the solvent and away from the Cu binding site.

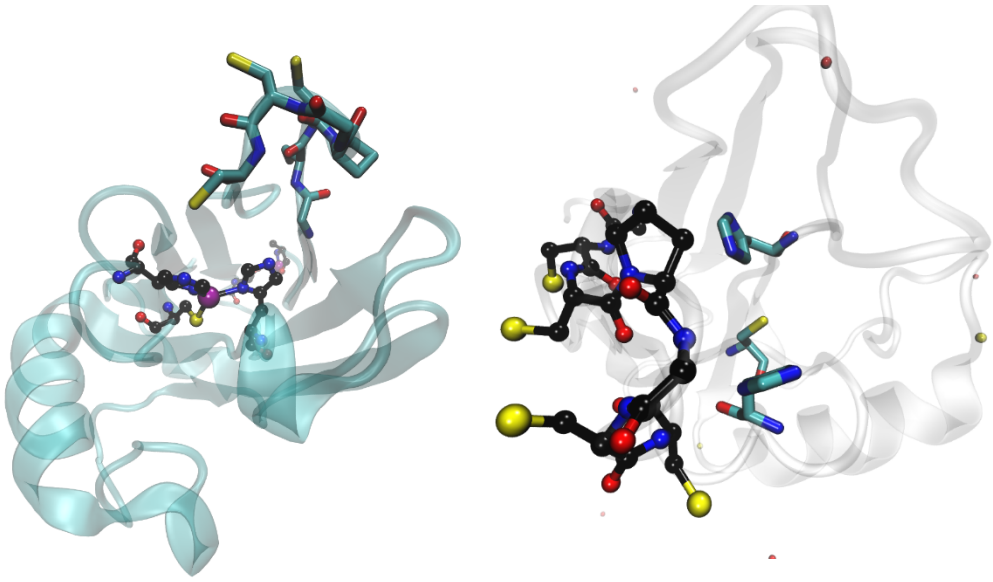

Figure 6.27. Models of Az-FlAsh_1 before (left) and after (right) simulation. Initial model was generated by I-TASSER.

In the second design the motif is inserted in loop 44 (loop containing residue 44, see figure 6.28). Such positioning will bring the FlAsH much closer to the Cu binding site. This design however has the drawback of being susceptible to disulfide formation. In addition, since it is very close to the Cu binding site, it may interfere with Cu binding.

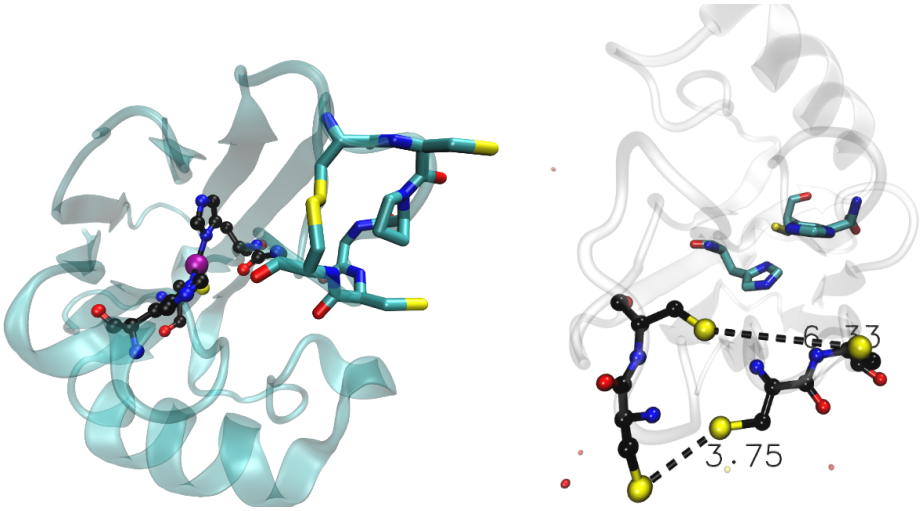

Figure 6.28. Models of Az-FlAsh_2 before (left) and after (right) simulation. Initial model was generated by I-TASSER.

Design 3 takes advantage of the study showing that FlAsH can bind to two separate peptides if each of them has a pair of di-Cys motif (figure 6.29). I incorporated one di-Cys motif in loop 12 and one in loop 44. This way, the FlAsH is forced to bind right on top of the Cu binding site

and has a lower chance of interfering with the site as it is kept in place by two different sites of the protein.

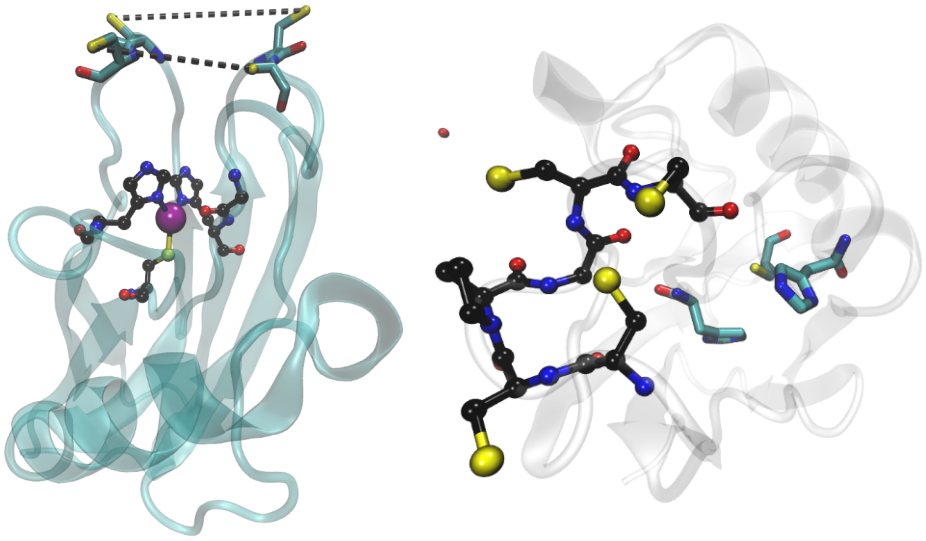

Figure 6.29. Models of Az-FlAsh_3 before (left) and after (right) simulation. Initial model was generated by I-TASSER.

SDS-PAGE showed that the small scale purification of all proteins resulted in yields enough for initial UV-vis and fluorescent studies. Figure 6.30 show a representative gel from construct 1:

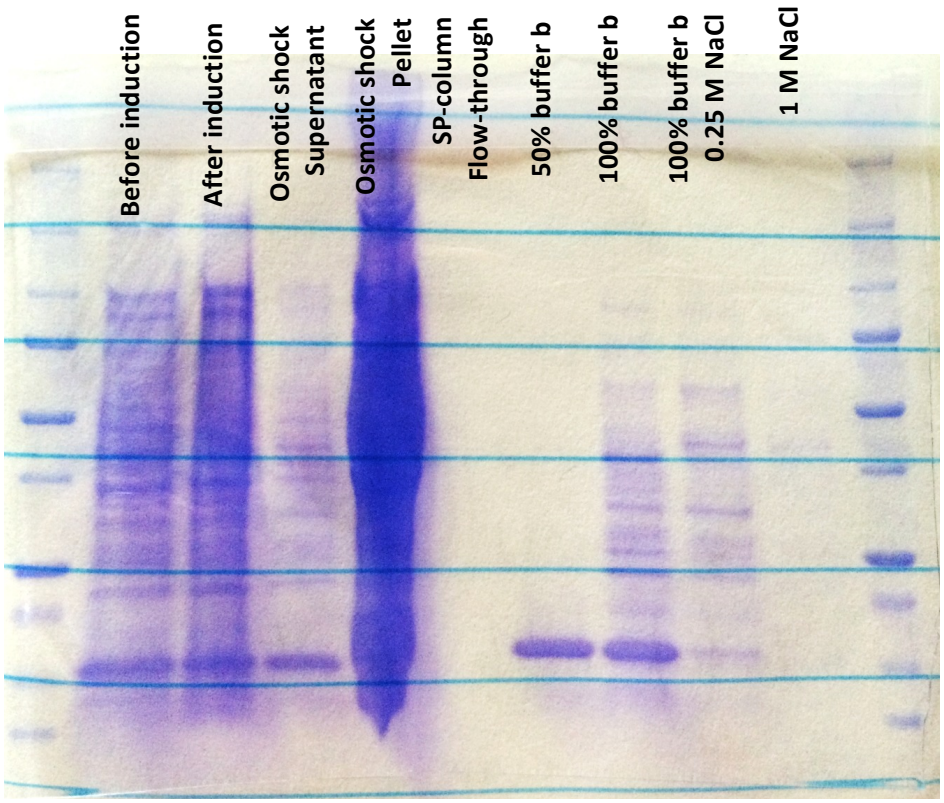

Figure 6.30. Monitoring the expression of Az_FlAsH_1 by SDS-PAGE.

6.5.3.2. Labeling of azurin with FlAsH

The fluorescent studies clearly show specific labeling of azurin variants with the Cys-Cys-Xxx-Xxx-Cys-Cys motif and not WT-Az (figure 6.31). Interestingly, FlAsH_3 construct showed better labeling efficiency. This observation can be either due to binding of two molecules of FlAsH per molecule of FlAsH_3 (since the motif is split) or due to better efficiency.

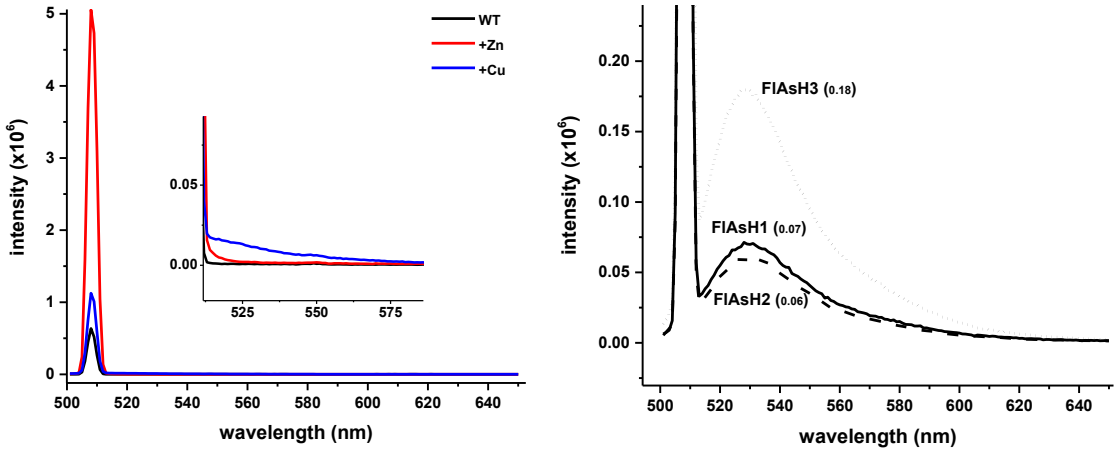

Figure 6.31. Fluorescent studies show efficient labeling of FlAsH designs.

Labeling the proteins under different conditions resulted in several findings: a) As expected, increasing protein concentration increased the fluorescent signal; b) TCEP is necessary for the efficient labeling. One can lower the amount of added TCEP to 2 molar equivalents to the protein, but without TCEP labeling efficiency is negligible. Interestingly in acetate buffer higher concentrations of TCEP abolished the binding; c) Tris buffer is not necessary for the binding and ammonium acetate buffer at pH 6 works just as well. An overview of the results is shown in figure 6.32.

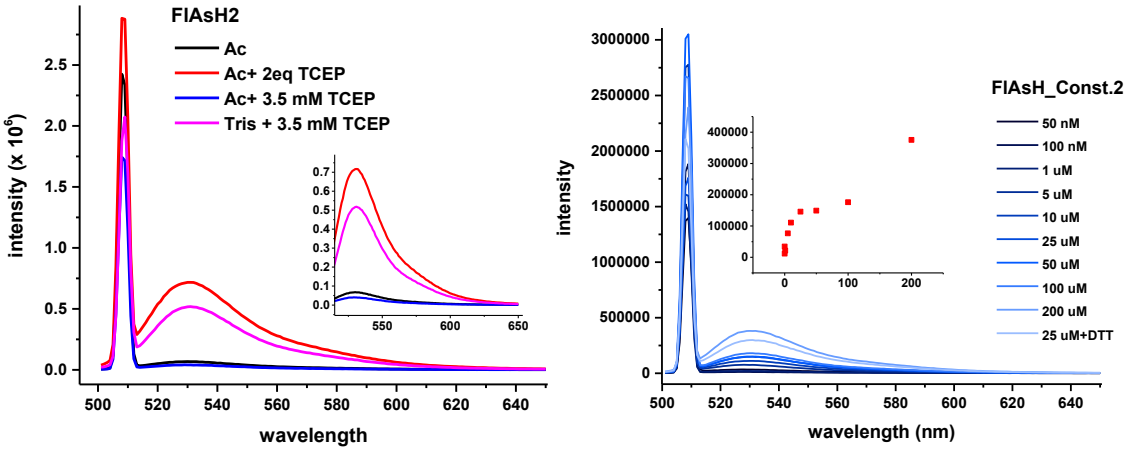

Figure 6.32. Fluorescent monitoring of FlasH binding in different conditions.

6.5.3.3. Quenching by Cu

In my initial Cu titration studies, I noticed that upon addition of Cu in excess to TCEP, fluorescent signal quenches beautifully. This quenching however, cannot be restored upon reducing the sample by ascorbate, even in excess. Representative results for FlAsH_1 is shown in fugure 6.33.

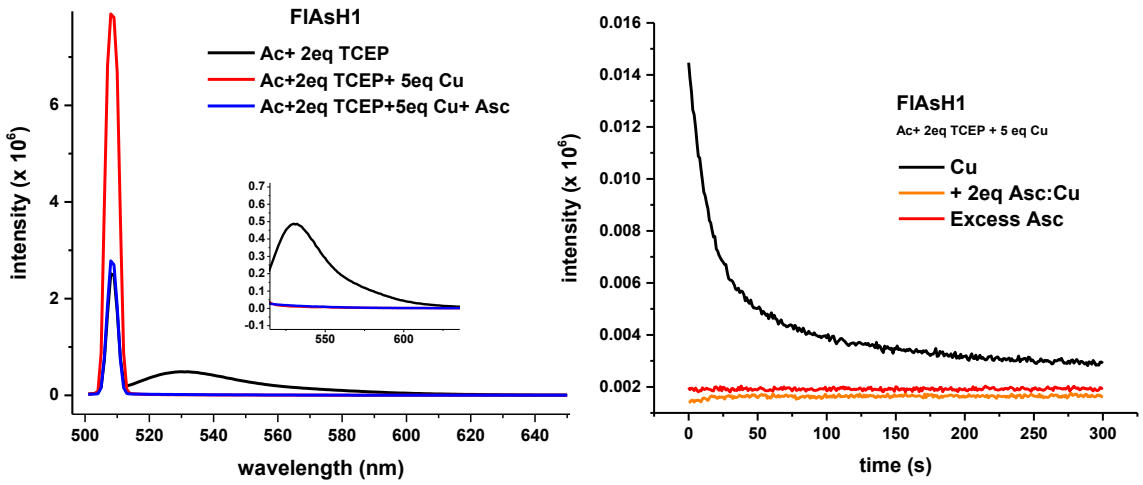

Figure 6.33. Quenching of FlAsH fluorescence by Cu titration.

To find out whether the protein still binds Cu, I performed UV-vis spectroscopy trying to monitor 625 nm peak, indicator of Cu binding in a typical type 1 Cu site. The UV-vis results (figure 6.34) showed that the binding is much lower than the expected value and that the presence of TCEP interferes with Cu binding. That is the main reason I continued with only two molar equivalent of TCEP to protein for further fluorescent studies. The results is further complicated by the fact that interaction of Cu with TCEP generates a peak at 625 nm which later shifts to close to 700 nm.

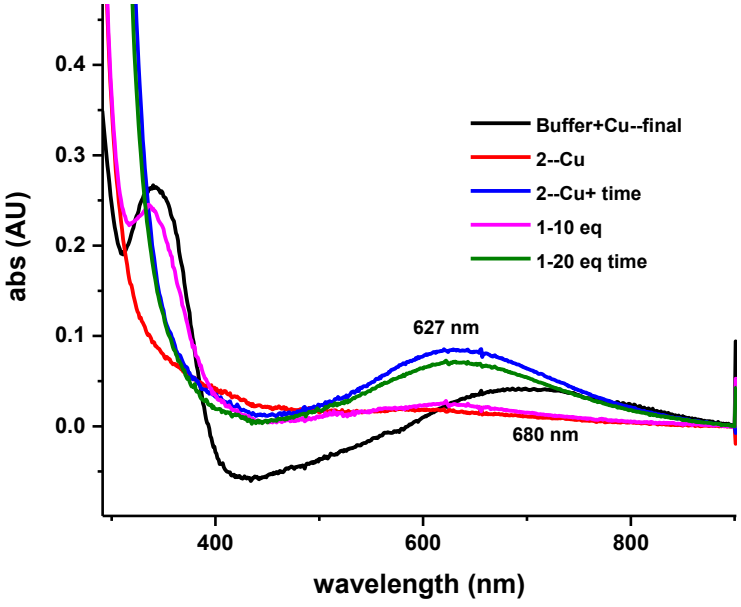

Figure 6.34. UV-vis results of Cu incorporation into Az_FlAsH variants.

Later I monitored the fluorescence quenching upon Cu addition, but not in a time course and I found out that addition of Cu resulted in a blue shift in fluorescent emission spectrum of all the samples (figure 6.35). Addition of Zn did not have such effect. The effect could not be reverted by ascorbate treatment and reduction of Cu (figure 6.35).

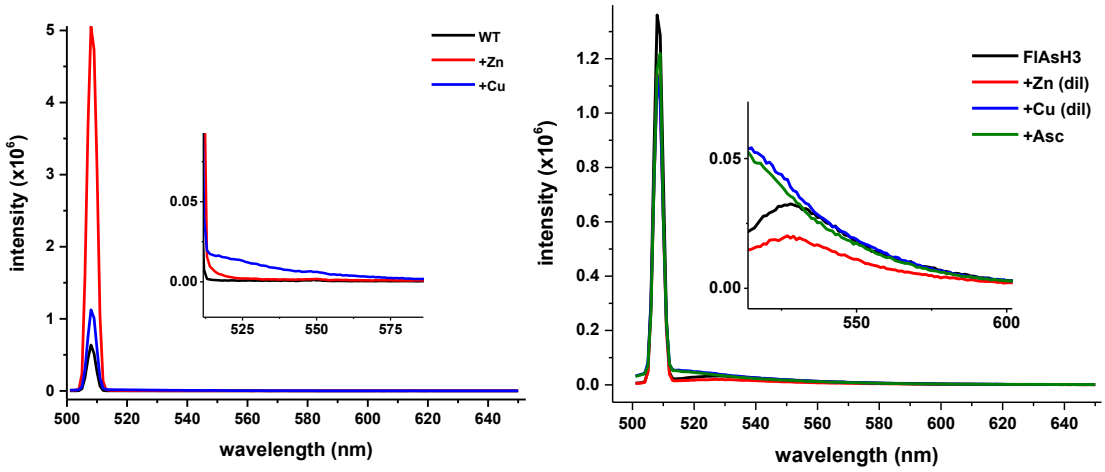

Figure 6.35. Fluorescent analysis of Az_FlAsH shows interference in emission upon Cu, and not zn, addition.

Interestingly, a distinct blue shift in the UV-vis spectra of the samples were also observed upon addition of Cu (figure 6.36).

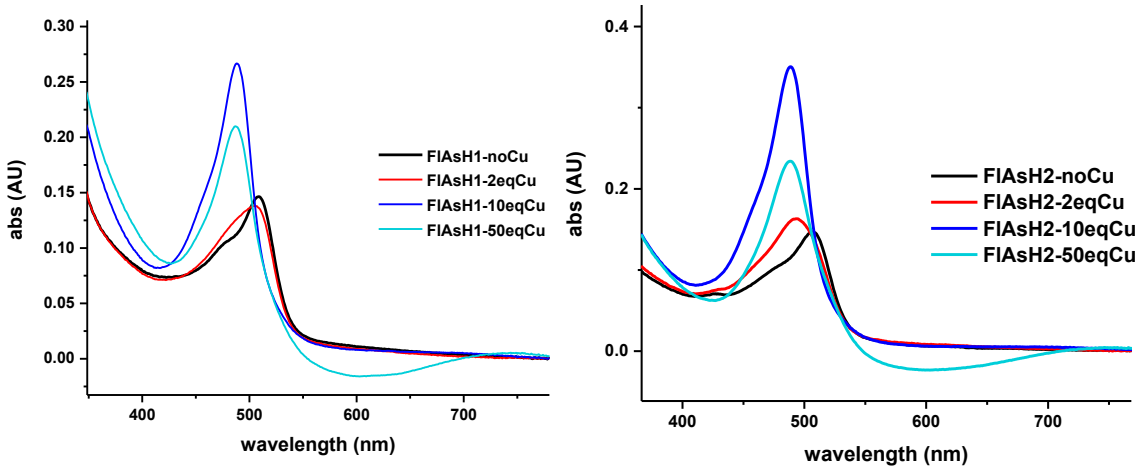

Figure 6.36. UV-vis analysis of FlAsH shows interference in emission upon Cu addition.

6.5.3.4. Interaction of the dye with metal ions

I knew that in all my samples, I had some amount of unreacted dye. I decided to check whether the dye itself reacts with metal ions or not. Since in the unbound state FlAsH does not

have a fluorescent signal, I used UV-vis to detect changes in the spectra and as shown in figure 6.37, metal addition has a noticeable effect on the UV-vis spectra of FlAsH. In the case of the non-redox active metal, Zn, the effect is limited to increase in absorption. Cu in contrast results in both an increase and a shift in the spectra. Adding excess Cu causes first an increase and then a decrease in the intensity of the peak (figure 6.37).

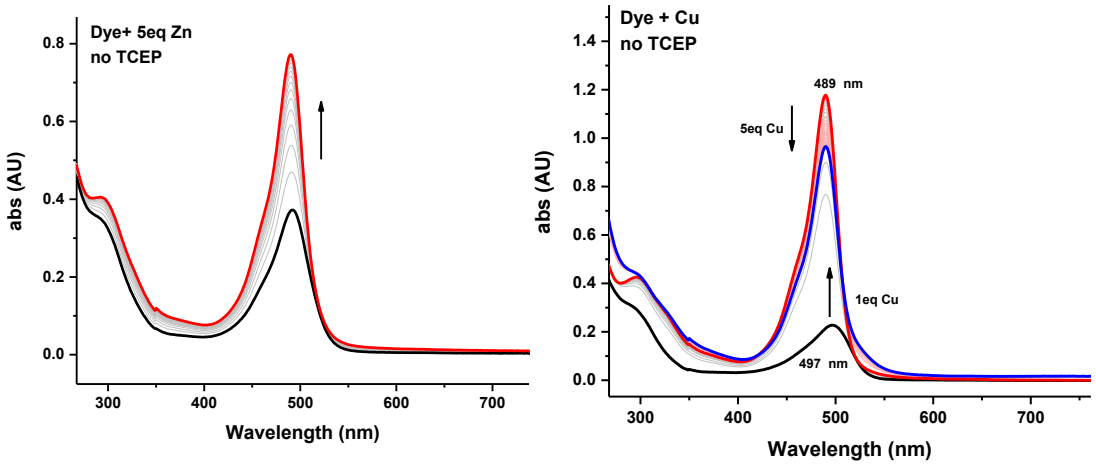

Figure 6.37. UV-vis analysis of FlAsH shows interference in emission upon Cu and Zn addition.

Being bound to protein resulted in a bigger blue shift and probably slower reaction as more equivalents of Cu was required to observe the decrease in intensity (figure 6.38).

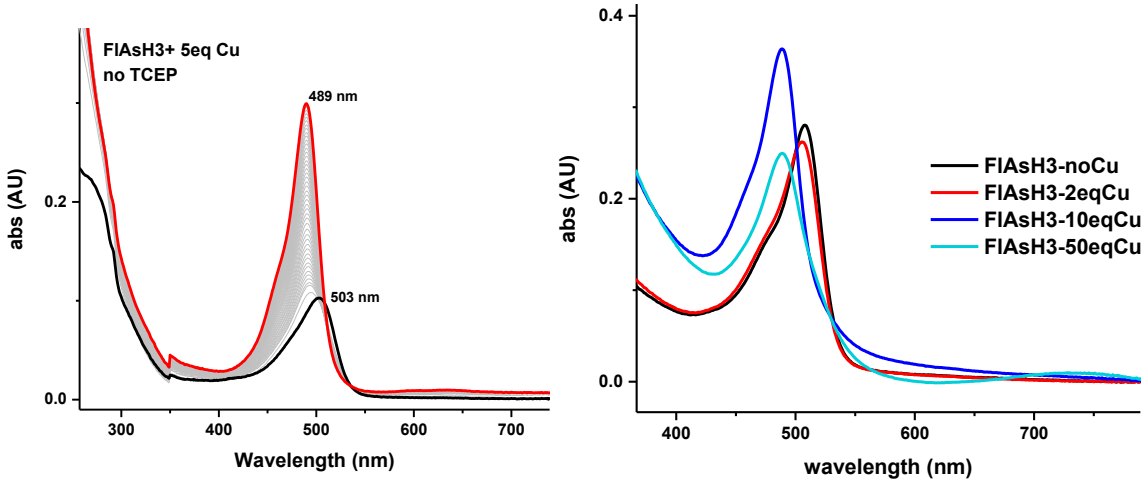

Figure 6.38. Binding to protein causes some changes in the interaction between FlAsH and Cu.

6.5.3.5. NMR

In order to find out whether the observed changes in UV-vis and fluorescent are a result of some structural changes in FlAsH or replacement of As with Cu, I planned to run NMR. Shiliang

ran NMR of samples of the dye, dye with Cu and dye with Zn in DMSO. However, he found out that the peaks were too broad.

6.6. Summary and future directions

Overall, our attempts to design a high-throughput screening set up to monitor the changes in redox state of the Cu in azurin was not very successful for different reasons.

In terms of conjugation with Alexa Fluor, the main concern was lack of efficient labeling, which would highly decrease the chances of sampling the whole library. Moreover, interaction with other Cys containing proteins and the cell culture itself may impede the labeling even more. However, one can think of using Alexa Fluor dyes with a more selective and efficient labeling moiety. The problem with cell culture interference can be overcome by carrying out the conjugation step after osmotic shock when the pellet is resuspended in another buffer such as PBS. The conjugation is worth trying as it gave the best result in terms of recovery after reduction of Cu by ascorbate.

Fusion of the protein with a fluorescent protein like mCherry is possibly the best method in terms of screening as one can be sure that all the proteins in the library are attached to the fluorophore. The current set up however suffers from two major problems. The first issue is the low amount of quenching observed upon Cu addition to the system. The quenching is similar to addition of free Cu and not quite enough for cell sorting. This low quenching can be a result of the distance between the two proteins. If that is the case, using more sophisticated methods to do the domain insertion,[60] can be useful. The other major problem is the inconsistency of the data when the protein is expressed on the surface. We already know that azurin does not fold on the surface of the yeast and initial studies on mCh-Az purified from the membrane also showed lack of Cu binding. More careful experiments are required to confirm the improper folding of azurin on the surface, but if that is the case, one needs to perform rounds of directed evolution on the surface of either bacteria or yeast to obtain folded azurin variants. An alternative approach is to use a cleaner display system which is closer to *in vitro* set up, the so-called “megavalent bead display”.[61] The approach is easy and doable and looks like a good new step.

In terms of ncAA, the fluorescent studies need to be repeated carefully with free ncAA to see if the reductant and Cu have effects on the ncAA as expected. If that works well, playing with

the positions may be an idea next step since ncAA benefit from being small and can offer shorter distances compared to any protein-fusion approach.

Finally, the FlAsH experiment failed due to undesired interaction of the metals with FlAsH. This interaction might be the reason why EDTA was added to binding buffer in previous reports. There is no report on this interaction and it worth being investigated.

6.7. References

(1) Marshall, N. M.; Garner, D. K.; Wilson, T. D.; Gao, Y.-G.; Robinson, H.; Nilges, M. J.; Lu, Y. Rationally tuning the reduction potential of a single cupredoxin beyond the natural range;*Nature* **2009**, *462*, 113.

(2) Yeung, N.; Lin, Y.-W.; Gao, Y.-G.; Zhao, X.; Russell, B. S.; Lei, L.; Miner, K. D.; Robinson, H.; Lu, Y. Rational design of a structural and functional nitric oxide reductase;*Nature* **2009**, *462*, 1079.

(3) Miner, K. D.; Mukherjee, A.; Gao, Y.-G.; Null, E. L.; Petrik, I. D.; Zhao, X.; Yeung, N.; Robinson, H.; Lu, Y. A designed functional metalloenzyme that reduces O_2 to H_2O with over one thousand turnovers;*Angew. Chem. Int. Ed.* **2012**, *51*, 5589.

(4) Arnold, F. H. Design by directed evolution;*Acc. Chem. Res.* **1998**, *31*, 125.

(5) Arnold, F. H. Redesigning enzyme recognition by directed evolution;*Book of Abstracts, 217th ACS National Meeting, Anaheim, Calif., March 21-25* **1999**, BTEC.

(6) Zhao, H.; Arnold, F. H. Directed evolution converts subtilisin E into a functional equivalent of thermitase;*Protein Engineering Design and Selection* **1999**, *12*, 47.

(7) Altamirano, M. M.; Blackburn, J. M.; Aguayo, C.; Fersht, A. R. Directed evolution of new catalytic activity using the alpha/beta-barrel scaffold;*Nature* **2000**, *403*, 617.

(8) Arnold, F. H.; Wintrode, P. L.; Miyazaki, K.; Gershenson, A. How enzymes adapt: lessons from directed evolution.;*Trends Biochem. Sci.* **2001**, *26*, 100.

(9) Farinas, E. T.; Bulter, T.; Arnold, F. H. Directed enzyme evolution;*Section Title: Enzymes* **2001**, *12*, 545.

(10) Reetz, M. T.; Rentzsch, M.; Pletsch, A.; Maywald, M. Towards the directed evolution of hybrid catalysts;*Chimia* **2002**, *56*, 721.

(11) Graddis, T. J.; Remmele, R. L., Jr.; McGrew, J. T. Designing proteins that work using recombinant technologies;*Current Pharmaceutical Biotechnology* **2002**, *3*, 285.

(12) Zhao, H.; Chockalingam, K.; Chen, Z. Directed evolution of enzymes and pathways for industrial biocatalysis;*Curr. Opin. Biotechnol.* **2002**, *13*, 104.

(13) Zhao, H.; Zha, W. Evolutionary methods for protein engineering;*Enzyme Functionality* **2004**, 353.

(14) Reetz, M. T. Directed Evolution of Enantioselective Enzymes: An Unconventional Approach to Asymmetric Catalysis in Organic Chemistry;*The Journal of Organic Chemistry* **2009**, *74*, 5767.

(15) McCullum, E. O.; Williams, B. A. R.; Zhang, J.; Chaput, J. C. Random mutagenesis by error-prone PCR.;*Methods Mol. Biol.* **2010**, *634*, 103.

(16) Reetz, M. T. In *Encyclopedia of Industrial Biotechnology*; Flickinger, M. C., Ed.; John Wiley & Sons, Inc.: 2010; Vol. 4, p 2212.

(17) Gaj, T.; Mercer, A. C.; Gersbach, C. A.; Gordley, R. M.; Barbas, C. F., 3rd Structure-guided reprogramming of serine recombinase DNA sequence specificity;*Proc Natl Acad Sci U S A* **2011**, *108*, 498.

(18) Reetz, M. T. In *Enzyme Catalysis in Organic Synthesis*; Drauz, K., Groeger, H., May, O., Eds.; Wiley-VCH Verlag GmbH & Co. KGaA: 2011; Vol. 1, p 119.

(19) Stevens, J. M.; Daltrop, O.; Allen, J. W. A.; Ferguson, S. J. C-type cytochrome formation: Chemical and biological enigmas;*Acc. Chem. Res.* **2004**, *37*, 999.

(20) Gray, H. B.; Malmstrom, B. G.; Williams, R. J. Copper coordination in blue proteins;*J. Biol. Inorg. Chem.* **2000**, *5*, 551.

(21) Lu, Y. In *Biocoordination Chemistry*; Que, J. L., Tolman, W. B., Meyer, T. J., Eds.; Elsevier: Oxford, UK, 2004; Vol. 8; 8, p 91.

(22) Solomon, E. I.; Heppner, D. E.; Johnston, E. M.; Ginsbach, J. W.; Cirera, J.; Qayyum, M.; Kieber-Emmons, M. T.; Kjaergaard, C. H.; Hadt, R. G.; Tian, L. Copper active sites in biology;*Chem Rev* **2014**, *114*, 3659.

(23) Liu, J.; Chakraborty, S.; Hosseinzadeh, P.; Yu, Y.; Tian, S.; Petrik, I.; Bhagi, A.; Lu, Y. Metalloproteins containing cytochrome, iron-sulfur, or copper redox centers;*Chem. Rev.* **2014**, *114*, 4366.

(24) Zinchenko, A.; Devenish, S. R.; Kintses, B.; Colin, P. Y.; Fischlechner, M.; Hollfelder, F. One in a million: flow cytometric sorting of single cell-lysate assays in monodisperse picolitre double emulsion droplets for directed evolution;*Anal Chem* **2014**, *86*, 2526.

(25) Chudakov, D. M.; Matz, M. V.; Lukyanov, S.; Lukyanov, K. A. Fluorescent proteins and their applications in imaging living cells and tissues;*Physiol. Rev.* **2010**, *90*, 1103.

(26) Kremers, G. J.; Gilbert, S. G.; Cranfill, P. J.; Davidson, M. W.; Piston, D. W. Fluorescent proteins at a glance;*J. Cell Sci.* **2011**, *124*, 157.
(27) Remington, S. J. Green fluorescent protein: a perspective;*Protein Sci.* **2011**, *20*, 1509.
(28) http://www.nobelprize.org/nobel_prizes/chemistry/laureates/2008/press.html.
(29) Boder, E. T.; Wittrup, K. D. Yeast surface display for screening combinatorial polypeptide libraries;*Nat. Biotechnol.* **1997**, *15*, 553.
(30) Wen, F.; Zhao, H. Construction and screening of an antigen-derived peptide library displayed on yeast cell surface for CD4+ T cell epitope identification;*Methods Mol. Biol.* **2013**, *1061*, 245.
(31) Harvey, B. R.; Georgiou, G.; Hayhurst, A.; Jeong, K. J.; Iverson, B. L.; Rogers, G. K. Anchored periplasmic expression, a versatile technology for the isolation of high-affinity antibodies from Escherichia coli-expressed libraries;*Proc. Natl. Acad. Sci. U. S. A.* **2004**, *101*, 9193.
(32) Sieracki, N. A.; Hwang, H. J.; Lee, M. K.; Garner, D. K.; Lu, Y. A temperature independent pH (TIP) buffer for biomedical biophysical applications at low temperatures;*Chem Commun (Camb)* **2008**, 823.
(33) Shao, Z.; Zhao, H.; Zhao, H. DNA assembler, an in vivo genetic method for rapid construction of biochemical pathways;*Nucleic Acids Res.* **2009**, *37*, e16.
(34) Carlson, H. J.; Cotton, D. W.; Campbell, R. E. Circularly permuted monomeric red fluorescent proteins with new termini in the beta-sheet;*Protein Sci.* **2010**, *19*, 1490.
(35) Shui, B.; Wang, Q.; Lee, F.; Byrnes, L. J.; Chudakov, D. M.; Lukyanov, S. A.; Sondermann, H.; Kotlikoff, M. I. Circular permutation of red fluorescent proteins;*PLOS ONE* **2011**, *6*, e20505.
(36) Nilsson, B. L.; Soellner, M. B.; Raines, R. T. Chemical synthesis of proteins;*Annu. Rev. Biophys. Biomol. Struct.* **2005**, *34*, 91.
(37) Meldal, M. Properties of solid supports;*Methods Enzymol.* **1997**, *289*, 83.
(38) Muir, T. W.; Sondhi, D.; Cole, P. A. Expressed protein ligation: a general method for protein engineering;*Proc. Natl. Acad. Sci. U. S. A.* **1998**, *95*, 6705.
(39) Severinov, K.; Muir, T. W. Expressed protein ligation, a novel method for studying protein-protein interactions in transcription;*J. Biol. Chem.* **1998**, *273*, 16205.
(40) Berrade, L.; Camarero, J. A. Expressed protein ligation: a resourceful tool to study protein structure and function;*Cell Mol. Life Sci.* **2009**, *66*, 3909.
(41) Vila-Perello, M.; Liu, Z.; Shah, N. H.; Willis, J. A.; Idoyaga, J.; Muir, T. W. Streamlined expressed protein ligation using split inteins;*J. Am. Chem. Soc.* **2013**, *135*, 286.
(42) Noisier, A. F. M.; Albericio, F. In *Amino Acids, Peptides and Proteins: Volume 39*; The Royal Society of Chemistry: 2015; Vol. 39, p 1.
(43) Wang, L.; Brock, A.; Herberich, B.; Schultz, P. G. Expanding the genetic code of *Escherichia coli*.;*Science* **2001**, *292*, 498.
(44) Wang, L.; Xie, J.; Schultz, P. G. Expanding the genetic code;*Annu. Rev. Biophys. Biomol. Struct.* **2006**, *35*, 225.
(45) Young, T. S.; Schultz, P. G. Beyond the canonical 20 amino acids: Expanding the genetic lexicon;*J. Biol. Chem.* **2010**, *285*, 11039.
(46) Xiao, H.; Chatterjee, A.; Choi, S. H.; Bajjuri, K. M.; Sinha, S. C.; Schultz, P. G. Genetic incorporation of multiple unnatural amino acids into proteins in mammalian cells;*Angew. Chem. Int. Ed. Engl.* **2013**, *52*, 14080.
(47) Wals, K.; Ovaa, H. Unnatural amino acid incorporation in E. coli: current and future applications in the design of therapeutic proteins;*Front. Chem.* **2014**, *2*, 15.
(48) Li, X.; Liu, C. C. Biological applications of expanded genetic codes;*Chembiochem* **2014**, *15*, 2335.
(49) Lang, K.; Davis, L.; Chin, J. W. Genetic encoding of unnatural amino acids for labeling proteins;*Methods Mol. Biol.* **2015**, *1266*, 217.
(50) Wang, J.; Xie, J.; Schultz, P. G. A genetically encoded fluorescent amino acid;*J. Am. Chem. Soc.* **2006**, *128*, 8738.
(51) Griffin, B. A.; Adams, S. R.; Tsien, R. Y. Specific covalent labeling of recombinant protein molecules inside live cells;*Science* **1998**, *281*, 269.
(52) Adams, S. R.; Tsien, R. Y. Preparation of the membrane-permeant biarsenicals FlAsH-EDT2 and ReAsH-EDT2 for fluorescent labeling of tetracysteine-tagged proteins;*Nat. Protoc.* **2008**, *3*, 1527.
(53) Luedtke, N. W.; Dexter, R. J.; Fried, D. B.; Schepartz, A. Surveying polypeptide and protein domain conformation and association with FlAsH and ReAsH;*Nat. Chem. Biol.* **2007**, *3*, 779.
(54) Goodman, J. L.; Fried, D. B.; Schepartz, A. Bipartite tetracysteine display requires site flexibility for ReAsH coordination;*Chembiochem* **2009**, *10*, 1644.
(55) Lowder, M. A.; Appelbaum, J. S.; Hobert, E. M.; Schepartz, A. Visualizing protein partnerships in living cells and organisms;*Curr. Opin. Chem. Biol.* **2011**, *15*, 781.
(56) Zhang, Y. I-TASSER server for protein 3D structure prediction;*BMC Bioinformatics* **2008**, *9*, 40.
(57) Roy, A.; Kucukural, A.; Zhang, Y. I-TASSER: a unified platform for automated protein structure and function prediction;*Nat. Protoc.* **2010**, *5*, 725.
(58) Yang, J.; Yan, R.; Roy, A.; Xu, D.; Poisson, J.; Zhang, Y. The I-TASSER Suite: protein structure and function prediction;*Nat. Methods* **2015**, *12*, 7.
(59) Phillips, J. C.; Braun, R.; Wang, W.; Gumbart, J.; Tajkhorshid, E.; Villa, E.; Chipot, C.; Skeel, R. D.; Kalé, L.; Schulten, K. Scalable molecular dynamics with NAMD;*J. Comput. Chem.* **2005**, *26*, 1781.

(60) Shah, V.; Pierre, B.; Kim, J. R. Facile construction of a random protein domain insertion library using an engineered transposon;*Anal Biochem* **2013**, *432*, 97.
(61) Diamante, L.; Gatti-Lafranconi, P.; Schaerli, Y.; Hollfelder, F. In vitro affinity screening of protein and peptide binders by megavalent bead surface display;*Protein Engineering, Design & Selection* **2013**, *26*, 713.

CHAPTER 7

TUNING THE ACTIVITY OF MNCCP, A FUNCTIONAL MIMIC OF MANGANESE PEROXIDASE, USING SECONDARY COORDINATION INTERACTIONS

* Portions of this chapter are from manuscript to be submitted "Exploring the role of secondary coordination interactions in a functional mimic of manganese peroxidase, MnCcP.1" (Hosseinzadeh P., Mirts E.N., Pfister T.D., Mayne C., Gao Y-G., Robnison H., Lu Y.) Mirts E.N. helped with some characterization and generated the figure for the activity assay of protein-free system. Pfister T.D. came up with original MnC*c*P.1 variants and some of the ideas for mutations.

7.1. Introduction

7.1.1. Lignin and its importance

Lignin is the second most abundant biopolymer on earth, exceeded only by cellulose. It is a heterogeneous polymer of aromatic compounds, the only naturally synthesized polymer of this kind.[1,2] Due to its richness of reducing equivalents, lignin represents a vast source of untapped, energety-producing molecules that could be used for the synthesis of commodity chemicals; especially aromatic compounds and biofuels. However, this highly polymerized molecule is very resistant to degradation.

7.1.2. Current chemical methods for lignin degradation and their limitation

The current chemical and thermochemical methods to degrade lignin are inefficient, often requiring either extreme conditions or expensive reagents.[3-5]

In contrast, nature has devised efficient tools to degrade lignin in order to unlock the potential energy stored in the biopolymer. There are a number of microorganisms with ligninolytic (lignin degrading) activity the best of which are white rot fungi. These fungi possess the ability to substantially degrade lignin by means of a complicated network of interactions among many proteins. Three enzymes are mainly responsible for ligninolytic activity: lignin peroxidases (LiPs), manganese peroxidases (MnP) and Laccases.[6-8]

MnP is the most common ligninolytic enzyme and is found in almost all species that efficiently degrade lignin.[4] Unlike LiP and Laccase that must bind to lignin, MnP oxidizes lignin indirectly via release of Mn(III). This is highly advantageous because it eliminates complicated heterogeneous catalytic kinetics and broadens MnP's substrate scope. MnP is a glycosylated heme protein secreted to the extracellular space. The reaction cycle of MnP is similar to other

peroxidases, starting by oxidation of a heme cofactor with hydrogen peroxide (H_2O_2). In the process of getting back to resting state, two equivalents of Mn(II) will be oxidized to Mn(III), which will be chelated by organic acids and released from enzyme. Mn(III) is, in turn, a potent oxidizing agent that can activate lignin and start its degradation, mainly by generation of radicals and oxidizing phenolic substrates. [1,4,8-10]

Despite the attractive peroperties of MnP for the degradation of lignin, its use has been limited due to difficulties in obtaining sufficient quantities. In its native system, MnP is produced only under nitrogen-limited conditions. Moreover, expression is limited by the availability of Mn and organic acids. Attempts to heterologously overexpress significant amounts of functional MnP in commonly used organisms like yeast and *E. coli* have not been successful thus far.[11,12]

To meet the above challenges, novel approaches in catalysis toward new and more challenging targets are needed. For many years, two fields of catalysis science, biocatalysis and chemical catalysis, have been developed independently, each with its own advantages and disadvantages. Enzymes, particularly metalloenzymes, catalyze some of the most difficult reactions in nature, such as biomass conversion, small molecule activation and water oxidation, with high efficiency and selectivity, under mild conditions and in environmentally benign ways (e.g., using water as solvent and biocompatible/biodegradable materials). However, enzymes remain difficult to study and too expensive to synthesize. On the other hand, while most chemical catalysts are easier to synthesize and study, they are often not as efficient, selective, or environmentally benign as enzymes for important reactions such as biomass conversion.

To combine the advantages of both bio- and chemical catalysis, biomimetic catalysts have been developed that use small organic molecules as ligands. These models provide much insight into the native systems that they mimic[13-30] and provide deeper understanding about reaction mechanisms of the enzymes. Moreover, these catalysts have moved forward to mimic complicated enzymatic systems such as those involved in H_2 generation,[31] water splitting,[32,33] and photosynthesis.[34,35]

While much progress has been made in this area, there are still challenges.[36] One critical barrier to success is the difficulty in designing and synthesizing highly structured ligands to stabilize functional transition states of the reactions. More importantly, long-range or non-

covalent interactions, such as hydrogen bonding and hydrophobicity, which are known to play critical roles in conferring and fine-tuning enzymatic reactivity and selectivity of the catalytic centers, are not easy to mimic using small organic molecules, as incorporating these structural features will require multiple step syntheses of complex macromolecular architectures with high rigidity and tunability.[37-39] To address the importance of non-covalent interactions and the role of protein environment in secondary sphere interactions, several studies focused on designing semi-synthetic models of enzymes that have a peptide conjugated to the synthetic core. Results of such experiments confirm the importance of non-covalent interactions in the activity. [40-43] While such success is promising, it remains difficult to apply to many other systems due to time, cost, and low yield.

7.1.3. Brief introduction to MnCcP engineering

Despite the attractive properties of MnP for lignin degradation, its application has been limited due to difficulties in obtaining sufficient quantities of functional protein, difficulty of genetic manipulation, and lack of thermal stability.[4,11,44,45] There have been reports on efficient conversion of lignin to fuel precursors using biosynthetic models or organic catalysts with considerable success.[46-51] However, most of these methods require extreme conditions such as high temperature and pressure.[52] In a complementary approach, we and other groups have used easy-to-express proteins such as cytochrome *c* peroxidase (C*c*P)[53,54] or DypB[55] as the scaffold to mimic MnP function.

CcP is a heme peroxidase natively found in baker's yeast that shares significant structural similarity with MnP, especially around the active site (Figure 7.1). The overall catalytic cycle is also the same between these two proteins diverging only in the type of substrate oxidized (Scheme 7.1). As opposed to MnP, CcP can be overexpressed in large amounts in *E.coli* in its functional form. Previously, the Lu group has reported successful construction of a manganese binding site in CcP. The so called MnCcP protein then went through further improvements by rational design to make MnCcP.1 which was capable of binding Mn(II) and oxidizing it into Mn(III). [56,57]

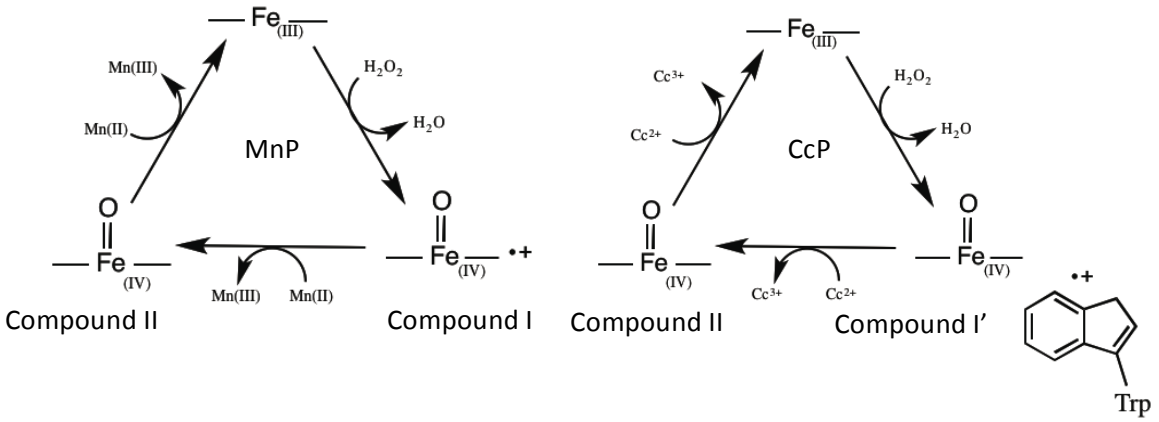

Scheme 7.1. Reaction cycles of MnP and CcP.

Previously, we have reported successful construction of a Mn(II)-binding site in C*c*P by structural comparison of the Mn(II)-binding site in MnP (Figure 7.1c) with the corresponding region of C*c*P (Figure 7.1d) and then Gly41Glu, Val45Glu and His181Asp mutations (called MnC*c*P). [53] The protein then was further optimized through replacing Asp181 by Glu, replacing Glu41 back to Gly and mutating Asp37 to Glu (called MnC*c*P.1),[58] which was capable of binding Mn(II) and oxidizing it into Mn(III) (Figure 7.1).

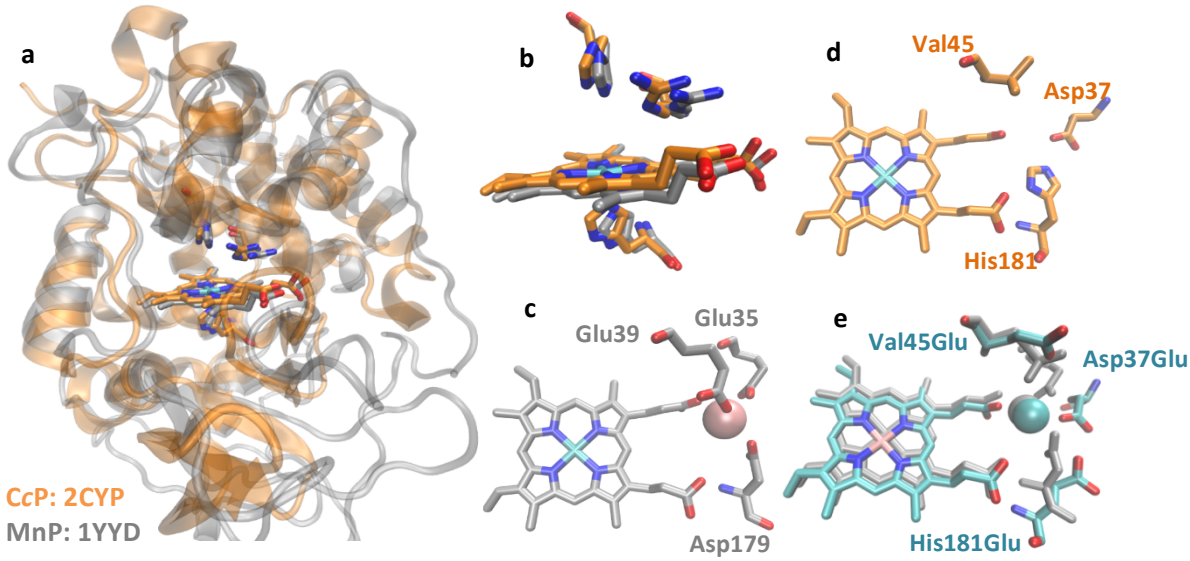

Figure 7.1. Structural comparison between MnP, CcP, and variants of MnCcP. (a) overlay of MnP (gray, PDB ID: 1YYD) and CcP (orange, PDB ID:2CYP) showing high structural similarities, especially in the heme-binding site (b). Mn(II)-binding site in MnP (c) and corresponding site in MnCcP (d). An overlay between Mn(II)CcP (cyan, PDB ID: X) and Mn(II)P (gray, PDB ID: 1YYD).

Although these MnC*c*P biosynthetic models are capable of Mn(II) oxidation, their catalytic efficiency (0.6 $mM^{-1}s^{-1}$ for the most active variant) is not comparable with that of the native MnP (390-4340 $mM^{-1}s^{-1}$, see Table 1). To improve the design and increase MnP activity, we report herein a crystal structure of Mn(II)-bound MnC*c*P (Figure 7.1e).

Structural comparison between Mn(II)P and Mn(II)MnC*c*P.1, and mutagenesis studies shed light on the roles of non-covalent interactions in the secondary coordination sphere of Mn(II) in tuning MnP activity, specifically mutations of Tyr36, Ile40, and Lys179 and their double and triple mutants (Table 7.1). We have found that H-bonding to primary ligands of Mn can have quite different effects, depending on the H-bonding acceptor atom. We have also demonstrated the importance of removing steric clashes and increasing flexibility, resulting in a mutant with ~8-fold increase of catalytic efficiency than our initial design and a K_M comparable to that of native MnPs. Finally, we show that such MnC*c*P mutants presented in this study display degradation activity towards phenolic lignin model compounds and alkali-treated lignin. In doing so, we have been able to shed additional light on the unique impacts of non-covalent interactions for imparting activity to metalloproteins.

Table 7.1. Kinetic parameters of different MnPs, MnP mutants, and MnP mimics.

enzyme	K_M**(mM)**	k_{cat}**(s^{-1})**	k_{cat}/K_M**($mM^{-1}s^{-1}$)**	**pH**
CcP (MI)[59]	3.2	0.19	0.06	5
MnCcP[59]	4.1	0.42	0.10	5
MnCcP.1[58]	1.9	0.47	0.25	5
MP6.8[54]	0.65	0.26	0.33	5
MnCcP2[59]	7.6	4.6	0.60	5
Y36F-MnCcP2	8	4.1	0.51	4.5
Y36F-MnCcP.1	0.37	0.10	0.28	4.5
I40G-MnCcP.1	0.28	0.46	1.63	4.5
K179R-MnCcP.1	0.40	0.19	0.47	4.5
I40G/K179R-MnCcP.1	0.48	0.39	0.81	4.5
Y36F/I40G-MnCcP.1	0.28	0.28	1.02	4.5
Y36F/K179R-MnCcP.1	1.10	0.62	0.56	4.5
Y36F/I40G/K179R-MnCcP.1	0.57	0.46	0.80	4.5

Table 7.1 cont.				
N246A-DypB[55]	17	39	2.3	5.5
Manganese peroxidase mutants				
PC-MnP(E35Q)[60]	4.4	0.77	0.18	4.5
PC-MnP(E39Q)[60]	2.0	1.2	0.6	4.5
PC-MnP(D179N)[61]	3.7	1.09	0.3	4.5
PC-MnP(E35Q-D179N)[60]	8.1	0.29	0.04	4.5
PC-MnP(R177E)[62]	3.9	25.5	6.5	4.5
PC-MnP(R177K)[63]	2.3	257	112	4.5
Native MnP				
PE-MnP PS3[64]	0.2	78	390	5
PE-MnP PS1[64]	0.048	79	1649	5
PC-MnP[65]	0.07	301	4340	4.5

7.2. Materials and methods

7.2.1. Materials and reagents:

All the materials and reagents used in these studies were purchased from either Sigma or Fisher chemicals except when otherwise mentioned.

7.2.2. Mutant protein generation, purification, and verification:

The mutants were generated based on common site directed mutagenesis techniques which consists of a quick change PCR step using Pfu-UltraII (Agilent) followed by removal of the parent plasmid by DpnI (NEB) treatment and transformation into NEB-Turbo cells as described by the provider. The PCR primers for each mutant are listed below. Primers were synthesized by IDT, Inc. (The reverse primer is complementary to the sequence shown):

Tyr36Phe: 5'- GGG AAG ATG ACG AAT TTG ACA ACT ATA TAG GC

Ile40Gly: 5'-CGA ATA TGA CAA CTA TGG CGG CTA TGG GCC C

Tyr36Phe/Ile40Gly: 5'- GGG AAG ATG ACG AAT TTG ACA ACT ATG GCG GCT ATG GGC CC

Tyr36Phe2: 5'- GGG AAG ATG ACG AAT TTG AAA ACT ATA TAG GC

Lys179Arg(His181Glu): 5'- CGC TCT GGG CAG AAC CGA GCT CAA G -3'

The plasmids were then extracted using QIAprep Spin Miniprep Kit and confirmed by sequencing in ACGT-Inc. sequencing company.

Mutation bearing plasmids then transformed into BL21-DE3* competent *E. coli* cells (Invitrogen). Protein purification was performed based on previously developed protocol in our lab. [53,58] Briefly, the cells were grown in a 5 ml Lauria Broth media starter culture (10 g bacto trypton (BD), 5 g yeast extract (BD), and 10g sodium chloride (Fisher chemicals) in 1L) at 37 °C for 8 hours. Two flasks of 2 liter rich media (10 g bacto trypton, 8 g of yeast extract, 5 g sodium chloride) was inoculated by 1 ml of starter culture and grown for 16 hours at 37 °C. The culture was then induced by 1mM IPTG (GoldBio) for 4 hours at 37 °C. The protein was purified from cytosol by sonication using Misonix ultrasonic liquid processor. The process time was 6:00 min with 6 s pulses on and 12 s pulses off and an amplitude of 70. The supernatant then was batch-bound to a DEAE column (GE Healthcare) and eluted with a gradient of KCl in phosphate buffer. The protein is then subjected to a sephedex S-100 gel filtration column (GE healthcare) and a second DEAE column. The mass of all proteins were verified using electron spray ionization mass spectroscopy (ESI-MS). ESI-MS were obtained on a Quattro II (Waters) ESI mass spectrometer maintained by the School of Chemical Sciences Mass Spectrometry Laboratory (Urbana, IL). Formic acid was used to ionize the protein upon injection.

7.2.3. Protein crystallization, data collection and structure determination:

The protein sample was concentrated using Centricon concentrators (10,000 molecular weight cutoff). Proteins were crystalized using a vapor diffusion hanging drop technique. One µL drop of 50 $mg \cdot ml^{-1}$ protein solution with 1mM $MnSO_4$ was placed on siliconized glass with 1 µL of well solution. The drop was then equilibrated against 500 µL of well solution, number 10 of PEG/ion screen HR2-126 from Hampton research. Crystals for suitable X-ray analysis began to appear after 1 week and finished growth after 2-3 weeks. The crystals were soaked for several minutes in 30% PEG 400 in the well solution before mounting. The diffraction data was collected at Brookhaven National Laboratory (BNL). The data was phased and refined using CCP4 and Shelx97 suites respectively. Molecular replacement was used as phasing model using WT-C*c*P structure as a model (PDB ID: 2CYP).

7.2.4. Kinetic experiments:

Kinetics experiments were performed on Agilent 8453 diode array (Agilent) instrument by monitoring increase in 270 nm absorption. The experiment begins by addition of 6-10 μM protein, 400 μL of different $MnSO_4$ concentrations in overall 3000 μL of 500 mM malonate buffer, pH=4.5. Reactions started with addition of 25 μl of 10 mM H_2O_2. The data were then transferred to Origin 9.1 for analysis. The values of k_{cat} and K_M were analyzed based on Michaelis-Menten curve fitting.

7.2.5. GC-MS studies:

GC-Ms studies were performed on a 6890N network GC system from agilent technology with a network GC system 5973 mass selective detector. The measurement begins at an initial temperature of 50 °C for 3 min and ramping to 300 °C at 40 °C/min, paushing at the final temperature for 2.5 min. Samples were extracted by ethyl acetate and dried in a sodium sulfate column prior to injection.

7.2.6. Molecular dynamics and simulation:

Molecular dynamics were performed using visual molecular dynamics (VMD)[66] and NAMD molecular dynamics simulation software.[67] The structure of mutants was modeled using obtained MnCcP.1 stcruture and MnP (PDB ID: 1YYD, 1MNP). PSF files were generated using the PSFGEN suite in VMD. Proteins were solvated in a water box with a 15 Å buffer, and the overall structure was neutralized by 0.1 M NaCl. MD simulations were performed using 1000 or 2000 steps of minimization followed by 2 ns of equilibration (2 fs/step) in a PVT format.

7.2.7. HPLC analysis:

Compounds 1, 2 were generously synthesized by Margaret Brown, from Michele Chang's lab in Berkley. The reactions were performed in 50 mM sodium acetate buffer pH=4.5 as previously described.[68] The reaction mixture contained 0.2or 50 uM protein (for compounds 1 or 2 respectively), 1 μM final compound 1 or 2, 1/2.5 mM $MnCl_2$ (1/2), and initiated with 1 mM H_2O_2. The reaction then stirred overnight at room temperature. Samples for HPLC analysis were prepared by centrifuging the reaction for 5 min at 20850 rcf in a bench top centrifuge. 10 uL of the samples were then injected into Agilent Eclipse XDB-C18 column (4.6*150, 5u) and run at 0.5 ml/min. The program was as follows:

A: water with 0.1% formic acid, B: Actonitrile with 0.1% formic acid
0-2 min, 10% B; 8-11.5min, 90% B; 12-16min, 10% B

Reactions for compound **1** were also carried out in the absence of $MnCl_2$. Reactions for compound **2** was also carried out in the presence of 0.1 M reduced glutathione which was added 10 min after addition of H_2O_2.

The reaction with alkali treated lignin was carried out in 3 mL of 500 mM malonate buffer pH=4.5. 100 μL of 0.5 mM protein was added to the reaction with or without 200 μL of 500 mM $MnSO_4$. 100 μL of 50 mM H_2O_2 was added and the reaction was shaking for 84 hours at 30 C or 24 hours at 37 C. The samples were prepared by addition of 40 ul of 100% CCl_3COOH to 400 uL of the reaction. After mixing, the samples were centrifuged for 10 min at 4000 rpm.

Samples were then loaded onto the column with 0.5 ml/min. The program was as follows:

A: water with 0.1% formic acid, B: methanol with 0.1% formic acid
0-10 min, gradient of 20-30% B; 10-24, gradient from 30% to 50% B; 24-50, gradient from 50% to 80% B.

7.2.8. Mn-dependent peroxidation in the absence of protein:

Reactions were carried out in stirring cuvette in a 1 mL volume containing 5 μL protein and $MnSO_4$ to 5 mM in 500 mM malonate buffer, pH 4.5. Reactions were initiated by the addition of various amounts of H_2O_2 (10, 25, 50 μM final concentration). Reactions proceeded for 2 min at room temperature and then filtered through a 10 kD centricon membrane for 4 min at 14,000 rpm in a tabletop centrifuge. The flow through was collected and diluted to a final volume of 2 mL with malonate buffer. Reduced ABTS was added to a concentration of 1 mM whereby it rapidly oxidized, and its concentration was assessed at 420 nm (ε_{420nm} = 36.8 mM^{-1} cm^{-1}).

7.3. Results and discussion

7.3.1. Crystal structure of Mn-bound MnCcP.1

While the overall alignment of the Mn(II) binding site in our designed MnC*c*P.1 and MnP are very similar (Figure 7.1), the activities are still very different (Table 7.1). In order to understand

structural features responsible for Mn(II) binding and MnP activity, we obtained x-ray crystal structure of Mn(II)-bound MnC*c*P.1 (see crystallographic parameters in Table 7.2).

Table 7.2. Data collection and refinement parameters for MnCcP-Mn crystal.

Data collection	
Space Group	$P2_12_12_1$
Cell dimension:	
a, b, c (Å)	44.43, 52.58, 136.48
α, β, γ(o)	90.0, 90.0, 90.0
Resolution (Å)	1.65
No. reflections	39,151
R-merge	0.092
I/σI	24.2
Redundancy	7.2
Completeness (%)	100
Refinement	
Resolution (Å)	10.0 – 1.65
Rwork/Rfree	0.216/0.2412
No. reflections	35,983
No. atoms	
Protein	2,356
Hem/Fe/Mn	42/1FE/1Mn
Water	210
B-factor	
Protein	25.04
Hem/Fe/Mn	16.5/14.3/32.3
Water	34.1
Rms. deviations	
Bond lengths(Å)	0.008
Bond angles (°)	2.026

A more detailed investigation of the overlay of Mn(II)-bound MnC*c*P and MnP shown in figure 7.2 suggests several differences between carboxylate ligands to Mn(II) ion in two proteins. The difference in ligand positions is evident between Glu37 in MnCcP and Glu35 in

MnP (figure 7.2). While the relative position of carboxylate ligands are similar, Glu37-MnC*c*P is further away from Mn(II) ion, incapable of coordinating to Mn(II) ion in an optimal fashion (3.09 Å in MnC*c*P vs. 2.40 Å in MnP). Upon further inspection, we found that this different positioning of the Glu ligands is mainly due to the difference in the structures of the loops that carry the ligands in MnP and C*c*P (figure 7.2a). While the exact structural position corresponding to Glu35-MnP is located in Gly41 (figure 7.2a), previous studies in our group have shown that Gly41Glu points away from the active site and cannot coordinate to Mn(II).[58] Furthermore, although the Glu181 ligand in MnC*c*P occupies the same structural position as Asp179- MnP, their orientations differ, causing a significant increase in distance from 2.41 Å in MnP to 4.26 Å in MnC*c*P.1 (figure 7.2).It was suggested that maybe a water ligand is directly coordinated to Mn that is stabilized by Glu181-MnC*c*P[58] however, such water ligand is not observed in Mn(II)-MnC*c*P.1 structure. Another, more subtle difference is in terms of observed freedom of the ligands. Comparison of two Mn(II)-bound crystal structures of MnP (PDB ID: 1MNP[69], 1YYD[70]) with that Mn(II)-free apo-MnP (PDB ID: 1YZP[70]) suggests that the greatest degree of flexibility is located in the Glu39-MnP. However, the corresponding Glu45 in MnC*c*P retained its position in all our MnCcP.1 crystal structures (apo-MnC*c*P.1-PDB ID: 2IA8[58], Co(II)-MnC*c*P.1-PDB ID: 2ICV[58], Mn(II)-MnC*c*P.1-PDB ID:). Lack of flexibility in this residue may explain why the Glu45-MnC*c*P rotamer that is better for coordinating to Mn(II), similar to Glu39-MnP, is not observed. Such difference between the rotamers in the same structural position resulted in a 1.84 Å difference in distance between the carboxylate and Mn(II) (3.94 Å in MnC*c*P vs. 2.10 Å in MnP, figure 7.2b,c). These observations strongly suggest that the ability of primary ligands in coordinating with Mn(II) ion is highly dependent on proper distance and orientation of the coordinating atoms and even slight deviations from the optimal geometry can influence metal binding and hence the activity.,

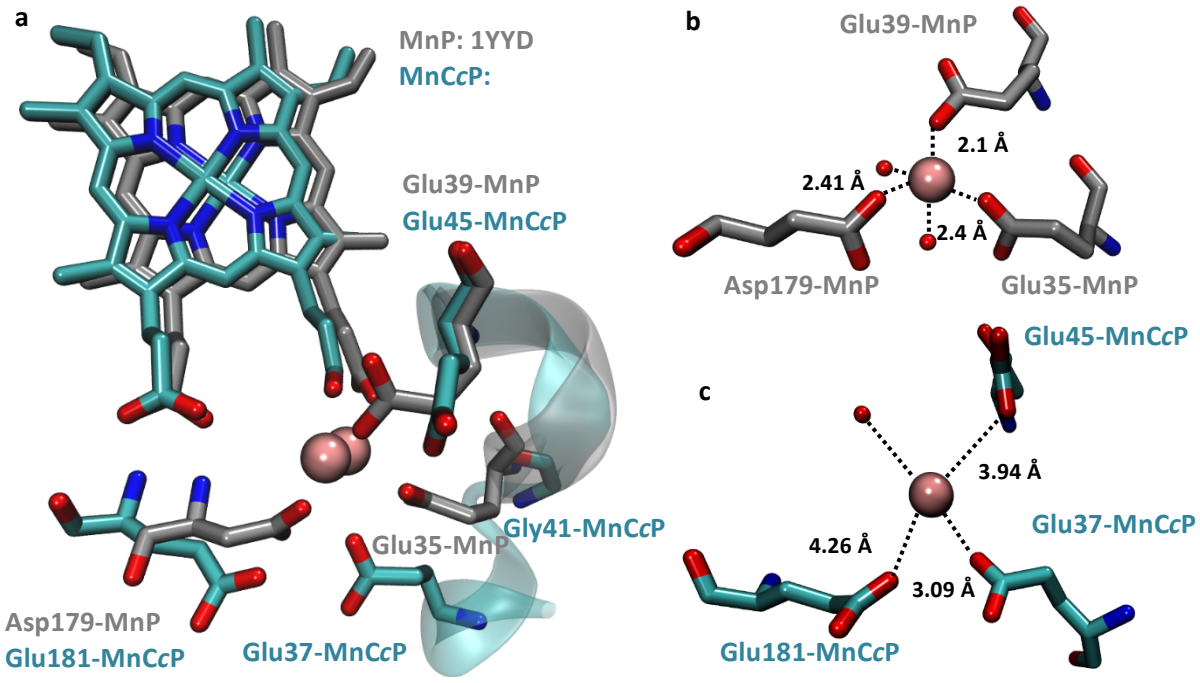

Figure 7.2. (a) Structural comparison between Mn(II) binding site of MnP (gray, PDB ID: 1YYD) and Mn(II)-MnC*c*P.1 (cyan, PDB ID:). (b) Primary ligands of Mn(II) in MnP. (c) Primary ligands of Mn(II) in MnC*c*P.1. Heme is not shown in b,c.

7.3.2. Removal of H-bond to primary ligands of Mn(II) by Tyr36Phe mutation

Structural analysis of Mn(II)-MnC*c*P.1 suggest that Tyr36 is within hydrogen bonding distance to the carboxylate of Glu45-MnC*c*P ligand of Mn(II) with a distance of 2.83 Å (Figure 7.3a). We hypothesized that this H-bond interaction may compete and thus weaken the ligand's ability to coordinate to Mn(II) and thus decrease the MnP activity. Such interaction can stabilize the rotamer of Glu45-MnC*c*P.1 that is observed in the crystal structures, resulting in the observed low flexibility of the ligand. Lack of any residues in hydrogen bonding distance to the corresponding residue in MnP, Glu39-MnP, further suggests that removing this interaction can enhance Mn(II) binding. To test this hypothesis, we mutated Tyr36 to Phe in the MnC*c*P.1. We chose Phe because it differs from Tyr only by the –OH group that is responsible for the H-bonding interactions, while minimizing other structural perturbations.

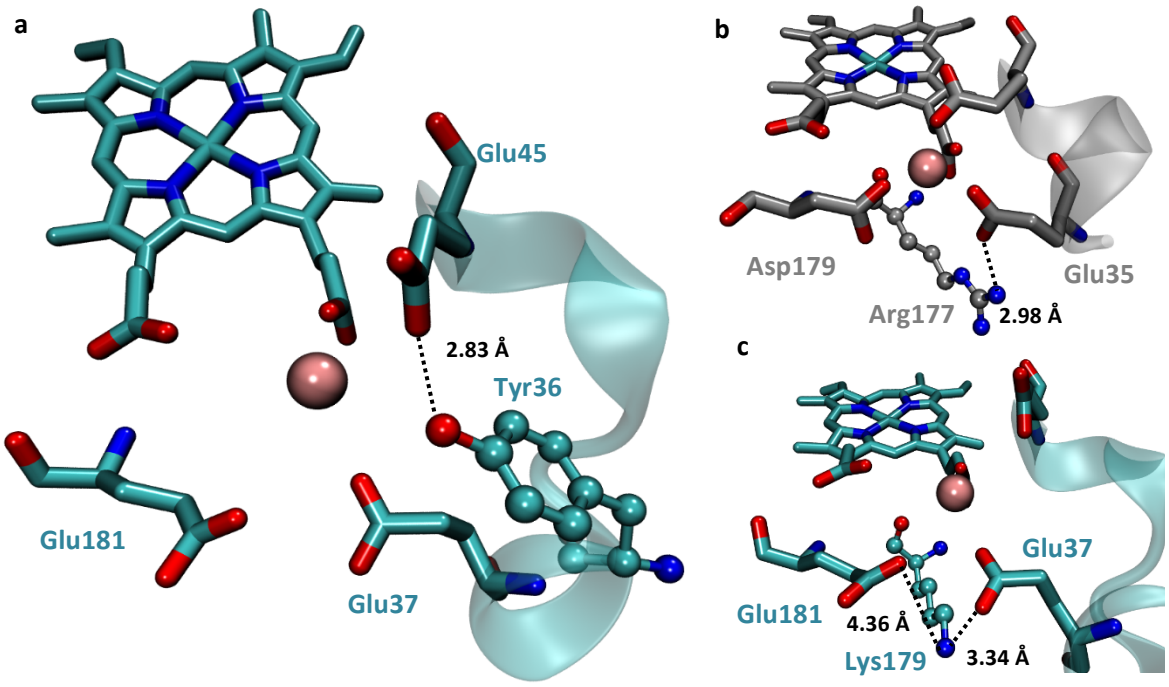

Figure 7.3. (a) Structure of Mn(II)-MnC*c*P.1 showing Tyr36 and its interaction with Glu45. (b) Salt bridge between Arg177 and Glu35 in MnP (PDB Id: 1YYD). (c) Possible H-bonding interaction between Lys179 and Glu37//Glu181 ligands in Mn(II)-MnC*c*P.1 structure (PDB ID:).

Activity assay (table 1, figure 2) showed thatTyr36Phe mutation improved the K_M by 5 folds, indicating that removing the hydrogen bonding interactions to the primary ligands by Tyr36Phe mutation indeed improved the binding to Mn(II) and thus K_M.

7.3.3. Improved orientation of Mn(II) ligand by introducing a H-bond through Lys179Arg mutation

There have been multiple reports on conserved hydrogen bonds that help position the active site residues or substrates in the proper orientation to fine-tune catalytic efficiency of enzymes or tune reduction potential of metal centers.[71-73] Inspired by such reports, we performed structure-based sequence analysis of MnPs from multiple organisms and found that they share a conserved Arg positioned below Glu35-MnP, corresponding to Glu37-MnCcP, which may play a key role in proper positioning of the Glu ligand through a salt bridge. Mutagenesis studies on MnP from *Phenorocheatea chrysosporium* showed that replacing this residue by negatively charged or neutral residues decreased the activity by ~700 fold (table 7.1).[62]

To investigate the role of this salt bridge in our MnC*c*P.1 model, we mutated Lys179 which occupies the same position as the conserved Arg in MnP, to an Arg. Both Lys and Arg have

positive charges and previous studies on native MnP have shown that mutation of Arg177 to Lys effects mostly K_M of the enzyme, presumably through disfavoring optimal conformation for Mn(II) binding (table 1).[63] However, analysis of MnP and MnC*c*P structures shows that the position of side chain of Arg177-MnP differs substantially from Lys179-MnC*c*P (Figure 4b,c). While Arg177-MnP is completely oriented towards Glu35-MnP and away from Glu179-MnP, Lys179-MnC*c*P is in between Glu37-MnCcP and Glu181-MnCcP. These observations suggest that Lys179Arg mutation may also affect k_{cat} of MnC*c*P.1 by favoring the correct salt bridge formation. The activity assay on this mutant showed a two fold increase in the catalytic efficiency, mainly due to decrease of K_M (table 1, figure 2), in agreement with starting hypothesis. Molecular dynamics simulations on Lys179Arg-MnC*c*P.1 showed an enhanced hydrogen bonding interaction between this residue and Glu37 (from 3.32 to 2.72 Å). Consistent with the design, Arg179 moved further away from Glu181-MnC*c*P ligand (an increase of 0.5 Å), resulting in re-orientation of this ligand toward Mn(II) so that their distance is closer by almost 2 Å. All mentioned observations are consistent with enhanced Mn(II) binding due to improved orientation of Mn(II) ligand.

7.3.4. Relaxation of steric clashes in the ligand-containing loop by Ile40Gly mutation

An overlay of MnP and MnC*c*P.1 suggests that the loop containing Glu35- and Glu39-MnP ligands differs substantially from the one containing Glu37- and Glu45-MnCcP ligands, leading to a different position of Glu37-MnCcP compared to Glu35-MnP (Figure 7.2a). A close inspection of Mn(II)-MnC*c*P.1 structure indicates that the side chain of Ile40-MnC*c*P can cause steric clashe with Glu37-MnC*c*P, preventing it from orienting towards Mn(II) (Figure 7.4a). To relieve this steric clash, we made the Ile40Gly mutation. By removing the steric clashes through Ile40Gly mutation, we give the Glu37 and Glu45 ligands in the loop of MnC*c*P.1 the freedom to better coordinate to Mn(II) ion, decreasing K_M and thus increase k_{cat}/K_M. Molecular dynamics simulations of Ile49Gly-MnC*c*P.1 showed that indeed the distances between Glu37 and Glu45 ligands decreased (figure 7.4b). As shown in table 7.1, Ile40Gly mutation results in the highest catalytic activity among all our mutations, arising primarily from a decrease in K_M by 6.7 fold.

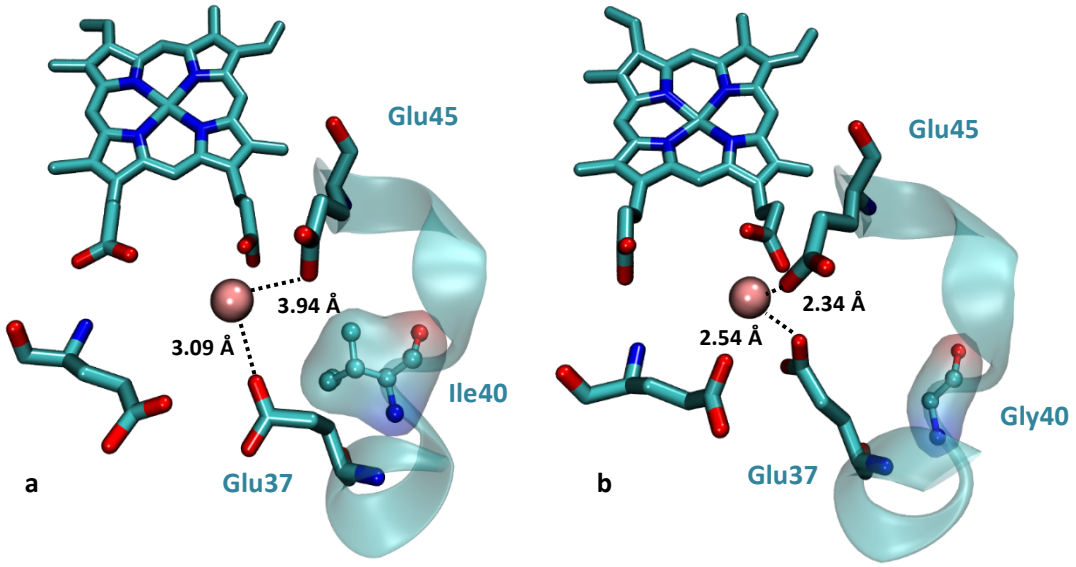

Figure 7.4. Mn(II)-binding site and corresponding distances between Mn(II) and Glu37 and Glu45 in (a) Mn(II)-MnC*c*P.1 cyrtsal structure (PDB ID:) and (b) MD simulated model of Ile40Gly-MnC*c*P.1 variant.

7.3.5. Cumulative effect of mutations on the activity of MnCcP.1

To investigate whether these mutations are accumulative, we made all possible double combinations of our mutants: Tyr36Phe/Lys179Arg, Tyr36Phe/Ile40Gly, Ile40Gly/Lys179Arg, and Tyr36Phe/Ile40Gly/Lys179Arg. As shown in Table 7.1 and Figure 7.5, Tyr36Phe/Lys179Arg double mutant showed MnP activity that equals to the combined activities of Tyr36Phe and Lys179Arg single mutant within the experimental error. This result is expected, since the Tyr36Phe and Lys179Arg mutations are involved in secondary sphere interactions to different ligands (Glu45 and Glu37/Glu181, respectively).

Based on the activity results, Ile40Gly is the most effective single mutation. However, the effect of Ile40Gly mutation on catalytic efficiency was diminished by combination with either of the other two mutations. In the case of the Ile40Gly/Lys179Arg double mutant, the decrease in the catalytic efficiency compared with Ile40Gly was mainly due to a larger K_M (Table 7.1), suggesting that the Lys179Arg and Ile40Gly mutations work antagonistically toward enhancing Mn(II) binding. This explanation makes sense because, while the Ile40Gly mutation increases the flexibility of the ligands in the loop to coordinate to Mn(II), the Lys179Arg mutation favors the formation of a salt bridge to the Glu37 ligand, hence rigidifying it. In contrast, while the Tyr36Phe/Ile40Gly double mutant displayed a similar K_M as that in Ile40Gly mutant, the k_{cat} decreased by two fold. Since Tyr36 is positioned in the same loop as Ile40, and both mutations

has the effect of increasing flexibility of the loop containing Glu37 and Glu45 ligands, it is possible that the combination of both mutations will lead to overall instability of the protein causing a lower k_{cat}.

The triple mutant, Tyr36Phe/Ile40Gly/Lys179Arg, has a K_M that is higher than most other single and double variants, except for Tyr36Phe/Lys179Arg. Such increase in K_M compared to other variants can be explained by the antagonist effect of mutations in enhancing Mn(II)-binding. The k_{cat} however stays relatively high, consistent with the dominant effect of Ile40Gly on increasing the k_{cat} in all variants. The presence of both Ile40Gly and Tyr36Phe will decrease the effect of both on the activity as explained above.

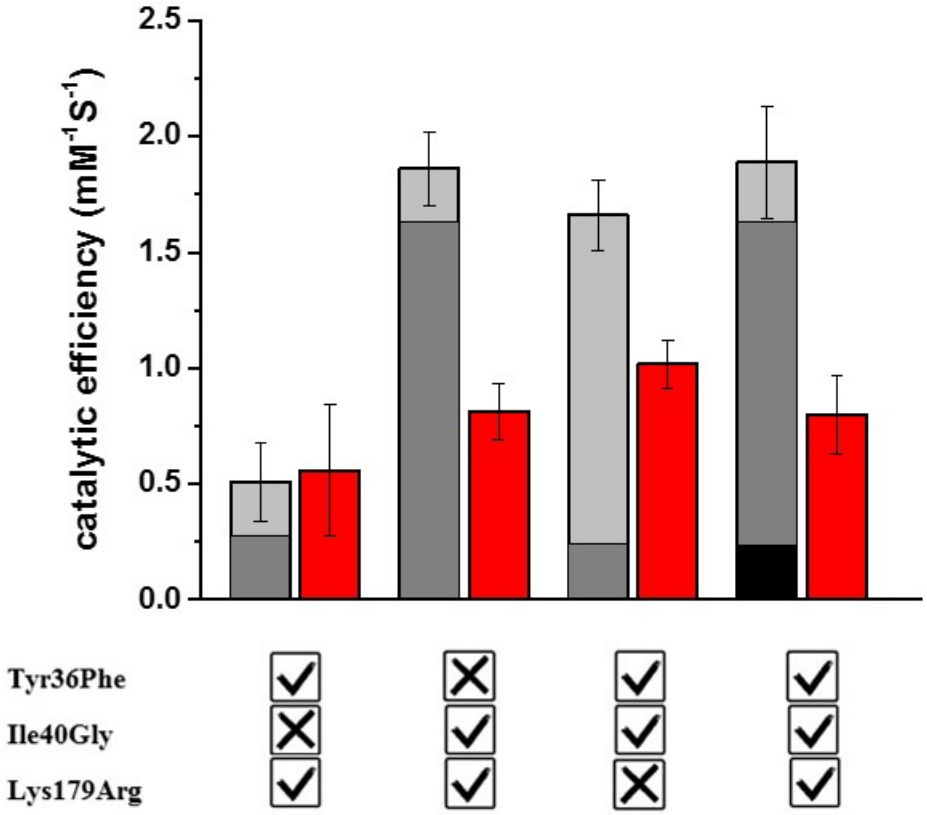

Figure 7.5. Catalytic efficiency of double and triple mutants of MnC*c*P.1. The observed effect is shown in solid red bars. The gray bars show the final catalytic efficiency expected if the effect of each mutation was additive.

7.3.6. Activity assays of the combined triple mutant, Tyr36Phe/Ile40Gly/Lys179Arg-MnCcP.1

Mn(III) that is produced by the activity of MnP is later chelated out of the enzyme by organic acids such as oxalate or malonate that are secreted by the fungus and degrades phenolic

components of lignin.[4,9,74,75] To demonstrate that our enzyme has the same activity and that Mn(III) is released from the active site, activity assays toward Mn(II) oxidation were performed with the triplet mutant.

In contrast to MnP that is solely dependent on the Mn(II) presence for its activity, MnC*c*P.1 mutants can perform peroxidation activity with both Mn-dependent and –independent pathways, with the latter being inherent to WT-C*c*P. To avoid the interference from the Mn(II)-independent pathway, we developed an assay in which we removed any reactive protein intermediates by membrane centrifugation and then assaying the flow-through for Mn-dependent catalytic activity. As was shown with MnP, Mn(III) produced in the reaction was capable of degrading phenolic compounds such as 2,2'-azino-bis(3-ethylbenzothiazoline-6-sulphonic acid) (ABTS) as detected by UV-Vis spectroscopic analysis (Figure 7.6). Several studies have shown that MnP can degrade non-phenolic compounds in the presence of reduced sulfur groups such as glutathione and unsaturated fatty acids such as tween 80.[4,76] However, we could not detect any degradation of veratryl alcohol by our protein in the presence of either of these compounds. High concentrations of Mn(III) in the presence of glutathione; however, could partially degrade veratryl alcohol to veratryl aldehyde (data not shown).

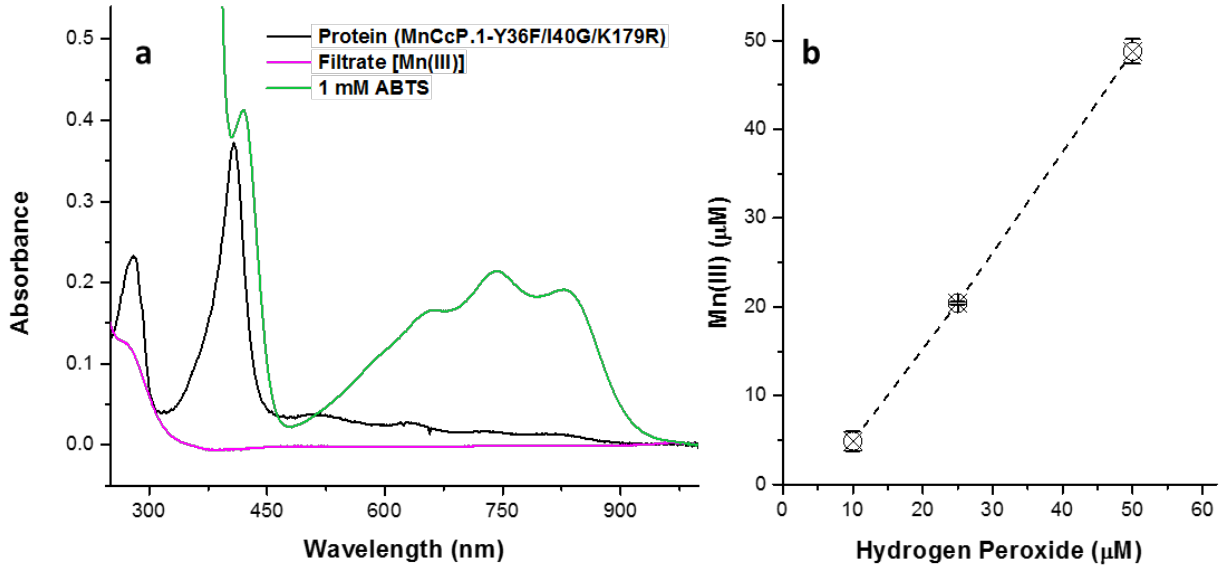

Figure 7.6. Substrate oxidation by Mn(III) in the absence of protein. (a) Representative spectra from a reaction initiated with 25 μM H_2O_2 show the complete removal of protein (black) from solution following filtration and Mn(III) absorbance at 270 nm (magenta). The oxidized substrate rapidly forms upon the addition of excess ABTS (green). (b) The amount of Mn(III) formed in the reaction could be controlled by the amount of peroxide in solution.

Further, we tested the activity of our triple mutant on two previously reported lignin model compounds using HPLC.[68] As with other hybrid MnPs,[7,10,77,78] our mutant was able to degrade phenolic model compound (figure 7.7a) in the presence or absence of Mn(II). The Mn-independent activity is consistent with previous observation with DyP2.[68]

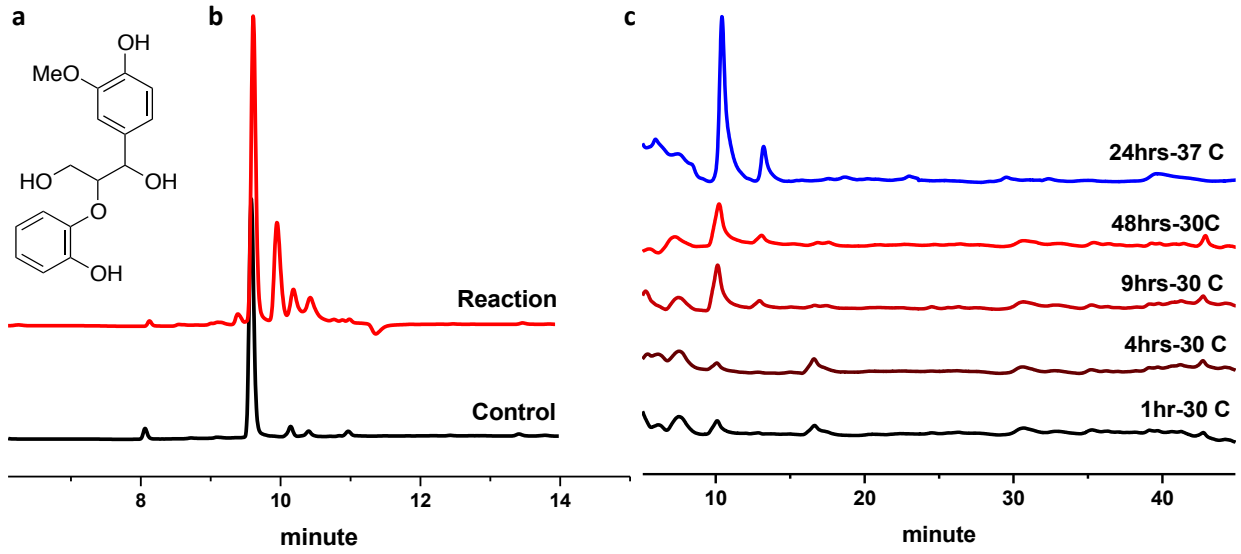

Figure 7.7. (a) Phenolic lignin model compound(b) The HPLC trace of degradation of the phenolic lignin model compound by Tyr36Phe/Ile40Gly/Lys179Arg. (c HPLC trace of alkali-treated lignin exposed to Tyr36Phe/Ile40Gly/Lys179Arg at different times.

The protein again failed to degrade non-phenolic model compounds even in the presence of tween 80 and glutathione (Figure 7.8).

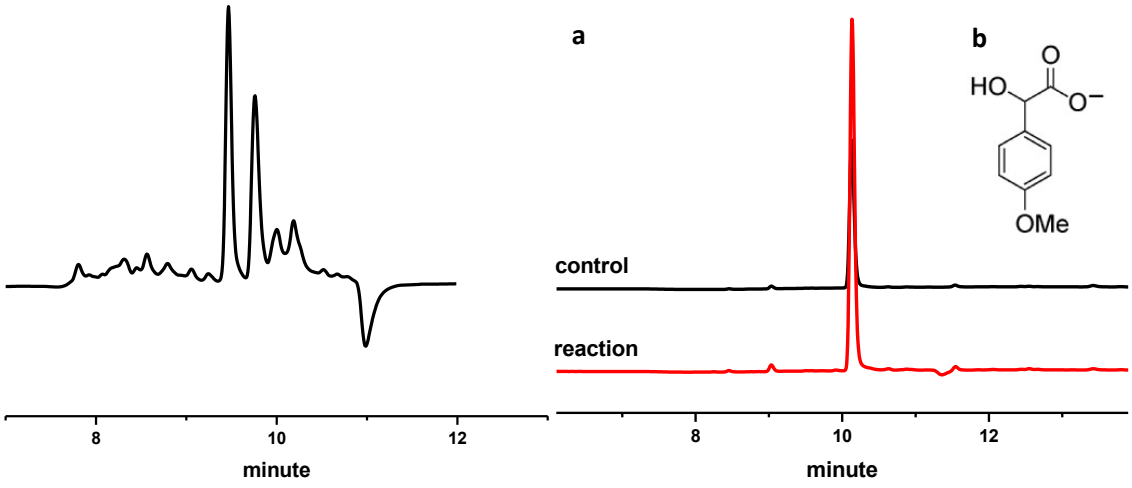

Figure 7.8. Degradation of phenolic lignin model compound by triple mutant without Mn (a) HPLC traces of control reaction and reactivity of triple mutant towards non-phenolic lignin model compound shown in (b)

Finally, we tested the activity of the triple mutant on alkali treated lignin using HPLC based on previously reported methods. The protein showed some degradation activity above that of WT-C*c*P although, the detected activity was low (Figure 7.7b). Nevertheless, these results indicates that our models are capable of lignin degradation.

7.4. Summary and conclusion

Here we reported an engineered mimic of MnP which has catalytic efficiency 8-folds higher than the starting scaffold and >25-folds increase over WT-C*c*P protein. We further demonstrated that our mutant is a functional model of MnP that mimics its activity both in Mn(II) oxidation and substrate oxidation (Figure 7.9). Moreover, we obtained a mutant with K_M value comparable to that of the native system (0.28 mM^{-1} for Ile40Gly and Tyr36phe/Ile40Gly vs. 0.2 for *Pleurotus eryngii* MnP PS3). Our study shed light into the role of non-covalent interactions around the metal binding site in improving the metal binding and overall activity. These overall guides can be used to enhance the activity of native enzymes or synthetic models to obtain better catalyst for biodegradation of aromatic compounds and delignification.

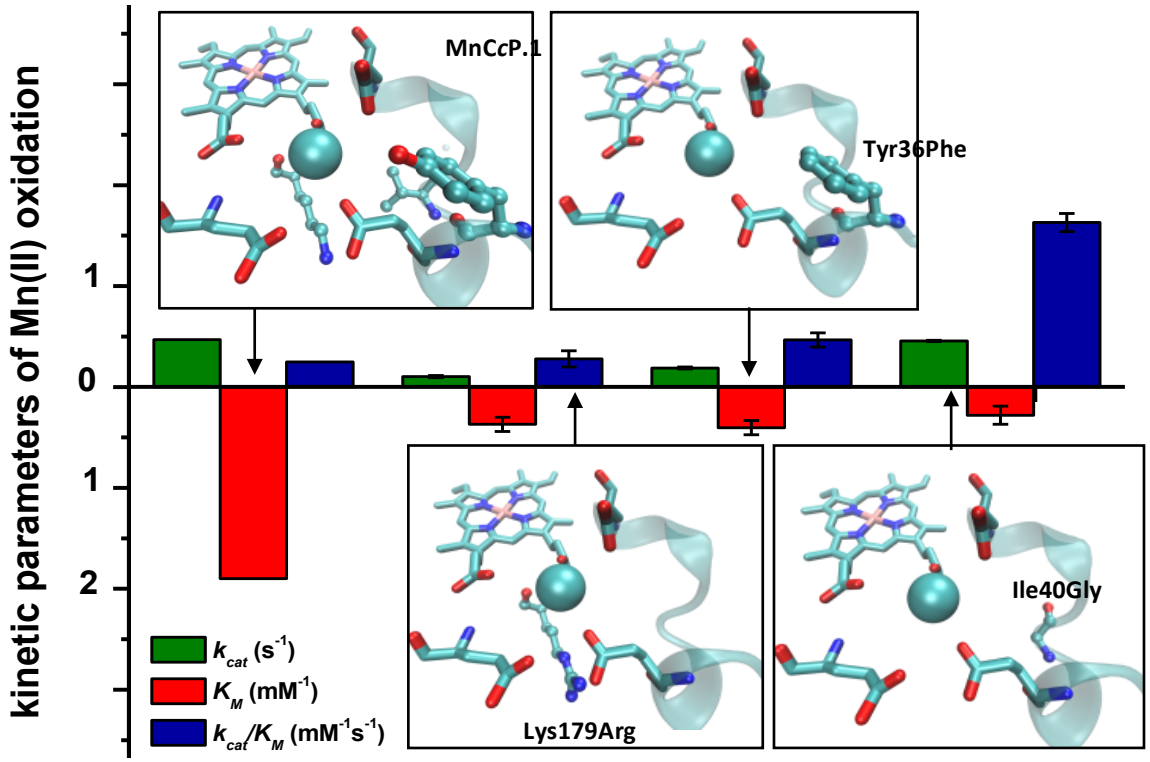

Figure 7.9. Different secondary sphere positions investigated in this study and their effect on activity and metal affinity of MnC*c*P.1

I have also performed several other mutagenesis studies to enhance the activity of MnC*c*P. Previously; we showed that addition of W51F and W191F to older generation MnC*c*P mutants resulted in enhanced activity.[58,79] Our previous data on W191F-MnCcP and W51F-MnCcP showed that the rate-limiting step in the activity of MnCcP is not reactivity of compound I', but the reactivity of compound II. Combination of these mutations with my highest activity MnC*c*P however, failed to generate enhanced activity. I think this is due to the fact that the compound I generation is no longer the rate limiting step in this series of mutants. In another attempt to increase the reactivity of CpdI and CpdII, I decided to increase the distance between His 175 and Fe in heme. It has been reported that the distance between proximal His and heme-Fe in MnP and LiP is longer than common peroxidases and this results in a relatively lower reduction potential and increased activity. In order to push the His away from heme, I designed a176S and A176T mutations. The idea was that addition of an H-bond to His will move it away from the heme. The a176S was designed after structural comparison of MnP and C*c*P structure. A176T failed to incorporate heme. Heme incorporation yield was low in case of A176S and the heme was degraded upon reaction with H_2O_2.

In my first three years I also designed a semi-high-throughput screening platform for directed evolution of MnC*c*P variants with enhance activity or stability. The screening method was based on using leucoberbelin blue (LBB) dye.[80] LBB is a dye with intense absorption and good linear dynamic range that can react with Mn(III) or Mn(IV) but not Mn(II), therefore MnCcP activity can be monitored by screening 96-well plates at 625 nm after a Mn(II) oxidation reaction.

Since we already have structural information about MnCcP in hand, [58] I used iterative saturation mutagenesis to generate our first rounds of libraries using MnCcP.[81] Assuming a sphere of 10 Å around the active site, I chose 8 sites as ISM locations each consisting of 1 to 3 amino acids (figure 7.10). Common site-directed mutagenesis techniques was used to generate the libraries using primers with NDT codons.[82] I chose this codon set because it has been shown to yield 95% coverage with less screening than required for the NNK set.[82] To increase transformation efficiency and therefore the sampling of the library, electroporation was used instead of chemical transformation.

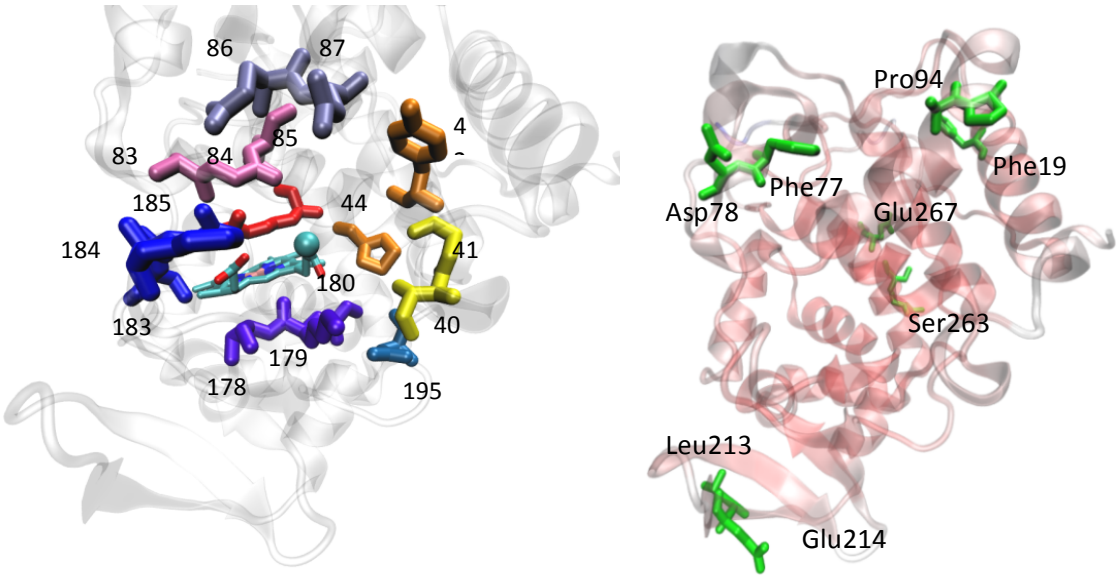

Figure 7.10. Positioning of 8 proposed ISM regions to increase activity. Regions are: A (40, 41), A' (42, 44), B (48), C (83, 84, 85), C' (86, 87), D (178, 179, 180), E (183, 184, 185), F (195). Right figure shows ISM sites for increasing the stability. The protein is colored based on B-factor (red, the lowest).

The variance was very high because I could not get consistent expression all the time. After sequencing the hits, I obtained only about 5% mutagenesis rate, which is an indication of low mutagenesis rate. Interestingly the mutants I obtained were mostly far from the site.

To increase the stability, I chose a combination of ISM and ep-PCR. The regions I chose for ISM are based on β-factors of residues in crystal structure as well as comparison between MnCcP and a thermophilic CcP (KLTH0F05170p from *Lachancea thermotolerans*). The sites with very high β-factor (>40)[83] or those that deviate significantly from a thermophilic CcP are the target sites for ISM. High β-factor is an indicator of high flexibility I protein structure. It has been shown that sites with higher β-factor usually have lower stability. We will also try to alter residues that are part of a secondary structure because increasing the rigidity of a secondary structure will contribute greatly to overall stability (Figure 7.10, right) The designed oligos were designed so that they can be also used in the so called iSOR method as a means to spike the activity library to enhance stability.[84]

7.5. References:

(1) Dashtban, M.; Schraft, H.; Syed, T. A.; Qin, W. Fungal biodegradation and enzymatic modification of lignin;*Int. J. Biochem. Mol. Biol.* **2010**, *1*, 36.
(2) Hammel, K. E.; CABI International: 1997; Vol. Chapter 2, p 33.
(3) Aust, S. D. Mechanisms of degradation by white rot fungi;*Environ. Health Perspect.* **1995**, *103*, 59.
(4) Hofrichter, M. Review: lignin conversion by manganese peroxidase (MnP);*Enzyme Microb. Technol.* **2002**, *30*, 454.

(5) Pandey, M. P.; Kim, C. S. Lignin Depolymerization and Conversion: A Review of Thermochemical Methods;*Chemical Engineering & Technology* **2011**, *34*, 29.
(6) ten Have, R.; Teunissen, P. J. M. Oxidative Mechanisms Involved in Lignin Degradation by White-Rot Fungi;*Chem. Rev.* **2001**, *101*, 3397.
(7) Cullen, D. In *The mycota : a comprehensive treatise on fungi as experimental systems for basic and applied research*; Springer: Agricultural applications. Berlin ; London, 2002; Vol. 11, p 71.
(8) Wong, D. Structure and Action Mechanism of Ligninolytic Enzymes;*Appl. Biochem. Biotechnol.* **2009**, *157*, 174.
(9) Wariishi, H.; Valli, K.; Gold, M. H. Manganese(II) oxidation by manganese peroxidase from the basidiomycete Phanerochaete chrysosporium. Kinetic mechanism and role of chelators;*J. Biol. Chem.* **1992**, *267*, 23688.
(10) Mendonça Maciel, M.; Castro e Silva, A.; Camarão Telles Ribeiro, H. Industrial and biotechnological applications of ligninolytic enzymes of the basidiomycota: A review;*Electronic Journal of Biotechnology* **2010**, *13*.
(11) Whitwam, R. E.; Gazarian, I. G.; Tien, M. Expression of Fungal Mn Peroxidase in E. Coli and Refolding to Yield Active Enzyme;*Biochem. Biophys. Res. Commun.* **1995**, *216*, 1013.
(12) Martìnez, A. T. Molecular biology and structure-function of lignin-degrading heme peroxidases;*Recent Advances in Lignin Biodegradation* **2002**, *30*, 425.
(13) Breslow, R. Biomimetic Chemistry and Artificial Enzymes: Catalysis by Design;*Acc. Chem. Res.* **1995**, *28*, 146.
(14) Costas, M.; Mehn, M. P.; Jensen, M. P.; Que, L. Dioxygen activation at mononuclear nonheme iron active sites: enzymes, models, and intermediates;*Chem. Rev.* **2004**, *104*, 939.
(15) MacKay, B. A.; Fryzuk, M. D. Dinitrogen Coordination Chemistry: On the Biomimetic Borderlands;*Chem. Rev.* **2004**, *104*, 385.
(16) Solomon, E. I.; Szilagyi, R. K.; DeBeer George, S.; Basumallick, L. Electronic Structures of Metal Sites in Proteins and Models: Contributions to Function in Blue Copper Proteins;*Chem. Rev.* **2004**, *104*, 419.
(17) Kuchar, J.; Hausinger, R. P. Biosynthesis of Metal Sites;*Chem. Rev.* **2004**, *104*, 509.
(18) Friese, S. J.; Kucera, B. E.; Young, V. G.; Que, L.; Tolman, W. B. Iron(II) Complexes of Sterically Bulky a-Ketocarboxylates. Structural Models for ÃŽÂ±-Ketoacid-Dependent Nonheme Iron Halogenases;*Inorg. Chem.* **2008**, *47*, 1324.
(19) Kirby, A. J.; Hollfelder, F. *From Enzyme Models to Model Enzymes*; Royal Society of Chemistry, 2009.
(20) Sattler, A.; Parkin, G. Cleaving Carbon-Carbon Bonds by Inserting Tungsten into Unstrained Aromatic Rings;*Nature* **2010**, *463*, 523.
(21) Rioux, R. *Model Systems in Catalysis-Single Crystals to Supported Enzyme Mimics*; Springerlink, 2010.
(22) Carroll, M. E.; Barton, B. E.; Gray, D. L.; Mack, A. E.; Rauchfuss, T. B. Active-Site Models for the Nickel-Iron Hydrogenases: Effects of Ligands on Reactivity and Catalytic Properties;*Inorg. Chem.* **2011**, *50*, 9554.
(23) Smith, S. E.; Yang, J. Y.; DuBois, D. L.; Bullock, R. M. Reversible Electrocatalytic Production and Oxidation of Hydrogen at Low Overpotentials by a Functional Hydrogenase Mimic;*Angew. Chem. Int. Ed.* **2012**, *51*, 3152.
(24) Carroll, M. E.; Barton, B. E.; Rauchfuss, T. B.; Carroll, P. J. Synthetic Models for the Active Site of the [FeFe]-Hydrogenase: Catalytic Proton Reduction and the Structure of the Doubly Protonated Intermediate;*J. Am. Chem. Soc.* **2012**, *134*, 18843.
(25) Yang, L.; Tolman, W. Type 1 copper site synthetic model complexes with increased redox potentials;*JBIC Journal of Biological Inorganic Chemistry* **2012**, *17*, 285.
(26) Jazdzewski, B.; Reynolds, A.; Holland, P.; Young, V., Jr.; Kaderli, S.; ZuberbÃƒÂ¼hler, A.; Tolman, W. Copper(I)-phenolate complexes as models of the reduced active site of galactose oxidase: synthesis, characterization, and O2 reactivity;*JBIC Journal of Biological Inorganic Chemistry* **2003**, *8*, 381.
(27) Li, F.; Chakrabarti, M.; Dong, Y.; Kauffmann, K.; Bominaar, E. L.; MÃƒÂ¼nck, E.; Que, L. Structural, EPR, and Mossbauer Characterization of (u-Alkoxo)(u-Carboxylato)Diiron(II,III) Model Complexes for the Active Sites of Mixed-Valent Diiron Enzymes;*Inorg. Chem.* **2012**, *51*, 2917.
(28) Tondreau, A. M.; Atienza, C. C. H.; Weller, K. J.; Nye, S. A.; Lewis, K. M.; Delis, J. G. P.; Chirik, P. J. Iron Catalysts for Selective Anti-Markovnikov Alkene Hydrosilylation Using Tertiary Silanes;*Science* **2012**, *335*, 567.
(29) McDonald, A. R.; Que, L. High-valent nonheme iron-oxo complexes: Synthesis, structure, and spectroscopy.;*Coord. Chem. Rev.* **2013**, *257*, 414.
(30) Frisch, J. R.; McDonnell, R.; Rybak-Akimova, E.; Que, L. Factors Affecting the Carboxylate Shift Upon Formation of Nonheme Diiron-O2 Adducts;*Inorg. Chem.* **2013**.
(31) Wang, M.; Chen, L.; Sun, L. Recent progress in electrochemical hydrogen production with earth-abundant metal complexes as catalysts;*Energy & Environmental Science* **2012**, *5*, 6763.
(32) Andreiadis, E. S.; Chavarot-Kerlidou, M.; Fontecave, M.; Artero, V. Artificial photosynthesis: From molecular catalysts for light-driven water Splitting to photoelectrochemical cells;*Photochem. Photobiol.* **2011**, *87*, 1478.
(33) Artero, V.; Fontecave, M. Light-driven bioinspired water splitting: Recent developments in photoelectrode materials;*Future of sciences, sciences for the future: Chemistry and its interfaces with biology and physics* **2011**, *14*, 799.
(34) Nocera, D. G. The Artificial Leaf;*Acc. Chem. Res.* **2012**, *45*, 767.
(35) Duan, L.; Bozoglian, F.; Mandal, S.; Stewart, B.; Privalov, T.; Llobet, A.; Sun, L. A molecular ruthenium catalyst with water-oxidation activity comparable to that of photosystem II;*Nat Chem* **2012**, *4*, 418.
(36) Collman, J. P.; Boulatov, R.; Sunderland, C. J.; Fu, L. Functional analogues of cytochrome *c* oxidase, myoglobin, and hemoglobin;*Chem. Rev.* **2004**, *104*, 561.

(37) MacBeth, C. E.; Gupta, R.; Mitchell-Koch, K. R.; Young, V. G., Jr.; Lushington, G. H.; Thompson, W. H.; Hendrich, M. P.; Borovik, A. S. Utilization of hydrogen bonds to stabilize M-O(H) units: synthesis and properties of monomeric iron and manganese complexes with terminal oxo and hydroxo ligands.;*J. Am. Chem. Soc.* **2004**, *126*, 2556.
(38) Borovik, A. S. Bioinspired hydrogen bond motifs in ligand design: The role of noncovalent interactions in metal ion mediated activation of dioxygen.;*Acc. Chem. Res.* **2005**, *38*, 54.
(39) Cukier, R. I.; Nocera, D. G. Proton-cpupled electron transfer;*Annu. Rev. Phys. Chem.* **1998**, *49*, 337.
(40) Peacock, A. F. A.; Iranzo, O.; Pecoraro, V. L. Harnessing natures ability to control metal ion coordination geometry using de novo designed peptides;*Dalton Trans.* **2009**, *0*, 2271.
(41) Jain, A.; Lense, S.; Linehan, J. C.; Raugei, S.; Cho, H.; DuBois, D. L.; Shaw, W. J. Incorporating Peptides in the Outer-Coordination Sphere of Bioinspired Electrocatalysts for Hydrogen Production;*Inorg. Chem.* **2011**, *50*, 4073.
(42) Jain, A.; Reback, M. L.; Lindstrom, M. L.; Thogerson, C. E.; Helm, M. L.; Appel, A. M.; Shaw, W. J. Investigating the Role of the Outer-Coordination Sphere in Ni(PPh2NPh-R2)2]2+ Hydrogenase Mimics;*Inorg. Chem.* **2012**, *51*, 6592.
(43) Jain, A.; Buchko, G. W.; Reback, M. L.; O'Hagan, M.; Ginovska-Pangovska, B.; Linehan, J. C.; Shaw, W. J. Active Hydrogenation Catalyst with a Structured, Peptide-Based Outer-Coordination Sphere;*ACS Catalysis* **2012**, *2*, 2114.
(44) Gu, L.; Lajoie, C.; Kelly, C. Expression of a Phanerochaete chrysosporium Manganese Peroxidase Gene in the Yeast Pichia pastoris;*Biotechnol. Progr.* **2003**, *19*, 1403.
(45) Jiang, F.; Kongsaeree, P.; Schilke, K.; Lajoie, C.; Kelly, C. Effects of pH and temperature on recombinant manganese peroxidase production and stability;*Appl. Biochem. Biotechnol.* **2008**, *146*, 15.
(46) Hurff, S. J.; Klein, M. T. Reaction pathway analysis of thermal and catalytic lignin fragmentation by use of model compounds;*Industrial & Engineering Chemistry Fundamentals* **1983**, *22*, 426.
(47) Futong, C.; David, D.; American Chemical Society: 1989; Vol. 399, p 519.
(48) Alonso, D. M.; Bond, J. Q.; Dumesic, J. A. Catalytic conversion of biomass to biofuels;*Green Chemistry* **2010**, *12*, 1493.
(49) Sergeev, A. G.; Hartwig, J. F. Selective, Nickel-Catalyzed Hydrogenolysis of Aryl Ethers;*Science* **2011**, *332*, 439.
(50) Parsell, T. H.; Owen, B. C.; Klein, I.; Jarrell, T. M.; Marcum, C. L.; Haupert, L. J.; Amundson, L. M.; Kenttamaa, H. I.; Ribeiro, F.; Miller, J. T.; Abu-Omar, M. Cleavage and hydrodeoxygenation (HDO) of C-O bonds relevant to lignin conversion using Pd/Zn synergistic catalysis;*Chemical Science* **2013**, *4*, 806.
(51) Strassberger, Z.; Alberts, A. H.; Louwerse, M. J.; Tanase, S.; Rothenberg, G. Catalytic cleavage of lignin small beta]-O-4 link mimics using copper on alumina and magnesia-alumina;*Green Chemistry* **2013**, *15*, 768.
(52) Yan, N.; Zhao, C.; Dyson, P. J.; Wang, C.; Liu, L. T.; Kou, Y. Selective degradation of wood lignin over noble-metal catalysts in a two-step process;*ChemSusChem* **2008**, *1*, 626.
(53) Yeung, B. K.; Wang, X.; Sigman, J. A.; Petillo, P. A.; Lu, Y. Construction and characterization of a manganese-binding site in cytochrome *c* peroxidase: towards a novel manganese peroxidase.;*Chemistry and Biology* **1997**, *4*, 215.
(54) Wilcox, S. K.; Putnam, C. D.; Sastry, M.; Blankenship, J.; Chazin, W. J.; McRee, D. E.; Goodin, D. B. Rational design of a functional metalloenzyme: introduction of a site for manganese binding and oxidation into a heme peroxidase;*Biochemistry* **1998**, *37*, 16853.
(55) Singh, R.; Grigg, J. C.; Qin, W.; Kadla, J. F.; Murphy, M. E. P.; Eltis, L. D. Improved Manganese-Oxidizing Activity of DypB, a Peroxidase from a Lignolytic Bacterium;*ACS Chemical Biology* **2013**.
(56) Jaeckel, C.; Kast, P.; Hilvert, D. Protein design by directed evolution;*Annual Review of Biophysics* **2008**, *37*, 153.
(57) Yeung, B. K. S.; Wang, X.; Sigman, J. A.; Petillo, P. A.; Lu, Y. Construction and characterization of a manganese-binding site in cytochrome c peroxidase: towards a novel manganese peroxidase;*Chemistry & biology* **1997**, *4*, 215.
(58) Pfister, T.; Mirarefi, A.; Gengenbach, A.; Zhao, X.; Danstrom, C.; Conatser, N.; Gao, Y.-G.; Robinson, H.; Zukoski, C.; Wang, A.; Lu, Y. Kinetic and crystallographic studies of a redesigned manganese-binding site in cytochrome c peroxidase;*J. Biol. Inorg. Chem.* **2007**, *12*, 126.
(59) Gengenbach, A.; Syn, S.; Wang, X.; Lu, Y. Redesign of Cytochrome c Peroxidase into a Manganese Peroxidase: Role of Tryptophans in Peroxidase Activity;*Biochemistry* **1999**, *38*, 11425.
(60) Kishi, K.; Kusters-van Someren, M.; Mayfield, M. B.; Sun, J.; Loehr, T. M.; Gold, M. H. Characterization of manganese(II) binding site mutants of manganese peroxidase;*Biochemistry* **1996**, *35*, 8986.
(61) Kusters-van Someren, M.; Kishi, K.; Lundell, T.; Gold, M. H. The manganese binding site of manganese peroxidase: characterization of an Asp179Asn site-directed mutant protein;*Biochemistry* **1995**, *34*, 10620.
(62) Gelpke, M. D.; Youngs, H. L.; Gold, M. H. Role of arginine 177 in the MnII binding site of manganese peroxidase. Studies with R177D, R177E, R177N, and R177Q mutants;*Eur. J. Biochem.* **2000**, *267*, 7038.
(63) Sollewijn Gelpke, M. D.; Moenne-Loccoz, P.; Gold, M. H. Arginine 177 is involved in Mn(II) binding by manganese peroxidase;*Biochemistry* **1999**, *38*, 11482.
(64) Camarero, S.; Sarkar, S.; Ruiz-Duenas, F. J.; Martinez, M. J.; Martinez, A. T. Description of a Versatile Peroxidase Involved in the Natural Degradation of Lignin That Has Both Manganese Peroxidase and Lignin Peroxidase Substrate Interaction Sites;*J. Biol. Chem.* **1999**, *274*, 10324.
(65) Mayfield, M. B.; Kishi, K.; Alic, M.; Gold, M. H. Homologous expression of recombinant manganese peroxidase in Phanerochaete chrysosporium;*Applied and Environmental Microbiology* **1994**, *60*, 4303.
(66) Humphrey, W.; Dalke, A.; Schulten, K. VMD: Visual molecular dynamics;*Journal of Molecular Graphics* **1996**, *14*, 33.
(67) Phillips, J. C.; Braun, R.; Wang, W.; Gumbart, J.; Tajkhorshid, E.; Villa, E.; Chipot, C.; Skeel, R. D.; Kale, L.; Schulten, K. Scalable molecular dynamics with NAMD;*J. Comput. Chem.* **2005**, *26*, 1781.

(68) Brown, M. E.; Barros, T.; Chang, M. C. Identification and characterization of a multifunctional dye peroxidase from a lignin-reactive bacterium;*ACS Chem. Biol.* **2012**, *7*, 2074.
(69) Sundaramoorthy, M.; Kishi, K.; Gold, M. H.; Poulos, T. L. The crystal structure of manganese peroxidase from Phanerochaete chrysosporium at 2.06-A resolution;*J. Biol. Chem.* **1994**, *269*, 32759.
(70) Sundaramoorthy, M.; Youngs, H. L.; Gold, M. H.; Poulos, T. L. High-Resolution Crystal Structure of Manganese Peroxidase:Substrate and Inhibitor Complexes;*Biochemistry* **2005**, *44*, 6463.
(71) Ju, K. S.; Parales, R. E. Control of substrate specificity by active-site residues in nitrobenzene dioxygenase;*Appl. Environ. Microbiol.* **2006**, *72*, 1817.
(72) Marshall, N. M.; Garner, D. K.; Wilson, T. D.; Gao, Y.-G.; Robinson, H.; Nilges, M. J.; Lu, Y. Rationally tuning the reduction potential of a single cupredoxin beyond the natural range;*Nature* **2009**, *462*, 113.
(73) Fukumoto, M.; Kudou, D.; Murano, S.; Shiba, T.; Sato, D.; Tamura, T.; Harada, S.; Inagaki, K. The role of amino acid residues in the active site of L-methionine gamma-lyase from Pseudomonas putida;*Biosci. Biotechnol. Biochem.* **2012**, *76*, 1275.
(74) Kuan, I. C.; Johnson, K. A.; Tien, M. Kinetic analysis of manganese peroxidase. The reaction with manganese complexes;*J.Biol.Chem.* **1993**, *268*, 20064.
(75) Onnerud, H.; Zhang, L.; Gellerstedt, G. r.; Henriksson, G. Polymerization of Monolignols by Redox Shuttle–Mediated Enzymatic Oxidation: A New Model in Lignin Biosynthesis I;*The Plant Cell Online* **2002**, *14*, 1953.
(76) Wariishi, H.; Valli, K.; Renganathan, V.; Gold, M. H. Thiol-mediated oxidation of nonphenolic lignin model compounds by manganese peroxidase of Phanerochaete chrysosporium;*J. Biol. Chem.* **1989**, *264*, 14185.
(77) Hofrichter, M.; Scheibner, K.; Schneegass, I.; Fritsche, W. Enzymatic combustion of aromatic and aliphatic compounds by manganese peroxidase from Nematoloma frowardii;*Appl Environ Microbiol* **1998**, *64*, 399.
(78) Moreira, M. T.; Sierra-Alvarez, R.; Lema, J. M.; Feijoo, G.; Field, J. A. Oxidation of lignin in eucalyptus kraft pulp by manganese peroxidase from Bjerkandera sp. strain BOS55;*Bioresour. Technol.* **2001**, *78*, 71.
(79) Pfister, T. D.; Gengenbach, A. J.; Syn, S.; Lu, Y. The Role of Redox-Active Amino Acids on Compound I Stability, Substrate Oxidation, and Protein Cross-Linking in Yeast Cytochrome c Peroxidase;*Biochemistry* **2001**, *40*, 14942.
(80) Anderson, C. R.; Johnson, H. A.; Caputo, N.; Davis, R. E.; Torpey, J. W.; Tebo, B. M. Mn(II) oxidation is catalyzed by heme peroxidases in "Aurantimonas manganoxydans" strain SI85-9A1 and Erythrobacter sp. strain SD-21;*Appl. Environ. Microbiol.* **2009**, *75*, 4130.
(81) Reetz, M. T.; Carballeira, J. D. Iterative saturation mutagenesis (ISM) for rapid directed evolution of functional enzymes;*Nat.Protocols* **2007**, *2*, 891.
(82) Reetz, M. T.; Kahakeaw, D.; Lohmer, R. Addressing the numbers problem in directed evolution;*Chembiochem* **2008**, *9*, 1797.
(83) Socha, R. D.; Tokuriki, N. Modulating protein stability - directed evolution strategies for improved protein function;*FEBS J.* **2013**, *280*, 5582.
(84) Herman, A.; Tawfik, D. S. Incorporating Synthetic Oligonucleotides via Gene Reassembly (ISOR): a versatile tool for generating targeted libraries;*Protein Engineering Design and Selection* **2007**, *20*, 219.

CHAPTER 8

CHARACTERIZATION OF AN UNUSUAL CYTOCHROME C PEROXIDASE VARIANT WITH A HEME-PROTEIN CROSSLINK

8.1. Introduction

Heme is one of the most common cofactor used in biology. Several classes of proteins from electron transfer cytochromes to enzymes with versatile activity such as P450 contain heme as their active site group. There are several classes of heme found in biology. One interesting aspect of hemoproteins is the fact that the heme can be covalently attached to the protein moiety. In the most well-known case of cytochromes *c*, the covalent attachment of heme to two or one cysteins in the protein is a prerequisite for stability of the system and the geometry of the heme.[1-3] The heme *c* mode of attachment has been reproduced in heme *b* containing proteins by introduction of cys residues.[4] More interesting are the systems in which the heme is cross-linked to the protein after a reaction. Covalent attachments of cofatcors usually result in enhanced enzymatic activity and stability.[5] It has been postulated that forming an adduct between heme and probably a glutamate residue in CYP4 family of proteins plays an important role in restricting the conformation of the heme and determining the specificity of the enzymes. [6,7]

There are several reports of heme-protein cross-link in literature. Heme-His crosslink was observed in an engineered hemoglobin via Leu75His mutation. The cross-link formation was induced by reduction of heme by dithionate.[8] Heme-His cross-link was observed in a hemoglobin before. Addition of dithionate in this case also resulted in complete cross-link formation. Interestingly, the authors showed that the reduction of heme is required and no crosslink was formed if a Zn-protophorphyrin was used.[9] Transient formation of heme-His cross-link was observed in the active site of a chaperon.[10]

Heme-Met cross-link is among the most common observed corss-links. These samples usually have a distinct green color and the Met usually forms a bond with the vinyl group on the heme. Such cross-link is observed in myeloperoxidase.[11] A mutant version of ascorbate peroxidase, S160M, also shows a heme-Met linkage in a hydrogen peroxide dependent manner.[12]

Heme-Tyr cross-links are also observed in several proteins. Mutation of residue 43 in myoglobin to a Tyr resulted in a crosslink between hydroxyl group of the Tyr and the heme

vinyl-4 group.[13] The authors suggested a mechanism in which the hydroxyl group of the Tyr first attacks the α-carbon and then a common Markonikov reaction takes place. A band at 553 in pyridine treated sample was indicative of saturation of one of the vinyls. Guanidine hydrochloride unfolding also showed a bis-His (403, 410 nm) rather than a free heme (370 nm) spectral feature. [13] A Tyr-heme crosslink was also observed in Ser160 variant of ascorbate peroxidase.[14] Structural studies of hydroxylamine oxidoreductase showed an unusual Tyr-heme crosslink in which the Tyr is linked to the heme by two linkages.[15]

Heme can be crosslinked to other residues such as Trp, [14] Asp, and Glu.[16]Also in several cases attachment of heme to more than two amino acids is observed. [11,14,16]

The mechanism of heme-protein cross-link formation can vary vastly even if the same amino acid is used as shown in case of cytochromes *c*.[1-3] Moreover, in most cases the mechanism is not known. Most of the linkages described either require the addition of H_2O_2[14] or are enhanced by that.[11,16] Herein, I describe the characterization of a C*c*P variant that has an unknown heme-covalent crosslink. The crosslink formation does not require H_2O_2 or reductant as shown by previous studies. It forms due to a change in the loop of C*c*P that contains residue 180 as well as presence of a Cys near propionate of the heme. Removal of the Cys abolishes the cross-link formation. However, the position of the Cys is not well suited to form a crosslink. MS/MS studies suggested Met172 as a possible site of attachment. The Met172 is very close to heme vinyl group and at the same structural position as reported for S160M ascorbate peroxidase. However, the spectroscopic features of the crosslinked protein and the lack of H_2O_2-dependence cast doubt on the possibility of this residue being the site of crosslink.

Another interesting feature about this protein is the observation of significant catalase activity in the "as-purified" form, which presumably had picked up some modified heme from the culture during the growth. Characterization and activity tests of this species is also discussed.

8.2. Materials and methods

8.2.1. Loop directed mutagenesis and construct design

The construction of the loop-directed variants was carried out using Gibson assembly. Below you may see the primer pairs used:

Loop_Cys:

Primers to get the vector

MnCcP_H181Loop_f: 5'- TTGTCCGCCTTGCCCAGAGCGTGAGC

MnCcP_H181Loop_r: 5'- CGATCGATGGGCCATGGGGAGCCGCTAACAACGTC

Gibson fragment (obtained by annealing the two complementary strands I ordered)

H181Loop: 5'- CGCTCTGGGCAAGGCGGATAAAGTGGATCAGACCATCGATGGGCCATGGGGAGC

The final fragment was sequenced by ACGT, Inc.

The Loop-Gly variant was obtained by sequencing another colony from the same plate of Loop-Cys!

Gibson fragments to get loop-Ser and loop-Val as well as the primers for the vector are shown below.

MnCcP_loop_f: 5'- CGCTAACAACGTCTTTACCAATGAGTTTT

MnCcP_loop_r: 5'- TCTCTGTCATTCATATTAAGTCTTTGAAAA

Cys-Val gblock: 5'- CAG AAC GTT TTT TCA AAG ACT TAA TAT GAA TGA CAG AGA AGT AGT TGC TCT TAT GGG GGC TCA CGC TCT GgT GAA GGC GGA TAA AGT GGA TCA GAC CAT CGA TGG GCC ATG GGG AGC CGC TAA CAA CGT CTT TAC CAA TGA GTT TTA CTT G

Cys-Ser gblock: 5'- CAG AAC GTT TTT TCA AAG ACT TAA TAT GAA TGA CAG AGA AGT AGT TGC TCT TAT GGG GGC TCA CGC TCT GAG CAA GGC GGA TAA AGT GGA TCA GAC CAT CGA TGG GCC ATG GGG AGC CGC TAA CAA CGT CTT TAC CAA TGA GTT TTA CTT G

The overall structure of the protein was predicted by uploading the protein sequence to I-TASSER server. [17-19]

8.2.2. Protein expression and purification

Protein was expressed and purified similar to previously described method for C*c*P. [20-22] In brief, 2 liters of Rich media was inoculated by 1 ml of starter culture and let grow overnight. The cells were then induced for four hours by addition of 1 mM IPTG. After sonication (details of sonication in chapter seven), the cells were diluted by adding water and buffer A (100 mM phosphate buffer pH 7 and 1 mM EDTA). The supernatant will then be added to equilibrated DEAE beads and the conductivity was set to be below 3 mΩ by adding water if necessary. After batch binding to the beads, the protein was eluted by a salt gradient. After the first DEAE column, the protein was concentrated and further purified by passing down a size exclusion column. After titrating heme into the protein, the holo-protein and free heme would be separated using a second DEAE column.

Addition of heme precursor, δ-amionlevulunic acid together with IPTG had no detectable effect on the yield of the green-C*c*P obtained.

The modified method for heme incorporation is as follows (adapted from myoglobin purification):[23] The protein is denatured by incubating for 20 min in 8 M guanidine hydrochloride. The denatured protein is then dripped into 750 ml of water, 33 mg potassium cyanide and 10 mg hemin. The hemin was previously dissolved in 2M KOH. The mixture is then stirred for one hour. It is then dialyzed against 10X volume of 100 mM potassium phosphate at pH 7 (or any other buffer) for four times, each time at least for four hours. The protein solution is then further purified by passing down a size exclusion column.

ESI-mass spectroscopy was used to confirm the protein. In some cases SDS-PAGE was used on 4-20% pre-catsed gel to track the purification or modifications of the protein.

8.2.3. Mn(II) oxidation assay

Mn(II) oxidation assay was performed as previously described in chapter 7. In brief, the protein was added to 50 mM malonate solution, pH 4.5 supplemented with different concentrations of Mn(II). The reaction starts by addition of excess H_2O_2 and monitored by increase of 270 nm peak due to Mn(III)-malonate formation, using $\varepsilon_{270} = 8500\ M^{-1}cm^{-1}$.

8.2.4. Mass spectroscopy analysis

Electrospray ionization mass spectroscopy (ESI-MS) was performed on a Waters ZMD quadropole instrument with a mass range of 2000 m/z in positive form.

Trypsin digestion was performed using the Trypsin kit from Sigma. The protein was exchanged into ammonium bicarbonate buffer and then a 1:50 mixture of trypsin:protein was used for the reaction. The reaction went to completion overnight at 37 C. Samples were then run down on HPLC and heme-containing fragemtns were pulled-down. The fragments were then lyophilized and the powder was submitted to MS/MS analysis in the Roy Jay Craver Biotechnology center, Protein Sciences division by Peter Yau and Brian Imai. The fragments were analazyed using Mascot software.

ICP-Ms was performed using a PerkinElmer-SCIEX ELAN DRCe instrument by Rudiger Laufhutt. 2 ml of 1 mM sample ws prepared and exchanged into water.

8.2.5. NMR sample preparation

Heme extraction was performed as follows: the protein was exchanged into cold water using a PD-10 column and was diluted to 100 μM (ε_{280} = 80 $mM^{-1}cm^{-1}$). 1% v/v 2N HCl is added to the protein solution to acidify the protein and dissociate the proximal His (a change in the color can be observed). Equal volume of cold MEK (2-butanone, saturated with water) was added to the sample. After iverting a few times, the sample kept still so that the MEK and water layer got separate. The heme layer was then removed by a glass Pasteur pipette (similarly, the protein part can be eluted using a separation funnel). The process of adding MEK was repeated 2-3 more times to make sure all the heme was extracted. The protein with only heme-bound fraction was then dialyzed for four hours against water twice to get rid of the remaining MEK and several times against phosphate buffer, 50 mM, pH 7.

The sample was prepared as Xiaotang Wang asked me to. I sent him 0.5 ml of about 2 M sample (for the green-C*c*P, I sent 2 M of the heme-containing fraction, about 10M of protein). The proteins were exchanged into 10% D_2O through several exchanges by PD-10. All then centricons that I used for concentration from here on are washed multiple times with D_2O. The final samples were frozen in liquid N_2 without addition of any glassing agent and shipped on dry ice.

8.2.6. HPLC analysis

HPLC of the digested peptide was carried out on a Waters Delta 600 model with a dual absorbance detector. The program I used was initially used by Arnab Mukherjee and Kyle Miner and is called KDM_XL_post_digest_2short_2. Water with 0.1% TFA and acetonitrile with 0.1% TFA were used as buffers A and B, respectively. A C18 column was used and was washed first by 100% isopropanol at 0.1 ml/min in backward direction to make sure the column is clean. Column was then washed in the correct direction using 100% acetonitrile and after that was equilibrated with buffer A. The heme part was monitored at 390 nm (due to limitations of the lamp) and the peptide was monitored at 280 (or 250) nm.

8.2.7. Spectroscopic analysis

UV-vis studies were performed on a photodiode array hp instrument or on a Cary 5E spectrophotometer. EPR was carried out on … at temperature of 15-5 K, 10 mW power, and modulation of 10 gauss. The samples were prepared with 20% glycerol as a glassing agent.

Circular dichroism (CD) was performed on the instrument in Grueble lab. The protein was exchanged into 10 mM phosphate buffer, pH 7.0 in concentrations of 2-3 μM. Scanning was performed on 200-250 range and 250-500 range to monitor the soret.

Hemochromogen assay was performed using a previously described protocol. The following solution was prepared as the buffer: 1 ml of 0.066 M NaOH, 660 μl of pyridine, 267 μl of water and 66 μl of sample or water. Protein concentration was set so that the intensity of the soret peak at the given solution is between 0.1 and 1 on hp. Use the above-mentioned solution as blank. Then add a small amount of dithionite (a tip) to the sample and keep taking spectra until the spectra gets stable. Blank again. Now repeat the same process of dithionite addition with the protein solution (don't blank again). Reduction by dithionite results in the growth of heme in pyridine (pyridine takes the heme out). The concentration is then calculated based on the known extinction coefficient of heme *b* in pyridine solution (ε_{556}= 36.4 $mM^{-1}cm^{-1}$). Assuming that all the heme is out of the protein, the extinction coefficient at 408 can be back-calculated using Beer's law.

8.2.8. Catalase assays

In order to generate verdoheme from Cu_B-Mb, I used the protocol below:[24] Cu_BMb purified by Ambika Bhagi-Domadaran was exchanged into 20 mM Tirs-HCl pH 8. The ε_{410} = 170 $mM^{-1}cm^{-1}$ was used and R/z of 4.5 was obtained. 100 molar equivalent of TMPD-ascorbate was added to the sample from a stock of 100 mM TMPD/1M ascorbate. After 5 min the reduced oxy from will generate. Upon addition of 2 molar equivalent Cu, vedoheme will form in 10 min. The protein was passed down PD-10 column to release free Cu and excess TMPD/ascorbate (protein is green at this stage). 1 μl of 10M H_2O_2 was added as with other H_2O_2 assyas.

The qualitative catalase assay was performed with some slight modification of a previously reported protocol.[25] In brief to 100 μl of protein sample in different concetrations, 100 μl of tween 20 and 100 μl of undiluted H_2O_2 solution (30%). Samples were mixed and then sit aat

room temperature. Calibration curve can be made by measuring the length of the foam generated with different concentrations of catalase standard.

The GC-MS studies were performed using 0.1 mM solution of protein with 100 molar equivalent of H_2O_2. 2 ml of the protein was degased using freeze-pump-thaw method. Four gas tight syringes with controlled release knob were placed above an empty flask and were under vacuum for half an hour. We had to use He gas for degassing as Ar has a signal close to O_2. To completely remove Ar out of the Schlenk line, one of the lines remained open and He pressure was increased for a couple of minutes. Before starting the reaction, some samples of headspace were taken as control. The reaction started with addition of 100 µl of 100 mM H_2O_2 and stirred for 10 min. Samples from headspace were taken using the gas tight syringes. GC-MS was carried out in the mass spec facility. We used an HP-PLOTQ column with 30 m length and internal diameter of 0.32 mm a film of 20 µm and temperature range of -60 to 270. The program we used was optimized for separation of NO and NO_2. It started with oven temperature of 50, initial temperature of 50 for 5 min. It then had a ramp of 25 deg/min and the final temperature was set to 200 for 20 min to wash everything out. We then changed the program a little to get better results. The intial temperature was set to 25 and the ramp was changed to 5 degree/min up to 100 and it stayed at 100 for 5 min.

A Clark-type O_2 electrode was used for more quantitative measurement of the catalase activity in the mutants. Reaction volume in the chamber was set to 500 µl. The protein was in 100 mM phosphate buffer pH 7.0. For catalase, different concentrations were set to 0, 5, 10, 50, 100, 500, 1000 units, diluted from a 2000 unit/ml stock. Reaction started by addition of 10 µl of 100 mM H_2O_2 solution using a syringe and mixing up a little. The rates were measured using the instrument settings itself. Since catalase has high binding, I washed the membrane with washing solution (1:10 dilution of 1L ethanol+500 ml 12 M HCl+500 ml water mixture). Each experiment was performed three times. Data were then analyzed with Origin 9.0 program to have another way of rate measurement.

8.2.9. Cyclic voltammetry

Cyclic voltammetry was performed using the previously reported protein film voltammetry technique.[26,27] The protein was placed on the electrode surface either alone or with DDAB as a coadsorbate. The voltammagram was collected with 200 mV/s scan range in different ranges.

8.3. Results and discussion

8.3.1. Design of the construct and the sequence

The initial idea behind the design was to enhance the activity of our MnC*c*P variants (see chapter seven for details of this mutant). Comparing the structures of MnP and C*c*P, I noticed two major differences in the heme access channel and the loop around His180 in C*c*P. First, the access channel is much smaller in MnP which can result in enhanced binding to Mn(II) ion. Second, the carboxylates of His180Glu in MnC*c*P points away from the Mn-binding site whereas the loop in MnP is designed to force the ligand to stay close to the Mn ion (Figure 8.1).

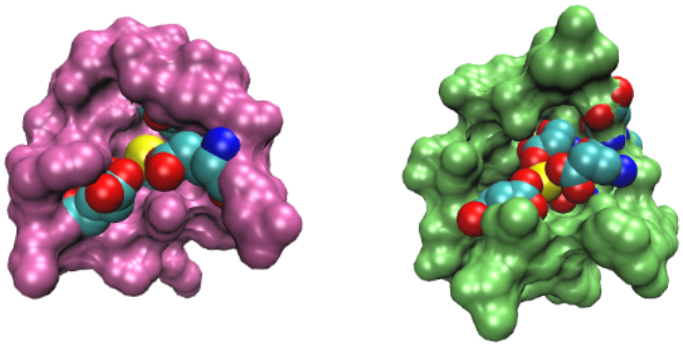

Figure 8.1. Comparison of the substrate-binding channel in MnC*c*P (not submitted to PDB yet, see chapter 7) in magenta and MnP (PDB ID 1YYD) in green.

In lieu of these observations, I performed the loop directed mutagenesis. Sequencing results showed Gly178Cys mutation (Figure 8.2) but I decided to keep the protein and continue with that. Below you may find the sequence as well as the position of the mutation in the structure.

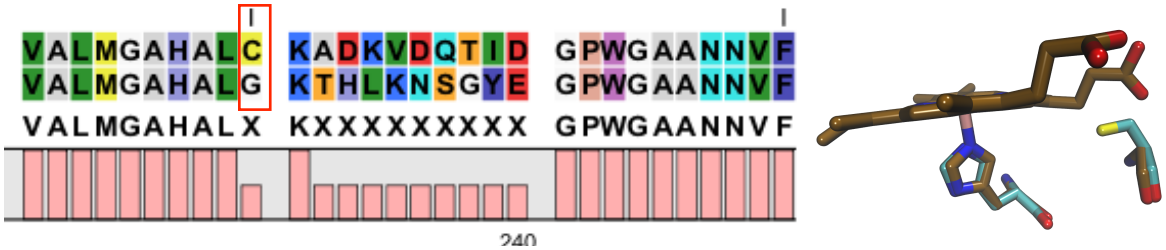

Figure 8.2. Sequence of the Loop-Cys variant if C*c*P. The position of cys mutation is shown in red box. The Cys is also shown in the overlay structure in cyan (the structure of MnC*c*P is shown in brown).

8.3.2. Protein purification and expression

To my surprise, the "apo-protein" came off as green (Figure 8.3). To my knowledge, none of the previous C*c*P mutants I purified had green pellet or green "apo" state. This state of protein will be called "Green-CcP" from now on. As observed by UV-vis spectra in figure 8.3, the protein contains some cofactor but in small amounts (about 15% or so, given the fact that the soret in C*c*P is usually same intensity as 280 nm peak).

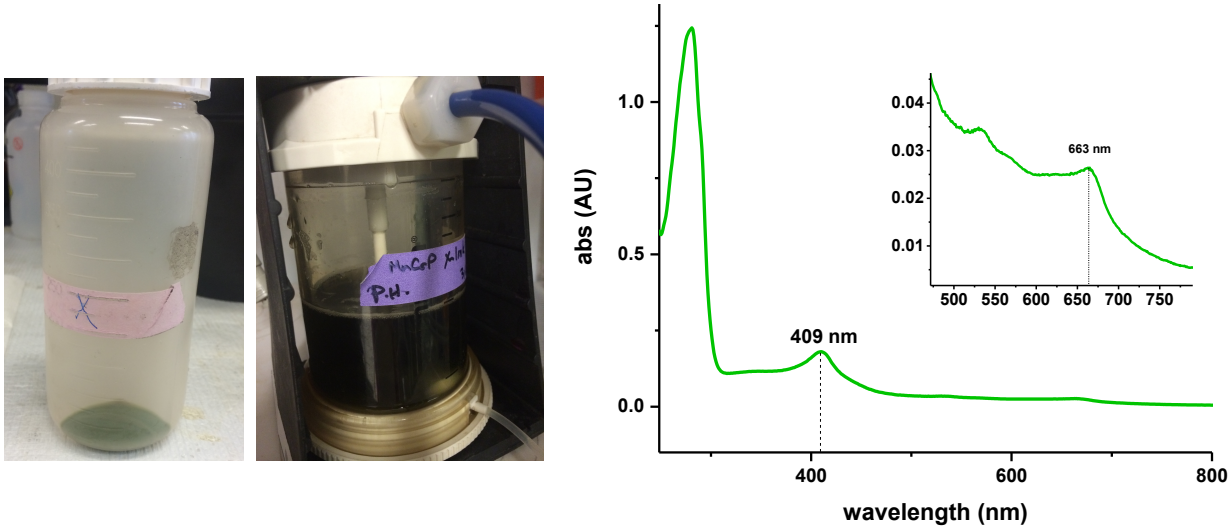

Figure 8.3. The pellet of "as-purified" loop-Cys is green as well as the protein before adding any heme. The spectra of green-C*c*P is shown in the right.

ESI-MS of the green protein (figure 8.4) showed a mass (33703±5) very similar to expected mass (33704 Da).The mass after heme incorporation and second DEAE was very messy and showed a major peak with a mass of 34354 ± 5 Da, 648 Da more than the other smaller peak corresponding to the estimated mass (figure 8.4). This heme-loaded version of loop-Cys is called "Red-C*c*P" from here on.

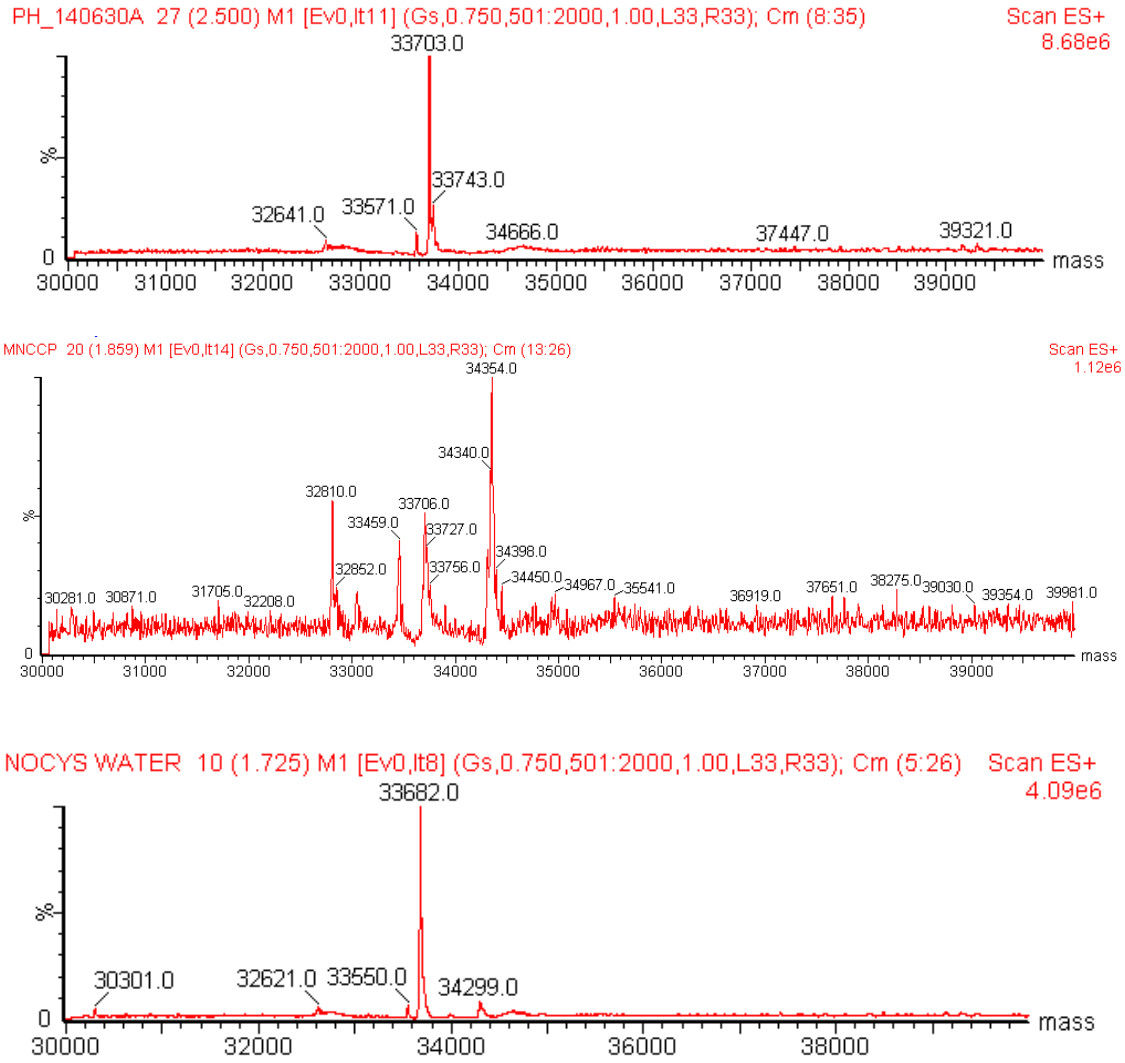

Figure 8.4. ESI-MS of green-C*c*P (top), red-C*c*P (middle) and loop-Gly (bottom)

Red sample has a normal UV-vis spectrum with the soret at 410 nm and R/z ratio of about 1, similar to other C*c*P mutants (figure 8.5).

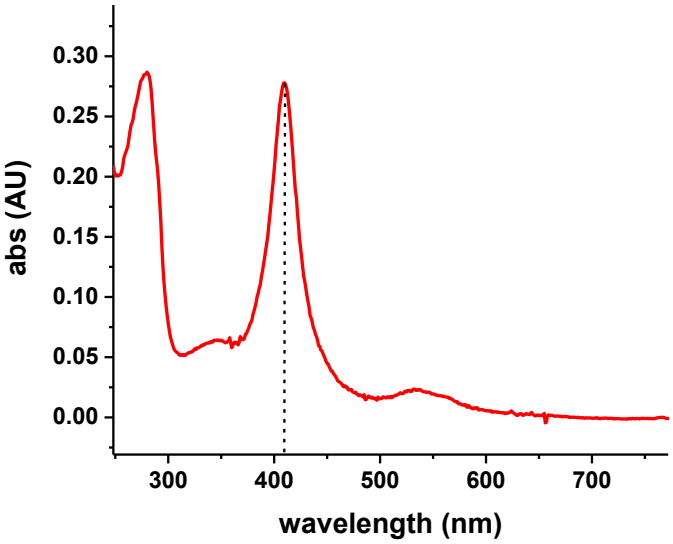

Figure 8.5. UV-vis of red-C*c*P shows a typical holo-C*c*P spectra.

Interestingly, the loop-Gly variant had normal cell pellets (golden-brownish) and a normal mass–spec (figure 8.4), as expected, even after heme addition (observed mass of 33682±5 Da, estimated mass of 33685.55).

Overnight incubation of samples with H_2O_2 resulted in little to no change in the green-C*c*P mass spectrum. Some amount of crosslink was observed in the loop-Gly sample. The red-C*c*P was dirty as usual, but no significant increase in the crosslink signal was observed. The data is not shown but are available on page 5 of PH notebook IX. It worth mentioning that one time, I got no crosslink upon heme titration into the green-C*c*P. With that sample, H_2O_2 addition caused crosslink to form as I observed by heme extraction experiments.

Further purification trials of the green-sample with DEAE column, Q-column and SEC showed that the reactive fraction is the one with the 680 nm shoulder. Since the Q-column was cumbersome and I lost lots of protein, I stopped doing that. Figure 8.6 shows a picture of the overall Q-column method and different peaks. The one in the green box is the most active fraction.

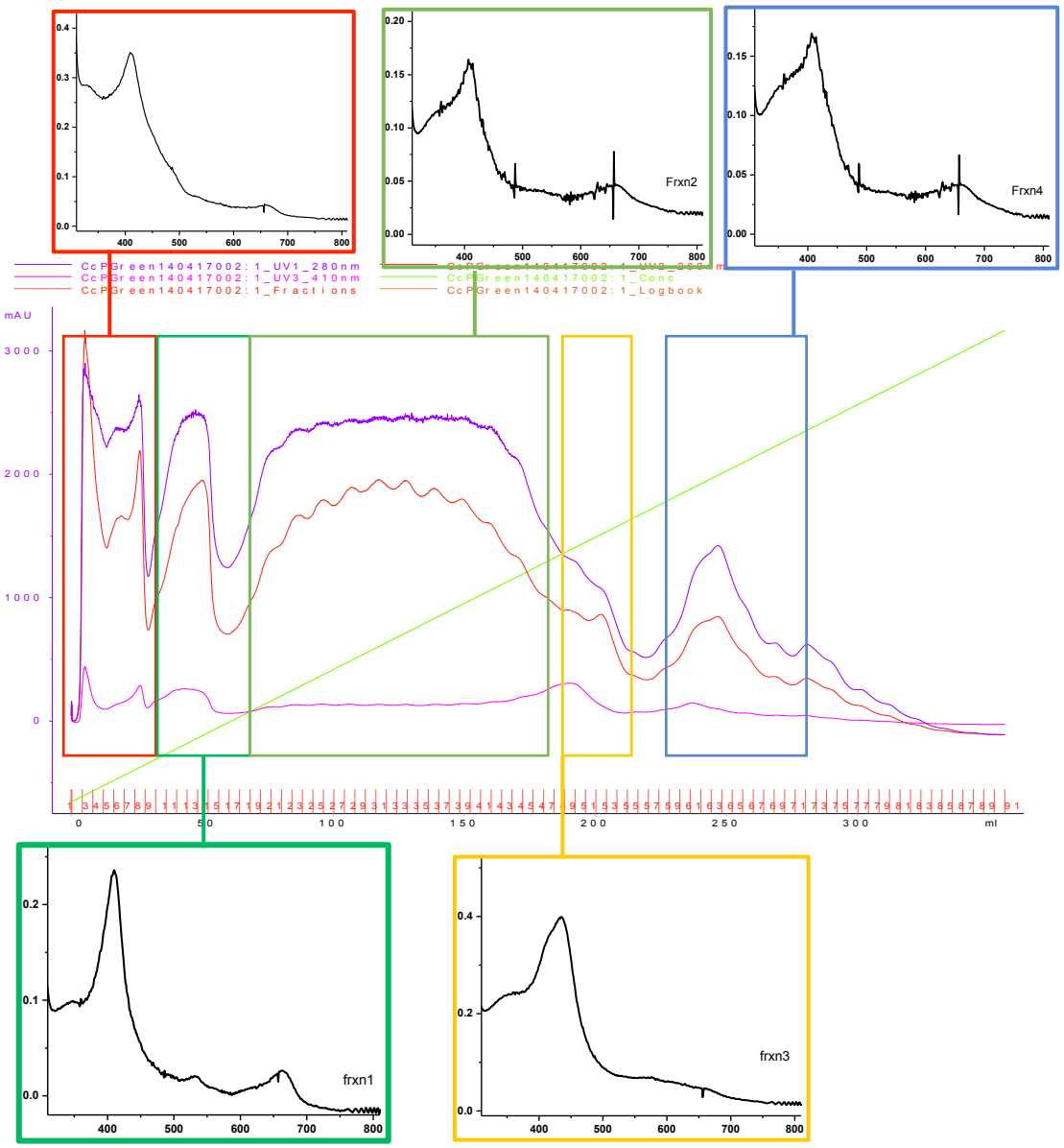

Figure 8.6. Q-column purification of green-C*c*P. The protein was eluted in a slow salt gradient.

The process of denaturing the protein and then refolding it in the presence of the heme gave almost pure cross-linked red-C*c*P. The mass is 34369±5 Da, which is about 666 bigger than the apo-protein peak (figure 8.7).

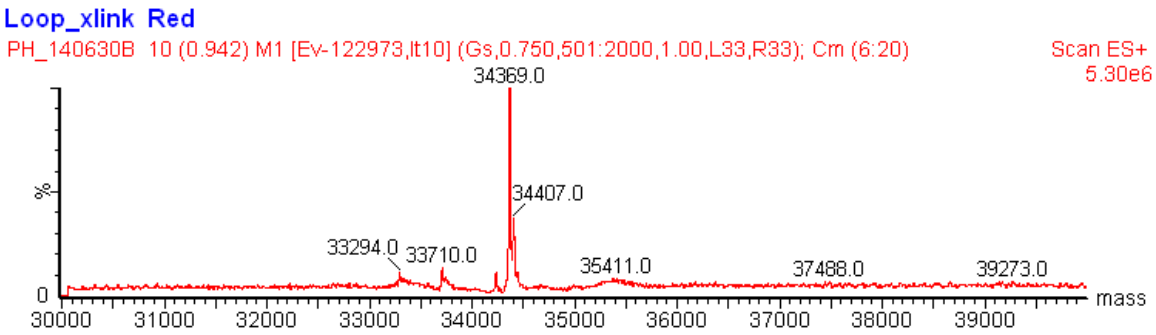

Figure 8.7. ESI-MS of red-C*c*P after denaturation and refolding in the presence of heme.

I tried to run SDS-PAGE with a reported method that showed heme-protein crosslink on gel,[8] but my gel turned out to look super ugly (page 63, PH notebook XI) and not conclusive at all. Gel analysis of older samples show clear degradation of the protein by time (page 149, PH notebook XI).

8.3.3. HPLC analysis

HPLC analysis (figure 8.8) showed that in the digested red sample, and only in red sample, there are peptide fragments that contain heme peaks as well. Such peaks were not observed either in the digested green sample or in the digested holo-Loop-Gly samples.

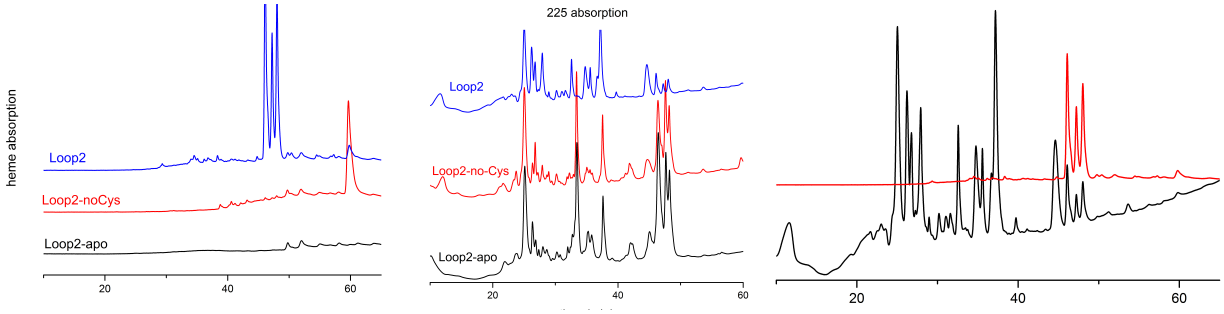

Figure 8.8. The left and middle plots show the HPLC trace monitored at 390 nm and 250 nm, respectively. Overlay of the two (right figure) for red-C*c*P shows peptide regions that overlap with heme absorption.

8.3.4. Mass spec analysis

After heme extraction, the majority of red-C*c*P remained heme-bound, suggesting a covalent linkage between heme and protein. Mass spec analysis of the small fractions of the heme that were successfully extracted gave a mass of 648 (figure 8.9), which is 32 units more than heme *b* (614), suggesting possible presence of O_2-bound heme. Even after trypsin digestion, the heme

remained in the water containing part, suggesting that probably a very positive peptide was attached to the heme.

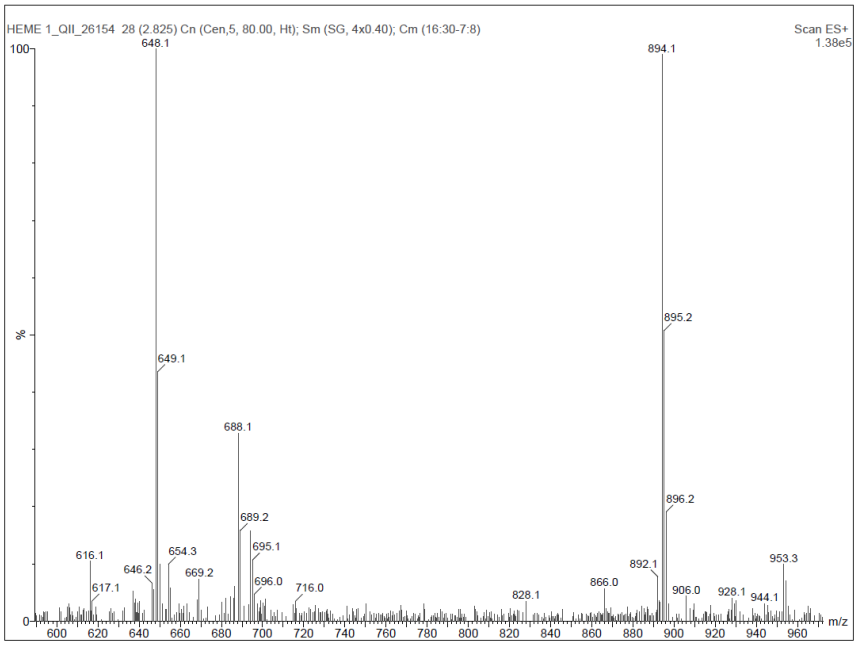

Figure 8.9. EI mas spectroscopy of extracted heme from red-C*c*P.

Initial MS/MS analysis of the data showed very low score Cys peptides and the modification was not clear. After getting the fully cross-linked red protein and upon some improvements on Mascot program, the MS/MS analysis yielded some peptides with the heme attached. Same peptide came out as a hit in some of my more concentrated samples from the red-C*c*P that was partially cross-linked. The mass search was done with heme *b* and heme *b* oxy, hyroxyheme, verdoheme and verdoheme oxy, ferric biliverdin and its oxy form. The search was set to find modifications on Cys, Asp, His, Met, and Arg residues. Overall, the best hit from Mascot showed a heme modification on Met 172 (figure 8.10). Why this cross-link does not form in other C*c*P mutants and whether the obtained peptide is real (since the Cys coverage is usually very low) is still a matter of doubt.

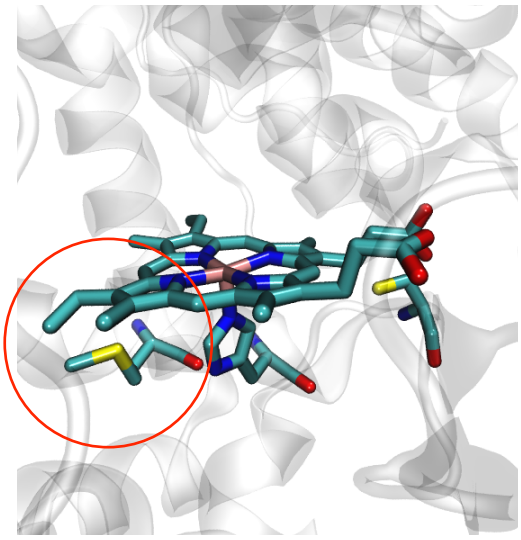

Figure 8.10. The predicted structure of loop-Cys. The possible site of crosslink (Met172) is shown in a circle.

ICP-MS data gave me a value of 11.25 ppm (or 11.25 g/1000L) of iron. Using this and given the molecular weight of iron (55.845) I calculated ε_{663}= 16.8 $mM^{-1}cm^{-1}$. Using Beer's law and assuming that the 663 nm peak and the 408 nm peak are from the same specie, I got ε_{408} = 77.33 $mM^{-1}cm^{-1}$ which is very reasonable for heme in C*c*P. It seems that it's not something with very high extinction coefficient, but only small amounts of it are present. The data is also close to the number I obtained from hemochromogen assay of the green-C*c*P (ε = 126.28 $mM^{-1}cm^{-1}$).

8.3.5. Spectroscopic studies

Running CD on the red-C*c*P and Loop-Gly variant showed similar features in 200-250 region, indicating very similar 3D composition between the two. However, the 250-500 region that has heme soret showed significant differences between the two proteins, suggesting a change in heme environment in the red protein (Figure 8.11). This change can be either due to the crosslink or different orientation of the heme in the pocket.

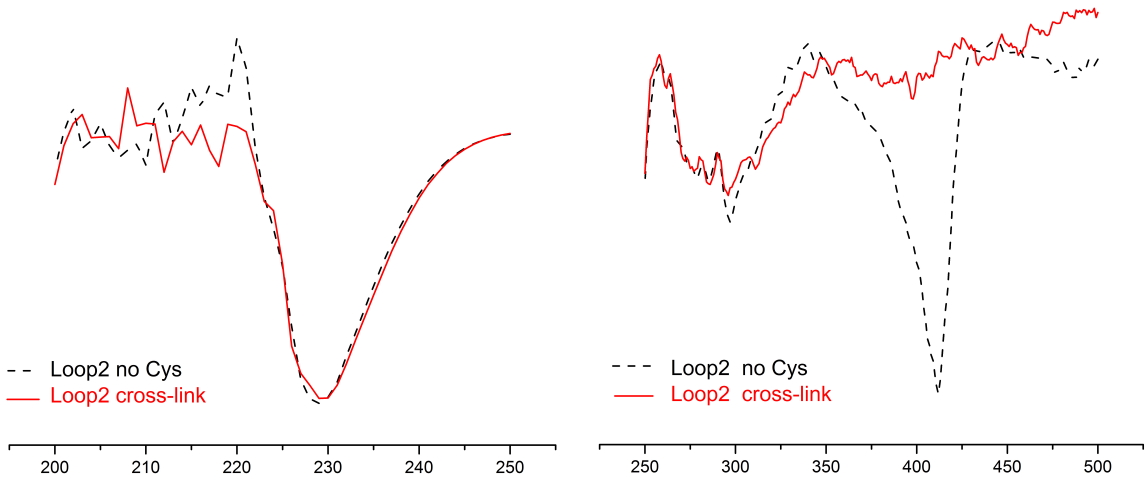

Figure 8.11. CD of red-C*c*P and loop-Gly in regions from 200-250 nm and 250-500 nm.

Hemochromogen assay gave a value of ε_{415} = 282.46 $mM^{-1}cm^{-1}$ for the red-C*c*P (figure 8.12).

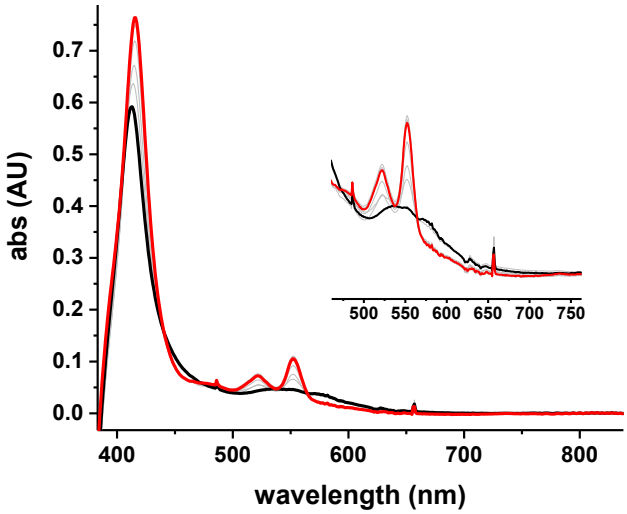

Figure 8.12. Hemochromogen assay of green-C*c*P. Initial and final spectra are shown in black and red lines, respectively.

EPR of red-C*c*P shows a low-spin state at higher pH and a high-spin state for the heme at lower pH values (Figure 8.13). The high spin signal goes away and instead a radical signal would appear as well as another signal as g = 4.2, similar to free Fe(III) or Fe(III)-biliverdin, an intermediate of heme degradation pathway.

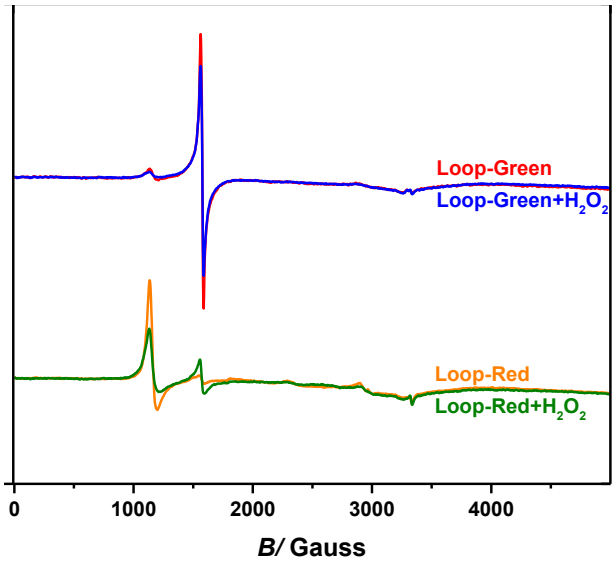

Figure 8.13. EPR spectra of red-C*c*P and green-C*c*P before and after H_2O_2 treatment. (10 mW power, 10 G modulation, 15 K)

There are several reasons that I think it is not verdoheme. First is that the protein had turnover during Mn(II) oxidation assay. Second reason is that 60% of the protein could be recovered after reaction with H_2O_2 and the third reason is that adding pyridine to the sample after H_2O_2 reaction did not give me the signature UV-vis of verdoheme (figure 8.14).

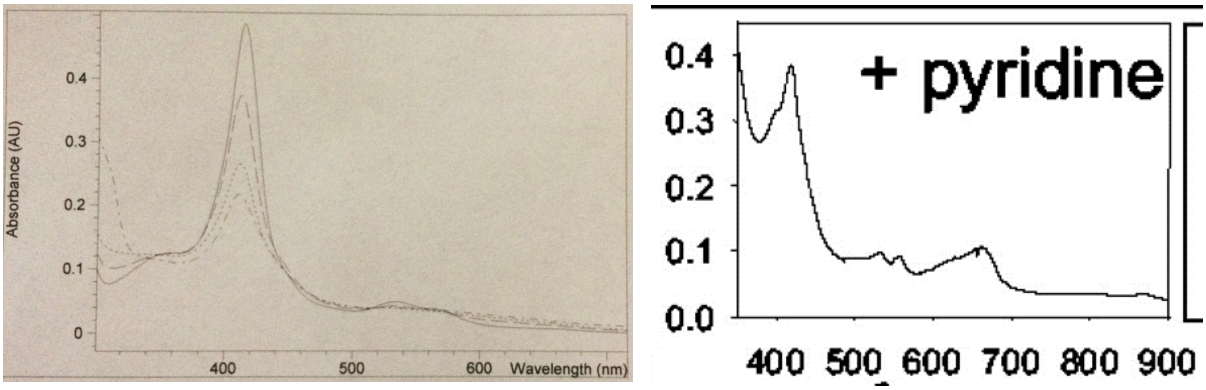

Figure 8.14. On the left the spectra of red-C*c*P is shown. The solid line is the initial spectrum. The dashed and dotted lines are after 5 and 10 molar equivalent addition of H_2O_2, respectively. the dash-dot line is after addition of pyridine. As can be seen that line lacks the significant 680 feature of verdoheme in pyridine shown in the right figure. Right figure is from ref [24]

Running the EPR on the pure cross-linked red-C*c*P and green-C*c*P (figure 8.15) showed that the red-C*c*P has normal heme signature in pH 7 and is a mixture if high spin and low spin heme. Interestingly the green-C*c*P has a signal at g = 4.22 which is consistent with what is observed

after reaction of red-C*c*P with a large amount of H_2O_2. The identity of the signal still remains elusive.

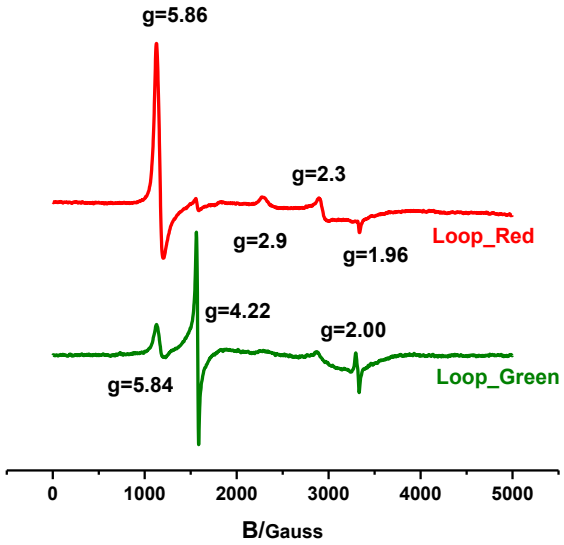

Figure 8.15. EPR spectrum of red-C*c*P (fully cross-linked) and green-C*c*P. (10 mW power, 10 g modulation, 15 K)

NMR of control loop-Gly showed normal C*c*P spectra, but with low spin heme. The green-C*c*P showed no paramagnetically shifted signal suggesting that it is either in Fe(II) state or is antiferromagentically coupled to a nearby radical. These results suggest that the EPR signal observed above is only a small percentage of the overall species there and most of it should be EPR silent. Adding potassium cyanide to the sample resulted in a shift in soret but no change in the visible region was observed.

In order to change the possible antiferromagnetic coupling between the heme-iron and a radical, I oxidized the green-C*c*P with ferricyanide. Not much spectral change was observed except for possible decay of peak at 668 (figure 8.16, left). EPR of the ferricyanide treated sample clearly showed a decrease in the g=4.22 sample but no increase in any other signal (figure 8.16, right).

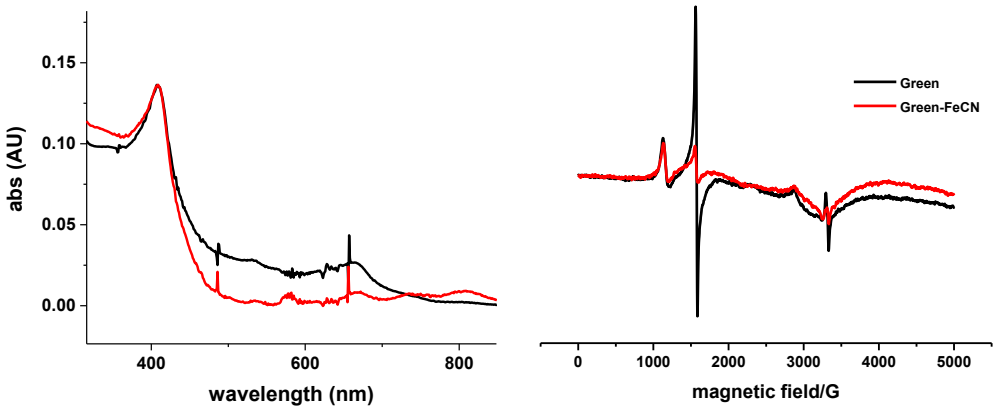

Figure 8.16. UV-vis and EPR spectra of green-C*c*P before and after reacting with excess ferricyanide. The protein is passed down PD-10 column to remove excess unreacted ferricyanide.

NMR of the red-C*c*P showed a broad signal typical of high spin Fe(III), consistent with observed dominance of high spin signal in EPR. The sample was converted to low spin by addition if cyanide. The obtained spectrum from the low-spin sample was completely different from those of other *b*-type hemoproteins. One possible explanation for that was the fact that the heme is corss-linked to the protein. Unfortunately further sampling of the sample didn't improve the signal to noise ratio and no more detailed structural information could be obtained.

8.3.6. Peroxidase activity assay

Mn(II) oxidation assay on the protein showed similar trends to my MnC*c*P.1 variants. However, the 410 nm soret peak didn't shift as is the case for those variants and would only go down.

Peroxidase assay with ABTS was adapted from Wiseman thesis.[28] Assays usually are performed in a 50 mM sodium acetate buffer pH 4.5. I tried several different buffers. 1 mM H_2O_2 and 0.4 mM ABTS are also present in the reaction solution. The protein is then added and the reaction is continued for 2 min. The activity is measured by dividing the final amount of oxidized ABTS (ε_{405} = 36800 $M^{-1}cm^{-1}$) by the time. One unit of enzymatic activity is defined by the amount of enzyme that decomposes 1 μmol of ABTS in 1 min at the buffer pH at room temperature.

The peroxidase activity assay showed that the proteins are less efficient in peroxidase activity compared to other active MnC*c*P variants (figure 8.17). There are two important things to note.

First, the red-C*c*P retains most of its activity at pH 7.0 (about 70%) while the I40G.1 variant (see chapter 7) only retains 10% of activity. This observation is consistent with a more robust system.

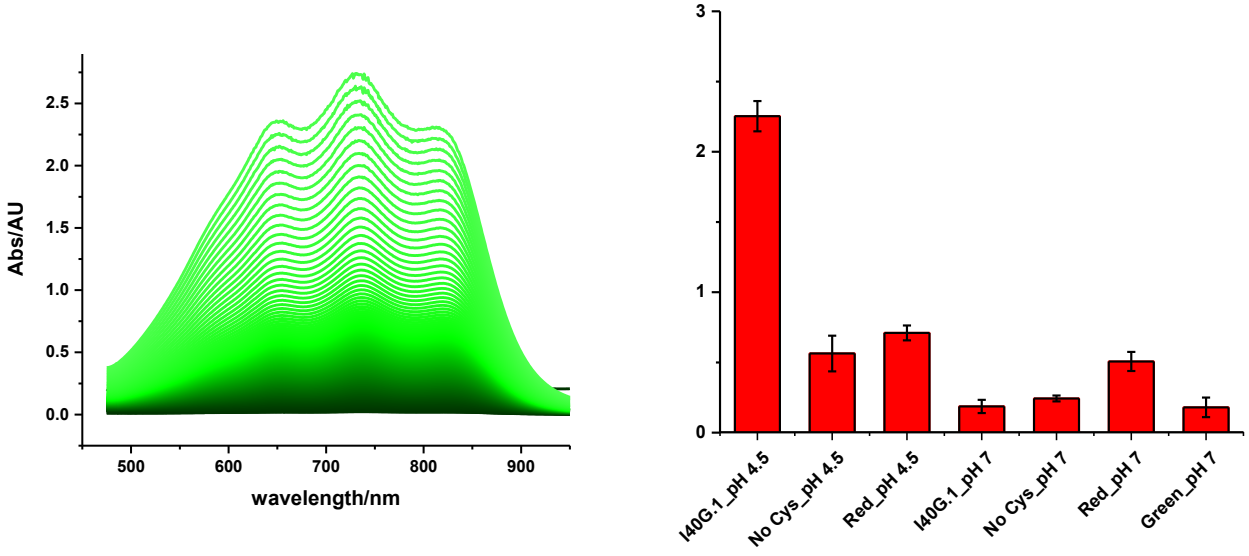

Figure 8.17. The left figure shows the overall trace of ABTS assay. On the right, the final results of the assay is shown.

Second, the peroxidase assay is an end point assay that monitors the activity over he course of 2 min. comparing the kinetic trace of the red-C*c*P and I40G.1 suggests that in longer time points, the red-C*c*P can reaches the activity of I40G.1 (figure 8.18) and it is much slower but not overall worst.

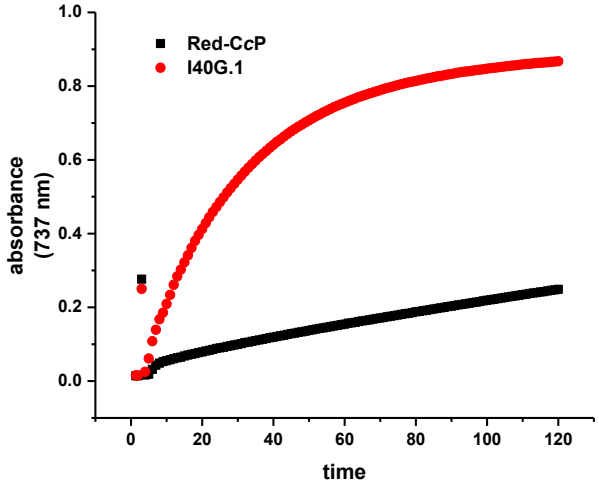

Figure 8.18. Time trace of ABTS assay for red-C*c*P and I40G.1.

8.3.7. Catalase activity assay

Unusual results during peroxidase assay as well as observation of bubbles in green-C*c*P suggested that the protein might have catalase activity. The bubble generation during H_2O_2 assay was so much that I couldn't take any more spectra and had a huge baseline shift (reaction of 200 µl protein with 1 µl of 10 M H_2O_2 in 2 ml final reaction buffer).

The same assay with Cu_BMb-verdoheme resulted in complete loss of heme signal, which is not the case with the green-C*c*P (figire 8.19).

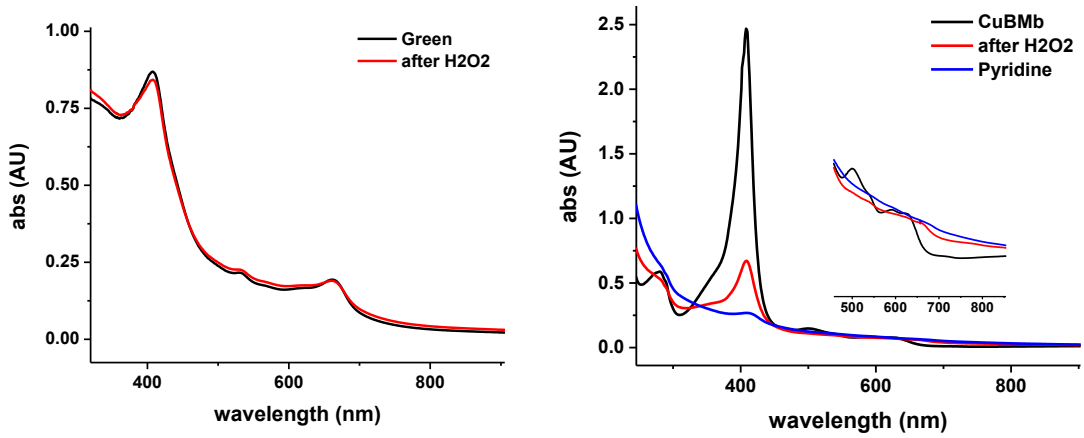

Figure 8.19. The left figure shows UV-vis of green-C*c*P before and after reaction with H_2O_2. The right figure shows the same thing for Cu_BMb.

The qualitative catalase assay showed O_2 formation (figure 8.20). The calibration curve was not very nice but it gave a nice qualitative fast way of comparing things. Interestingly the red-C*c*P has almost no catalase activity compared to the green one.

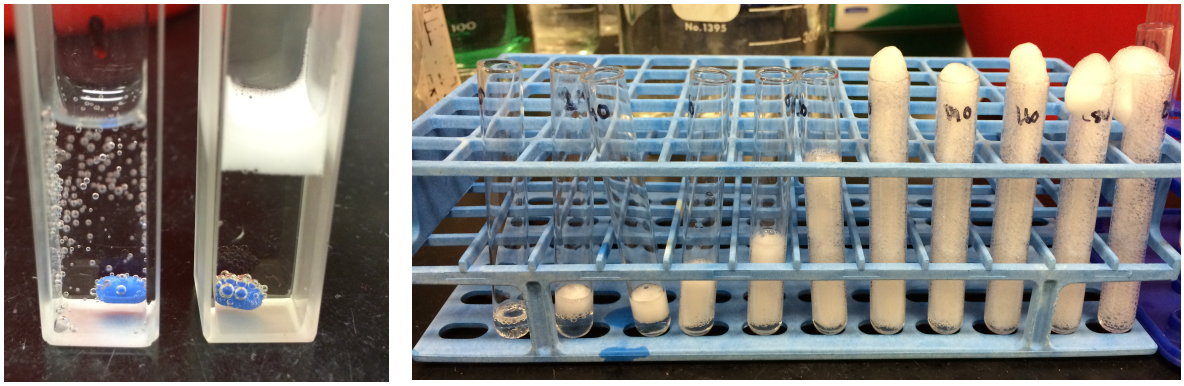

Figure 8.20. Green-C*c*P generates bubbles in the cuvette when reacting with H_2O_2 as shown in the left figure. The left-most cuvette contains catalase as a control. The tubes on the right show the qualitative assay of catalase. Moving to the right, the amount of protein (here catalase) is increasing.

GC-Ms studies clearly showed the presence of O_2 in our samples (figure 8.21). The amount observed was suggestive of a catalytic reaction with turnovers. The two different programs we tried didn't give us better separation. Probably the best way to go is to use a more specialized column (the one I found is MolSeive 5A columns). The O_2 signal is completely absent in the control sample (not shown in here, available on pages 11 and 14 of PH notebook X).

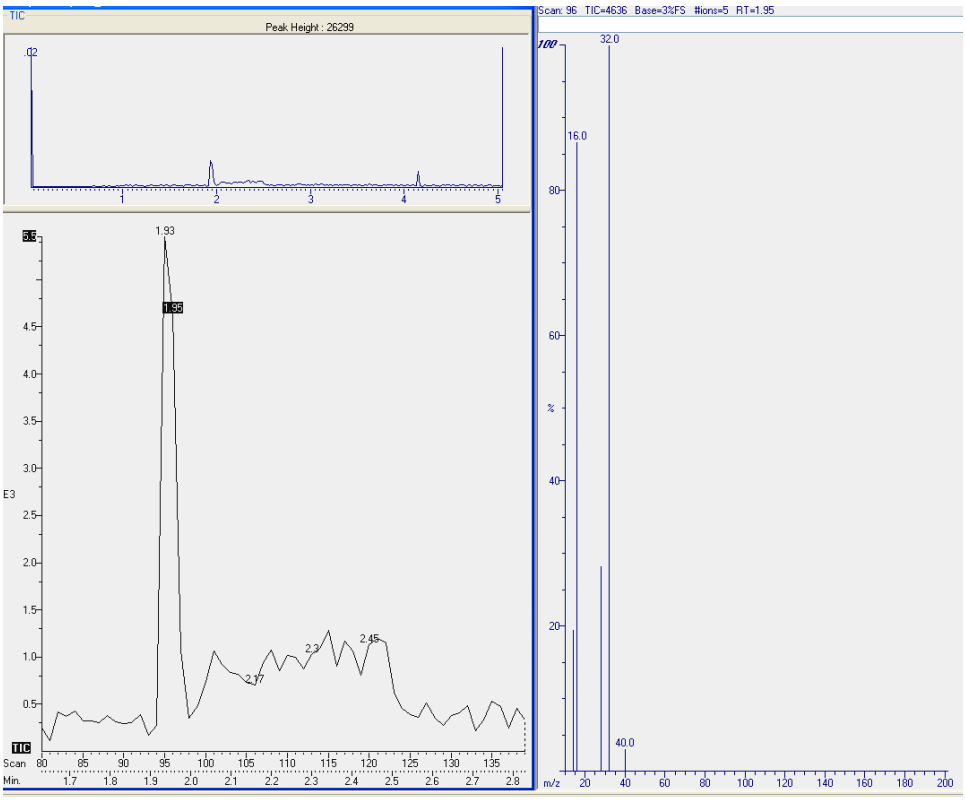

Figure 8.21. GC-MS of the head space gas after reaction of green-C*c*P with H_2O_2 shows clear formation of O_2.

Results from the O_2 production studies with O_2 electrode showed that the protein is not an efficient catalase in most [H_2O_2]. The initial calculations showed an activity of 1500-3750 U/mg for the green-C*c*P depending on the method used for calculating the rates (compare to 2000-5000 U/mg for catalase). Taking into account that catalase is twice as big as C*c*P, the enzyme has about 35% activity of catalase activity. It should be noted that this activity happens only at high concentrations of H_2O_2.

Later experiments showed that most C*c*P variants at that concentration have catalase activity (figure 8.22). This observation contradicts my previous observations of the huge amount of

bubbles formed by the green-C*c*P and not any other C*c*P variants. It may be due to saturation of the spectra or the concentrations being off.

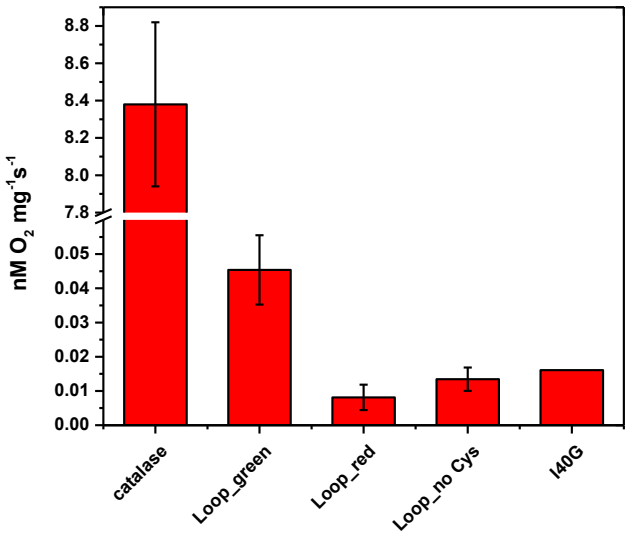

Figure 8.22. Quantification of O_2 production from different C*c*P variants and catalase based on data from O_2 electrode.

8.3.8. Cyclic voltammetry analysis

The green-C*c*P did not show any signal in CV. However, the red protein gave a nice reversible peak at about -70 mV vs. SHE (figure 8.23). This value is much higher than normal C*c*P mutants (usually about -200) and very close to D235N variant. The higher reduction potential can explain why the protein is not an amazing peroxidase.

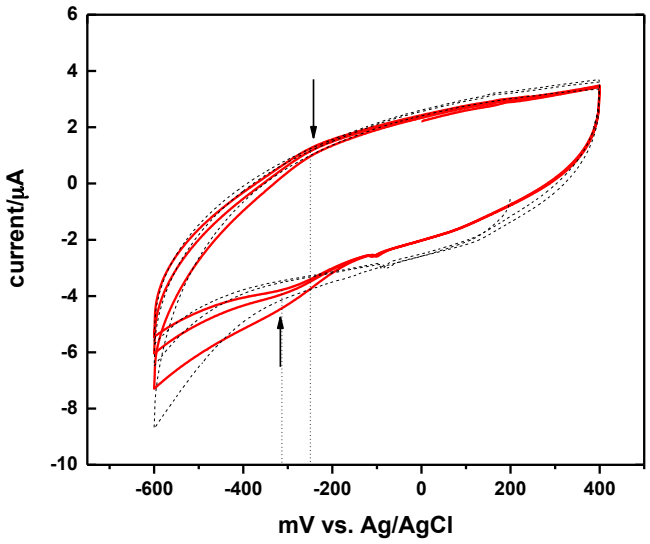

Figure 8.23. voltammagram of red-C*c*P obtained using protein film voltammetry in a scan rate of 200 mV/sec.

8.3.9. Loop-Ser purification and characterization

I obtained the loop-Ser variant after Gibson assembly. The purification protocol was exactly similar to the green and I obtained greenish pellet but less than the one from loop-Cys (about 3% compared to 20%, see figure 8.24). Below you may find the UV-vis of the fractions. The mass spec showed a mass of 33696±5 Da, which is about the calculated mass of 33688. Interstingly this variant showed an impressive amount of catalase activity.

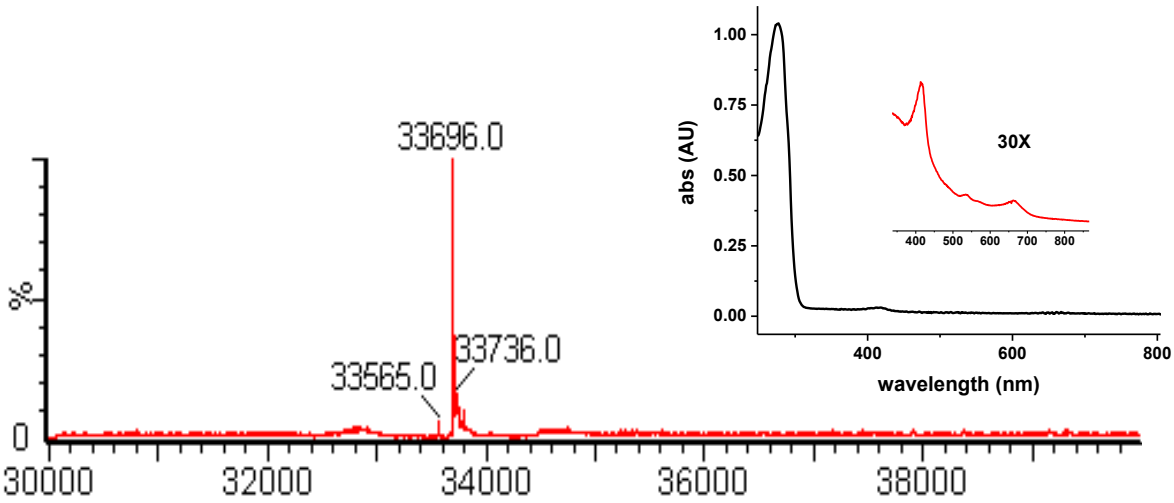

Figure 8.24. UV-vis and ESI spectrum of loop-Ser variant shows small, but observable amount of green cofactor.

8.4. Conclusion and future directions

Overall, this loop-Cys C*c*P variant shows interesting features that worth pursuing. In terms of the green-C*c*P, my best guess is that the protein is taking up something from the media. This take up relies on the presence of Cys or some polar group as I observed the green species in the loop-Ser variant too. Another confirmation to the claim is the fact that the amount of green species I obtain is highly dependent on my culture conditions. One way to go about this is to reduce the protein and then oxidize it again and see if we get the same species and if not it shows that there is a modification on the heme. The best way to go is to take the cofactor out using heme extraction and run NMR on that. Since the cofactor is not cross-linked, this should not be impossible to perform.

As for the red-C*c*P, the best way to go is to obtain the structure by NMR. I am planning to send the peptide to Xiaotang Wang to give him a better chance to obtain the structure. Another way to go is to just run overall NMR on the sample. There are several possible other things to do

to obtain the mechanistic insight such as addition of heme in the presence or absence of O_2 or reductant. It seems that the crosslink formation is O_2 dependent so addition of heme in the anaerobic chamber can be a good way to go. Whether the protein is linked to the Met172 or not is still a matter of doubt. This is the same position that the crosslink was observed in the engineered ascorbat peroxidase. However, as suggested by the authors C*c*P has mechanisms to prevent this reaction. Also, in contrast to the ascorbate peroxidase study, the cross-link forms without the need to use H_2O_2 and the final species is red and not green. These observations cast doubt on the correctness of Met-heme crosslink. One way to test this is to mutate Met172 and see if the cross-link still forms.

Loop-Val variant is a good control to see if the uptake of the cofactor is a result of the presence of more bulk in the place of original Gly or it needs a polar group as well. Since Loop-Ser has very high catalytic activity but not an indicator of crosslink formation as far as I tested, it suggests that probably the heme environment and not the crosslink is responsible for catalase activity. Maybe the uptaken heme is reoriented in these variants or these variants took up a special type of modified heme.

8.5. References

(1) Stevens, J. M.; Daltrop, O.; Allen, J. W. A.; Ferguson, S. J. C-type cytochrome formation: Chemical and biological enigmas;*Acc. Chem. Res.* **2004**, *37*, 999.

(2) Bertini, I.; Cavallaro, G.; Rosato, A. Cytochrome *c*: occurrence and functions;*Chem. Rev.* **2006**, *106*, 90.

(3) Kranz, R. G.; Richard-Fogal, C.; Taylor, J. S.; Frawley, E. R. Cytochrome *c* biogenesis: mechanisms for covalent modifications and trafficking of heme and for heme-iron redox control;*Microbiol. Mol. Biol. Rev.* **2009**, *73*, 510.

(4) Lin, Y. W.; Wang, W. H.; Zhang, Q.; Lu, H. J.; Yang, P. Y.; Xie, Y.; Huang, Z. X.; Wu, H. M. Converting Cytochrome *b*5 into cytochrome *c*-like protein;*Chembiochem* **2005**, *6*, 1356.

(5) Garner, D. K.; Liang, L.; Barrios, D. A.; Zhang, J.; Lu , Y. The important role of covalent anchor positions in tuning catalytic properties of a rationally designed MnSalen-containing metalloenzyme;*ACS Catalysis* **2011**, *1*, 1083.

(6) Henne, K. R.; Kunze, K. L.; Zheng, Y. M.; Christmas, P.; Soberman, R. J.; Rettie, A. E. Covalent linkage of prosthetic heme to CYP4 family P450 enzymes;*Biochemistry* **2001**, *40*, 12925.

(7) LeBrun, L. A.; Hoch, U.; Ortiz De Montellano, P. R. Autocatalytic mechanism and consequences of covalent heme attachment in the cytochrome P450 4A family;*J. Biol. Chem.* **2002**, *277*, 12755.

(8) Rice, S. L.; Preimesberger, M. R.; Johnson, E. A.; Lecomte, J. T. Introduction of a covalent histidine-heme linkage in a hemoglobin: a promising tool for heme protein engineering;*J. Inorg. Biochem.* **2014**, *141*, 198.

(9) Vu, B. C.; Vuletich, D. A.; Kuriakose, S. A.; Falzone, C. J.; Lecomte, J. T. J. Characterization of the heme-histidine cross-link in cyanobacterial hemoglobins from Synechocystis sp. PCC 6803 and Synechococcus sp. PCC 7002;*JBIC, Journal of Biological Inorganic Chemistry* **2004**, *9*, 183.

(10) Lee, D.; Pervushin, K.; Bischof, D.; Braun, M.; Thony-Meyer, L. Unusual heme-histidine bond in the active site of a chaperone;*J. Am. Chem. Soc.* **2005**, *127*, 3716.

(11) Fiedler, T. J.; Davey, C. A.; Fenna, R. E. X-ray crystal structure and characterization of halide-binding sites of human myeloperoxidase at 1.8 A resolution;*J. Biol. Chem.* **2000**, *275*, 11964.

(12) Metcalfe, C. L.; Ott, M.; Patel, N.; Singh, K.; Mistry, S. C.; Goff, H. M.; Raven, E. L. Autocatalytic Formation of Green Heme: Evidence for H2O2-Dependent Formation of a Covalent Methionine-Heme Linkage in Ascorbate Peroxidase;*J. Am. Chem. Soc.* **2004**, *126*, 16242.

(13) Yan, D.-J.; Li, W.; Xiang, Y.; Wen, G.-B.; Lin, Y.-W.; Tan, X. A Novel Tyrosine–Heme C-O Covalent Linkage in F43Y Myoglobin: A New Post-translational Modification of Heme Proteins;*ChemBioChem* **2015**, *16*, 47.

(14) Pipirou, Z.; Bottrill, A. R.; Svistunenko, D. A.; Efimov, I.; Basran, J.; Mistry, S. C.; Cooper, C. E.; Raven, E. L. The reactivity of heme in biological systems: autocatalytic formation of both tyrosine-heme and tryptophan-heme covalent links in a single protein architecture;*Biochemistry* **2007**, *46*, 13269.
(15) Cedervall, P.; Hooper, A. B.; Wilmot, C. M. Structural studies of hydroxylamine oxidoreductase reveal a unique heme cofactor and a previously unidentified interaction partner;*Biochemistry* **2013**, *52*, 6211.
(16) Colas, C.; Kuo, J. M.; Ortiz de Montellano, P. R. Asp-225 and glu-375 in autocatalytic attachment of the prosthetic heme group of lactoperoxidase;*J. Biol. Chem.* **2002**, *277*, 7191.
(17) Zhang, Y. I-TASSER server for protein 3D structure prediction;*BMC Bioinformatics* **2008**, *9*, 40.
(18) Roy, A.; Kucukural, A.; Zhang, Y. I-TASSER: a unified platform for automated protein structure and function prediction;*Nat. Protoc.* **2010**, *5*, 725.
(19) Yang, J.; Yan, R.; Roy, A.; Xu, D.; Poisson, J.; Zhang, Y. The I-TASSER Suite: protein structure and function prediction;*Nat. Methods* **2015**, *12*, 7.
(20) Pfister, T. D.; Gengenbach, A. J.; Syn, S.; Lu, Y. The Role of Redox-Active Amino Acids on Compound I Stability, Substrate Oxidation, and Protein Cross-Linking in Yeast Cytochrome c Peroxidase;*Biochemistry* **2001**, *40*, 14942.
(21) Pfister, T.; Mirarefi, A.; Gengenbach, A.; Zhao, X.; Danstrom, C.; Conatser, N.; Gao, Y.-G.; Robinson, H.; Zukoski, C.; Wang, A.; Lu, Y. Kinetic and crystallographic studies of a redesigned manganese-binding site in cytochrome c peroxidase;*J. Biol. Inorg. Chem.* **2007**, *12*, 126.
(22) Miner, K. D.; Pfister, T. D.; Hosseinzadeh, P.; Karaduman, N.; Donald, L. J.; Loewen, P. C.; Lu, Y.; Ivancich, A. Identifying the elusive sites of tyrosyl radicals in cytochrome *c* peroxidase: implications for oxidation of substrates bound at a site remote from the heme;*Biochemistry* **2014**, *53*, 3781.
(23) Miner, K. D.; Mukherjee, A.; Gao, Y.-G.; Null, E. L.; Petrik, I. D.; Zhao, X.; Yeung, N.; Robinson, H.; Lu, Y. A designed functional metalloenzyme that reduces O_2 to H_2O with over one thousand turnovers;*Angew. Chem. Int. Ed.* **2012**, *51*, 5589.
(24) Sigman, J. A.; Kim, H. K.; Zhao, X.; Carey, J. R.; Lu, Y. The role of copper and protons in heme-copper oxidases: Kinetic study of an engineered heme-copper center in myoglobin;*Proc. Natl. Acad. Sci. U S A* **2003**, *100*, 3629.
(25) Iwase, T.; Tajima, A.; Sugimoto, S.; Okuda, K.; Hironaka, I.; Kamata, Y.; Takada, K.; Mizunoe, Y. A simple assay for measuring catalase activity: a visual approach;*Sci. Rep.* **2013**, *3*, 3081.
(26) Armstrong, F. A. Insights from protein film voltammetry into mechanisms of complex biological electron-transfer reactions;*J. Chem. Soc., Dalton Trans.* **2002**, 661.
(27) Hwang, H. J.; Ang, M.; Lu, Y. Determination of reduction potential of an engineered CuA azurin by cyclic voltammetry and spectrochemical titrations;*J. Biol. Inorg. Chem.* **2004**, *9*, 489.
(28) Wiseman, B., Manitoba, 2010.